Determining Factors of Skin Colouration: A Light and Electron Microscopic Study of the Distribution of Melanin and Its Degradation in the Human Epidermis

Dissertation

Accepted by the Department of Chemistry,
Faculty of Mathematics, Informatics and Natural Sciences of the University of Hamburg
for the degree of Doctor of Natural Sciences
(Dr. rer. nat.)

Miriam Susanna Droste
Hamburg, Germany
2006

Reviewers of doctoral thesis:

Prof. Dr. Stephan Förster
Institute of Physical Chemistry, University of Hamburg

Prof. Dr. Horst Weller
Institute of Physical Chemistry, University of Hamburg

Examining committee:

Prof. Dr. Stephan Förster
Institute of Physical Chemistry, University of Hamburg

Prof. Dr. Ulrich Hahn
Institute of Biochemistry and Molecular Biology, University of Hamburg

Dr. Kathrin Hoppe
Institute of Physical Chemistry, University of Hamburg

Dr. Roger Wepf
Electron Microscopy Centre of the ETH Zurich, Swiss Federal Institute of Technology Zurich

Defence of doctoral thesis: 23rd of March 2007

The work described in this thesis was accomplished at the Paul Gerson Unna-Forschungszentrum, Beiersdorf AG, Hamburg under the academic supervision of Dr. Roger Wepf, now head of the Electron Microscopy Centre (EMEZ), ETH Zurich, and Prof. Dr. Stephan Förster, Institute of Physical Chemistry, University of Hamburg.

ZUSAMMENFASSUNG

Die menschliche Hautfarbe wird im Wesentlichen von der Menge des vorhandenen Pigmentes Melanin, sowie seiner Verteilung in der Epidermis beeinflusst. Die Unterart des Melanins spielt dabei eine untergeordnete Rolle, da das in der Epidermis vorkommende Melanin zu einem Großteil aus den Polymeren des Eumelanins gebildet wird. Dies gilt für alle Hauttypen, mit der Ausnahme des Phototyps I, in dem das Phäomelanin ein Fünftel des gesamten Melaningehaltes ausmacht. Melanin wird von dendritischen Zellen, den Melanozyten, die in der Basalschicht der Epidermis ansässig sind, in spezialisierten Organellen, den so genannten Melanosomen gebildet. Die Melanosomen werden an die benachbarten Keratinozyten abgegeben, wo sie u.a. eine Schutzfunktion gegen UV Strahlung übernehmen, indem sie das einfallende Licht streuen und absorbieren.
Innerhalb der Keratinozyten liegen die Melanosomen entweder als einzelne Partikel vor oder sind zu Clustern zusammengefasst. Dieses Verteilungsmuster wird von der Art des Transfers von den Melanozyten zu den Keratinozyten bestimmt. Elektronenmikroskopische Untersuchungen haben gezeigt, dass vermutlich mehrere verschiedene Transfermechanismen parallel existieren. Am wahrscheinlichsten ist jedoch die exozytotische Abgabe der Melanosomen in den Interzellularraum, wo sie als membranfreie Partikel vorliegen und sofort von den benachbarten Keratinozyten über Phagozytose aufgenommen werden.
In allen Hauttypen wird die größte Konzentration an Melanosomen im *Stratum basale* beobachtet. Zu den oberen Epidermisschichten nimmt der Melanosomengehalt ab, wobei im *Stratum corneum* fast keine oder nur sehr wenige Melanosomen festzustellen sind. Der hier zugrunde liegende Abbaumechanismus basiert auf der oxidativen Zersetzung des Biopolymers Melanin durch Wasserstoffperoxid. Dieses entsteht intrazellulär aus Superoxid Anion, das von dem membranständigen Enzymkomplex NADPH Oxidase gebildet wird. Die Beteiligung dieses Enzymkomplexes am Abbau von Melanin konnte in diesem Projekt gezeigt werden.
Je dunkler die Haut, desto mehr Melanosomen sind in den tiefen Schichten der Epidermis vorhanden. Da die Melanosomen in allen Hauttypen gleich stark abgebaut werden, die Ausgangsbasis jedoch unterschiedlich ist, erreichen in dunklerer Haut mehr Melanosomen die oberen Epidermisschichten. Diese Anreicherung beeinflusst die Wahrnehmung der Hautfarbe dahingehend, dass einstrahlendes Licht bereits in höheren Epidermisschichten gestreut und absorbiert wird, was zu einer dunkleren Erscheinung führt, als es bei Hauttypen mit einem geringeren Melanosomengehalt in den oberen Schichten der Epidermis der Fall ist. Daher erscheint Kaukasische Haut, die einen geringen Melanosomengehalt aufweist, hell, während Negroide Haut mit einem deutlich höheren Anteil an Melanosomen als dunkel empfunden wird. Ungleich anders verhält es sich in Altersflecken und Sommersprossen, hier bestimmt die Assoziation von Melanosomen zu kleinen Aggregaten, bei relativ hohem Melanosomengehalt in allen Schichten der Epidermis, den Farbunterschied zw. hellen Hautstellen und den dunklen Hautflecken.

ABSTRACT

The colour of the human skin is predominantly determined by the present quantity of the pigment melanin and its epidermal distribution patterns. The subtype of melanin plays a subordinate role, as eumelanin polymers constitute the major component of melanin particles in all skin phenotypes, with the sole exception of Fitzpatrick' skin phototype I, where pheomelanin accounts for one fifth of the total melanin content. Melanin is synthesized by dendritic cell, the melanocytes, located in the basal layer of the epidermis, in specialized organelles, so-called melanosomes. These melanosomes are transferred to the surrounding keratinocytes, providing – among other functions – protection against UV light by scattering and absorption interactions with the incident light.

Within the keratinocytes, the melanosomes are either distributed individually or agglomerated into clusters. This dispersal is governed by the mode of transfer from melanocyte to keratinocyte. Electron microscopic evidence gathered in this study indicates multiple co-existing modes of transfer, most likely involving exocytosis from the melanocytes, resulting in melanosomes free of surrounding membranes in the intercellular space, that are immediately internalized by adjacent keratinocytes via phagocytic processes.

In all skin types, the largest amount of melanosomes is observed in the *Stratum basale*, with gradually decreasing numbers toward the *Stratum corneum*, where no or only few melanosomes are left. The underlying degradation process is based on the oxidative breakdown of the biopolymer melanin by hydrogen peroxide, arising from superoxide anion produced via the membrane-associated enzyme complex NADPH oxidase, and the involvement of this enzyme in melanin degradation is demonstrated in this project.

The darker the skin, the larger the constitutional amount of melanosomes in the *Stratum basale*. And as the degradation process is equally efficient in all skin types, this leads to an accumulation of melanosomes in the upper epidermal layers of dark skin types, as more melanosomes reach the *Stratum corneum*. This influences the perception of the skin colour, since incident light is already absorbed and/or diffusely scattered in the upper epidermal layers, resulting in a darker appearance than experienced for skin with lower melanosome content. Hence Caucasian skin, containing only small amounts of melanosomes is perceived as white, while Negroid skin with considerably higher melanosome content is experienced as dark brown-to-black. In contrast, the outward appearance of age spots and freckles is determined by the association of melanosomes into clusters, while maintaining high levels of melanosomes throughout all epidermal layers. As a consequence, the lesion is experienced as a dark spot compared to its surroundings.

In nature's infinite book of secrecy a little I can read.

William Shakespeare, Anthony and Cleopatra

CONTENTS

A Introduction **1**

B Skin Pigmentation and Its Analysis **3**

I The Skin and Its Diversity in Colour *3*

I.1 Physiology of the Skin 3

I.2 Constitutive Skin Colour: The Pigment Melanin 5

I.2.1 Formation of Eumelanin and Pheomelanin 5

I.2.2 The Pigment Producing Cells: Melanocytes 9

I.2.3 Developmental stages of Melanosomes 10

I.2.4 Transfer of Melanosomes to Keratinocytes 11

I.2.5 Melanosome Distribution in Keratinocytes and Throughout the Epidermis 15

I.3 Facultative Skin Colour: Tanning and Whitening 16

I.4 Dysfunctions of Pigmentation – Age Spots and Freckles 17

I.5 The Unknown Fate of Melanin 18

I.5.1 Melanin Dust or Degradation of the Polymer Structure? 18

I.5.2 NADPH Oxidase – a Candidate for Mediating Melanin Degradation 19

II Investigation and Evaluation of Skin Pigmentation *20*

II.1 Noninvasive Measurement of Skin Colour 20

II.2 Microscopic Analysis of Pigmentation 22

II.2.1 Histological and Cytochemical Methods to Investigate Pigmentation 23

II.2.2 Electron Microscopy as a Tool to Study Pigmentation 24

II.2.3 Cytochemical Demonstration of NADPH Oxidase Activity 24

II.3 Chemical Analysis of Melanin Content in Biological Samples 25

III The Project – Challenging Questions of Skin Pigmentation *27*

C Materials & Methods 29

I Standard Buffers 29

II Skin Samples 30

III Sample Preparation for Microscopy 32

III.1 Fixation 32

III.1.1 Chemical Fixation 33

III.1.2 Cryofixation 35

III.1.2.1 Plunge-Freezing 35

III.1.2.2 High-Pressure Freezing 36

III.1.2.3 Freeze-Drying 36

III.2 Dehydration and Embedding 37

III.2.1 Room Temperature Dehydration and Embedding 37

III.2.2 Freeze Substitution and Low-Temperature Embedding 39

III.3 Sectioning 41

III.3.1 Cryostat Sectioning 41

III.3.2 Ultramicrotomy 42

IV Staining Techniques for Melanocytes and Melanosomes 42

IV.1 Common Histological Staining Techniques 42

IV.1.1 Hematoxylin and Eosin Stain 43

IV.1.2 Toluidine Blue Staining 43

IV.2 Specific Histochemical Reactions 44

IV.2.1 Nile Blue Staining 44

IV.2.2 DOPA Oxidase Reaction 45

IV.2.3 Fontana-Masson Silver Staining 46

IV.3 Immunofluorescence Assay 48

IV.4 Staining for Transmission Electron Microscopy 51

V Cytochemical Localisation of NADPH Oxidase Activity 52

VI Chemical Analysis of Melanin in Biological Samples 56

VI.1 Chemical Analysis of Total Eumelanin and Pheomelanin Content 56

VI.2 Melanin Degradation *In Vitro* 57

VI.3 Analysis of Melanin Degradation Products by SEC 57

VI.4 Analysis of Melanin Degradation Products by ESI-MS 57

VII Microscopic Documentation 58

VII.1 Light Microscopy 58

VII.2 Confocal Laser Scanning Microscopy 58

VII.3 Transmission Electron Microscopy 59

VII.4 Reflectance Spectroscopy 59

VIII Image Processing 60

VIII.1 Image Archiving 60

VIII.2 3D-Reconstruction and Visualization 60

VIII.3 Image Assembly 60

VIII.4 Counting Melanosomes 61

VIII.5 Automated Analysis of Melanosome Distribution 63

D Skin Pigment Characterization by Light and Electron Microscopy 65

I Identification of Melanocytes in the Context of Human Epidermis 65
I.1 Staining of Melanocytes by DOPA Oxidase Reaction 65
I.2 Identification of Melanocytes by Immunohistochemistry 66
I.3 Identification of Melanocytes in Transmission Electron Micrographs 71

II Characterization and Analysis of Melanosomes and Their Distribution in the Human Epidermis 73
II.1 Melanosome Staining by Histochemistry 74
II.2 Nile Blue Staining of Melanosomes 75
II.3 Fontana-Masson Staining for the Detection of Melanin 76
II.4 Melanosomes in CLSM Images of Resin Embedded Samples 81
II.5 Melanosomes imaging by Transmission Electron Microscopy 84

E Results 87

I Epidermal Melanosome Distribution and Melanin Content 87
I.1 Stereological Analysis of Epidermal Melanosome Distribution 88
I.1.1 Caucasian, Asian and Negroid Skin 88
I.1.2 Fitzpatrick's Skin Phototypes I vs. VI 91
I.1.3 Lentigo Senilis and Perilesional Adjacent Areas 92
I.1.4 Melanosome Organisation within the Keratinocytes of Different Skin Types 93
I.1.5 Epidermal Distribution of Melanin Particles in Different Phenotypes 96
I.1.6 Benchmark Test of the Manual Analysis 98
I.2 Automated Analysis of Epidermal Melanosome Distribution 100
I.2.1 Capability and Limitations of the Automated Analysis 102
I.2.2 Comparison of Manual and Automated Analysis on the Basis of Lentigo Samples 103
I.3 Chemical Analysis of Epidermal Melanin Content 105
I.4 Investigation of Skin Colour by Reflectance Spectroscopy 107

II Melanocyte Distribution in the Epidermis 108
II.1 The Epidermal Melanin Unit 108
II.2 Melanocyte Distribution in Fitzpatrick's Skin Phototypes I -VI 110
II.3 Melanocyte Distribution in *Lentigo Senilis* and Adjacent Areas 112

III Characteristics of Lentigo Senilis 114
III.1 Dermal – Epidermal Interleaving 114
III.2 Ultrastructural Characteristics 119
III.3 Corrected Melanosome Distribution 122

IV Melanosome Transfer – Search for Evidence 124
IV.1 Melanosome Transfer in Co-Cultures of Keratinocytes and Melanocytes 124
IV.2 Ultrastructural Organisation of Melanosomes within Melanocytes and after Transfer to Keratinocytes 126
IV.3 Melanosomes in the Intercellular Space 130
IV.4 Melanosomes at the Interface of Melanocytes and Keratinocytes 131

V Melanin Degradation In Vitro and Its Detection Ex Vivo 133
V.1 Degradation of Melanin by Hydrogen Peroxide 133
V.2 Localisation of NADPH Oxidase Activity 139

F Discussion & Conclusions 143

I Epidermal Melanosome Distribution Quantified by TEM 143

II Constitutive Pigmentation of Normal Skin Investigated by Microscopy, Chemical Analysis and Reflectance Spectroscopy 146

III Facultative Pigmentation of Age Spots and Freckles 151

IV The Epidermal Melanin Unit Revisited 155

V Melanosome Transfer – Microscopic Evidence and Its Implications 157

VI The Impact of Epidermal Melanosome Distribution on the Visual Perception of Skin Colour 160

VII The Influence of Temporary and Chronic UV Irradiation on Pigmentation 162

VIII Degradation of Melanin by H_2O_2 Controls the Skin Colour 164

G Summary & Outlook 169

H References 173

I Appendix 185

I Punch Biopsy Studies 185

I.1 Ethics Proposal (Ethikantrag) 185

I.2 Declaration of Consent (Einwilligungserklärung) 189

I.3 Information on Study Participants 192

I.3.1 Study 10684 192

I.3.2 Study 18655 193

II Safety Information for the Applied Chemicals and Reagents 195

III Curriculum Vitae 199

IV Publications & Conference Contributions 201

V Acknowledgements 203

VI Eidesstattliche Versicherung 205

LIST OF FIGURES

Figure 1: Layers of the skin. *4*
Figure 2:Monomers of eumelanin. *5*
Figure 3: Monomers of pheomelanin. *6*
Figure 4: Pathway of melanin synthesis. *7*
Figure 5: Potential mechanism of assembly of eumelanin polymers. *8*
Figure 6: Location of melanocytes in the epidermis. *9*
Figure 7: Development of eumelanosomes. *10*
Figure 8: Mechanism of melanosome transport into the dendrites of the melanocyte. *12*
Figure 9: Four possible mechanisms for melanosome transfer to keratinocytes. *13*
Figure 10: Melanosome distribution patterns in different ethnic skin types. *15*
Figure 11: Oxidative breakdown of eumelanin. *26*
Figure 12: Reductive hydrolysis of pheomelanin. *26*
Figure 13: Annotated TEM-mosaic. *61*
Figure 14: Definition of single melanosomes and melanosome clusters. *62*
Figure 15: DOPA oxidase reaction. *66*
Figure 16: Comparison of antibodies directed against melanosomal proteins. *69*
Figure 17: Antibody combinations for the identification and description of melanocytes. *70*
Figure 18: Double labelling for Mel-5 and α-collagen IV. *71*
Figure 19: TEM image of a melanocyte. *72*
Figure 20: Histochemical standard stains. *74*
Figure 21: Nile blue staining for melanin. *75*
Figure 22: Fontana-Masson staining for melanin. *77*
Figure 23: Fontana-Masson benchmark. *78*
Figure 24: Reflection signal of fluorophore-stained, resin embedded skin samples. *82*
Figure 25: Histological benchmark of the reflection signal. *83*
Figure 26: TEM images of melanosomes and melanosome clusters. *84*
Figure 27: Epidermal melanosomes distribution in ethnic skin types. *89*
Figure 28: Epidermal melanosome distribution in Asian phenotypes. *90*
Figure 29: Epidermal melanosome distribution in Fitzpatrick's skin phototypes I and VI. *91*
Figure 30: Epidermal melanosome distribution in lentigo senilis, lesional and perilesional. *93*
Figure 31: Melanosome distribution in SC and SB of different skin types. *94*
Figure 32: Epidermal distribution of melanin particles in ethnic skin types and phototypes I and VI. *96*
Figure 33: Epidermal distribution of melanin particles in lentigo senilis. *97*
Figure 34: TEM mosaic used for benchmarking the manual analysis. *98*
Figure 35: Benchmark test of the manual analysis of melanosome and melanin particle numbers. *99*
Figure 36: Annotated TEM images illustrating the detection of melanosomes by ZETA. *100*
Figure 37: Comparison of automated and manual analysis. *104*
Figure 38: Data of the automated and manual analysis of a perilesional sample (A75-5). *105*
Figure 39: Eu- and pheomelanin content in Fitzpatrick's skin phototypes I -VI. *106*
Figure 40: Reflectance spectroscopy of Fitzpatrick's skin phototypes I-IV and VI. *107*

Figure 41: The epidermal melanin unit. *109*
Figure 42: Melanocyte location in the epidermis of skin phototype II and VI. *111*
Figure 43: Melanocyte density per millimetre BM and SG in Fitzpatrick's skin phototypes. *112*
Figure 44: Melanocyte location in lentigo senilis. *113*
Figure 45: Melanocyte density per millimetre BM and SG in lentigo senilis. *114*
Figure 46: Classification of senile lentigines and freckles according to the integration index. *115*
Figure 47: Histological overview of lesional and perilesional samples of senile lentigines. *116*
Figure 48: Histological overview of lesional and perilesional samples of freckles. *117*
Figure 49: Determination of the fringe integration index. *119*
Figure 50: Fringe integration index of the basement membrane of lentigo senilis and freckles. *120*
Figure 51: Basement membrane under keratinocytes and melanocytes in lentigo senilis. *121*
Figure 52: Macromelanosomes in lentigo senilis. *122*
Figure 53: Melanosome distribution in senile lentigines and freckles. *123*
Figure 54: Melanosome transfer observed in co-cultures of melanocytes and keratinocytes. *125*
Figure 55: Melanosomes within melanocytes and melanocyte dendrites. *127*
Figure 56 (left & right): Solitary melanosomes and melanosome clusters in keratinocytes of the lower epidermis. *129*
Figure 57: Melanosomes in the intercellular space. *130*
Figure 58: Interaction of melanocyte and keratinocyte. *132*
Figure 59: Fragmentation of Sepia melanin by hydrogen peroxide. *134*
Figure 60: SEC chromatogram of Sepia melanin degraded with H_2O_2. ..... *135*
Figure 61: SEC chromatogram of a suspension of human epidermis. *135*
Figure 62: Mass spectrum of the third fraction of the SEC-analysis. *137*
Figure 63: Light microscopic detection of the cerium precipitate demonstrating H_2O_2. ..... *139*
Figure 64: Electron microscopic detection of NADPH oxidase. *140*
Figure 65: Demonstration of cerium by EFTEM. *142*
Figure 66: Melanosome detection in SC poses a problem for the ZETA image analysis tool. *145*
Figure 67: Comparison of microscopic and chemical analysis of epidermal melanin content. *147*
Figure 68: Potential pathway for the degradation of eumelanin by hydrogen peroxide. *165*

LIST OF TABLES

*Table 1: Fitzpatrick's skin phototypes**..... 21
Table 2: Designated use of samples for this project...... 31
Table 3: Sample preparation and resulting microscopic applications...... 32
Table 4: Protocol for room temperature dehydration and embedding...... 38
Table 5: Protocol for freeze-substitution and low temperature embedding...... 40
Table 6: Protocol for Fontana-Masson silver staining...... 47
Table 7: Protocol for immunofluorescence assay...... 49
Table 8: Primary antibodies...... 50
Table 9: Secondary antibodies and nuclear stains...... 51
Table 10: Protocol for heavy metal staining of resin sections for TEM...... 52
Table 11: Protocol for the cytochemical demonstration of NADPH oxidase...... 54
Table 12: Staining results of all tested antibodies depending on the pre-treatment of the sample...... 67
Table 13: Antibody combinations for the description of melanocytes...... 68
Table 14: Analyses of melanin content and melanosome distribution..... 87
Table 15: Percentage of individual melanosomes in the epidermal layers of different skin types...... 95
Table 16: Melanin content in Fitzpatrick's skin phototypes I -VI and percentage of eu- and pheomelanin...... 107
Table 17: Percentage of individual melanosomes in the epidermal layers of lentigo senilis and freckles...... 123
Table 18: List of polymers, corresponding to the mass spectrum obtained from the third fraction of the SEC-analysis...... 138

ABBREVIATIONS AND UNITS

Units are applied according to the International System of Units (SI). Exceptions are listed.

2D	two-dimensional
3-AHP	3-amino-4-hydroxyphenylalanine
3D	three-dimensional
4-AHP	4-amino-3-hydroxyphenylalanine
α (antigen)	antibody directed against (antigen)
AHP	amino-hydroxyphenylalanine
approx.	approximately
Aqua bidest.	double distilled water
BSA	bovine serum albumin
BSA	bovine serum albumin
CLSM	confocal laser scanning microscopy
DAB	diaminobenzidine
DAB	diaminobenzidine
DHI	dihydroxyindole
DHICA	dihydroxyindole 2-carboxylic acid
DMEM	Dulbecco's modified Eagle medium
DMSO	dimethyl sulfoxide
DNA	deoxyribonucleic acid
DOPA	3,4-dihydroxyphenylalanine
DPI	diphenyleneiodonium chloride
EFTEM	energy-filtered transmission electron microscopy
EM	electron microscopy
ESI-MS	electrospray ionisation mass spectroscopy
eumel.	eumelanin
h	hour(s)
HAADF	high-angle annular dark field
HI	hydrogen iodide; hydriodic acid
HPLC	high performance liquid chromatography
IEM	immuno-electron microscopy (fixative)
IFA	immunofluorescence assay
IgG	immunoglobulin G
LM	light microscopy
lSSp	lower SSp
mel.	melanosomes
melc.	melanocyte(s)
min	minute(s)
NA	numerical aperture
NADPH	β-nicotinamide adenine dinucleotide 2' phosphate

PAR-2	protease-activated receptor 2
PBS	phosphate buffered saline
PDCA	pyrrole-2,3-dicarboxylic acid
PFA	paraformaldehyde
PFA	paraformaldehyde
pheomel.	pheomelanin
PTCA	pyrrole-2,3,5-tricarboxylic acid
resp.	respectively
ROI	region of interest
ROS	reactive oxygen species
rpm	revolutions per minute
SB	Stratum basale
SC	Stratum corneum
SEC	size exclusion chromatography
SEM	scanning electron microscopy
SG	Stratum granulosum
SSp	Stratum spinosum
SEM	scanning electron microscopy
STEM	scanning transmission electron microscopy
T	temperature
TEM	transmission electron microscopy
temp.	temperature
TFA	trifluoroacetic acid
TGN	trans-Golgi network
TRP-1	tyrosinase-related protein 1
TRP-2	tyrosinase-related protein 2 or dopachrome tautomerase
uSSp	upper SSp
UV	ultra violet (light)

A INTRODUCTION

The concept of beauty has been, is and will ever be as variable as culture and emotions of mankind. Notions of what is considered beautiful are countless and prone to change with fashion, even in terms of skin complexion. Until the dawn of the 20th century, a pale complexion was considered beautiful and noble, a sign of prosperity. Today it is regarded as unhealthy and unattractive, and wealth nowadays is demonstrated by extensive outdoor activities – a "healthy tan" providing the proof. A year-round tan is highly valuable, and is purchased at any cost (Rawe, 2006). However, this applies to Western Europe and North America. But throughout Asia, dark skin tones are considered akin to evil, and sophisticated cosmetic treatments and even surgery to become "fair and handsome" become increasingly popular. Skin colour in Asia can even nowadays be used as an argument for discrimination and exclusion of dark-skinned individuals from certain parts of society. This constitutes more than just a problem of fashion or beauty, but endangers freedom and constitutional rights of individuals (Perry, 2005).

In addition one aspect of skin colour is universally disliked: uneven skin tone. Local changes in skin colour, caused by loss (hypopigmentation) or overproduction of skin pigment (hyperpigmentation) are unpopular, irrespective of otherwise differing beau ideals. Age spots, freckles, melasma or vitiligo are just a few examples of dyspigmentations regarded as problematic worldwide.

Accountable for the diversity of skin tones is the pigment melanin, the name being derived from the Greek word "melas", meaning dark or black (Nordlund *et al.*, 1998). Melanin is a complex biopolymer, comprising of two subtypes: eumelanin and pheomelanin, but the exact chemical structure remains yet unknown. Eumelanin is of a dark blackish-brown colour, while pheomelanin is described as yellow or reddish. Apart from the skin, melanin is found in the hair and the pigmented epithelium underlying the retina of the eye and several other tissues. Melanin occurs also in animals, plants and fungi. It is ascribed several functions, including camouflage, free radical scavenging and neutralizing of bacterial toxins, but the most common one is the protection from harmful and mutagenic UV light (Mackintosh, 2001).

In the skin, melanin is synthesized by specialized cells of the basal layer of the epidermis, the melanocytes. Within the melanocyte, the melanin synthesis is enclosed in organelles, the so-called melanosomes. Melanocytes are dendritic cells, their extensions reaching between the surrounding cells of the epidermis (keratinocytes) to transfer the melanosomes. The exact mechanism of this transfer remains yet unknown, but several hypotheses concerning uptake via phagocytosis are being discussed (Van Den Bossche *et al.*, 2006). The transferred melanosomes are dispersed in the cytoplasm of the keratinocytes, locating to the apical pole of the nucleus, to protect it from UV light. As the amount of melanin present in the keratinocytes decreases toward the upper layers of the epidermis, it is assumed that the melanin is degraded somehow, although this process is yet not elucidated. Due to the exceptional complexity of the biopolymer, it yields only to strong oxidizing agents, most of which are incompatible with cellular vitality. The only reagent qualified for intracellular localisation and melanin degradation is hydrogen peroxide which can arise within keratinocytes via NADPH oxidase (Borovanský and Elleder, 2003).

The skin colour is assumed to depend on the type and amount of melanin synthesized by the melanocytes, as well as by the distribution and degradation of the melanin in the epidermis. Detailed investigation of the distribution of melanosomes in the epidermis and within keratinocytes in skin of different phenotypes of normal skin and hyperpigmented skin like age spots (*lentigo senilis*) could provide basic knowledge to understand the determining factors of visual perception of skin colour as well as insights into development and triggering factors of hyperpigmentation. Understanding the mechanism by which melanosomes are transferred from melanocytes to keratinocytes and the melanin degradation pathway would explain the melanosome distribution patterns in keratinocytes and throughout the epidermis.

A thorough understanding of these processes is imperative for the identification of potential targets for cosmetic influence on skin pigmentation. Effective tanning and whitening agents are required, which produce a natural skin tone without harmful side effects. Aimed enhancement or inhibition of the proliferation and subsequent transfer of melanosomes, as well as the ensuing degradation process would produce the desired tanning or whitening effects.

B SKIN PIGMENTATION AND ITS ANALYSIS

I The Skin and Its Diversity in Colour

The skin (*Integumentum commune*) is often referred to as "the largest organ of the human body". For the average adult human, the skin has a surface area of 1.5-1.8 m². It is 1.5-4 mm thick and accounts for about 15 % of the body weight (Matoltsy, 1986b; Haake and Holbrook, 1999). The skin constitutes a barrier against water loss of the body and impacts of the environment, e.g. providing protection against pathogens or UV light. Further functions are insulation and temperature regulation, sensation and vitamin D and B synthesis (Leonhardt, 1987; Montagna *et al.*, 1992).

I.1 Physiology of the Skin

The skin comprises of three primary layers: the epidermis, the dermis and the hypodermis (see Figure 1). Skin appendages, like hair, sweat glands or nails, arise from the epidermis, but are located mainly in the dermal compartment, some even reach into the underlying hypodermis, an adipose tissue-rich subcutaneous region. The dermis is a connective tissue, comprising mainly of collagen and elastic fibres, providing elasticity and tensile strength, and thus protection from mechanical injury (Matoltsy, 1986a).

The epidermis is a stratified squamous epithelium that is continually renewed within approx. 28 days. It is approximately 0.4-1.5 mm in thickness. The epidermis can be further subdivided into layers of differentiation, so-called *strata* (beginning with the outermost layer): *Stratum corneum* (SB), *Stratum granulosum* (SG), *Stratum spinosum* (SSp), and *Stratum basale* (SB). The majority of epidermal cells are keratinocytes. Attached to the basement membrane are mitotically active keratinocytes of columnar shape, the so-called stem cells. Daughter cells are pushed up the *strata* by newly dividing cells, forming layers of progressively more differentiated cells. The cells of the SSp are polygonal in shape, with a round nucleus and an abundance of desmosomes (junctions contacting neighbouring cells). In the SG, the keratinocytes undergo a change, from metabolic cell to a finally differentiating cell, leading to

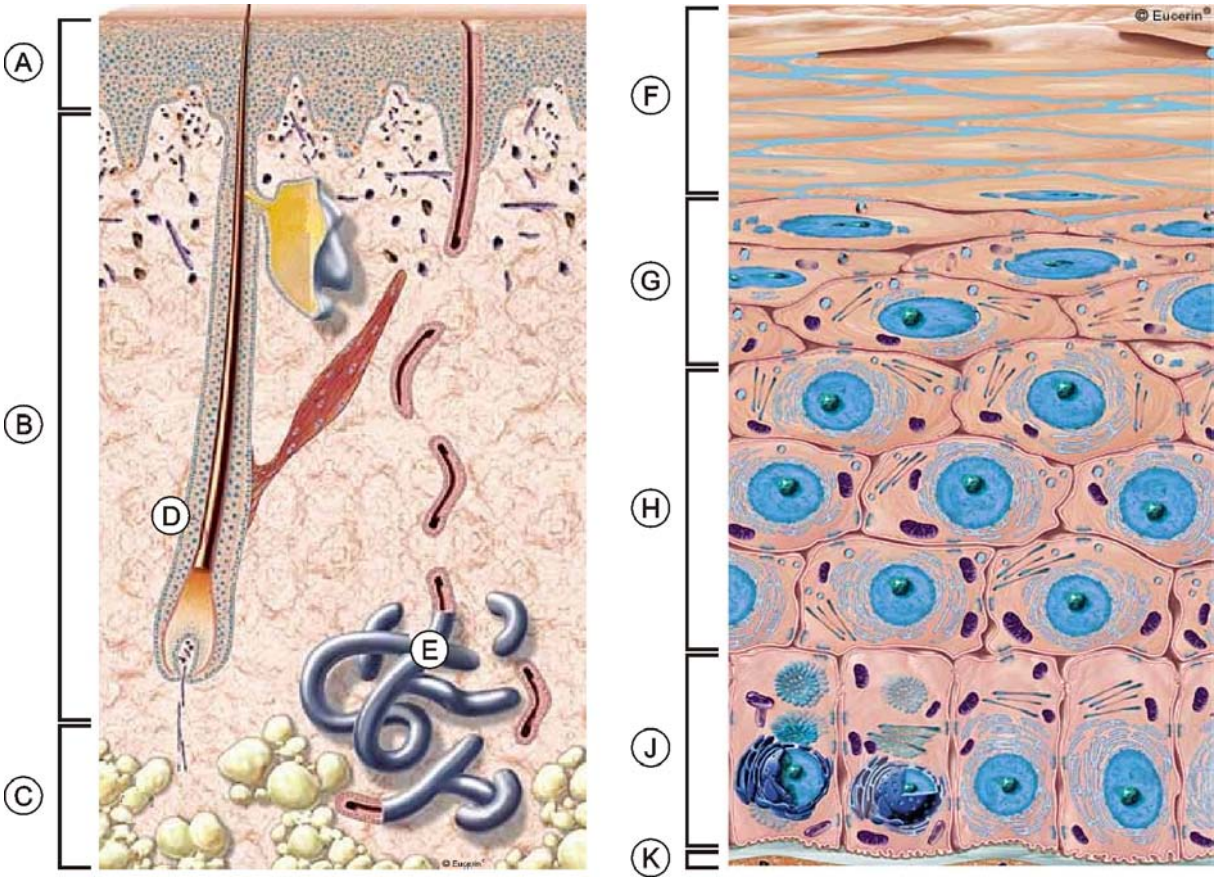

Figure 1: Layers of the skin. The skin consists of three layers: epidermis (A), dermis (B), and hypodermis (C). Skin appendages like hairs (D) and sweat glands (E) are located in the dermis. The epidermis is a stratified squamous epithelium, that is subdivided into epidermal layers: the *Stratum corneum* (F), the *Stratum granulosum* (G), the *Stratum spinosum* (H) and the *Stratum basale* (J). The epidermis is connected to the dermis by the basement membrane (K). Modified from www.eucerin.de.

a controlled process of keratinisation and ultimately to cell death. These cell finally form a sealing barrier against water loss. This process and structural reorganization of the organelles and the nucleus gives the cells a granulous and flattened appearance. The cells of the SC, the corneocytes, are flat, polyhedral, dead horny cells, highly interleaved to form a protective barrier against mechanical injury and dehydration. Eventually, these cells are chipped off (desquamation). The entire process of differentiation from basal keratinocytes to corneocytes and desquamation takes approx. 28 days (Bloch *et al.*, 1927; Haake and Holbrook, 1999).

Interlaced among the keratinocytes are several other cell types, including the pigment producing melanocytes, Langerhans' cells, that are part of the immune defence of the skin, and Merkel cells, that are associated with the sense of touch (Leonhardt, 1987; Montagna *et al.*, 1992).

I.2 Constitutive Skin Colour: The Pigment Melanin

Human skin colour features an abundance of phenotypes, ranging from almost black to pinkish white. In general, skin colour correlates with the geographical position – mainly the latitude – and the resulting exposure to the sun. However, globalisation and cultural exchange gave rise to a broad spectrum of skin colour shades. These are further diversified by a multitude of exogenous and endogenous influences, such as solar radiation, hormones or other environmental factors. The genetically determined level of pigmentation, excluding all other influences, is referred to as *constitutive skin colour*. An induced level of pigmentation, on the other hand, is termed *facultative skin colour* (Kochevar *et al.*, 1999; Astner and Anderson, 2004).

I.2.1 Formation of Eumelanin and Pheomelanin

Two major biological pigments account for the skin colour: haemoglobin and melanin. Oxygenated haemoglobin in the micro-capillary network of the dermis provides the skin with a reddish hue, the intensity varying with the blood flow. Melanin, on the other hand, is synthesized in the epidermis and remains in the epidermal cells. Short-time variations are not possible, although exogenous and endogenous factors can induce changes in the level of pigmentation within several days (Jimbow *et al.*, 1986; Aroca *et al.*, 1993; Yamaguchi *et al.*, 2006).
Two main classes of melanins are predominant in the human skin, accounting for different colour shades. The dark brown-to-black *eumelanin* is insoluble in acid and alkali, and yields only to strong oxidizing agents, such as hydrogen peroxide, although the process is slow (S. Ito and Jimbow, 1983; Napolitano et al., 2000). On the other hand, the polymer is a powerful reducing agent (Churukian, 2002). Eumelanin consists primarily of two types of polymers (Figure 2), 5,6-dihydroxyindole (DHI) and 5,6-dihydroxyindole-2-carboxylic acid (DHICA),

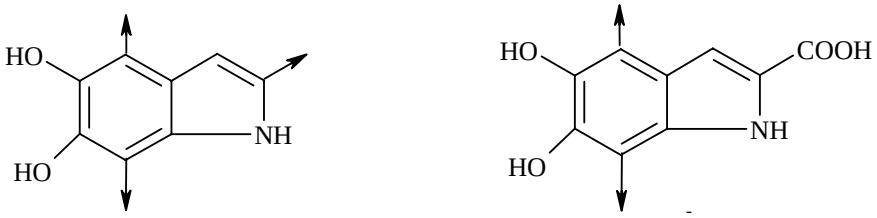

Figure 2:Monomers of eumelanin. Left: 5,6-dihydroxyindole (DHI). Right: 5,6-dihydroxyindole-2-carboxylic acid (DHICA). It is assumed, that these monomers are linked via carbon-carbon bonds (indicated by arrows), or by hydrogen bonds and π-stacking to form the eumelanin-polymer.

that are linked via carbon-carbon bonds, hydrogen bonds or π-stacking to form the eumelanin-polymer (Clancy and Simon, 2001; Wakamatsu and Ito, 2002). Eumelanin has a general absorption in the range of 200-2400 nm, without any characteristic maxima, and only the infrared spectra in the rage of 2.5-10 µm show absorption maxima at 3 µm and 6 µm (Jimbow *et al.*, 1999).

The second class of melanins is termed *pheomelanin*, a yellow-to-reddish-brown pigment. It is formed by a modification of the eumelanin synthesis pathway in the presence of cysteine, accounting for the high content of sulphur (9-12 %) and nitrogen (8-11 %). Eumelanin, on the other hand, contains 6-9 % nitrogen, but no sulphur (0-1 %). And unlike eumelanin, pheomelanin shows solubility in alkali solutions (S. Ito and Jimbow, 1983). The pheomelanin-polymer again comprises two major monomers: 5-S-benzothiazinylalanine and 2-S-benzothiazinylalanine (Figure 3) that are interlinked in the same way as the eumelanin-monomers.

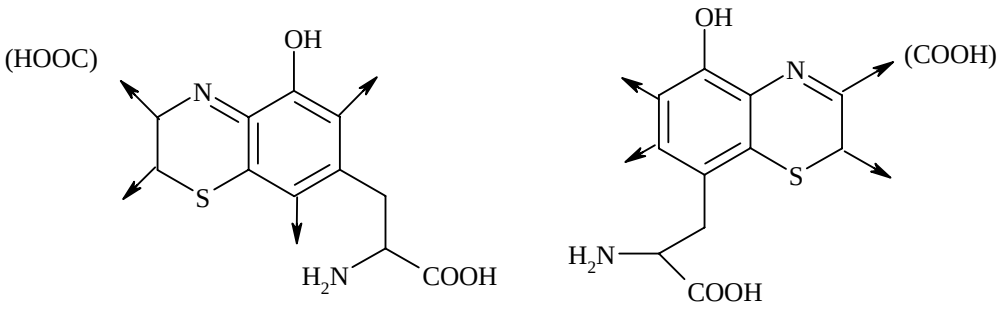

Figure 3: Monomers of pheomelanin. Left: 5-S-benzothiazinylalanine. Right: 2-S-benzothiazinylalanine. It is assumed, that these monomers are linked via carbon-carbon bonds (indicated by arrows), or by hydrogen bonds and π-stacking to form the pheomelanin-polymer.

Both types of melanin arise from tyrosine, that is hydroxylated to 3,4-dihydroxyphenylalanine (DOPA), that subsequently oxidized to dopaquinone. In the presence of sulphydryl compounds, e.g. cysteine or glutathione, dopaquinone is converted to cysteinyldopas that give rise to pheomelanin through the formation of benzothiazine metabolites.

However, if no cysteine is present, dopaquinone is converted to dopachrome, that spontaneously decarboxylates to produce 5,6-dihydroxyindole (DHI). DHI is rapidly oxidized by tyrosinase to from indole-5,6-quinone, which is then converted to the blackish (DHI-derived) eumelanin. Alternatively, dopachrome can be rearranged to form 5,6-dihydroxyindole-2-carboxylic acid (DHICA) with the enzymatic assistance of tyrosinase- related protein 2 (TRP-2),

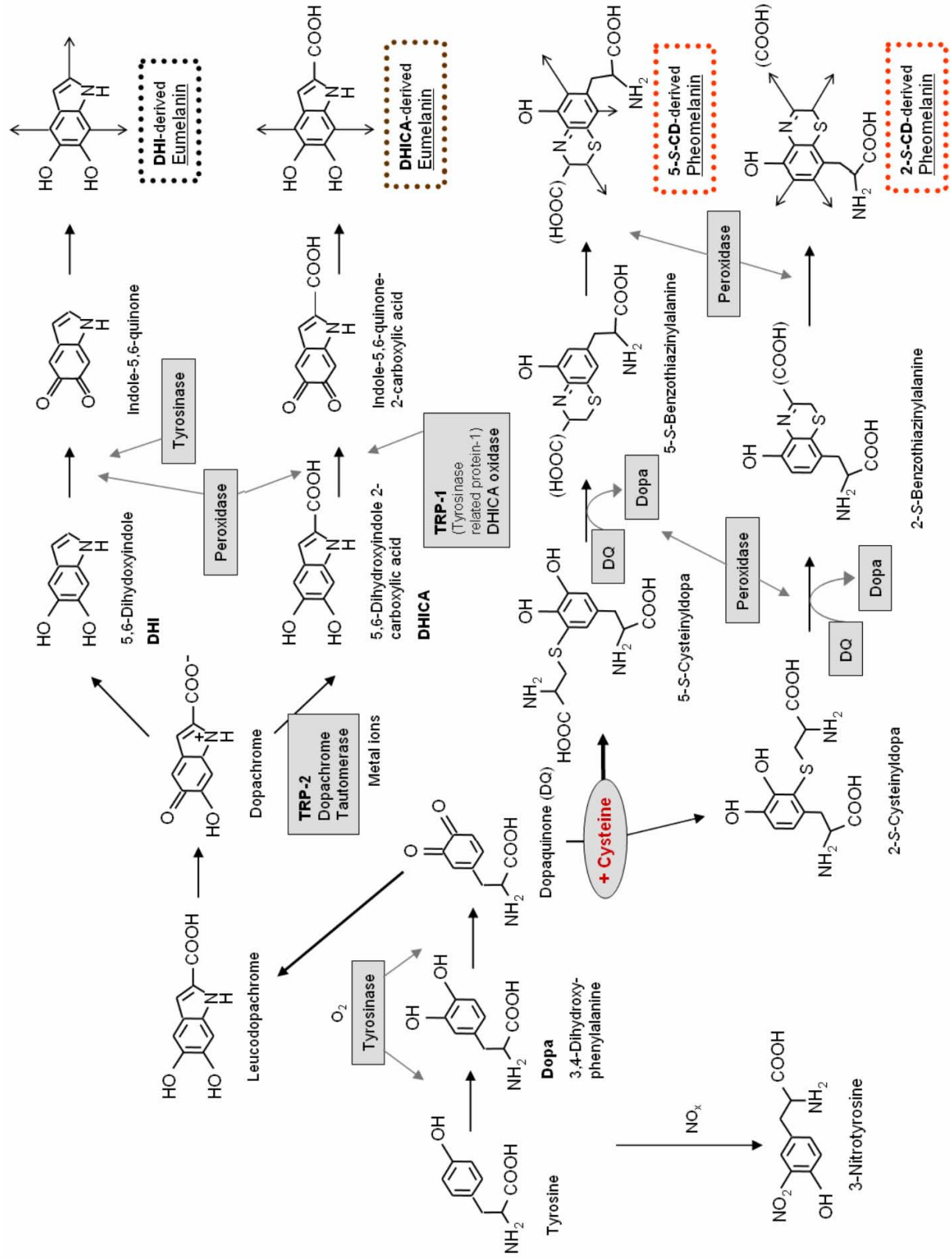

Figure 4: Pathway of melanin synthesis. Eumelanin and pheomelanin share a biogenetic synthesis pathway (arising from tyrosine), in which dopaquinone forms a crucial intermediate. Dopaquinone is converted to dopachrome, which is autooxidised to DHI and further converted to form eumelanin. However, in the presence of TRP-2, DHICA and the derived eumelanin polymer is formed instead. But, if dopaquinone encounters cysteine, pheomelanin is synthesized via cysteinyldopa intermediates.

also called dopachrome tautomerase. DHICA autooxidises to give rise to the dark brown-to black (DHICA-derived) eumelanin (Prota, 1980; Jimbow *et al.*, 1986; Nordlund *et al.*, 1998; Bolognia and Orlow, 2003). The entire pathway of the melanin synthesis is summarized in Figure 4.

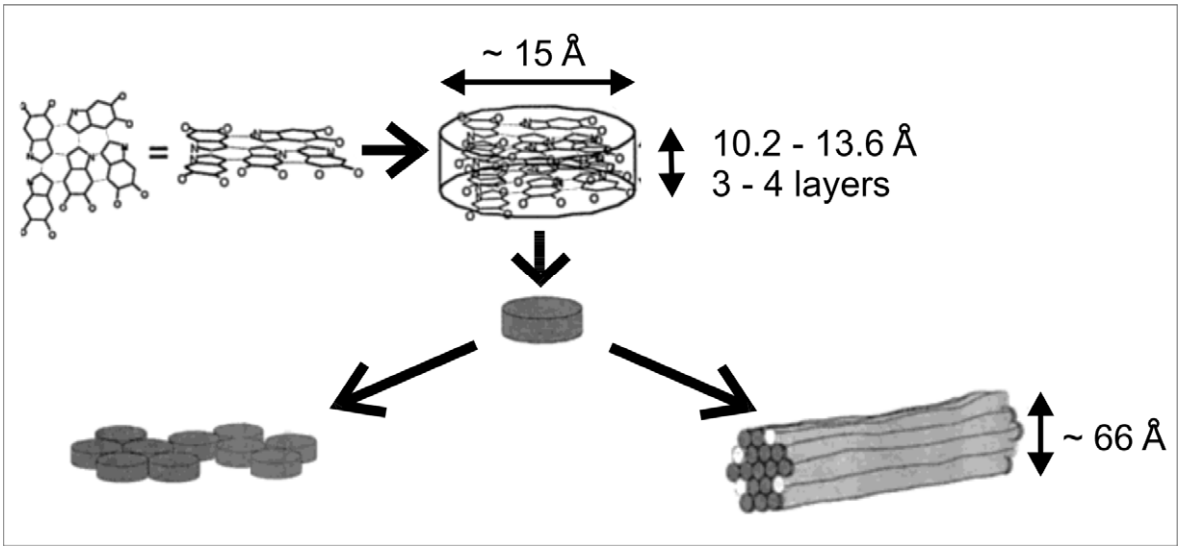

Figure 5: Potential mechanism of assembly of eumelanin polymers. The basic molecular unit is assumed to be a planar oligomer consisting of DHI and DHICA polymers. Three or four of these planar oligomers are supposed to assemble through π-stacking and side on interactions, to from a puck-like structure, that further assembles either sideways in a planar fashion (left) or are stacked one upon the other, forming filament-like shapes. These filaments could then aggregate into bundles (right). Adapted from Clancy and Simon (2001).

It is assumed, that the eumelanin and pheomelanin monomers are linked via carbon-carbon bonds, or by hydrogen bonds and π-stacking to form the respective polymer. The structural organisation of synthetic melanins is relatively well characterised (Cheng *et al.*, 1994a; Cheng *et al.*, 1994b; Zajac *et al.*, 1994). However, the exact composition and molecular structure of natural melanin remains largely unknown (Liu and Simon, 2003; Cheun, 2004). Using isolated eumelanin from the ink sacs of the cuttlefish *Sepia officinalis*, which is commonly used as a model for human eumelanin, Clancy and Simon (2001) proposed a possible structural organization of the biopolymer (see Figure 5). They hypothesized a planer oligomer consisting of 5 units of DHI and/or DHICA that assemble through π-stacking and side-on interactions. Three or four of these planar oligomers are π-stacked to form a flattened cylinder or puck-like structure, that is then further assembled to planer agglomerates or stacked vertically to form filaments, that could then further assemble into bundles.

I.2.2 The Pigment Producing Cells: Melanocytes

Melanocytes are dendritic cells that derive from the neural crest and migrate into the skin during the embryonic period. They are located in the basal layer of the epidermis. Their dendrites contact keratinocytes not only in the *Stratum basale*, but as high up as the mid *Stratum spinosum*. Each melanocyte is reported to associate with 30-40 keratinocytes and supply them with pigment. This functional symbiosis is called *epidermal melanin unit*. Melanocytes do not proliferate *in situ* and the quantity of functioning melanocytes within the epidermis is more or less constant, but gradually decreased with age (Nordlund *et al.*, 1998; Haake and Holbrook, 1999; Jimbow *et al.*, 1999).

Microscopically, melanocytes can be distinguished from keratinocytes by their pale-staining cytoplasm, devoid of keratin filaments, the lack of desmosomal junctions with neighbouring keratinocytes, an oval nucleus and the presence of the characteristic pigment granules. These pigment granules – *melanosomes* – are specialized, lysosome-related organelles that harbour the synthesis of melanin (Ackerman *et al.*, 1997; Haake and Holbrook, 1999; Bolognia and Orlow, 2003). Pigment production is triggered and regulated by a multitude of factors, UV irradiation ranking foremost, but it can also be influenced by hormones, such as melanocytes-stimulating hormone and β-endorphin, and other extrinsic factors (Kauser *et al.*, 2003). And although the production of melanin is confined to the melanocytes, it is the keratinocytes that provide the stimulating factors and determine the ratio of eumelanin and pheomelanin in the synthesized pigment (Duval *et al.*, 2001; Duval *et al.*, 2002).

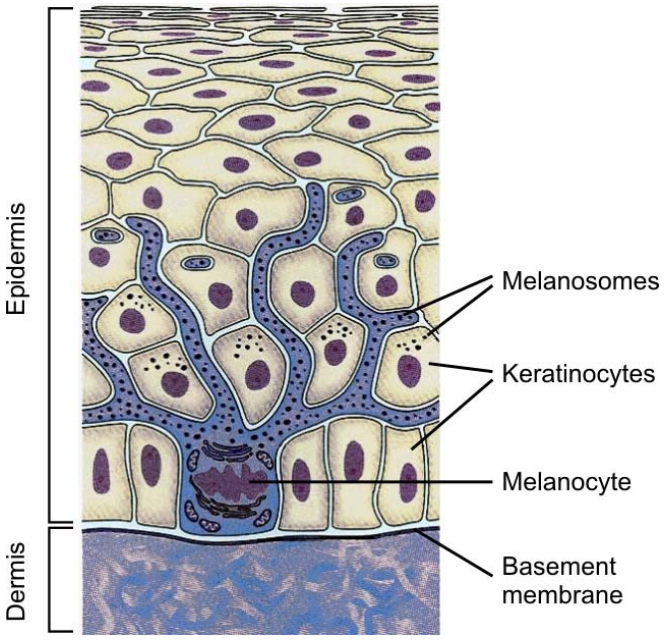

Figure 6: Location of melanocytes in the epidermis. Melanocytes are pigment producing cells that derive from the neural crest and are situated in the basal layer of the epidermis. Their dendritic processes contact keratinocytes from the SB to the mid SSp, and supply them with melanosomes – pigment containing granules (featured as black dots). One melanocyte (displayed in blue) and 30 – 40 keratinocytes are associated in a functional symbiosis, called epidermal melanin unit.

I.2.3 Developmental stages of Melanosomes

Melanosomes represent a distinct lysosome-related organelle, discernible from endosomes and lysosomes, although they share several characteristics with lysosomes, such as the presence of lysosomal proteins and a low luminal pH, which are also required for the synthesis of melanin. The melanin precursors and intermediate products of the biosynthesis, i.e. phenols, quinones and indoles, are highly oxidizing reactants that endanger other cellular components of the melanocyte. The melanin synthesis is therefore sequestered to melanosomes, that render reaction and reaction products harmless (Jimbow *et al.*, 1986; Raposo *et al.*, 2001; Raposo and Marks, 2002; Bolognia and Orlow, 2003).

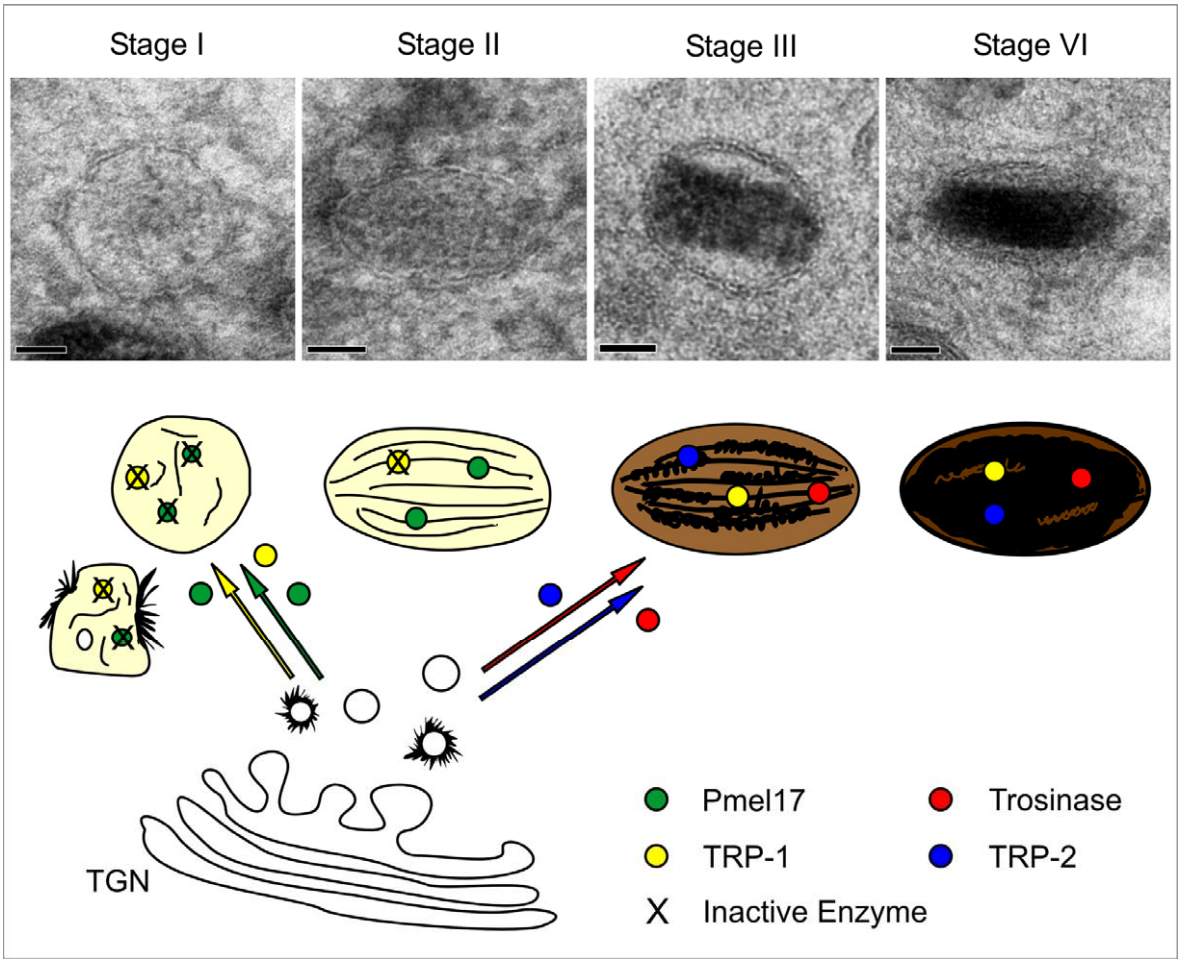

Figure 7: Development of eumelanosomes. Premelanosomes arise from endosomal organelles, that fuse with structural proteins derived from the endoplasmatic reticulum. Melanosomal enzymes are assembled in the TGN and are trafficked toward the melanosomes by early endocytic organelles. Stage I premelanosomes are poorly organized, spherical structures. Pmel17 and TRP-1 are already present at this stage, but remain inactive. In stage II, the characteristic oval, striated structure becomes apparent. Pmel17 is found active, driving the formation of the striations. Tyrosinase activity, starting the process of melanin synthesis, is first detected in stage III, when melanisation of the preformed intraluminal striations is observed. The mature eumelanosome (stage IV) is fully melanised and the intraluminal structure is masked completely.

TGN = trans Golgi network; TRP = Tyrosinase-related protein

Melanosome biogenesis covers four developmental stages, which differ slightly depending on the type of melanin synthesized. In the initial stage, both eumelanosomes and pheomelanosomes are more or less spherical vacuoles arising from endosomal organelles that contain poorly organized structural proteins, presumably assembled in the endoplasmatic reticulum (Figure 7). Melanogenic enzymes, such as Pmel17, tyrosinase and tyrosinase-related protein 1 (TRP-1; see Figure 4) are delivered from the trans-Golgi network (TGN).

Pmel17 and TRP-1 fuse with the preformed *stage I* premelanosomes, but remain inactive until later stages of melanosome development (Kushimoto *et al.*, 2001). In *stage II*, eumelanosomes become elliptical and the internal matrix condenses to form lamellar striations, running the length of the organelle in an organized array. These striations are non-membranous fibres and their formation is driven by Pmel17, which is active predominantly during this stage (Raposo *et al.*, 2002). Tyrosinase, TRP-1 and TRP-2 activity are first detected in *stage III* and melanin synthesis becomes apparent. Regular, periodic melanin depositions are observed along the striations. The intraluminal structure is gradually obscured and the organelle is filled with pigment, until – in *stage IV* – the melanosomes appears as a highly melanised, electron-dense structure (Berson *et al.*, 2001; Raposo and Marks, 2002). Pheomelanosomes on the other hand, remain spherical, less well organized structures, without lamellar matrix. Mature pheomelanosomes appear less dense and electron-lucent (Jimbow *et al.*, 1986).

I.2.4 Transfer of Melanosomes to Keratinocytes

As the melanosome mature, they are transported toward the tip of the dendrites of the melanocyte (Figure 8). The anterograde transport toward the plus end of the microtubule is facilitated by motor proteins of the kinesin superfamily (Hara *et al.*, 2000; Vancoillie *et al.*, 2000). Pure microtubule-dependent melanosomes transport is bidirectional, and the retrograde movement toward the minus ends of the microtubules, which are situated in the cell centre, is established via cytoplasmic dynein, that traps its cargo via dynactin. In the dendrite tip, the melanosomes are tethered to actin filaments, to prevent their retrograde transport and enable transfer to neighbouring keratinocytes. This is assisted by Rab27a, which recruits myosin Va, an actin-based motor, to the melanosomes via melanophilin, and thus enables the peripheral capture of melanosomes within the dendrites (Nordlund *et al.*, 1998; Wu *et al.*, 2001; Seabra and Barral, 2004)

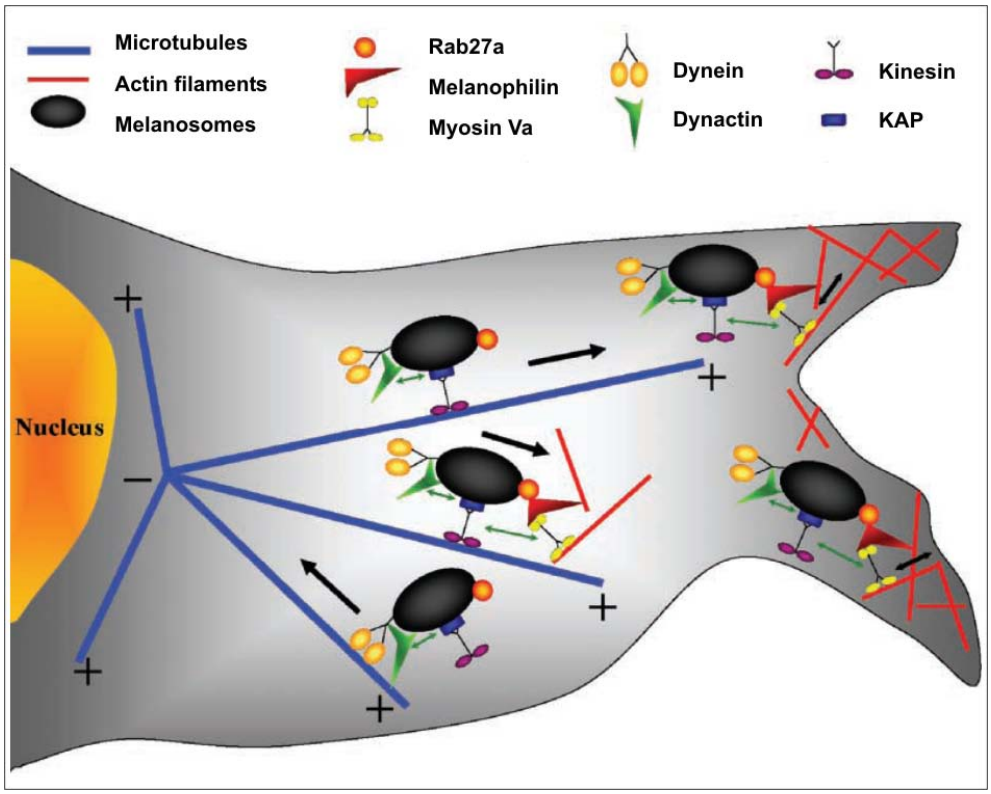

Figure 8: Mechanism of melanosome transport into the dendrites of the melanocyte. Within the melanocytes, melanosomes are transported along microtubules. Movement toward the plus end of the microtubule, which is situated in the tip of the dendrite is mediated by kinesin. The retrograde movement is powered by dynein. In the dendrite tips, the melanosomes are captured by a complex formed by Rab27a, melanophilin and myosin Va, and bound to present actin filaments. From Seabra and Barral (2004).

How the actual transfer from melanocyte to keratinocyte is accomplished is jet unknown. However, four hypotheses have emerged, each probable and confirmed by the observations of the respective investigators (Figure 9): (A) cytophagocytosis, (B) exocytosis of melanosomes into the intercellular space, followed by endocytosis by the recipient keratinocyte, (C) direct inoculation, enabled by membrane fusion of both cells, and (D) transfer via membrane vesicles pinched off from the melanocyte (Yamamoto and Bhawan, 1994; Nordlund *et al.*, 1998).

Cytophagocytosis involves the cellular engulfment of any particle larger than 0.5 µm in diameter. The phagocytic nature of keratinocytes has been described *in vitro* and *in vivo* (Blois, 1968; Potter and Medenica, 1968). In the case of melanosome transfer, a part of an intact melanocyte, namely the dendrite tip, would be engulfed and eventually pinched off by a keratinocyte. This process would result in intra-keratinocyte vesicles containing one or several melanosomes, the melanosomal membranes intact, and surrounded by two membranes, the outer one arising from the keratinocyte and the inner membrane derived from the melano-

cyte dendrite. Okazaki *et al.* (1976) described the transfer mechanism as follows: in the initial stage, the dendritic process of the melanocyte penetrates into the keratinocyte and is enfolded with a cell membrane, followed by squeezing and pinching off of the dendrite. While the resulting pouch gradually moves toward the nucleus of the keratinocyte, the inner membrane and the melanosome membranes are digested, leaving a single membrane surrounding several melanosomes. These are then released into the cytoplasm in groups – enveloped in membrane fragments, accounting for melanosome clusters – and singles (Mottaz and Zelickson, 1967; Klaus, 1969a; Ackerman *et al.*, 1997).

A second possible pathway for melanosome transfer was described by Swift (1964) and Yamamoto and Bhawan (1994). They observed "naked melanin" – melanosomes that were

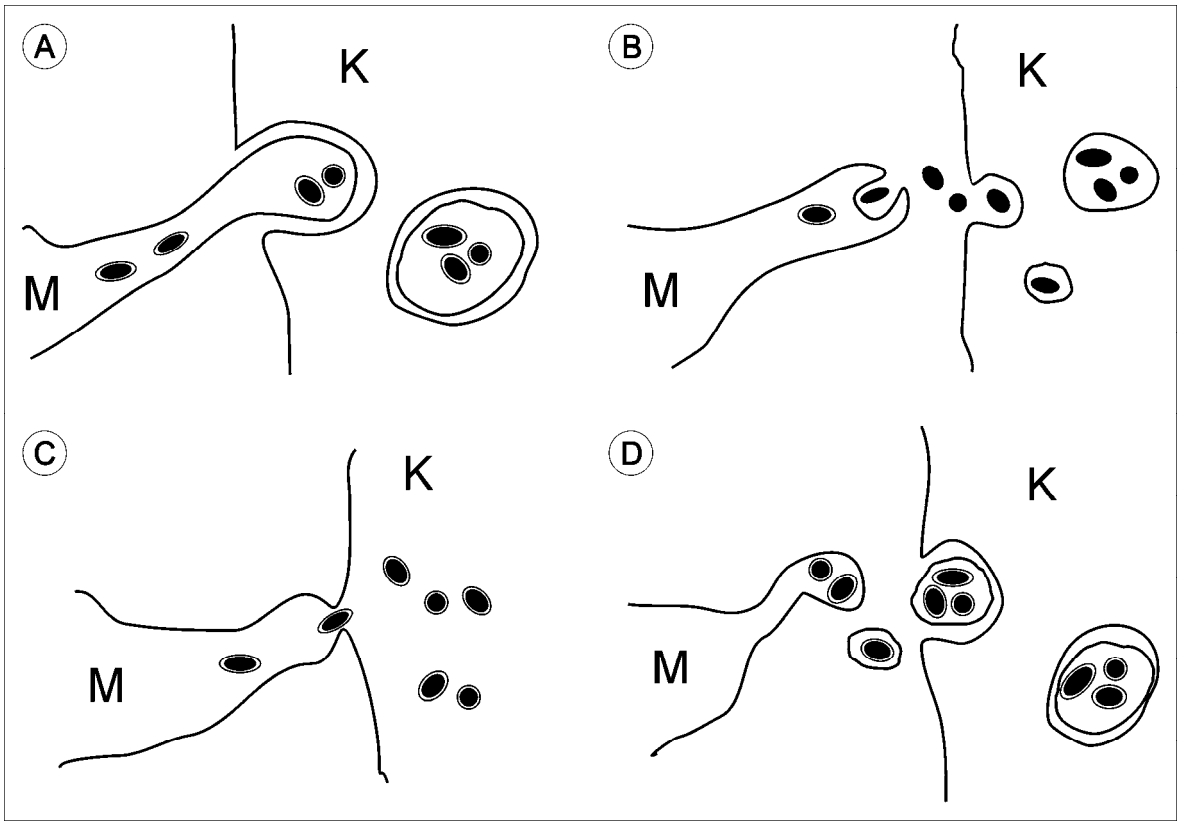

Figure 9: Four possible mechanisms for melanosome transfer to keratinocytes. (A) Cytophagocytosis: the melanocyte dendrite tip containing melanosomes is enfolded and pinched off by the keratinocyte. Inside the keratinocyte, the melanosomes are contained in a vesicle surrounded by two membranes, the inner one derived from the melanocyte, the outer membrane deriving from the keratinocyte. (B) Exocytosis of melanosomes into the intercellular space, followed by endocytosis by the keratinocyte. In the intercellular space, the melanosomes are devoid of surrounding membranes, while within the keratinocyte one or several melanosomes are enveloped by one membrane, derived from the keratinocyte. (C) Membrane fusion of melanocyte and keratinocyte: the melanosomes are transferred directly and are distributed individually within the keratinocyte. (D) Shedding of melanosome containing vesicles by the melanocyte, which are internalized by the keratinocyte via endocytosis. In the intracellular space, the melanosomes are surrounded by a single membrane, while within the keratinocyte two membranes (one from the melanocyte, one from the keratinocyte) are present.

M = melanocyte; K = keratinocyte; the black line represents a bilayer lipid membrane

not surrounded by a membrane or part of a dendrite – in the intercellular space, and hypothesized *exocytosis* of melanosomes by the melanocytes, resulting in extracellular melanosomes, and ensuing *phagocytosis* of the released melanosomes by the adjacent keratinocytes. In this case, the melanosome membrane would fuse with the plasma membrane of the melanocyte dendrite during the exocytosis. The extracellular melanosomes would be without enveloping membrane, and within the keratinocyte, "naked" single melanosomes or melanosome aggregations would be surrounded by one membrane, derived from the keratinocyte. It has been demonstrated *in vitro*, that melanocytes discharge melanin into the extracellular space. Electron microscopic investigation showed the discharged melanosomes was not surrounded with membranes, which was taken as proof for exocytosis (Virador *et al.*, 2002; Van Den Bossche *et al.*, 2006).

A third possible transfer mechanism involves *membrane fusion* of melanocyte and keratinocyte, resulting in a channel that connects the cytoplasms of both cells and enables direct transmission of melanosomes. Filopodia were implicated to act as means of contact, creating a tubular structure, 50 – 200 nm in diameter, through that melanosomes are transported. In this case, the melanosomal membranes would remain intact and the melanosomes would be distributed individually within the cytoplasm of the keratinocytes. The existence of melanosome clusters, however, would not be explained (Scott *et al.*, 2002).

A fourth option, *transfer via membrane vesicles*, is generally not considered as probable transfer mechanism, although is has been demonstrated that sections of membrane can be transferred from cell to cell. Detaching of melanosome containing membrane vesicles from the melanocyte dendrite, followed again by phagocytosis, would lead to membrane-surrounded melanosomes observable in the intercellular space and melanosome aggregates enveloped by a double membrane within keratinocytes (Van Den Bossche *et al.*, 2006).

Definite proof for any of the described transfer pathways is still lacking, and speculations arise, whether melanosome transfer *in vivo* may involve more than one – if not all – of the described mechanisms. In any case, phagocytosis seems to be a necessary step, a hypothesis supported by the presence of the protease-activated receptor 2 (PAR-2) in keratinocytes. PAR-2 is given a leading role in the receptor-mediated phagocytosis, and stimulation of this receptor increases both, the phagocytosis rate of keratinocytes, and melanosome transfer *in vitro* as well as *in vivo* (Seiberg *et al.*, 2000a; Scott *et al.*, 2001; Scott *et al.*, 2003).

I.2.5 Melanosome Distribution in Keratinocytes and Throughout the Epidermis

After transfer to the keratinocyte, the melanosomes are assembled predominantly to the apical pole of the nucleus, facilitated again by microtubule transport. This supranuclear melanin cap effectively absorbs and scatters incident UV light, providing protection against mutagenic damage (Boissy, 2003; Byers *et al.*, 2003; Yamashita *et al.*, 2005; Van Den Bossche *et al.*, 2006). The structural organisation of melanosomes within the keratinocytes varies according to skin type. In dark skin of Fitzpatrick's skin phototypes V and VI, melanosomes measure approximately 100 – 250 nm lengthwise and up to 100 nm across, and are maintained as individual organelles throughout the cytoplasm. Lighter skin types usually exhibit smaller melanosomes (50 – 150 nm along, 50 – 80 nm across), the oval shape being more pronounced than in dark skin. A characteristic feature of light skin types (Fitzpatrick's skin types I and II), is the aggregation of melanosomes into clusters of 2-10 organelles. Skin of phototypes III and

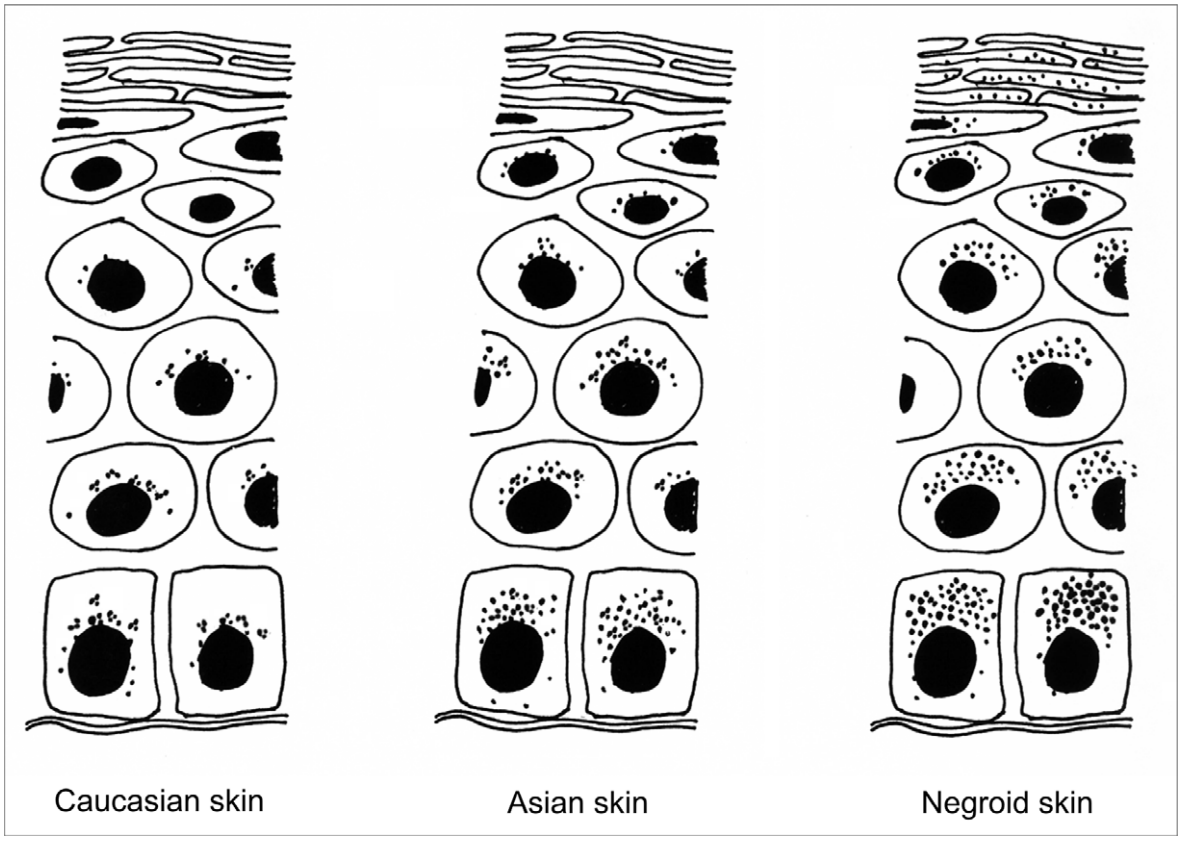

Figure 10: Melanosome distribution patterns in different ethnic skin types. Independently of the skin type, the largest amount of melanosomes is observed in the SB, and number decrease toward the skin surface. In skin phototypes I to III, i.e. Caucasian skin, melanosomes are predominantly aggregated into clusters, and disappear until the mid SSp. In skin types IV and V, i.e. Asian skin, melanosomes are visible until the SG, while they are even present in the surface corneocytes in very dark skin (Negroid skin).

IV, and sometimes type V, present a combination of both distribution patterns, i.e. individual and clustered melanosomes (Szabo *et al.*, 1969; Konrad and Wolff, 1973; Boissy, 2003).
In all skin types, the majority of melanosomes is observed in the basal keratinocytes, and melanosome number decrease toward the surface of the skin (Figure 10). But while in skin phototype I to III, i.e. Caucasian skin, the melanosomes disappear until the mid SSp, they are still present in the SG of skin types IV and V, i.e. Asian skin. In dark skin types, predominantly phototype VI, i.e. dark Asian and Negroid skin, melanosomes are observed throughout the entire epidermis and remain visible in the corneocytes. The amount of clustered melanosomes decreases toward the upper layers of the epidermis, and only individual melanosomes are observed from the SG upward (Lu *et al.*, 1996; Alaluf *et al.*, 2002a; Thong *et al.*, 2003)

I.3 Facultative Skin Colour: Tanning and Whitening

The constitutive level of pigmentation can be influenced by several factors, resulting mostly in an increase of pigmentation, i.e. tanning, but the reverse effect, so-called whitening of the skin, can also arise. Melanocytes respond to diverse extrinsic factors, including melanocyte-stimulating hormone, several growth factors and cytokines. But the most important stimulating factor is the sun, or more correctly UV irradiation (Virador *et al.*, 2002; Vincent J. Hearing, 2005a). On the one hand, UV irradiation induces tyrosinase activity, resulting in increased pigment production. On the other hand, it triggers transfer of pre-existing melanosomes to the neighbouring keratinocytes by inducing phagocytosis, via the activation of PAR-2 (Gilchrest *et al.*, 1979; Nordlund *et al.*, 1998; Seiberg *et al.*, 2000a). Additionally, pre-existing melanosomes are redistributed throughout the epidermis, shifting from the SB to the upper layers, thus temporarily reducing the melanosome content in the SB by approx. 10 % (Yoon *et al.*, 2003; Tadokoro *et al.*, 2005). Tanning effects can also be achieved cosmetically by artificial tanning agents. These usually contain dihydroxy acetone that merely stains the outer layers of the SC, but the melanin content of the skin remains unchanged (Matissek, 1984).
But tanning is no always desired: hyperpigmentation disorders and different beau ideals have created a need for cosmetic depigmenting agents. Depigmentation can be achieved by either (1) influencing the transcription and activity of melanosomal enzymes, (2) interfering with the transfer mechanism of melanosomes to the keratinocytes, or (3) affecting the melanin degrading system and the turnover of pigmented keratinocytes. Most of the available whitening compounds, including hydroquinone, kojic acid, hinokitiol, 25-hydroxycholesterol and many

more, target the melanosomal enzymes, thus reducing the melanin synthesis (Briganti *et al.*, 2003; Hall *et al.*, 2004; Choi *et al.*, 2006; Y. Ito *et al.*, 2006). A few other whitening agents, like niacinamide, act by reducing the transfer of melanosomes to keratinocytes (Hakozaki *et al.*, 2002; Greatens *et al.*, 2005). Exfoliants are also employed to achieve skin lighting, merely by facilitating the removal of pigmented keratinocytes at the skin surface (Briganti *et al.*, 2003).

I.4 Dysfunctions of Pigmentation – Age Spots and Freckles

The pigmentation of the skin shows variations between different areas of the body, depending on the average sun exposure of the respective body parts. E.g., the face and forearms generally appear more pigmented than non-exposed areas like the nates. Moreover, even small areas of the skin are not evenly pigmented, although macroscopically it may appear homogeneous. Extreme aberrations from the constitutive skin colour, sometimes accompanied by alterations of the skin texture, are frequent manifold. Acquired hyperpigmentation disorders include freckles, melasma, post-inflammatory hyperpigmentation, and senile *lentigo* – more commonly known as ages spots. Vitiligo represents a hypopigmentation disorder, characterized by the gradual loss or dysfunction of melanocytes in patches of the skin (Nordlund *et al.*, 1998; Kitamura *et al.*, 2004). Scars also appear paler than the surrounding skin, but here, melanocyte number and activity, and thus also the pigmentation are comparable to the unaffected skin. The cause for the paleness is rather due to vascular and optical factors of the thickened skin (Velangi and Rees, 2001).

A *lentigo* is defined as a small pigmented lesion, measuring 1-5 mm, which is surrounded by normal appearing skin. Macroscopically, many lesions are not distinguishable: e.g. freckles and age spots affect the same sun exposed areas of the body, i.e. the face, the back of the hands and forearms. Microscopically, both are characterized by increased pigmentation in the SB and a variable number of melanocytes, but several histopathological differences can be noted. Freckles commonly affect individuals with light skin, especially redheads, their colour varies and tends to deepen after sun exposure. Apart from the hyperpigmentation in the SB, the skin is not altered, and melanocyte number as well as development of the rete ridges is normal (Rahman and Bhawan, 1996).

Age spots, or *lentigo senilis*, on the other hand affect mostly middle-aged and elderly people. Their distribution is not even and their quantity slowly increases with time. Microscopically,

they exhibit massively hyperpigmented, elongated and club-shaped rete ridges, often branching out and fusing at the base. Melanocyte numbers are increased and the melanocytes concentrate along the rete ridges. Melanosomes are numerous, not only in the SB, but throughout the epidermis (Rahman and Bhawan, 1996; Virador *et al.*, 2001). Additionally, ultrastructural modifications are reported, including melanocytes sinking into the dermis below the keratinocytes, and perturbations of the dermal-epidermal junction. But up to date, the exact cause of this hyperpigmentation and the underlying molecular mechanisms are not fully understood (Noblesse *et al.*, 2006; Unver *et al.*, 2006).

I.5 The Unknown Fate of Melanin

Once transferred from the melanocytes, the melanosomes ascend with the recipient keratinocytes toward the skin surface and are removed from the epidermis during exfoliation with the corneocytes. It is assumed that the melanosomes remain within the keratinocytes. Export of melanosomes from the keratinocytes into the extracellular space or to other cells has – up to date – not been reported. But as melanosome numbers markedly decrease toward the SC, it is a generally accepted hypothesis, that the melanosomes and the contained melanin are somehow degraded within the keratinocytes (Nordlund *et al.*, 1998; Jimbow *et al.*, 1999). Since the discovery of the melanosome by Seiji *et al.* (1961), research was aimed at exploring the molecular mechanism, by which this degradation is achieved. But up to date, this riddle remains unsolved (Borovanský and Elleder, 2003).

I.5.1 Melanin Dust or Degradation of the Polymer Structure?

Histological investigation of the skin, using special melanin-specific stains, such as the Fontana-Masson silver stain (see chapter C.IV.2.3), gave rise to the hypothesis of decomposition and breaking up of melanosomes into smaller units. The products of this melanosome disintegration were believed to remain in the keratinocytes, and to be removed from the epidermis by desquamation. In the SC, the remaining melanin was assumed to exist as fine powder, so-called “melanin dust” – a theory not jet invalidated (Rothman and Lorincz, 1963; Odland, 1991; Nordlund *et al.*, 1998).

The presence of acid phosphatase in melanosomes, together with the aggregation of melanosomes within the keratinocytes into membrane-bound clusters, funded the assumption, that the melanosomes are internalized by secondary lysosomes, that somehow mediate the break-

up of melanosomes and the following degradation of the enclosed melanin (Hori *et al.*, 1968; Seiji and Kikuchi, 1969; Olson *et al.*, 1970; Nakagawa *et al.*, 1984). The fact, that melanosome clusters are abundant in the basal layer, but vanish nearly completely in the upper layers of the epidermis, seemed to support this theory (Thong *et al.*, 2003).

However, melanin proved to be very resistant to both, acid phosphatase and lysosomal hydrolases. Lysosomal digestion merely degraded the protein and lipid moieties of the melanosomes, but the melanin contingent remained intact (Otaki and Seiji, 1971; Saito and Seiji, 1976; Borovanský *et al.*, 1999). No lysosomal enzyme has been found, that is capable of degrading melanin (Borovanský and Elleder, 2003).

I.5.2 NADPH Oxidase – a Candidate for Mediating Melanin Degradation

Melanosomes can be disintegrated by treatment with alkaline pH (Borovanský and Elleder, 2003). However, the required extreme pH can be ruled out as an intracellular degradation mechanism, as it is not compatible with cell survival. Degradation of the melanin polymer, i.e. chemical destruction of the original structure and conversion into metabolites or degradatory products, can be achieved *in vitro* by oxidation with potassium permanganate or hydrolysis with hydrogen iodide – both extremely unlikely in living cells (S. Ito and Wakamatsu, 2003). The only remaining possible degradation pathway consistent with the structure of the melanin oligomer as supposed by Clancy and Simon (2001, see also chapter I.2.1) points to oxidative degradation (Borovanský *et al.*, 1999; Elleder and Borovanský, 2001).

Hydrogen peroxide is a powerful oxidizing agent, capable of degrading melanin *in vitro* (Korytowski and Sarna, 1990). Hydrogen peroxide arises in several cells types present in the skin, e.g. endothelial cells, phagosomes and fibroblasts, and has also been demonstrated for keratinocytes and even melanosomes (Glickman *et al.*, 1993; Turner *et al.*, 1998; Bokoch and Knaus, 2003). NADPH oxidase – a membrane-associated, multi-subunit enzyme complex – is indicated as a possible source for the hydrogen peroxide (Borovanský and Elleder, 2003). NADPH oxidase catalyzes the formation of superoxide anion by transferring electrons from NADPH to molecular oxygen. Superoxide anion subsequently dismutates, either spontaneously or catalyzed by superoxide dismutase, to form hydrogen peroxide (Bokoch and Knaus, 2003; Robinson *et al.*, 2004).

But although the reduction or complete loss of melanosomes toward the SC indicates, that biodegradation of melanosomes is possible, a convincing demonstration of melanin degradation *in vivo* and the characterization of the possible degradatory products is still lacking (Schraermeyer, 1993; Borovanský and Elleder, 2003).

II Investigation and Evaluation of Skin Pigmentation

Since the discovery of the melanocyte as a specialized cell type of the human epidermis in the 19th century, a large variety of microscopic investigation techniques have arisen to study these cells and their major synthesis product, the melanosomes. With the formation of dermatology as an independent field of research, noninvasive investigation techniques for medical application and diagnosis gained more importance.

II.1 Noninvasive Measurement of Skin Colour

Susan Taylor (2006) states, that "the human eye remains the ultimate assessment tool" for the description and classification of skin colour. But as the perception varies exceedingly among different investigators, several tools have been developed – and are currently in use – to standardize the measurement and reduce the range of variation. These tools include photography, Wood's light examination, reflectance spectroscopy and *in vivo* or *intra vital* microscopy.

The system of Fitzpatrick's skin phototypes was introduced 1975, to standardize the assessment of skin colour, replacing the then commonly used race-oriented classification of skin colour (Astner and Anderson, 2004). Fitzpatrick's classification system relies on the patient's or study participant's own report of responses to sunlight exposure. Together with the visual assessment of the constitutive skin colour, determined on unexposed skin, the sunburn and tanning history defines the phototype according to Table 1. Some investigators include eye and hair colour in this enquiry, as these factors are often related. Red hair combined with green or blue eyes, e.g., are almost exclusively found in individuals with phototype I, while persons with phototype V or VI generally have dark hair and eyes. Table 1 gives an overview of the six designated phototypes and the corresponding constitutive skin colour and response to UV radiation. Additionally, the average minimal erythema dose (MED) for UV-A and UV-B radiation, i.e. the lowest dose of radiation that induces minimally perceptive erythema, is displayed for the different phototypes.

Table 1: Fitzpatrick's skin phototypes*. The minimal erythema dose (MED) is displayed for UV-A and UV-B radiation, for the different skin phototypes. The MED is determined as the minimum dose that induces minimally perceptive erythema.

Phototype	Sunburn & tanning history (defines the phototype)	Constitutive skin colour (unexposed buttock skin)	UV-A MED (mJ/ cm²)	UV-B MED (mJ/ cm²)
I	burns easily, never tans	ivory white	20-35	10-30
II	burns easily, tans minimally with difficulty	fair white	30-45	25-40
III	burns moderately, tans moderately and uniformly	darker white	40-55	30-50
IV	burns minimally, tans moderately and easily	beige-olive, lightly tanned	50-80	40-60
V	rarely burns, tans profusely	moderate brown or tanned	70-100	90-90
VI	never burns, tans profusely	dark brown or black	100	90-150

* Adapted from Fitzpatrick's Dermatology in General Medicine (Fitzpatrick *et al.*, 1999)

But as simple visual assessment is scientifically and clinically inadequate, the above mentioned methods aimed at standardizing measurements of skin colour, are employed in medicine and science. Wood's light with an emission wavelength of 360 nm is used in the diagnosis of pigmentary disorders, measuring local reflection and absorbance of the penetrating UV light. Areas of the skin with high epidermal melanin content, e.g. *lentigo senilis*, appear darker than normal skin, while scars or areas with increased collagen deposition are not detected, due to their melanin concentration, that is comparable to normal skin (Taylor et al., 2006).

As melanin yields a strong reflectance, reflectance-mode *in vivo* confocal microscopy can be used to determine the epidermal melanin content by measuring the reflectance signal from the skin. The reflectance signal displays a good correlation to the epidermal melanin content, which increases with the phototype. Additionally, confocal microscopy enables three-dimensional investigation of the epidermal distribution of melanin (C.A. Charles *et al.*, 2002; Yamashita *et al.*, 2005; Taylor *et al.*, 2006). But as the resolution of *in vivo* confocal microscopy does not enable to image single melanosomes, it provides only qualitative information on reflecting particles in the epidermis, i.e. mainly the epidermal melanin distribution – quantitative assessment is not possible (Sauermann *et al.*, 2002). Multiphoton spectroscopy and microscopy allows 3D measurement or visualization of pigment content and distribution in a more quantitative way, as it also distinguishes between eumelanin and

pheomelanin by means of excitation and emission spectra (Masters *et al.*, 1997; Konig, 2000). However, these methods are not commonly used.

For more than 50 years, reflectance spectroscopy has been in use – and remains the most common technique – to objectively measure skin colour. The most widely employed standard colour system for reflectance spectroscopy is the Commission International d'Eclairage (CIE) *L*a*b** system. The *L** value measures the reflectance or lightness of the skin, *a** quantifies the colour saturation from red to green, and *b** measures the colour saturation from yellow to blue. This technique provides a means to assess and directly compare different states of pigmentation, but supplies no information of the epidermal melanin concentration or composition (Alaluf *et al.*, 2002b; Taylor *et al.*, 2006).

II.2 Microscopic Analysis of Pigmentation

Due to insufficient resolution, *in vivo* imaging techniques provide only limited information on the epidermal distribution of melanin. Improving microscopic resolution requires an amplification of the energy source, and hence reduction of the wavelength, which can be achieved either by the employment of mercury arc lamps, laser beams, or – in the case of electron microscopy – electron beams (Flegler *et al.*, 1995; Pawley, 1995). The energy introduced into the tissue by either of these energy sources, inevitably causes damage to the investigated tissue, rendering *in vivo* investigation nearly impossible, with the exception of multiphoton laser microscopy. Moreover, microscopic resolution is improved by minimizing the thickness of the sample, which is either achieved by noninvasive optical sectioning as e.g. accomplished by confocal laser scanning microscopy (CLSM), or invasively sectioning perpendicular to the skin surface to gain an overview of all layers of the skin (Hayat, 2002). The latter requires the draft of biopsies from the skin for *ex vivo* examination.

The *ex vivo* investigation should primarily be aimed at displaying the physiological condition of the sample, preserving natural cell shape, cell contacts and intracellular components. However, the removal of tissue from its natural context entails the induction of biochemical and morphological changes within the extracted tissue fraction (Hayat, 2002). To preserve the sample in a natural or at least the nearest possible natural condition, it needs to be fixed either by chemical fixatives or physically, i.e. by freezing. Subsequent dehydration and embedding in a stabilizing matrix, such as wax or resin, facilitates the sectioning process: the more solid (but not hard or brittle) the embedding medium, the thinner the sections that can be produced.

A more detailed description of the employed preparation methods is given in chapter C – Materials & Methods.

Each step in the entire preparation procedure carries with it the risk of introducing artefacts, either in the form of cell shrinkage, agglomeration or disintegration of intracellular components, ice crystal formation that causes damage to the cellular ultrastructure, or modulation of enzymatic conformations (Echlin, 1992; Monaghan *et al.*, 1998; Pfeiffer *et al.*, 2000; Skepper, 2000; Murk *et al.*, 2003). The appropriate combination of fixation method and following dehydration and embedding procedure is chosen considering the aim of the intended investigation as well as the designated mode of microscopy, as it always requires compromising between minimizing artefacts and reducing preparative effort.

II.2.1 Histological and Cytochemical Methods to Investigate Pigmentation

Histology comprises the investigation of tissue sections, administering different staining techniques to demonstrate biological structures in their morphological context. Routine staining techniques, such as hematoxylin eosin, toluidine blue or Nile blue staining, not only afford a general characterization of skin samples but additionally provide a melanin-specific staining that allows a general assessment of the epidermal melanin distribution (Romeis, 1968). Additionally, several histological techniques exist explicitly for the identification and description of melanin and melanocytes (Romeis, 1968; Churukian, 2002). The most commonly used techniques include reducing methods such as the Fontana-Masson silver staining (Barbosa *et al.*, 1984), enzyme methods such as the DOPA reaction (Sasai *et al.*, 1978), and methods based on solubility and bleaching properties of melanin (see chapter C.IV.2). Solubility and bleaching methods are aimed rather exclusively at the identification of melanin and are not appropriate for the quantification of melanin.

The DOPA reaction, a cytochemical method to demonstrate melanocytes that actively synthesize pigment in tissue samples is nowadays replaced by immunocytochemistry. A wide range of antibodies are commercially available for the identification of nearly every melanocytic enzyme (Smoller *et al.*, 1991; Bhawan, 1997; Dean *et al.*, 2002). The use of fluorophore-coupled secondary antibody together with the application of confocal laser scanning microscopy (CLSM) additionally provides a means to display the investigated structures in 3D (Pawley, 1995).

II.2.2 Electron Microscopy as a Tool to Study Pigmentation

While light microscopy enables the demonstration of epidermal melanin content and sometimes even facilitates the imaging of single melanosomes, the resolution is not sufficient to describe the ultrastructure of melanocytes, their interaction with the neighbouring keratinocytes or even the melanosomal organisation before and after transfer from melanocyte to keratinocyte. Especially the later task involves the identification and quantification of melanosomal membranes, forming vesicles of 150 – 300 nm in diameter (see chapter I.2.4).
The visualization of membranes in biological tissues not only affords the superior resolution of transmission electron microscopy (TEM), but additionally requires sophisticated preparation techniques. Chemical fixation is not well suited for this task, as it induces shrinkage and conglomeration artefacts, which especially effect melanocytes and would hinder the investigation of melanocyte-keratinocyte interactions. High-pressure freezing, followed by freeze-substitution in the presence of uranyl acetate and low-temperature embedding in Lowicryl® HM20 – although by far the most time-consuming and demanding preparation procedure – produces the best results regarding lipid preservation and structural integrity of skin samples (Pfeiffer *et al.*, 2000; Giddings, 2003).
TEM is also the most suitable microscopic investigation technique for the measurement of the epidermal melanin content, as it facilitates the detection and direct quantification of individual as well as clustered melanosomes (see chapter C.VIII.4). Sophisticated stereological analysis of the ultrathin TEM sections even creates the possibility to extend the two-dimensionally obtained melanosome numbers into the third dimension to achieve more correct information (Griffiths, 1993).

II.2.3 Cytochemical Demonstration of NADPH Oxidase Activity

Direct detection and localisation of ROS is complicated by the fact that ROS are short lived and rapidly catalyzes by intracellular scavenging systems. Briggs and Karnovsky introduced a cytochemical technique to localize NADPH oxidase enzyme activity in biological tissues (Briggs *et al.*, 1975a; Karnovsky, 1994).
According to Feigl (1958), cerium ions react with ammonia and hydrogen peroxide, forming cerium perhydroxide, which is an insoluble, electron opaque precipitate, that accumulates at the intracellular production sites of H_2O_2 and is easily detected in EM or in reflection-mode CLSM (Briggs *et al.*, 1975b; Ellis *et al.*, 1998; Telek *et al.*, 1999).

To demonstrate the activity of NADPH oxidase in biological tissues, the samples are incubated with a reaction medium containing cerium chloride, the substrate NADPH, and specific inhibitors of other enzymes potentially producing ROS, such as catalase or xanthine oxidase. The specificity of the reaction is confirmed by the either omitting the substrate NADPH or including a specific inhibitor for NADPH oxidase, diphenyleneiodonium chloride (DPI) in the reaction medium (Ellis *et al.*, 1998; Ellis and Grant, 2002).

In addition to detecting the cerium perhydroxide precipitate by CLSM or EM, the precipitate can be used for polymerization and cyclization of diaminobenzidine (DAB), resulting in an amplification of the primary reaction product, that can be visualized by conventional light microscopy. Cobalt chloride can be used to enhance the contrast (Gossrau *et al.*, 1989).

II.3 Chemical Analysis of Melanin Content in Biological Samples

A microanalytical method to quantify the content of eumelanin and pheomelanin in biological tissues was devised by Ito *et al.* (S. Ito and Jimbow, 1983; S. Ito and Fujita, 1985). The method does not require the isolation of the melanin from the tissue, but is applied to the entire homogenized skin or hair sample instead.

Oxidative reduction of eumelanin with permanganate (Figure 11) yields a specific degradation product: pyrrole-2,3,5-tricarboxylic acid (PTCA) is gained from DHICA-derived eumelanin, while DHI-derived eumelanin yields pyrrole-2,3-dicarboxylic acid (PDCA). Reductive hydrolysis of pheomelanin with hydrogen iodide (HI) specifically produces amino-hydroxyphenylalanine (AHP) isomers (Figure 12), depending on the originating pheomelanin polymers: 4-amino-3-hydroxyphenylalanine (4-AHP) is produced from 5-*S*-DC-pheomelanin, and 2-*S*-SC-pheomelanin yields 3-amino-4-hydroxyphenylalanine (3-AHP). But only 4-AHP is used an indicator for pheomelanin, as the specificity exceeds that of total AHP, due to a considerable background level of AHP originating from melanin precursors (Wakamatsu *et al.*, 2002).

These specific degradation products can be analyzed and quantitated by high performance liquid chromatography (HPLC). 4-AHP is produced at a yield of 11 %, the PTCA yield measures only 2.8 %, and the yield for PDCA is negligible. This renders the introduction of conversion factors necessary, to determine the actual concentration of eumelanin and pheomelanin in the investigated samples. The conversion factor for 4-AHP is 9. The amount of eumelanin was initially determined by multiplying the measured PTCA content of the sample

with a factor of 35, but this factor has been corrected to 160, due to reports of massive under-estimation of the eumelanin content (Alaluf *et al.*, 2001; Wakamatsu and Ito, 2002).

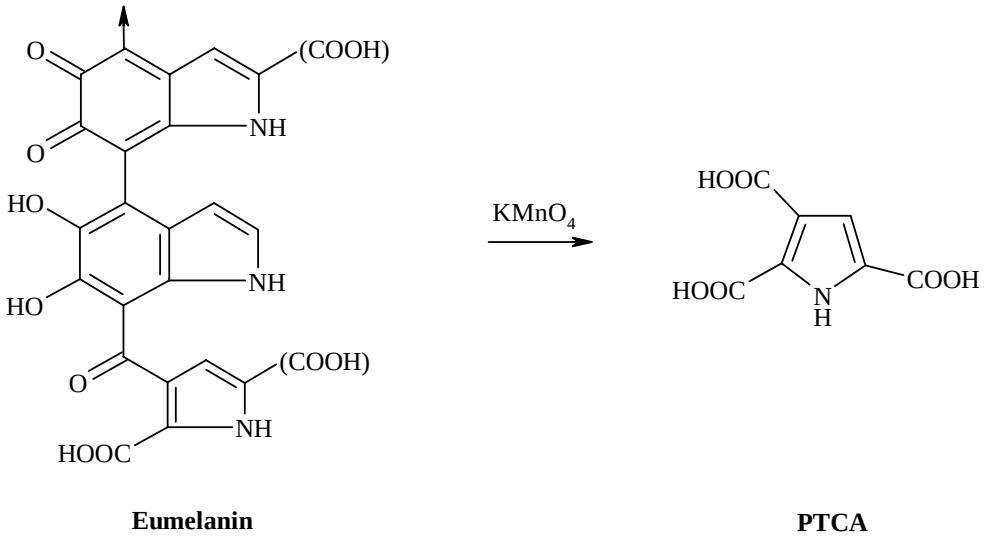

Eumelanin **PTCA**

Figure 11: Oxidative breakdown of eumelanin. Eumelanin is degraded oxidatively with potassium permanganate ($KMnO_4$), resulting in specific degradation products: pyrrole-2,3,5-tricarboxylic acid (PTCA) and pyrrole-2,3-dicarboxylic acid (PDCA). PTCA is produced at a yield of 2.8 %, while the yield of PDCA is negligible. The degradation products are detected and quantified by HPLC, and PTCA is used as a specific indicator for eumelanin. The measured amount of PTCA is multiplied by a conversion factor of 160 to determine the actual eumelanin content of the investigated sample.

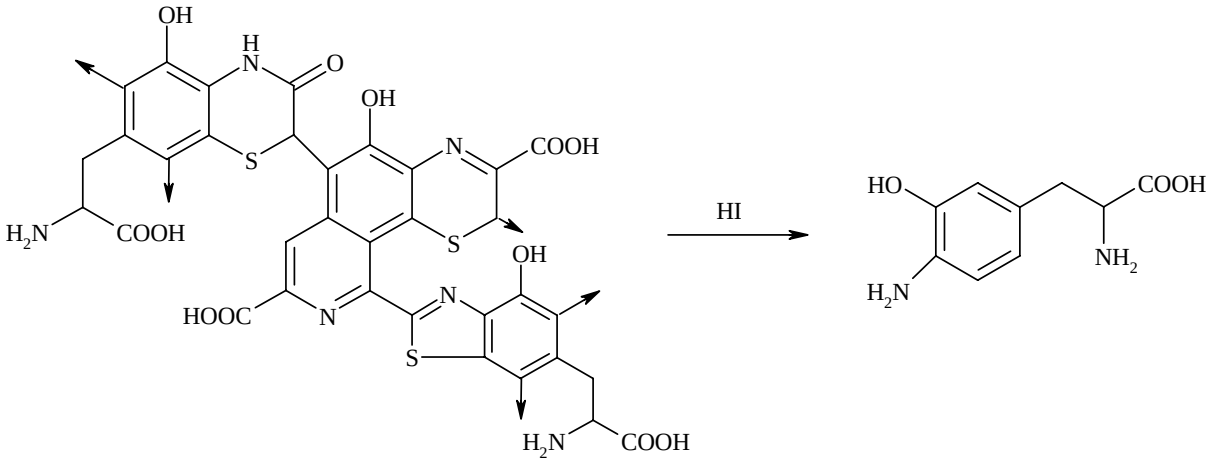

Pheomelanin **AHP**

Figure 12: Reductive hydrolysis of pheomelanin. Pheomelanin is chemically degraded by hydrogen iodide, producing the pheomelanin-specific marker 4-amino-3-hydroxyphenylalanine (4-AHP) at a yield of 11 %. 4-AHP can be quantitatively determined by HPLC. The obtained 4-AHP content of the respective sample is multiplied by a conversion factor of 9 to determine the pheomelanin content.

III The Project – Challenging Questions of Skin Pigmentation

The type and amount of melanin and its epidermal distribution pattern determines the actual skin colour. But while the biosynthesis of melanin within the melanocytes is well characterized, neither transfer of melanosomes from the melanocytes to the surrounding keratinocytes, nor the ultimate fate of transferred melanosomes within the keratinocytes are elucidated up to date (Borovanský and Elleder, 2003; Van Den Bossche *et al.*, 2006). This project therefore aims at finding morphological and biochemical functional clues for the description of melanin processing and its degradation pathway. A further aim is to establish potentially unique criteria for various skin types, including dyspigmentations, and the potential relation to their morphological and functional background.

As understanding the metabolism of melanin requires basic knowledge of its epidermal distribution, a first step is to investigate the distribution of melanin and/ or melanosomes in different epidermal layers in skin of Caucasian, Asian and Negroid origin. A further step covers the morphological description of melanosomes before and after transfer from melanocyte to recipient keratinocyte, with a special focus on the number of melanosomal membranes to find proof for one or more of the existing theories regarding melanosome transfer. The mode of transfer is of special interest, as it may provide an explanation for the distribution patterns within the keratinocytes as well as the ensuing processing of the melanosomes. Further emphasis is put on the distinctions of *lentigo senilis* compared to normal elderly skin, including the number of melanocytes, the epidermal distribution of melanosomes and the ultrastructure of the skin. Several staining and microscopy techniques are available for the characterization of skin pigmentation, and an appropriate method for each respective task is to be identified. Supplementary, a chemical analysis of the total eumelanin and pheomelanin content of skin biopsies is performed, and a comparison of the results of this method with microscopic investigation is aspired.

Based on the assumption of Borovanský and Elleder (2003; see also chapter I.5.2), that NADPH oxidase may be involved in the melanin degradation process by providing ROS capable of degrading the extremely stable polymer, a cytochemical assay is established to demonstrate the sites of hydrogen peroxide production in the epidermis and identify a potential colocalisation with melanosomes or cellular structures implied in melanin processing.

C MATERIALS & METHODS

I Standard Buffers

Buffers that are repeatedly used for different applications are listed in this chapter. The preparation of specific solutions and buffers is described in the respective chapters. Chemicals and reagents are usually purchased from Sigma-Aldrich, Munich, Germany. Variant suppliers are mentioned additionally.

Dulbecco's Modified Eagle Medium (DMEM)

The cell culture medium is readily purchased from Invitrogen, Karlsruhe, Germany.

Phosphate-Buffered Saline (PBS) pH 7.2

The Buffer is readily purchased from Invitrogen, Karlsruhe, Germany.

HEPES Buffer 0.05 M, pH 7.4

HEPES (N-2-Hydroxyethyl piperazine-N´-2´-ethane sulphonic acid) (Roth, Karlsruhe, Germany)	11.91 g
Aqua bidest.	ad 1000 ml
Sodium hydroxide solution (Merck, Darmstadt, Germany)	ad pH 7.4

Sodium Cacodylate Buffer 0.1 M, pH 7.4

Sodium cacodylate trihydrate	21.4 g
Aqua bidest.	ad 1000 ml
Hydrochloric acid	ad pH 7.4

Sodium Cacodylate Buffer 0.15 M, pH 7.4

Sodium cacodylate trihydrate	32.1 g
Aqua bidest.	ad 1000 ml
Hydrochloric acid	ad pH 7.4

Sodium cacodylate contains arsenic and is therefore toxic.

Tris Hydrochlorine Buffer (Tris-HCl Buffer) 0.05 M, pH 7.6

Tris (Tris[hydroxymethyl]aminomethane) (USB Corp., Cleveland, Ohio, USA)	6.06 g
Aqua bidest.	ad 1000 ml
Hydrochloric acid	ad pH 7.6

All buffers can be stored at 4 °C for several weeks.

II Skin Samples

For this project three different sample collectives were investigated, that were obtained during two studies approved by the Hamburg ethics committee (internal Beiersdorf AG study numbers: 10684 and 18655). And all participants were required to give informed consent before partaking.

During the first study (2000 - 2001) biopsies of the nates (diameter 4-5 mm) were obtained from thirty volunteers with healthy skin of the following ethnic groupings: European (n = 10), Asian (n = 10) and African (n = 11). Further eleven volunteers contributed biopsies from the back of their hands (diameter 2-3 mm), one each covering an age spot (*lentigo senilis*, lesional) and one from the periphery of the respective age spot (perilesional). Biopsies were taken in the University Medical Centre Hamburg-Eppendorf and placed – epidermis upward – onto cellulose, soaked in cell culture medium (DMEM), to ensure adequate supply of nutrients and to prevent desiccation during transport to Beiersdorf AG. The biopsies were processed for high-pressure freezing immediately, yielding five samples per volunteer, and stored in liquid nitrogen until further processing.

During a second study (2005) additional thirty volunteers – five of each of Fitzpatrick's skin phototypes I-VI – gave two punch biopsies each (diameter 4 mm) from the nates. The samples were transported from the University Medical Centre to Beiersdorf AG as described before. After removal of the adipose tissue, one biopsy of each volunteer was processed for microscopic investigation, while the other biopsy was prepared for chemical analysis of the melanin content by Dr. Wakamatsu of the Fujita Health University in Toyoake, Japan (S. Ito and Jimbow, 1983; Wakamatsu and Ito, 2002).

For microscopy, each biopsy was divided into six smaller parts: three 2 mm-punch biopsies were extracted and high-pressure frozen followed by low-temperature dehydration and em-

bedding (see chapters III.1.2.2 and III.2.2). One part was fixed in IEM and uranyl acetate for room temperature dehydration and embedding (chapters III.1.1 and III.2.1) and the remaining two parts were plunge-frozen for immunohistochemistry (III.1.2.1). The second biopsy was weighted to determine the moist mass, before plunge-freezing, followed by freeze-drying and shipment to Japan for chemical analysis. Table 2 displays the usage and applied investigative techniques of the different sample collectives.

Additionally, discard material from cosmetic surgery was used for several microscopic investigations, including the assessment of staining techniques and the NADPH oxidase detection assay. Patients gave written consent. The cosmetic surgery biopsies were transported and stored as described earlier.

Sections of paraffin embedded Negroid skin samples were obtained from Dr. Brandner, Laboratory for Cell Biology, Department of Dermatology and Venerology, University Medical Centre Hamburg-Eppendorf.

Table 2: Designated use of samples for this project.

Sample collective		Investigation of…	Microscopy mode	Results described in chapter:
BDF-Study Nr. 10684	Caucasian, Asian and Negroid skin	Melanosome distribution and melanin clearing	TEM	E.I.1.1
		Structural organisation of melanosomes	TEM	E.IV.2
	Lentigo senilis lesional and perilesional	Melanocyte distribution	CLSM	E.II.3
		Melanosome distribution and melanin clearing	TEM	E.I.1.3, E.I.2.2, E.III
		Characteristics of *lentigo senilis*	LM	E.III
BDF-Study Nr. 18655	Fitzpatrick's Skin Phototypes I-VI	Melanocyte distribution	CLSM	E.II.2
		Melanosome distribution and melanin clearing	LM and TEM	E.I.1.2
		Structural organisation of melanosomes	TEM	E.IV.2
		Chemical analysis of melanin content	-	E.I.3
Cosmetic surgery discard material		Assessment of staining techniques	LM, CLSM and TEM	D
		NADPH oxidase detection assay	LM and TEM	E.V.2

III Sample Preparation for Microscopy

The procedure of sample preparation for microscopy comprises four major steps: (1) fixation, (2) dehydration and embedding, (3) sectioning and (4) staining. For each step various alternatives and modifications are possible and the suitable variant is chosen depending on the respective experiment and intended mode of microscopy, sometimes also requiring combinations of two methods. The preparative techniques applied during this project are described in the following chapter. Table 3 gives an overview of the employed combinations. Chemically fixed samples are either processed for resin embedding at room temperature, or plunge-frozen and sectioned in the cryostat. Physically or cryofixed specimen can also be transferred directly to the cryostat for sectioning or freeze substituted, followed by cryostat cutting or low-temperature embedding and subsequent ultramicrotomy. After suitable staining, cryostat sections and semithin resin sections can be investigated using a light microscope (LM) or confocal laser scanning microscopy (CLSM). Ultrathin resin sections are stained with heavy metal salts for transmission electron microscopy (TEM).

Table 3: Sample preparation and resulting microscopic applications.

Fixation	Dehydration	Embedding	Sectioning	Staining	Microscopy
Chemical sample fixation	At room temp.	At room temp.	Ultramicrotomy	Histocytochemistry	LM
				Heavy metal staining	TEM
Chem. & phys. fix.	-	-	Cryostat	Histocytochemistry Immunofluorescence	LM
Physical sample fixation	-	-	Cryostat	Histocytochemistry Immunofluorescence	LM CLSM
	Freeze substitution	-	Cryostat	Immunofluorescence	CLSM
		Low-temp. embedding	Ultramicrotomy	Histocytochemistry	CLSM
				Heavy metal staining	TEM

III.1 Fixation

When removed from their surrounding compound, most tissues immediately initiate autolysis processes. To prevent cellular disintegration and to preserve the structural integrity of the tis-

sue, the biopsy needs to be fixed as soon as possible after its extraction. Fixation can be achieved either chemically or physically, depending on the demands of the respective method of investigation. Several methods for chemical as well as physical fixation are available, including the combination of both fixation forms.

III.1.1 Chemical Fixation

Glutaraldehyde and paraformaldehyde are the two most commonly used fixatives, either individually or in combination. Both aldehydes crosslink proteins or components of proteins. Formaldehyde forms methylene bridges between two amino acids within a protein that are mostly reversible, while glutaraldehyde forms irreversible intramolecular and intermolecular protein crosslinks (Griffiths, 1993; Hayat, 2002). Uranyl acetate and osmium tetroxide are used as secondary fixatives after protein fixation, mostly combined with the first step of the embedding procedure. These heavy metals salts react primarily with lipid moieties.

Skin samples are cut into 2 mm pieces, in order to minimize the duration of the fixation, thus ensuring the penetration of the entire sample, and at the same time minimizing extracting effects of the fixative. The samples are usually treated with chemical fixatives for 24 h at 4 °C. Uranyl acetate is generally added to the primary fixative, while osmium tetroxide is applied for one hour prior to dehydration (see chapter III.2.1). Variations from this standard are described in the respective chapters. The applied fixatives and their preparation are listed below.

The samples are then either dehydrated and embedded in resins (see chapter III.2), plunge-frozen (see chapter III.1.2.1) or immediately sectioned with the cryostat (see chapter III.3.1). Before plunge-freezing, the samples are infiltrated with sucrose solution after chemical fixation for further 24 h at 4 °C, providing a protection against the formation of ice crystals.

Paraformaldehyde stock solution 8 % (w/v)

Paraformaldehyde (Plano, Wetzlar, Germany)	8.00 g
0.05 M HEPES buffer	ad 100 ml
Hydrochloric acid	ad pH 7.2

Paraformaldehyde (PFA) is dissolved with stirring at 60 °C. Sodium hydroxide solution is added drop by drop until the solution becomes clear, and the pH-value is adjusted to 7.2 with hydrochloric acid. The solution can be stored at -20 °C for several months.

Paraformaldehyde fixative (4 %)

PFA-stock solution 8 % (w/v)	50 ml
0.05 M HEPES buffer	ad 100 ml

The solution can be stored at -20 °C for several months.

Fixative for immuno-electron microscopy (IEM-fixative)

PFA-stock solution 8 % (w/v)	50 ml
Glutaraldehyde solution 25 % (w/v) (Plano, Wetzlar, Germany)	40 µl
0.05 M HEPES buffer	ad 100 ml
Hydrochloric acid	ad pH 7.2

The solution should be mixed under inert gas (e.g. nitrogen), as glutaraldehyde is unstable in the presence of oxygen. The solution can be stored at -20 °C for several months.

Uranyl acetate 2 % (w/v)

Uranyl acetate (SERVA, Heidelberg, Germany)	0.20 g
Aqua bidest.	ad 10 ml

Uranyl acetate is applied at a concentration of 1 % for fixation. The solution can be stored at 4 °C for several weeks. Security guidelines for protection against radiation need to be considered when working with uranyl acetate.

Osmium tetroxide solution 1 % (w/v)

Osmium tetroxide (Plano, Wetzlar, Germany)	1.00 g
Aqua bidest.	100 ml

Bidest. water is filled into a brown glass bottle with ground glass stopper. The ampoule with osmium tetroxide is cleaned on the surface with ethanol and put into the water-filled glass bottle. The ampoule is forced open with a pestle under water to prevent the release of osmium vapours. The osmium tetroxide is totally dissolved with stirring and filtered. The solution can be stored at 4 °C for several weeks, the refrigerator needs to be equipped with ventilation.

Sucrose solution 30 % (w/v)

Sucrose (Merck, Darmstadt, Germany)	30.00 g
Aqua bidest.	100 ml

The solution can be stored at 4 °C for several weeks.

III.1.2 Cryofixation

Cryofixation, or physical fixation, presents an alternative to chemical fixation that is not only faster but also eliminates side effects of chemical cross-linking, like the reorganization of the ultrastructure of cell membranes and cytoplasm. The term “cryofixation” describes the rapid cooling of a specimen to preserve a snapshot of its solution state. A major problem when it comes to cooling a specimen to subzero temperatures is the formation of ice crystals. If the ultrastructure of a sample is to be investigated, this must be avoided, as ice crystals seriously deform cell components (Echlin, 1992). As this can only be achieved by a very high cooling rate, samples should be chosen as small as is consistent with the physiological and morphological aims of the experiment. It is also possible to combine chemical and physical fixation methods to ensure stabilization against cryo-damage (B.M. Humbel and Müller, 1984).

III.1.2.1 Plunge-Freezing

The specimen is plunged into a suitable liquid cryogen as rapidly as possible. Propane or ethane are the most commonly used liquid cryogens. The sample size should not exceed 4 mm in diameter to ensure an efficient cooling rate. Sample and sample holder need to be configured to ensure that the sample is the first object to enter the cryogen.

Procedure

The cryogen, in this case liquid ethane, is contained in a metal reservoir and sitting in a bath of liquid nitrogen. The edge of the sample is held by a pair of tweezers that are clamped into a spring-loaded mechanical plunging device positioned above the cryogen bath. It is necessary to ensure that the injector is prevented from bouncing back and the sample does not hit the bottom of the cryogen container. The sample is injected into the cryogen with a velocity of approximately 5-6 m s^{-1}. The average cooling rate for plunge-freezing is 10-12 $\cdot 10^3$ K s^{-1}. The sample is stored in liquid nitrogen until further preparation steps.

In this project, fresh skin biopsies without any pre-treatment and IEM-fixed, sucrose-infiltrated samples were preserved by plunge-freezing and processed for light microscopy, i.e. cryostat sectioning with subsequent staining (see chapter IV).

III.1.2.2 High-Pressure Freezing

High-pressure freezing takes advantage of the fact that water can remain liquid well below its equilibrium freezing point without the formation of ice crystals. At atmospheric pressure this undercooling is possible until -38 °C. Below -130 °C water can be transferred into a stable non-crystalline condition, referred to as amorphous ice or vitrified water. In the temperature range between -38 °C and -130 °C nucleation, i.e. ice crystal formation, takes place. The application of high pressure (approx. $2.4 \cdot 10^5$ kPa) while cooling hinders the volume expansion associated with crystallization, and thus reduces the freezing point as well as the nucleation rate. Undercooling now continues until -92 °C without the interference of nucleation effects. This reduces the temperature (and time) range between the state of undercooled and vitreous water during which nucleation occurs.
Although the cooling rate of this procedure (approx. $0.5 \cdot 10^3$ K s^{-1}) is much lower than that of plunge-freezing, the reduction of cryoinjury of the sample makes it superior when it comes to investigating ultrastructure.

Procedure

Skin samples are taken using standard biopsy punches (diameter 2-4 mm). The subcutis is carefully removed and the sample is cut into small pieces of about 500-2000 µm in diameter and 200 µm in thickness. The samples are placed in standard aluminium platelets filled with incompressible 1-hexadecene to improve energy transfer and to protect the specimen. The samples are frozen in an HPM 010 high-pressure freezer (Bal-Tec AG, Balzers, Liechtenstein). Ethanol is used to apply the pressure ($2.4 \cdot 10^5$ kPa) before cooling the specimen by a jet of liquid nitrogen.
The specimens are stored in liquid nitrogen until further processing.

III.1.2.3 Freeze-Drying

Frozen specimens can also by dehydrated by low-temperature vacuum sublimation. For total removal of residual water the samples are warmed to room temperature under high-vacuum.
Plunge-frozen samples of skin phototypes I-VI (see chapter II) were freeze-dried to facilitate transport to the Laboratory of Dr. Wakamatsu in Toyoake, Japan. The samples were stored in liquid nitrogen and transferred into the high-vacuum chamber of a BAF 060 Freeze-Fracture System (Bal-Tec AG, Balzers, Liechtenstein), equipped with a specimen stage, that can be

tempered from -170 °C to +50 °C. The vacuum chamber was pre-cooled to -140 °C and the vacuum-pressure was adjusted to $8 \cdot 10^{-6}$ Pa. The temperature was gradually increased in steps of 30 °C every half hour. In a final step, the samples remained at -20 °C for one hour, before releasing them from vacuum and transfer to 1.5 ml Eppendorf tubes. The Eppendorf tubes were deposited in transport containers with anhydrous silica gel to ensure dry conditions during transport to Japan.

As the samples were disintegrated for chemical analysis, the unavoidable molecular or structural damage brought about by shrinkage or collapse of the tissue during the desiccation process was no concern.

III.2 Dehydration and Embedding

After fixation the samples are further processed to enable easy handling during the sectioning process and to simplify storage. Therefore the samples are dehydrated and embedded in resin. First the water bound in the tissue – liquid or vitreous – is replaced by an organic solvent, which is, in turn, substituted by resin, that is subsequently polymerized. Common dehydration agents are ethanol or acetone. This process can be performed either at room temperature for chemically fixed specimen, or the entire process is accomplished at low temperatures if the samples were cryofixed. Different types of resins are utilized for each application, epoxy resins are used for room temperature embedding, while Lowicryl® resins are adapted to low-temperature infiltration and polymerization. Fluorescent dyes can be introduced during the dehydration process, to enable multiple microscopic investigations of the same sample (Biel *et al.*, 2003).

Besides, chemically fixed or plunge-frozen samples can be transferred directly into the cryostat for sectioning (see chapter III.3.1).

III.2.1 Room Temperature Dehydration and Embedding

The procedure of dehydration and embedding can be performed manually or partly automated using the Leica EM TP tissue processor (Leica, Wetzlar, Germany). The chemically fixed samples are gradually dehydrated by a graded series of ethanol. The solvent is then replaced by an epoxy resin. The epoxy-solvent ratio is gradually increased until pure epoxy resin is used. During infiltration the vials containing the samples and the respective solution are gently agitated to ensure thorough infiltration of the tissue with resin. The specimens are then

transferred into molds containing pure liquid resin and are finally placed into an oven (T = 60 °C) to polymerize the resin to form a solid block. The sample is positioned at the tip of the embedding container and aligned for sectioning later on, to achieve sections perpendicular to the skin surface and include all epidermal layers. The exact protocol of the procedure is displayed in Table 4.

It is of exceeding importance to keep the dehydration solvents sealed tightly, as they will absorb water from the air to an extent that makes them incapable of eliminating water in the sample. Therefore, molecular sieves are used to desiccate the solvents. When replacing one dehydration agent with the next solution it is important to do so rapidly to avoid water uptake.

Any dehydration solvent is a powerful extractor of lipids. Osmium tetroxide or uranyl acetate can therefore be used during or after fixation to help stabilize the lipids during the dehydration process. Fixation steps are usually followed by washing with HEPES buffer.

Table 4: Protocol for room temperature dehydration and embedding.

Step	Media	Duration	Temperature
	HEPES buffer, pH 7.4	2 x 10 min	room temp.
	Osmium tetroxide 1 % *	1 h	room temp.
	HEPES buffer, pH 7.4 *	2 x 10 min	room temp.
dehydration	30 % ethanol	15 min	room temp.
	50 % ethanol	15 min	room temp.
	70 % ethanol	30 min	room temp.
	90 % ethanol	30 min	room temp.
	100 % ethanol	1 h	room temp.
	100 % ethanol	1 h	room temp.
embedding	30 % Epon in ethanol	1 h	room temp.
	50 % Epon in ethanol	1 h	room temp.
	70 % Epon in ethanol	1 h	room temp.
	90 % Epon in ethanol	1 h	room temp.
	100 % Epon	over night	room temp.
	100 % Epon	2 h	room temp.
	100 % Epon	72 h	60 °C

* not obligatory

Epon (Fluka, Munich, Germany)

Stock solution I

Epoxy embedding medium	62 g
Hardener DDSA (dodecenyl succinic anhydride)	100 g

Stock solution II

Epoxy embedding medium	100 g
Hardener NMA (nadic methyl anhydride)	89 g

Epon

Stock solution I	40 g
Stock solution II	60 g
Accelerator DMP 30 (2,4,6-tridimethylamino methyl phenol)	1 g

Epon should be freshly prepared for final embedding and polymerization steps. Excess Epon can be stored at -20 °C for several weeks and used for initial infiltration steps with low epoxy-ethanol ratio. The stock solutions can be stored at 4 °C for several months. Heating should be avoided while thoroughly mixing the stock solutions to prepare embedding medium.

III.2.2 Freeze Substitution and Low-Temperature Embedding

High-pressure frozen samples are ideally dehydrated below the recrystallization temperature of -130 °C, but this would be far too slow and only few solvents are able to dissolve ice at these temperatures. But recrystallization usually does not occur in hydrated specimens until approximately -80 °C and several solvents are available that dissolve ice in this temperature range in reasonable time. Anhydrous acetone is most commonly used as substitution medium (B.M. Humbel and Müller, 1984). For this project, acetone saturated with uranyl acetate and fluorescent dyes was applied.

Prior to freeze-substitution, excess 1-hexadecene is cautiously removed from the specimen under liquid nitrogen conditions and the sample is removed from the aluminium platelet. The samples are transferred into 1.5 ml Eppendorf tubes filled with precooled substitution medium, contained in transfer vessels (Hohenberg *et al.*, 1994). The freeze substitution is performed in an Leica automatic freeze substitution system EM AFS (Leica, Bensheim, Germany), leaving the samples in the dehydration medium for 40 h at -90 °C. Once the substi-

tution is completed, the specimens are allowed to slowly warm to -50 °C over a period of 20-24 h and washed twice with acetone and subsequently with ethanol until excess fluorescent stain is removed. The exact protocol is listed in Table 5. Subsequently the samples are infiltrated with low-temperature embedding resin (Lowicryl® HM20; Polysciences, Eppelheim, Germany). Concentrations of 30 % and 70 % of HM20 in ethanol are applied twice, each time for one hour, followed by pure HM20 over night. Prior to UV polymerization fresh HM20 is applied and the resin is cured at -35 °C, followed by further polymerization at room temperature.

Table 5: Protocol for freeze-substitution and low temperature embedding.

Step	Media	Duration	Temperature
dehydration	UAc & fluorescent stains [1] in acetone	40 h	-90 °C
	no change [2]	12 h	-70 °C
	no change	8-12 h	-50 °C
	acetone	1 h	-50 °C
	acetone	1 h	-50 °C
	ethanol	1 h	-50 °C
	ethanol	1 h	-50 °C
	ethanol	1 h	-50 °C
	ethanol	1 h	-50 °C
embedding	30 % HM20 in ethanol	1 h	-35 °C
	30 % HM20 in ethanol	1 h	-35 °C
	70 % HM20 in ethanol	1 h	-35 °C
	70 % HM20 in ethanol	1 h	-35 °C
	HM20	15-18 h	-35 °C
	HM20	2 h	-35 °C
	HM20 & UV polymerization	72 h	-35 °C
	UV polymerization	72 h	room temp.

[1] Nile blue sulphate (Merck, Darmstadt, Germany) & DiIC18 (Molecular Probes, Leiden, the Netherlands), or Safranine O (Merck, Darmstadt, Germany)

[2] if the specimen are still held in HPF-platelets, they are carefully loosened without removing them from the substitution medium

Lowicryl® HM20

Crosslinker D	2.98 g
Monomer E	17.02 g
Initiator C	0.10 g

Crosslinker and monomer are mixed gently by slowly rocking the vial from side to side. The formation of air bubbles or foaming needs to be avoided, as incorporation of oxygen impairs with polymerization. HM20 should be freshly prepared for final infiltration steps polymerization. Excess HM20 can be stored at -20 °C for several weeks and used for low concentration infiltration steps. Polymerization should be tested prior to application.

III.3 Sectioning

Very thin samples are required for the majority of microscopic techniques to enable the transmission of light or electrons for imaging. Therefore, sections of varying thickness are prepared, according to the intended microscopic application. Cryostat sections are used for many light microscopic investigations such as immunofluorescence (see chapter IV.3) or Fontana-Masson staining for melanin (see chapter IV.2.3). Semithin sections of resin embedded samples are also processed for light microscopy, while ultrathin sections are required for transmission electron microscopy.

III.3.1 Cryostat Sectioning

The frozen skin sample is transferred from liquid nitrogen into the cool chamber (T = -30 °C) of the Cryostat Leica CM 3050 (Leica, Bensheim, Germany) and embedded in TissueTek® (Leica, Bensheim, Germany). Bubbles within the TissueTek® need to be avoided as they may affect section quality. The TissueTek® is applied directly on the sample holder, adjusting the sample perpendicularly to the blade, so that cross-sections can be achieved that comprise every layer of the epidermis. To ensure consistent section thickness and avoid detaching of the sample from the TissueTek®, the embedded sample is allowed to adjust to the chamber temperature for 30 min before sectioning. Disposable steel blades (Leica, Bensheim, Germany) are used, that are aligned at an angle of 5 degrees. Section thickness varies from 2-25 µm. For standard immunofluorescence applications (see chapter IV.3) sections of 5-7 µm are obtained. The sections are picked up on silanized coated glass slides (Histobond®, Marienfeld, Lauda-Königshofen, Germany), dried at room temperature and stored at -20 °C.

III.3.2 Ultramicrotomy

Resin embedded skin samples are cut using an ultramicrotome Ultracut UCT (Leica Bensheim, Germany). The samples are trimmed to remove excess surrounding resin and to create a plain sample surface (blockface) using a diamond trimming knife (Diatome, Biel, Switzerland). The edges of the blockface should be approximately parallel, forming a trapezoid or rectangle. If the sample has been treated with fluorescent dyes prior to embedding, the blockface can be examined in a confocal laser scanning microscope.

The sample is then cut into semithin sections (200-500 nm) for light microscopic investigations, or ultrathin sections (50-90 nm) for electron microscopy. The tilt of 35° of the utilized diamond knife (Diatome, Biel, Switzerland) is specially adapted for sectioning Lowicryls and relatively soft non-homogenous specimens like skin. The clearance angle of the ultramicrotome is 6 °. The sections are collected on a water surface, adjacent to the knife, and smoothed out by chloroform vapours. The thickness of the sections can then be controlled by means of a colour scale.

Semithin sections are picked up in a droplet of water using a metal loop (Perfect Loop, Diatome, Biel, Switzerland), mounted on adhesive microscope slides (Histobond®, Marienfeld, Lauda-Königshofen, Germany) and dried on a hot plate at 60 °C. Ultrathin sections are mounted directly on carbon coated copper grids (Quantifoil®, Jena, Germany).

IV Staining Techniques for Melanocytes and Melanosomes

Several staining techniques were employed for this project to enable general evaluation of the samples as well as specific description of melanocytes and melanin distribution, using plain frozen sections and differently embedded specimen. All sections are mounted in Leica CV Ultra® mounting medium, using a Leica CV5030 fully automated glass coverslipper (Leica Microsystems, Wetzlar, Germany).

IV.1 Common Histological Staining Techniques

Two general staining methods – hematoxylin eosin stain and toluidine blue stain – were used for the general characterization and evaluation of the skin samples.

IV.1.1 Hematoxylin and Eosin Stain

The hematoxylin eosin stain is the most widely used staining method in histology and histopathology. It involves the combinations of the basic dye hematoxylin, which colours nuclei with blue-purple hue, and alcohol-based acidic eosin Y, which colours the cytoplasm bright pink. Melanin is stained brown. The stain is applied to semithin resin sections (200-500 nm).

Procedure

The sections are etched in hydrogen peroxide for one hour prior to staining in hematoxylin solution over night at room temperature. The sections are washed in running tap water for 30 minutes and stained in eosin solution for 5 minutes at 60 °C. Subsequently, the sections are washed in distilled water, and air dried before mounting.

Hematoxylin staining solution

Hematoxylin solution, Harris Modified	50 ml
Hematoxylin solution, Gill No. 3	50 ml

The solution is freshly prepared and centrifuged and filtered before usage.

Eosin staining solution

Eosin yellowish solution (Fluka, Munich, Germany)	1 ml
Aqua bidest.	ad 100 ml
Acetic acid	1 drop

The solution can be stored at room temperature for several months. It needs filtering before usage.

IV.1.2 Toluidine Blue Staining

Toluidine blue is another general histological stain, yielding purplish-blue staining of cytoplasm and nuclei while melanin appears dark bluish-black. This staining method is easier to use and faster than hematoxylin and eosin stain. It is also applied to semithin resin sections.

Procedure

After etching with hydrogen peroxide solution for one hour, the sections are stained on a hot plate for 20 minutes. If the stain is too intense, it can be modified by briefly washing in ethanol. The sections are washed in distilled water and mounted.

Sodium tetraborate decahydrate buffer

Sodium tetraborate decahydrate	10 g
Aqua bidest.	1000 ml
Sodium hydroxide solution (Merck, Darmstadt, Germany)	ad pH >12

Toluidine blue staining solution

Toluidine blue (Fluka, Munich, Germany)	5 g
Sodium tetraborate decahydrate buffer	100 ml

The solutions can be stored at room temperature for several months, but need to be filtered before usage.

IV.2 Specific Histochemical Reactions

A number of methods are described explicitly for the identification of melanin and melanocytes (Romeis, 1968; Churukian, 2002). The most commonly used techniques, including the Fontana-Masson silver staining, the DOPA reaction and immunohistochemistry are described in this chapter.

IV.2.1 Nile Blue Staining

Lillie's Nile blue staining (Romeis, 1968) is a histological method applied to paraffin or frozen sections, that yields dark green staining for melanin against a light blue background of cytoplasm and nuclei.

Procedure

Paraffin sections are deparaffinized in xylene for 10 minutes, followed by hydration in descending concentrations of ethanol (100 %, 90 %, 60 % and 30 %).
All sections are taken to distilled water for 5 minutes and subsequently stained in Nile blue solution for 20 minutes. The sections are then washed in running tap water for 10-20 minutes and rapidly rinsed in 1 % sulphuric acid. The sections are then dehydrated in a series of increasing concentrations of ethanol (30 %, 60 %, 90 % and 100 %) for 10 minutes in each solution. Paraffin sections are cleared in xylene for 10 minutes and the sections are mounted in Leica CV Ultra® mounting medium.

Lillie's Nile blue staining solution

Nile blue (hydrogen sulphate) (Merck, Darmstadt, Germany)	0.05 g
Sulphuric acid, extra pure (Merck, Darmstadt, Germany)	1 ml
Aqua bidest.	ad 100 ml

The solution can be stored at room temperature for several months, but needs to be filtered before usage.

IV.2.2 DOPA Oxidase Reaction

In the initial steps of melanogenesis, tyrosinase or DOPA oxidase, acts on tyrosine to produce dihydroxy-phenylalanine (DOPA), which is subsequently further oxidized by the same enzyme to form an intermediate pigment which then polymerizes to produce melanin (see chapter B.I.2.3). Bloch first described the possibility to demonstrate tyrosinase activity by administering synthetic DOPA, which is oxidized to form an insoluble brown-black pigment in fresh frozen tissue sections (Bloch *et al.*, 1927). This method can be utilized to identify melanocytes but not for the visualization of melanosomes in keratinocytes, as the enzyme tyrosinase is no longer active in mature melanosomes.
Fresh frozen sections or frozen sections fixed in PFA-fixative for no longer than 2-3 hours can be used, the best results are described for postfixed cryostat sections. Frozen sections with and without postfixation were tested, as well as PFA-fixed paraffin-embedded tissue.

Procedure

Paraffin sections are deparaffinized and hydrated as described above. A part of the frozen sections is postfixed in IEM-fixative for 10 min, the other part is left without fixative treatment. After washing in distilled water for a few minutes, the sections are placed in the DOPA incubating solution for 30 minutes at 37 °C. Control sections are treated with sodium cacodylate-buffer. Then the incubating solution is replaced with fresh solution and the developing reaction is examined microscopically every 30 minutes. The reaction is completed in 2-4 hours. The sections are washed in aqua bidest. and counterstained in neutral red for 5 minutes. The sections are then dehydrated in a graded series of ethanol (see above). Paraffin sections are additionally cleared in xylene before mounting using the Leica CV5030 fully automated coverslipper.

DOPA incubating medium

Dihydroxy-phenylalanine (DOPA)	0.1 g
Sodium cacodylate-buffer, pH 7.4	100 ml

Aqueous Neutral red 0.5 % (w/v)

Neutral red	0.5 g
Aqua bidest.	100 ml

The solutions can be stored at room temperature for several weeks. Neutral red solution needs to be filtered before usage.

IV.2.3 Fontana-Masson Silver Staining

The Fontana-Masson silver staining is a histological staining technique that is based on the argentaffin properties of melanin. Melanin as a powerful reducing agent can reduce ammoniacal silver solutions to form metallic silver without the use of an extraneous reducer. Black silver granules deposit on the melanin, that can be visualized with light microscopy (Romeis, 1968). Masson's method (1914) using Fontana's silver solution (1912) and its various modifications are now a widely used routine method for the detection of melanin (and its precursors) in skin and other tissues.

The method is described to work on all kind of sections, including resin sections, although some adjustments are said to be necessary (Churukian, 2002). Paraffin and frozen sections are most commonly used with PFA being the preferred fixative.

For this project, the Fontana-Masson staining was applied to cryostat sections (with IEM-prefixation and without), and PFA-fixed, paraffin-embedded sections were used as a control. HM20-resin sections were also investigated.

Procedure

Paraffin sections are deparaffinised as described in chapter IV.2.1. Frozen sections (only sections without chemical pretreatment) are postfixed with PFA-fixative for 10 min. Resin sections are etched in hydrogen peroxide solution for one hour.

Prior to treatment with the ammoniacal silver solution the sections are washed in three changes of bidest. water. The sections are stained in a glass Coplin jar covered with aluminium foil over night. Control sections are kept in aqua bidest. during incubation. Subsequently, the sections are washed in several changes of double distilled water and treated

with aqueous sodium thiosulphate for one minute. After repeated washing the sections are lightly counterstained with aqueous neutral red (see above) for 5 minutes.

Paraffin and frozen sections are then dehydrated in a series of ascending concentrations of ethanol (see above). Paraffin sections are additionally cleared in xylene before mounting. Resin sections are not dehydrated. The entire procedure is performed at room temperature, following the protocol displayed in Table 6. It is essential to use only absolutely clean glass-ware, as the silver solution reacts with any residual contamination and false-positive precipitates will form on the sections.

Table 6: Protocol for Fontana-Masson silver staining.

Step	Reagent	Duration
washing	Aqua bidest.	3 x 10 min
staining	Fontana's silver solution	over night
washing	Aqua bidest.	3 x 10 min
secondary antibody labelling	5 % aqueous sodium thiosulphate (hypo)	1 min
washing	Aqua bidest.	3 x 10 min
counterstain	0.5 % aqueous Neutral red	5 min
washing	Aqua bidest.	3 x 10 min
dehydration *	graded ethanol series	10 min for each solution
mounting	Leica CV Ultra® mounting medium	let dry over night

* not necessary for resin sections

Fontana's silver solution

Silver nitrate (Sigma-Aldrich, Munich, Germany)	10 g
Aqua bidest.	100 ml
Ammonia, concentrated (Merck, Darmstadt, Germany)	

20 ml of aqueous silver nitrate solution (10 %) are placed in a glass flask. Concentrated ammonia is added drop by drop while constantly agitating the flask, until the formed precipitate dissolves and a faint opalescence is observed. If too much ammonia is added, the opalescence can be restored by the addition of a few drops silver nitrate solution. This titration is critical if the method is to work consistently well. 20 ml double distilled water is added and the solution is filtered into a dark glass bottle. The solution can be stored at 4 °C for up to 4 weeks. Ammoniacal silver solutions are potentially explosive if stored incorrectly.

Aqueous Sodium thiosulphate (hypo) 5 % (w/v)

Sodium thiosulphate	5 g
Aqua bidest.	100 ml

The solution should be prepared directly before use.

IV.3 Immunofluorescence Assay

The immunofluorescence assay (IFA) is a technique based on the highly specific and sensitive detection of proteins or rather a small region of the protein, the epitope, by IgG-antibodies. Some immunostaining agents can be applied in a single step procedure, where the primary antibody is directly linked to a colouring agent, in this case a fluorophore. But most commonly two sets of antibodies are employed: a primary antibody binds directly to the antigen of interest and is subsequently targeted by a dye-coupled secondary antibody, recognizing an epitope of the primary antibody specific for the host species in which it was generated. This results in an amplification of the signal, as multiple secondary antibodies will bind to a primary antibody.

Procedure

Cryostat sections are thawed and dried and the tissue sections are encircled using a delimiting pen (Dako Pen, DAKO, Glostrop, Denmark) to prevent excessive spreading of the reagents. The respective solution (see protocol; Table 7) is pipetted onto the tissue sections (volume will depend on tissue size, usually 50 µl per section) and the glass slides are covered with a Petri dish and aluminium foil to prevent drying-up and possible bleaching of the fluorescent stains during incubation. The droplets are removed with a pipette to avoid mixing of different incubation solutions. Antibody dilutions and nuclear stains are prepared with blocking buffer. Blocking, washing and incubation steps are carried out at room temperature.

Blocking buffer

Bovine Serum Albumin (BSA) (Merck, Darmstadt, Germany)	0.80 g
Gelatine from cold water fish skin	1.00 g
PBS	ad 100 ml

The buffer can be stored at -20 °C for several months.

Table 7: Protocol for immunofluorescence assay.

Step	Reagent	Duration
blocking of unspecific binding sites	Normal Donkey Serum	120 min
washing	blocking buffer	2 x 5 min
primary antibody labelling	species 1-α-protein 1 species 2-α-protein 2	120 min
washing	blocking buffer	2 x 5 min
secondary antibody labelling	Cy3 species 3-α-species 1 Cy5 species 3-α-species 2	30 min
washing	blocking buffer	2 x 5 min
nuclear staining	Sytox Green® or DAPI	10-30 min
washing	blocking buffer	2 x 5 min
mounting	Leica CV Ultra® mounting medium	let dry over night

Prior to antibody application, unspecific binding sites are blocked with normal donkey serum. The sections are washed twice with blocking buffer and incubated for two hours with the primary antibody. Specifications of the investigated antibodies and the applied dilutions are listed in Table 8. The optimal working concentration is determined for each antibody separately. If the concentration recommended by the supplier is not appropriate, the antibody is applied in twofold concentration as well as twofold and fivefold dilution, compared to the recommended dilution. If no information is provided by the supplier, the antibody is used initially in tenfold dilution and the optimal concentration is approached in twofold dilution steps. Each antibody is tested on frozen sections with and without chemical pre-fixation and a negative control is always performed, using blocking buffer instead of the primary antibody. However, for some antibodies no specific labelling can be achieved; these are indicated in Table 8. After repeated washing, the secondary antibody is applied for 30 min. Cy2- and Cy3-conjugated antibodies are administered in two-hundredfold and the Cy5-conjugated antibodies in hundredfold dilution (for specifications see Table 9). Subsequently, the nuclei are stained either with DAPI for 10 min or with Sytox Green® for 30 min and the sections are mounted in Leica CV Ultra® mounting medium, using the Leica CV5030 fully automated glass coverslipper. The sections are stored at 4 °C and in a darkened place to minimize photo bleaching. The sections are investigated using a confocal laser-scanning microscope (CLSM) that is equipped with three different excitation wavelengths, which can be recorded simultaneously, thus enabling “triple-labelling”.

Table 8: Primary antibodies.

Antibody (antigen)	Labelled Cell Type/ Structure	Host Species	Clonality	Supplier	Dilution
α-Clathrin	membrane vesicle marker	goat	polyclonal	Abcam	1: 20 (1)
α-Collagen IV	basement membrane	rabbit	polyclonal	Novus Biologicals	1: 200
α-EEA 1 (early endosomal antigen 1)	early endosomes	rabbit	polyclonal	Abcam	1: 250 (2)
α-Keratin	cytoskeleton/ keratinocytes	rabbit	polyclonal	BioTrend	1: 200
α-Laminin 2	basement membrane	rat	monoclonal (4H8-2)	Sigma	1: 200 (3)
α-MiTF (Microphthalmia transcription factor)	melanocytes	mouse	monoclonal (C5 + D5)	Neo Markers	1: 25 - 1: 50 (1)
α-S100	dendritic cells	rabbit	polyclonal	BioTrend	1: 800 (2)
α-S100	dendritic cells	rabbit	polyclonal	Serotec	1: 40 (2)
α-Tubulin	cytoskeleton	rat	monoclonal (2Q467)	US Biological	1: 10 (1)
α-Tyrosinase	melanocytes	mouse	monoclonal (T311)	Oncogene	1: 10 - 1: 30 (1)
α-Vimentin	cytoskeleton/ melanocytes	goat	polyclonal	US Biological	1: 40 (3)
Mel-1 (GD3)	melanocytes	mouse	monoclonal (R24)	Signet	1: 40 (1)
Mel-5 (TRP1)	melanocytes	mouse	monoclonal (Ta99)	Signet	1: 400
Melanoma Ab-1 (gp100)	melanocytes	mouse	monoclonal (HMB45)	Neo Markers	1: 40 - 1: 80 (1)
Melanoma Ab-2 (gp100)	melanocytes	mouse	monoclonal (HMB50)	Neo Markers	1: 100 (3)
Melanoma Ab-3 (gp100)	melanocytes	mouse	monoclonal (HMB45 + 50)	Neo Markers	1: 100 (3)
Melanoma Ab-5 (gp100)	melanocytes	mouse	monoclonal (NKI/beteb)	Neo Markers	1: 100 (3)
Phalloidin Alexa Fluor® 488	cytoskeleton	toxin	-	Molecular Probes	1: 400 (2)
Phalloidin Alexa Fluor® 568	cytoskeleton	toxin	-	Molecular Probes	1: 200 (2)

(1) no staining results – dilution recommended by supplier
(2) only IEM-fixed frozen sections
(3) only frozen sections without chemical pre-treatment

Table 9: Secondary antibodies and nuclear stains.

Antibody	Host Species	Conjugate	Supplier	Dilution
α-goat, Cy 2	donkey	Cy2 (Carbocyanin)	Dianova	1: 200
α-goat, Cy 3	donkey	Cy3 (Indocarbocyanin)	Dianova	1: 200
α-goat, Cy 5	donkey	Cy5 (Indodicarbocyanin)	Dianova	1: 100
α-mouse, Cy 2	donkey	Cy2 (Carbocyanin)	Dianova	1: 200
α-mouse, Cy 3	donkey	Cy3 (Indocarbocyanin)	Dianova	1: 200
α-mouse, Cy 5	donkey	Cy5 (Indodicarbocyanin)	Dianova	1: 100
α-rabbit, Cy 2	donkey	Cy2 (Carbocyanin)	Dianova	1: 200
α-rabbit, Cy 3	donkey	Cy3 (Indocarbocyanin)	Dianova	1: 200
α-rabbit, Cy 5	donkey	Cy5 (Indodicarbocyanin)	Dianova	1: 100
α-rat, Cy 2	donkey	Cy2 (Carbocyanin)	Dianova	1: 200
α-rat, Cy 3	donkey	Cy3 (Indocarbocyanin)	Dianova	1: 200
α-rat, Cy 5	donkey	Cy5 (Indodicarbocyanin)	Dianova	1: 100
Normal Donkey Serum	donkey	-	Dianova	1: 10
DAPI	-	-	Molecular Probes	1: 10000
Sytox Green®	-	-	Molecular Probes	1: 10000
Sytox Orange®	-	-	Molecular Probes	1: 10000

IV.4 Staining for Transmission Electron Microscopy

Compounds of heavy metals such as lead or uranium are used to enhance the contrast for TEM investigation. The dense electron clouds of the heavy atoms interact strongly with the electron beam of the electron microscope and since the heavy atoms deposit selectively in the sample they give contrast between different structures and thus enhance structural detail.

Procedure

Ultrathin resin sections mounted on copper grids are placed upside down on a droplet of the respective solution. Afterwards the grids are carefully dried on filter paper. The exact protocol is listed in Table 10. The stained sections are examined in a Tecnai 12 transmission electron microscope (FEI, Eindhoven, the Netherlands).

Table 10: Protocol for heavy metal staining of resin sections for TEM.

Step	Reagent	Duration
staining	Uranyl acetate	30 min
washing	double distilled water	2 x 5 min
staining	Lead citrate	1 min
washing	Sodium hydroxide solution 0,02 M	30 s
washing	double distilled water	2 x 5 min

Uranyl acetate 1 % (w/v)

Uranyl acetate · 2 H_2O, research grade (SERVA, Heidelberg, Germany)	0.10 g
Ethanol (Merck, Darmstadt, Germany)	5 ml
Aqua bidest.	ad 10 ml

The solution can be stored at 4 °C for several weeks. The solution should be centrifuged before application, to remove crystals of uranyl acetate.

Lead citrate, alkaline

Lead citrate · 3 H_2O, pure (SERVA, Heidelberg, Germany)	1.33 g
Tri-Sodium citrate dihydrate, extra pure	1.76 g
Aqua bidest.	ad 50 ml
Sodium hydroxide solution (Merck, Darmstadt, Germany)	

Bidest. water is boiled and cooled. Tri-sodium citrate dihydrate is dissolved, then the lead citrate is added. Sodium hydroxide solution is added until the solution becomes clear. Incorporation of oxygen should be avoided. The solution can be stored at 4 °C for several weeks, but should not be used in case of turbidity. The solution should be centrifuged before application, to remove crystalline lead carbonate.

V Cytochemical Localisation of NADPH Oxidase Activity

The demonstration of NADPH oxidase in the human epidermis is realized by adapting a protocol for the cytochemical detection of hydrogen peroxide in biological tissues, published by Ellis and Grant (2002). The assay employs the principles of cerium capture cytochemistry.

H_2O_2 produced via NADPH oxidase reacts with cerous ions to form a fine electron-dense precipitate (cerium perhydroxide), that can be visualized by CLSM or TEM. Further amplification with diaminobenzidine (DAB) enables the visualization by conventional light microscopy.

Procedure

Skin biopsies are fixed in cold fixation buffer for one hour as soon as possible after procurement. The samples are washed four times in cold sodium cacodylate buffer containing DMSO and sucrose to remove the fixative. The specimens are kept in washing buffer over night in the refrigerator and until further processing the following day. Then, the samples are brought to room temperature during two more washing steps with 0.1 M glycine added to the washing buffer to remove unbound aldehydes.

The samples are preincubated for 30 minutes in a shaking water bath (T = 37 °C) followed by four changes of complete incubation medium, each for 30 minutes at 37 °C. Preincubation is indispensable to ensure sufficient penetration of cerium, because of its slow penetration into tissues or cells. The addition of triton X-100 to the incubation media supports the penetration. Any H_2O_2 produced by catalase or glutathione peroxidase during the reaction is scavenged by specific inhibitors such as aminotriazole or sodium azide in the preincubation and reaction medium. After two hours, the reaction is stopped by washing once in cold sucrose-containing tris-maleate buffer (pH 7.5) followed by cold 0.1 M sodium cacodylate buffer with sucrose. Phosphate buffers need to be avoided, because phosphates react with cerium to form non-specific precipitates. Controls for the specificity of the reaction are performed by either omitting the substrate (β-NADPH) for the reaction, or including specific inhibitors of NADPH oxidase (DPI) and other H_2O_2 generating enzymes, such as xanthine oxidase (inhibitor allopurinol). The inhibitors are included in the preincubation medium.

Depending on the intended microscopic investigation, the samples are then postfixed overnight at 4 °C in osmium tetroxide for electron microscopy or processed for LM-investigation. The samples are incubated with amplification medium for 30 minutes at 40 °C. Fresh incubation medium is applied after 15 minutes and the reaction is stopped by washing in cold tris-HCl buffer (pH 7.6). The exact protocol is displayed in Table 11. The specimens are then either dehydrated and embedded in Epon or plunge frozen and sectioned for LM-examination. Resin sections can be investigated in TEM without post-staining or in the reflection mode of CLSM.

Table 11: Protocol for the cytochemical demonstration of NADPH oxidase.

Step	Reagent	Duration	Temp.	Comment
fixation	fixative	1 h	4 °C	agitate
stop of fixation	washing buffer, pH 7.4	4 x 15 min	4 °C	agitate
washing	washing buffer, pH 7.4	over night	4 °C	
washing	0.1 M glycine in washing-buffer, pH 7.4	2 x 15 min	room temp.	agitate
preincubation	preincubation medium	30 min	37 °C	agitate
incubation	complete reaction medium	4 x 30 min	37 °C	agitate
stop of reaction	7 % sucrose in tris-maleate buffer, pH 7.5	5 min	0 °C	
washing	7 % sucrose in 0.1 M Na-cacodylate buffer, pH 7.4	5 min	0 °C	
followed by:				
amplification for **LM**	amplification medium	2 x 15 min	40 °C	agitate
stop of amplification reaction & washing	Tris-HCl buffer, p 7.6	3 x 5 min	0 °C	
or				
post-fixation for **TEM**	1 % osmium tetroxide 7 % sucrose in 0.1 M Na-cacodylate buffer, pH 7.4	over night	4 °C	
washing	7 % sucrose in 0.1 M Na-cacodylate buffer, pH 7.4	2 x 15 min	4 °C	

Fixative

Acrolein, puriss. (Fluka, Munich, Germany)	5 ml
0.1 M Sodium cacodylate buffer, pH 7.4	ad 100 ml

The fixative should be prepared fresh. Acrolein should be handled only in a properly functioning fume hood. Bisulphite should be available to neutralize acrolein.

Washing buffer

Sucrose	50 g
Dimethyl sulfoxide (DMSO)	10 g
0.15 M Sodium cacodylate buffer, pH 7.4	1000 ml

Tris-maleate buffer 0.1 M, pH 7.5

Tris maleate salt	23.72 g
Aqua bidest.	1000 ml
1 M Maleic acid	ad pH 7.5

Buffers can be prepared ahead of time and are stored at 4 °C for several weeks.

Triton X-100 stock solution

Triton X-100	1 ml
Aqua bidest.	ad 100 ml

Preincubation medium

Cerium chloride	74.5 mg
3-Amino-1,2,4-triazole	84.1 mg
Sucrose	7 mg
Tris maleate buffer, pH 7.5	100 ml
Triton X-100 stock solution	10 drops

For controls of specificity of the reaction the preincubation medium includes:

Diphenyleneiodonium chloride (DPI) (inhibitor of NADPH oxidase)	31.5 mg
or Allopurinol (inhibitor of xanthine oxidase)	13.6 mg

Complete reaction medium

Preincubation medium	10 ml
β-Nicotinamide adenine dinucleotide 2’ phosphate, reduced tetrasodium salt (β-NADPH)	5.68 mg

Aminotriazole and β-NADPH are toxic. Inhalation, swallowing and contact with skin and eyes must be avoided.

Amplification medium

Cobalt chloride	1 mg
3,3′-Diaminobenzidine tetrahydrochloride (DAB)	0.05 mg
Hydrogen peroxide solution 35 % (Fischer Scientific GmbH, Schwerte, Germany)	0.02 ml
Tris-HCl buffer, pH 7.6	ad 100 ml

Preincubation medium, complete reaction medium and amplification medium should be prepared fresh immediately before use and must be filtered.

VI Chemical Analysis of Melanin in Biological Samples

VI.1 Chemical Analysis of Total Eumelanin and Pheomelanin Content

Thirty skin samples, five of each Fitzpatrick's skin phototype I-VI were analyzed for eumelanin and pheomelanin content by Dr. Wakamatsu of the Fujita Health University in Toyoake, Japan (S. Ito and Jimbow, 1983; Wakamatsu and Ito, 2002). The samples were freeze-dried and stored in Eppendorf tubes and packed in transport containers with anhydrous silica gel to ensure dry conditions for shipment.

Procedure

Samples and synthetic melanins investigated as high standards are dried over diphosphorus pentoxide and sodium hydroxide overnight under vacuum conditions, and are then equilibrated with moisture over saturated calcium chloride solution to constant weight. The samples are homogenized in double distilled water (5 mg synthetic melanin in 1 ml, or 3 – 5 mg skin sample in 0.5 ml) and disintegrated by ultrasound. Aliquots of 200 µl (100 µl for melanin standards) are used for the chemical degradation. Oxidation of eumelanin with potassium permanganate ($KMnO_4$) yields the specific degradation product PTCA, which is quantified by HPLC. Pheomelanin is determined by HPLC-analysis of the specific degradation product 4-AHP, produced by HI reductive hydrolysis. All chemicals used are of highest purity available. PTCA and 4-AHP content of the samples is determined from the HPLC results using the following formulae.

Calculation formula for PTCA values (ng PTCA/ mg wet sample):

$$\frac{\text{peak height of sample}}{\text{peak height of standard}} \times \frac{1000 \text{ ng/ml}}{\text{sample weight (mg)}} \times \frac{80 \text{ µl}}{80 \text{ µl}} \times 0.2 \text{ ml}$$

Calculation formula for 4-AHP values (ng 4-AHP/ mg wet sample):

$$\frac{\text{peak height of sample}}{\text{peak height of standard}} \times \frac{500 \text{ ng/ml}}{\text{sample weight (mg)}} \times \frac{730 \text{ µl}}{100 \text{ µl}} \times \frac{10 \text{ µl}}{10 \text{ µl}} \times 0.2 \text{ ml}$$

The amount of eumelanin contained in a sample is obtained by multiplying the amount of PTCA by a conversion factor of 160. For pheomelanin the conversion factor for the amount of 4-AHP is 9.

VI.2 Melanin Degradation *In Vitro*

Melanin extracted from the ink of *Sepia officinalis* (readily purchased from Sigma-Aldrich) is incubated with hydrogen peroxide in a 1 ml Eppendorf tube for 48 h, either in the dark or under a UV lamp. The solution is subsequently dried using a vacuum pump. The residue is eluted in PBS buffer and analyzed in size exclusion chromatography (SEC).

VI.3 Analysis of Melanin Degradation Products by SEC

Size exclusion chromatography (SEC) is widely used for the purification and analysis of polymers, such as proteins, polysaccharides, and nucleic acids. It is a chromatographic method in which molecules are separated based on the size of the molecules in their respective solvent (the so called hydrodynamic volume). Molecules of different sizes will elute through a stationary phase at retention volumes.
PBS buffer is used as eluent for both, the degradation products of *Sepia* melanin and the suspension of human skin (see chapter E.V.1). The eluent is collected after passing the column (Viscotek aqueous column G3000PWXL, Viscotek, Houston, Texas, USA), and a triple detector array (TDA^{TM} Model 302, Viscotek), including light scattering detector, viscosimeter detector and refractive index detector. The collected fractions are further analyzed by ESI-MS.

VI.4 Analysis of Melanin Degradation Products by ESI-MS

Electrospray ionisation (ESI) is a technique used in mass spectrometry (MS) to produce ions. The analyte is dissolved in a polar solvent, which is usually more volatile than the analyte itself, e.g. water, alcohols or acetonitrile. The analyte is present either in a protonated form or as an anion. This liquid is pushed through a charged metal capillary. The liquid pushes itself out of the capillary, because of the repelling effect of equal charges within the solution. Thus, an aerosol of approx. 10 µm droplets is formed.

Nitrogen gas is used as a carrier gas to help nebulize the liquid and evaporate the solvent. During evaporation, the repulsive Coulombic forces between charged analyte molecules cause the droplets to break up, producing gaseous ions. These ions are then separated according to their mass-to-charge ratio and analyzed by mass spectroscopy.
The fractions collected after SEC are dissolved in water or trifluoroacetic acid (TFA), desalinated, and analyzed using an Esquire LC ESI-MS (Bruker Daltonik GmbH, Bremen, Germany).

VII Microscopic Documentation

VII.1 Light Microscopy

Histological stains such as hematoxylin and eosin, toluidine blue and the melanin-specific stains are documented using a Zeiss Axioscope (Carl Zeiss, Jena, Germany) equipped with a digital colour camera Leica DFC 300 FX. An oil-immersion objective (40x/ NA 1.0) is used. Overlapping images are acquired spanning the entire epidermis of each sample. The images are subsequently stitched together using the photomontage mode of ImageAccess database and image processing software (Imagic AG, Glattbrugg, Switzerland).

VII.2 Confocal Laser Scanning Microscopy

Immunofluorescently labelled cryostat sections are examined by confocal laser scanning microscopy (CLSM), which enables the recording of high-resolution, three-dimensional images stacks. The employed Leica TCS SP CLSM (Leica Microsystems, Wetzlar, Germany) is equipped with an argon/ krypton laser with excitation wavelengths of 488 nm, 568 nm and 647 nm. With a spectrometer prism and three photomultiplier tubes, it is possible to detect up to three fluorescence signals simultaneously, enabling the investigation of multi-labelled specimen. Since most fluorophores have a broad emission spectrum, excitation and detection can be controlled sequentially, avoiding artefacts.
For optimal image quality oil-immersion objectives are used (20x/ NA 0.7, 40x/ NA 1.0, 63x/ NA 1.3; all from Leica). Three-dimensional image stacks are obtained by varying the plane of focus in 0.2-0.5 µm-steps, the single images have a size of 1024 x 1024 pixel^2. For small volumes, a maximum projection can be generated displaying the maximum intensity pixel of

each sampling point of the image stack, superimposed along the projection axis. Larger volumes can be visualized and reconstructed using Imaris 4.0 (Bitplane, Zurich, Switzerland; see chapter VIII.2).

The reflection mode of the CLSM is applied to visualize the cerium precipitate formed in skin samples by cytochemical NADPH oxidase localisation reaction (see chapter V). Melanosomes in resin-embedded skin samples can also be visualized in this way.

VII.3 Transmission Electron Microscopy

The transmission electron microscope Tecnai G^2 12 BioTwin (FEI, Eindhoven, the Netherlands) is equipped with a lanthanum hexaboride (LaB_6) cathode, that is operated with an acceleration voltage of 120 kV yielding a beam current of 2-3 µA. A single tilt holder (Gatan, Pleasanton, CA, USA) is used to insert the specimen into the microscope. Images are recorded in bright field mode using a wide angle CCD camera (image resolution 1024 x 1024 $pixel^2$). The microscope is additionally equipped with a post-column energy filter (Gatan GmbH, München, Germany) to enable electron energy loss spectroscopy (EELS).

A semi-automatic tool facilitates the recording of mosaics, i.e. a series of high-magnification images that combine to make a large overview of the specimen area investigated. The Tecnai Photomontage option ensures sufficient overlap between images necessary for reassembly and minimizes the number of images needed to cover the entire region of interest (ROI). Reassembly is performed either manually using CorelDRAW® (Corel Corp., Ottawa, Ontario, Canada) or ImageAccess, or automatically employing RIA2D, a mosaic generating tool (see chapter VIII.3).

VII.4 Reflectance Spectroscopy

Objective measurement of visible skin colour is performed by reflectance spectroscopy using a Dr. Lange Spectro-pen® (Dr. Bruno Lange GmbH, Düsseldorf, Germany). Fivefold measurements are conducted. The results are displayed in the Commission International d'Eclairage (CIE) *L*a*b** colour system, in which colours are described by their lightness value (*L**), the amount of green or red (*a**), and the amount of yellow or blue (*b**) they contain. The *L** value among with the *b** value is used to measure pigmentation, the *a** value best captures erythema or skin redness.

VIII Image Processing

VIII.1 Image Archiving

ImageAccess Enterprise 5 (Imagic AG, Glattbrugg, Switzerland) is utilized for digital image archiving. The database simplifies management of large amounts of images and enables directed retrieval of single image. Additionally, the software features some aspects of image processing, such as calibration, measurement and annotation as well as interactive image assembly. This image assembly tool is designed to handle small amounts of images (up to 20 images at a time) and is used to reassemble LM or CLSM-images to generate overviews of entire sections and even small mosaics of TEM-images. However, most TEM-mosaics comprise of 80-100 (or more) images and overextend the capacity of this tool.

VIII.2 3D-Reconstruction and Visualization

CLSM image stacks are processed with the Imaris® visualization software for microscopic 3D data, release 4.0 (Bitplane AG, Zurich, Switzerland). Imaris® facilitates the visualization of three-dimensional image stacks as well as the modification of individual image parameters, such as channel colour, geometrical settings or threshold cut-off if necessary. In addition to displaying, the image stacks in 3D, Imaris features the calculation of isosurfaces, 3D-representaions as a solid surface. The isosurface represents the voxels of the image stack of an intensity range defined by thresholding.

VIII.3 Image Assembly

The mosaic generating tool RIA2D (Rigid Image Aligner in 2D) was especially developed to reassemble mosaics of TEM images, acquired with the Photomontage tool of the employed Tecnai G^2 12 BioTwin. It refers to the text file, generated by the Photomontage tool, to determine the approximate position of each single image before applying the cross-correlation based algorithm for exact image assembly. A minimum image overlap of 10 % is required to achieve adequate results. An example of reassembled TEM-images is displayed in Figure 13.

VIII.4 Counting Melanosomes

The TEM-mosaics are acquired to give an overview of the entire epidermis. This allows the investigation of whole cells and avoids double analysis of the same cell in different images, covering adjacent areas. The melanosome distribution is determined per cell by counting melanosomes and melanosome clusters, considering the amount of melanosomes that form the respective clusters, and correlating the numbers to the area of the analyzed cell.

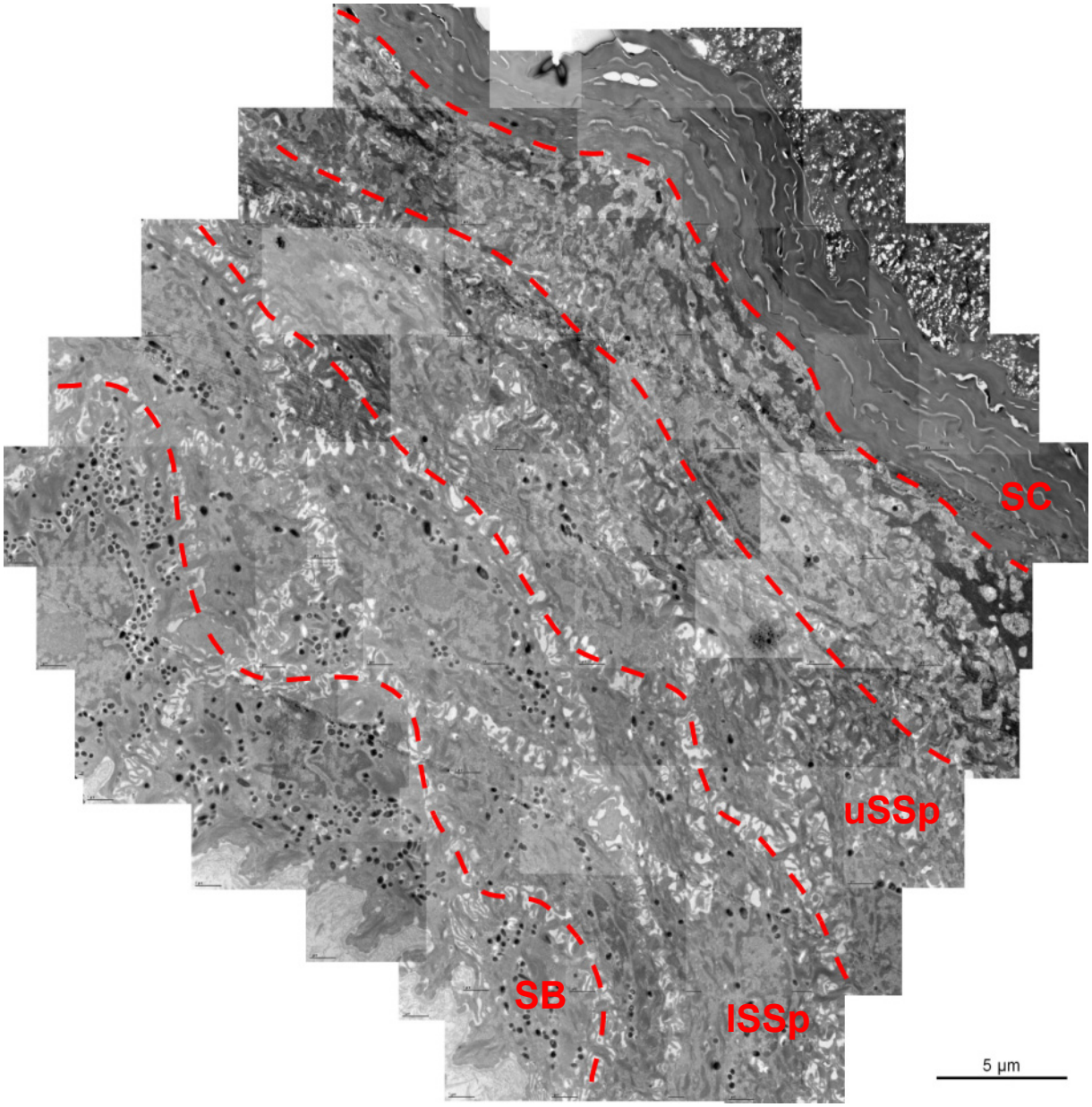

Figure 13: Annotated TEM-mosaic. The mosaic covers the entire epidermis from SC (on top) to basement membrane (bottom). The boundaries of the epidermal layers – *St. corneum*, upper *St. spinosum*, lower *St. spinosum* and *St. basale* – are marked in red. The *Stratum granulosum* (between SC and uSSp) is not analyzed. Ten cells of each layer are investigated. Melanosome numbers and the area of the respective cell are determined. *Bar: 5 µm*

Four layers of the epidermis are distinguished: the *Stratum corneum* (SC), the *Stratum spinosum* which is further divided into an upper (uSSp) and lower (lSSp) part, and the *Stratum basale* (SB). The *Stratum granulosum* is not examined due to the high density of the cells, which makes it difficult to distinguish melanosomes and other electron dense material. Figure 13 shows an example of a TEM-mosaic (African skin) demonstrating the location of the boundaries of the individual epidermal layers. A minimum of 10 cells per epidermal layer is analyzed.

A melanosome is a melanin-filled organelle. In TEM images, melanosomes appear as black, electron dense particles of roundish or oval shape, 100-200 nm in size. They occur within the keratinocyte either as individual particles (single melanosome) or appear in agglomerations of 2-3, sometimes up to ten or more particles (cluster). Both, single melanosomes and clusters are delimited by a surrounding single membrane.

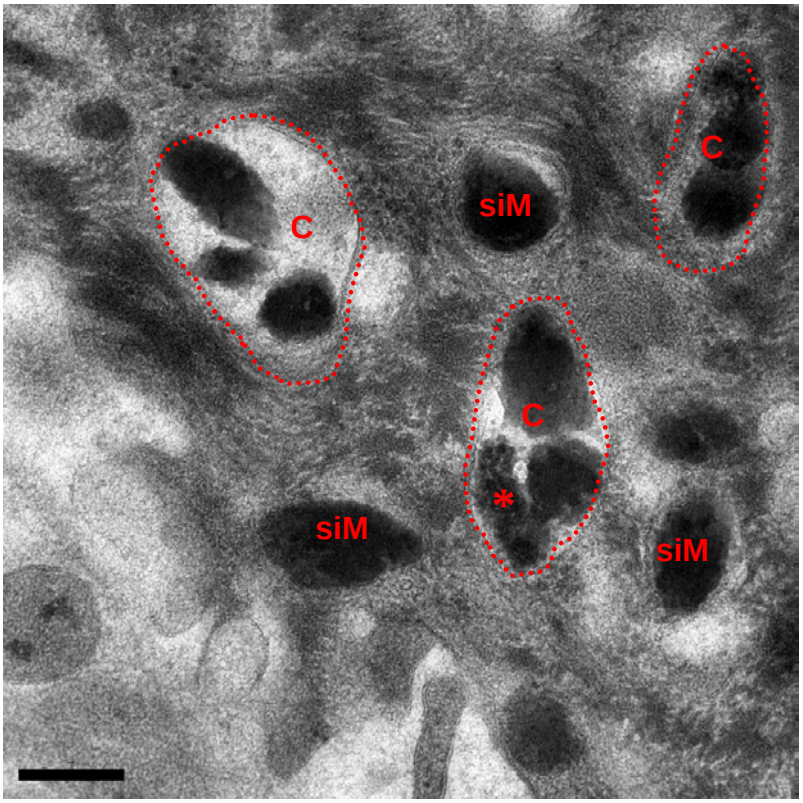

Figure 14: Definition of single melanosomes and melanosome clusters. Melanosome clusters are defined as two or more melanin particles grouped together within an organelle with a visible surrounding membrane. If only one melanin particle is contained within the organelle, it is referred to as single melanosome. If no membranes are visible because of poor sample preservation, clusters are defined by the size of the individual particles and the distance between them. In addition, the shape of clustered particles matches that of the flanking particles; an example is marked with an asterisk.

siM = single melanosome, C = cluster of melanosomes *Bar: 200 nm*

In a first approach, single particles and clusters are each rated as one melanosome. Notwithstanding, the numbers of particles within one cluster are documented for further analysis. Figure 14 demonstrates the classification of melanosomes. If, due to poor structural preservation of the sample, surrounding membranes can not be discerned, other criteria such as size, shape and proximity of the melanin particles are used to define a cluster. The particles within a cluster are usually smaller than individually distributed melanosomes. Furthermore, clustered particles show an adjustment in shape to match the adjacent particles, reducing the distance between them (marked with an asterisk). A single membrane is clearly visible surrounding the single melanosomes (siM) as well as clusters (C).
A second approach to counting melanosomes rates every melanin particle as one melanosome. The obtained melanosome numbers are correlated to the area of each analyzed cell and a mean value is calculated for each of the epidermal layers. Both, counting and measurement of cell area are done using the measurement tool of ImageAccess.

VIII.5 Automated Analysis of Melanosome Distribution

To shorten the process of data acquisition, an image analysis tool for the automated identification and counting of melanosomes in TEM-images was developed by FIT, the Fraunhofer Institute for Applied Information Technology in Sankt Augustin, Germany. The analysis tool is based on the FIT-devised software ZETA (Schwarz *et al.*, 2006). This software is trained to identify melanosomes by manually annotating sample images. Melanosomes are labelled by mouse-click. In a second step, structures that resemble melanosomes either in shape, or appear as electron dense as melanosomes, are denoted to prevent false-positive identification. Two training data sets were generated, one for the identification of melanosomes in the lower epidermal layers (SB to SG) and one to match the image quality of the SC, where the melanosomes are smaller than in the underlying layers.
The results are listed as comma separated values (csv), including information on

- the investigated epidermal layer
- the total number of identified melanosomes per image
- the number of isolated melanosomes per image
- the number of clusters per image
- the number of particles allocated to a cluster

- total area allocated to identified melanosomes per image
- a melanosome ID, corresponding to the annotation of the image

The automated processing also provides an annotated image, showing the detected melanosomes to control the quality of the detection. Isolated melanosomes are denoted in red, melanosome clusters are marked in yellow, with a frame indicating which melanosomes belong to the cluster. Each identified melanosome is labelled with an ID to enable the allocation to the particular set of values in the text file. False-positive results can thus be eliminated from the text file.

D SKIN PIGMENT CHARACTERIZATION BY LIGHT AND ELECTRON MICROSCOPY

A large variety of imaging and staining techniques are available specifically for the analysis of skin pigmentation. However, the investigation and especially the quantification of melanocytes require different staining methods and microscopic imaging techniques compared to the quantification and evaluation of their product, the melanosomes. This chapter covers the tested staining and ensuing imaging methods and includes an evaluation concerning the usefulness of the individual methods for the respective task of morphological and quantitative investigation.

I Identification of Melanocytes in the Context of Human Epidermis

When examined through a conventional light microscope, melanocytes appear as clear cells, at least after standard chemical fixation. The clear space actually is an artefact of fixation during which cytoplasm collapses around the nucleus (Griffiths, 1993). But as this phenomenon can be observed for all kinds of dendritic cells, it is no suitable criterion for the identification of melanocytes. Furthermore, it is not desirable to employ artefact-based imaging methods, if melanocytes and their interaction with keratinocytes have to be accurately described. It was therefore necessary to find imaging techniques that enable both, artefact-free identification of melanocytes as well as the description of the surrounding tissue.

I.1 Staining of Melanocytes by DOPA Oxidase Reaction

The DOPA oxidase reaction provides a possibility to demonstrate tyrosinase activity within the skin and can therefore be used to identify melanocytes. This method is described to work only in freshly prepared frozen sections or briefly postfixed frozen sections, as the enzyme activity is impaired by chemical fixatives and embedding (Bloch *et al.*, 1927; Churukian, 2002). In unfixed frozen sections, the reaction produced two degrees of blackish-brown stain

in basal cells (Figure 15.A). Nearly all of the basal cells showed an indefinite light brown colouration at least in parts of the cell, and only a few were totally stained dark brown. These can be assumed to be melanocytes, as indications of dendrites could be perceived. But the sections were damaged by the redox reaction resulting in nuclei breaking away (arrows). Even the IEM postfixed frozen sections showed a faint reaction: discrete dark brown spots were visible in the SB (Figure 15.B, marked by arrowheads). Dendrites or even single melanosomes were not perceptible. The reaction produced no effect on paraffin sections (Figure 15.C), the light brown stain being melanin that did not react to DOPA incubation. Control sections that were incubated with buffer only, showed no reaction.

Although this method enables the identification of melanocytes, it is not suitable for the description of their morphology nor for the analysis of interactions with keratinocytes due to artefacts and the poor resolution of conventional light microscopy compared to the sample thickness.

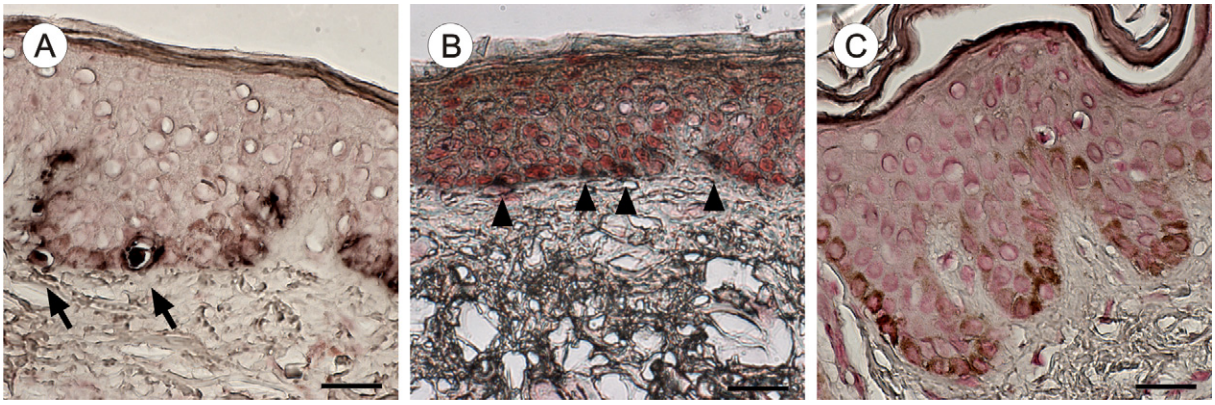

Figure 15: DOPA oxidase reaction. This reaction marks melanocytes by reducing DOPA to form a blackish-brown melanin precipitate. (A) shows the result for frozen sections (7 µm) of Caucasian skin (Fitzpatrick's skin phototype II). (B) IEM postfixed frozen section (7 µm) of the same sample. (C) Result obtained with PFA-fixed, paraffin embedded skin samples (4 µm) of skin phototype VI is shown. *Bars: 25 µm*

I.2 Identification of Melanocytes by Immunohistochemistry

Immunohistochemistry presents another possibility to detect melanosomal proteins, which has several advantages compared to histochemical reactions. Immunolabelling is based on highly specific binding of IgG-antibodies to target proteins. Direct or indirect labelling of these antibodies with fluorescent dyes enables very precise detection of the target proteins by fluorescent light microscopy and CLSM. In addition, by double labelling with a combination of

complementary antibodies an explicit identification of melanocytes and further information, e.g. on morphology and location can be achieved.

Several antibodies were tested, directed either against melanosomal enzymes or melanocyte-specific components. The staining results of most of the antibodies are dependent on the pre-treatment of the sample. Any kind of fixation – chemical or physical – influences structure and properties of the target proteins and therefore their availability for antibody-binding. This conformational change may be necessary to make the antigen available for the antibody, but it may also result in total masking or destruction of the antigen (Griffiths, 1993; Hayat, 2002). Some antibodies, e.g. both tested S100 antibodies or the actin-labelling toxin phalloidin, worked only on chemically pre-fixed frozen sections, while others (e.g. α-EEA1 or the Melanoma antibodies) produced results only when fixatives were avoided. Only a few antibodies, i.e. α-collagen IV, α-keratin and Mel-5 are independent of sample pre-treatment. Some antibodies, like α-clathrin, α-tyrosinase or α-tubulin showed no staining at all. A full list of tested antibodies and the achieved staining results in dependence of the type of frozen section is displayed in Table 12. The optimal working dilution was determined individually for each antibody based on recommendations of the supplier. The applied dilutions are listed in chapter C.IV.3.

Table 12: Staining results of all tested antibodies depending on the pre-treatment of the sample.

all kinds of frozen sections	frozen sections, no pre-treatment	frozen sections, chemical fixation	no staining results
α-Collagen IV	α-Laminin 2	α-EEA1	α-Clathrin
α-Keratin	α-Vimentin	α-S100	α-MiTF
Mel-5	Melanoma Ab-2	Phalloidin	α-Tubulin
	Melanoma Ab-3		α-Tyrosinase
	Melanoma Ab-5		Mel-1
			Melanoma Ab-1

For the identification of melanocytes, a combination of two antibodies was employed: an antibody labelling one enzyme involved in melanosome formation or melanin polymerisation was combined with markers for specific components of the cytoskeleton or melanocyte-associated proteins that are not directly involved in melanogenesis. But due to the differences in the affinity for the type of frozen sections, the range of combinations is restricted. Suitable antibody combinations are listed in Table 13.

Melanoma Ab-2 (HMB50) and Ab-5 (NKI/ beteb) are two different clones of antibodies

directed against gp100, an enzyme that promotes the biogenesis of premelanosomes. The staining results of both antibodies are comparable. Melanoma Ab-3 is a mixture of Ab-1 (clone HMB45) and Ab-2 and is not described, as the results are identical to Ab-2. HMB45 is described to label epidermal and dermal melanoma cells, but no melanocytes in normal adult epidermis (Smoller *et al.*, 1991). Accordingly, Ab-1 did not show any labelling results.

Table 13: Antibody combinations for the description of melanocytes. Only the antibodies, which showed reproducible, specific labelling results are listed.

	Mel-5 (α-TRP1)	**Melanoma Ab-2** (α-gp100)	**Melanoma Ab-5** (α-gp100)
α-Collagen IV	++ (3)	+ (2)	++ (3)
α-EEA 1	+ (1)	-	-
α-Keratin	++ (3)	+ (2)	+ (3)
α-Laminin 2	+ (2)	+ (2)	+ (2)
α-S100	++ (1)	-	-
α-Vimentin	+ (2)	+ (2)	+
Phalloidin	++ (1)	-	-

(1) these combinations work only for chemically pre-fixed frozen sections
(2) these combinations require frozen sections without chemical fixation
(3) these combinations work well for both, frozen sections with, and without chemical pre-fixation
(++) intensive labelling (+) moderate labelling (-) combination not possible

Mel-5 labels another enzyme involved in melanin polymerisation, i.e. TRP-1, which is active in melanosome stages III and IV (Bhawan, 1997). This antibody was found to be the most sensitive of the tested melanocyte markers. A direct comparison of the three antibodies applied to serial sections is displayed in Figure 16. All three antibodies detect melanocytes in corresponding locations of the sample, but the amount of details varies, Melanoma Ab-2 (Figure 16.A) displaying the least and Mel-5 the most details (Figure 16.C). This findings are in accordance with Dean *et al.* (2002) who also found Mel-5 to be the most sensitive of melanocyte markers. In addition, this antibody is not dependent on sample pre-treatment and produced very good staining results at high dilutions. Therefore, Mel-5 was used as melanocyte marker for further investigations.

Nevertheless, Mel-5 recognises a protein that is found active in melanosome stages III and IV. As melanosomes at this stage of development are already transferred to keratinocytes, it was necessary to determine, whether this antibody detects melanocytes only, or whether any melanosomes within keratinocytes, that still exhibit TRP-1 activity are recognized as well.

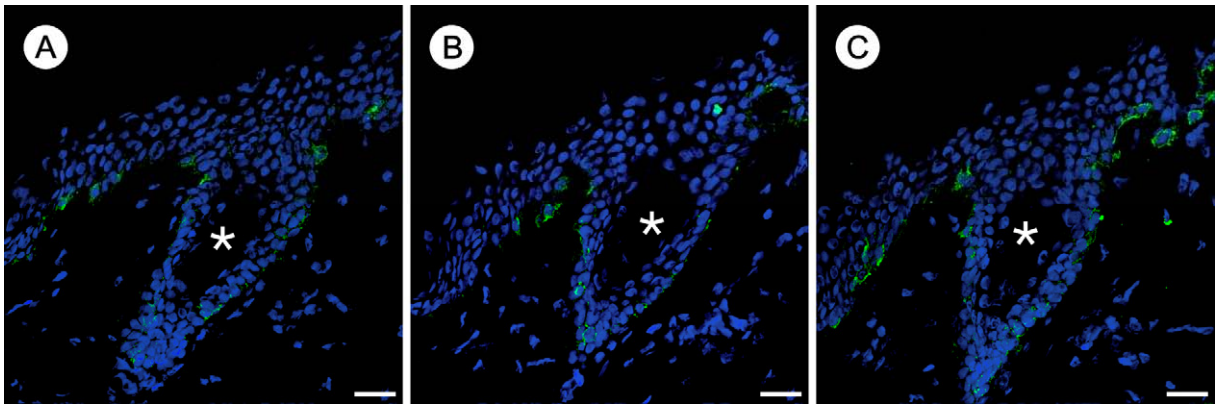

Figure 16: Comparison of antibodies directed against melanosomal proteins. Consecutive serial sections of epidermis including a hair follicle (asterisk). Melanocytes are displayed in green, nuclei in blue. (A) Staining result for Melanoma Ab-2, an antibody directed against gp100, an enzyme involved in premelanosome formation (clone HMB50). Melanocytes can be distinguished in the basal layer of the epidermis, as well as in the hair follicle. (B) Staining result for Melanoma Ab-5 (clone NKI/beteb) directed against gp100. Melanocytes are detected in places corresponding to (A), but more details are visible. (C) Melanocytes are labelled with Mel-5. This antibody recognizes TRP1, an enzyme involved in melanin polymerization, found in late developmental stages of melanosomes. Again, melanocytes are detected in places corresponding to the previous section. This antibody provides the most detailed staining. *Bars: 25 µm*

Hence, additional properties of melanocytes, such as the cytoskeleton, were included in the investigation. The intermediate filaments of melanocytes are made of vimentin, while the keratinocytes contain keratin. An α-vimentin antibody can therefore be used as a direct marker, while α-keratin provides an indirect marker, i.e. a negative image of melanocytes. Another direct marker is the early endosome marker α-EEA1, as melanosomes derive from early endosomes (Wilson *et al.*, 2000; Raposo and Marks, 2002). The S100 protein is present in all cells derived from the neural crest and detects any kind of cells forming dendrites (Donato, 2003). In combination with a melanogenesis-associated marker, α-S100 provides clear identification of melanocytes as well as a means to describe their morphology. Antibodies directed against components of the basement membrane, like α-collagen IV and α-laminin 2, as well as the cytoskeleton marker phalloidin can be employed to describe the positioning of melanocytes in the epidermis and their interactions with keratinocytes.

Figure 17 exhibits examples for double labelling with Mel-5 to identify melanocytes (Mel-5 labelling is displayed in green). Mel-5 and α-keratin show complementary staining patterns, α-keratin provides a negative image of the melanocytes and no colocalisation is observed (Figure 17.A). The intermediate filaments of melanocytes were labelled with α-vimentin (Figure 17.C). The antibody displayed only a low affinity for epidermal cells, while dermal cells like fibroblasts were clearly stained. Yet Mel-5 positive cells also show small spots of colocalisation with α-vimentin (marked with white arrowheads). Double labelling with α-S100

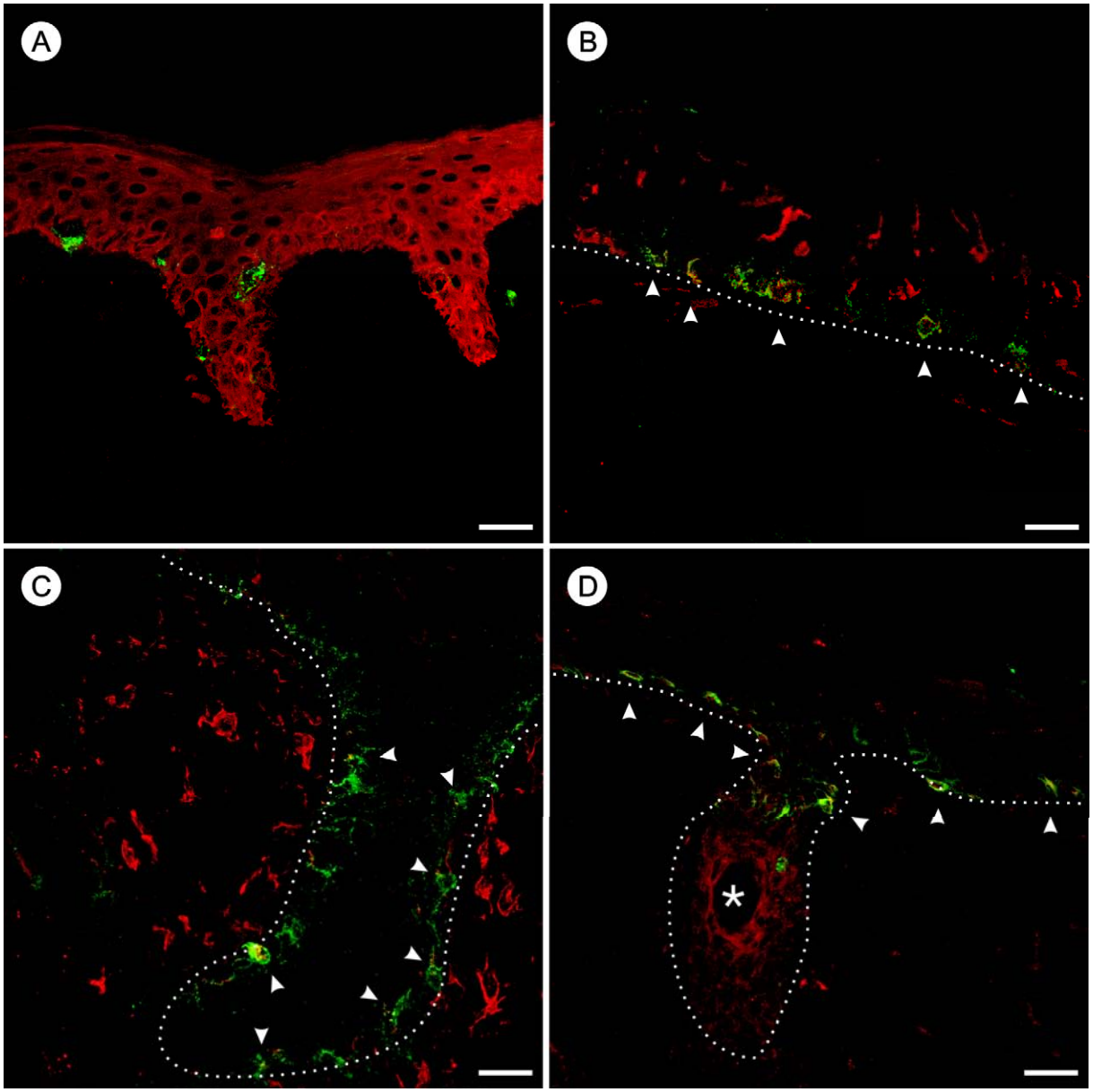

Figure 17: Antibody combinations for the identification and description of melanocytes. Frozen sections without chemical pre-fixation were used for A & C, and with IEM pre-fixation for B & D. The melanocyte marker Mel-5 is displayed in green, colocalisation with the respective marker appears yellow. The SC is positioned at the top of the images, the dotted white line represents the basement membrane. (A) Double labelling for Mel-5 and α-keratin. All Mel-5 positive cells are negative for α-keratin and v.v. (B) Mel-5 combined with a marker for dendritic cells, α-S100. Cells that show double labelling (arrowheads) are clearly identified as melanocytes. (C) Double labelling for Mel-5 and α-vimentin. The cytoskeleton of melanocytes contains vimentin instead of keratin, while keratinocytes do not contain vimentin. The α-vimentin antibody labels mostly dermal cells, i.e. fibroblasts, but a few epidermal cells are positive for vimentin (arrowheads). (D) Combination of Mel-5 and α-EEA1 (early endosome marker) labelling. Premelanosomes are of endosomal origin, and α-EEA1 is present in melanocytes. Cells positive for both markers are indicated by white arrowheads. α-EEA1 displays unspecific labelling in keratinocytes surrounding a hair follicle (asterisk). *Bars: 25 µm*

revealed several dendritic cells in the upper layers of the epidermis (Figure 17.B). In the SB, most of the stained cells are positive for both, Mel-5 and α-S100 (marked with white arrow-heads), although a few dendritic cells are present, which are not identified as melanocytes.

This staining result underlines the positioning of melanocytes along the basement membrane. The double staining with Mel-5 and α-EEA1 shows colocalisation in most of the recognized cells (Figure 17.D, indicated by white arrowheads). The intracellular location of the α-vimentin and α-EEA1 labelling is near the nuclei, as would be expected. Hence, these antibodies can be used for the identification of melanocytes only, but not for the description of their morphology and interactions with keratinocytes. In contrast, Mel-5 and α-S100 stain cytoplasm and dendrites of the melanocytes.

These findings confirm the specificity as well as the high sensitivity of Mel-5 as a suitable marker for melanocytes. In combination with α-collagen IV, Mel-5 provides detailed information on morphology and interaction of melanocytes with keratinocytes (Figure 18). This combination was used to determine the density and distribution of melanocytes and describe the epidermal melanin unit (see chapter II.1).

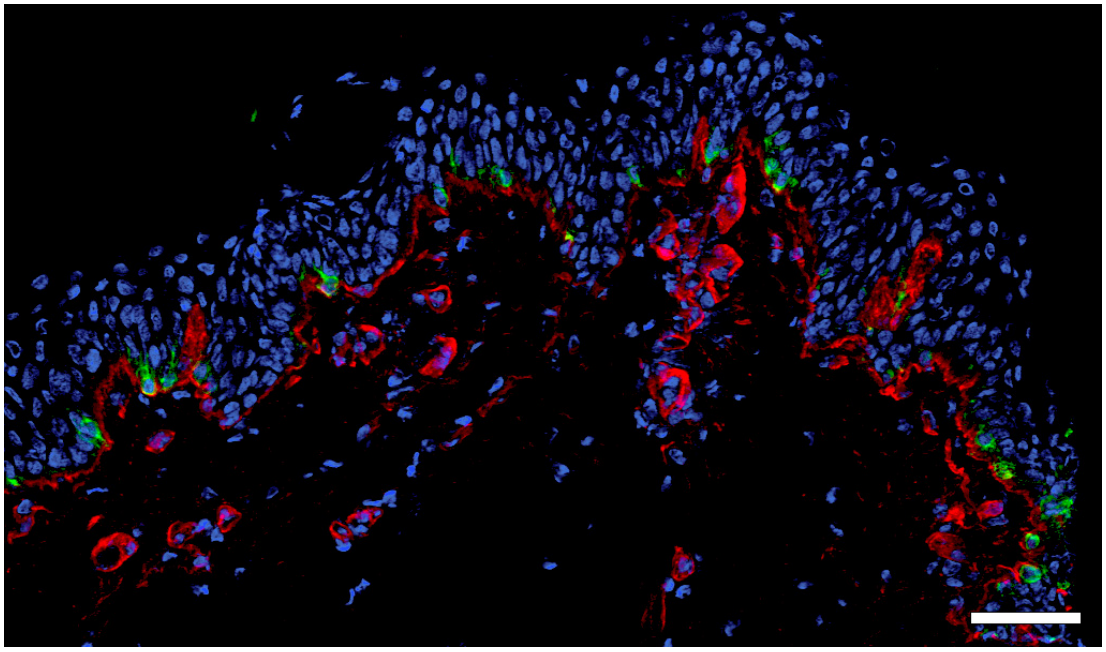

Figure 18: Double labelling for Mel-5 and α-collagen IV. Melanocytes are represented in green, the basement membrane (labelled with α-collagen IV) in red and nuclei (labelled with Sytox Green) are displayed in blue. This antibody combination is useful to describe the exact localisation of melanocytes relative to the basement membrane and their density in the epidermis (see chapter E.II: Melanocyte Distribution). *Bar: 50 µm*

I.3 Identification of Melanocytes in Transmission Electron Micrographs

Despite the precision of the confocal imaging, the resolution is still not sufficient to describe the ultrastructure of melanocytes (especially the dendrites) and investigate melanosome formation and their translocation to keratinocytes. This can only be achieved by transmission

electron microscopy (TEM). But here the identification of melanocytes is complicated by the lack of antibodies suitable for the application to sections of resin embedded tissue. The most sensitive melanocyte markers Mel-5 and Melanoma Ab-2 and Ab-5 were tested on HM20 sections, showed no affinity binding of antibodies and hence no specific labelling.

Therefore ultrastructural characteristics had to be used for identification, such as the presence of dendrites and melanosomes in various maturation stages. But here again, a major distinguishing characteristic is the fact, that melanocytes appear as “clear cells” (Clark and Hibbs, 1958; A. Charles and Ingram, 1959). Even after high-pressure freezing, freeze-substitution

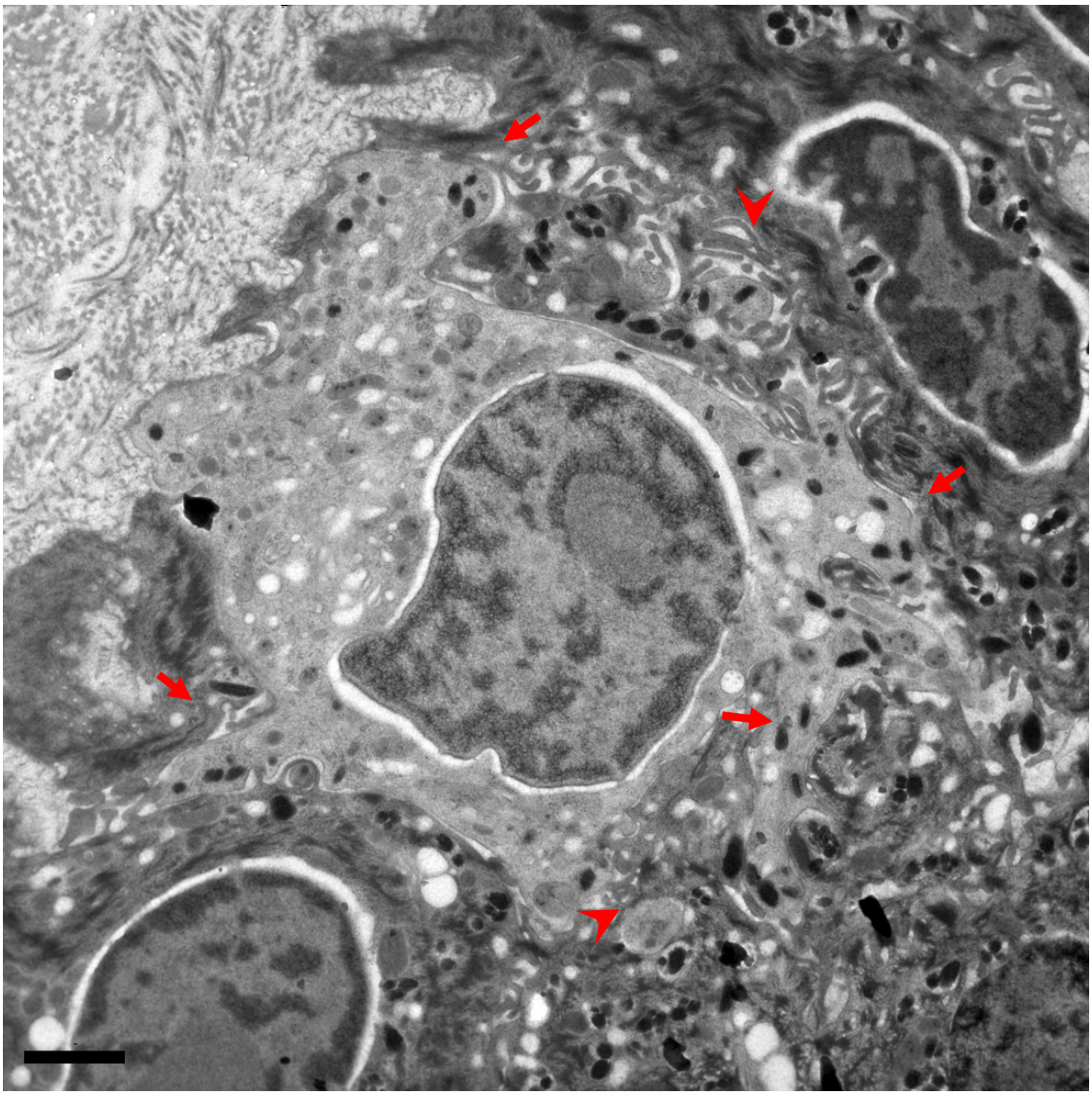

Figure 19: TEM image of a melanocyte. The cytoplasm of the melanocyte appears lighter than that of the surrounding keratinocytes, no tonofibrils are visible. Short dendrites and continuations of the dendrites, that appear to be pinched-off (arrowheads), are perceptible, reaching between the surrounding keratinocytes. Melanosomes in various stages of development can be discerned near the dendrite tips (marked with arrows). Details of the dendrites are displayed in Figure 58. *Bar: 1 µm*

and low-temperature resin embedding – a method designed for minimizing structural artefacts – the cytoplasm of melanocytes appears lighter than that of surrounding keratinocytes. On the other hand, this staining pattern might not be an artefact at all, but merely the result of a different composition of the cytoplasm of melanocytes. E.g. the lack of keratin fibres may lead to less binding of staining reagents.

Figure 19 shows an example of a TEM image of a melanocyte: the cytoplasm is lighter than that of keratinocytes and no tonofibrils are perceptible. Cross sections of dendrites are visible in the intracellular space, mainly between keratinocytes, but also in direct vicinity of the melanocyte. Extensions of dendrites that appear pinched-off are also visible in the intracellular space (arrowheads). Melanosomes and other organelles are present in abundance in all stages of development. The late stages III and IV are situated near the dendrite tips, ready for transfer to the keratinocytes (arrows).

Due to it's superior resolution, TEM is the only appropriate microscopy technique for the analysis of melanocyte and melanosome morphology as well as the investigation of melanosome translocation to keratinocytes. The resolution of light microscopy is not sufficient to capture this process in relation to intracellular membranes, the cytoskeleton and the plasma membranes in the tissue context. However, the lower preparative effort combined with better practicability of 3D-imaging and a larger field of view render CLSM of immunolabelled cryostat sections sufficient for the investigation of melanocyte location and density as well as for the description of the epidermal melanin unit (see chapter E.II).

II Characterization and Analysis of Melanosomes and Their Distribution in the Human Epidermis

The description and quantitative analysis of melanosomes, and consequently the microscopic description of melanin content in the skin represents a problem. An antibody that directly recognizes melanin does not exist. And even then, the detection of small structures as melanosomes would probably be difficult with light microscopy. However, several more or less specific histochemical staining methods for melanin are described, Merck's Nile blue staining and Fontana-Masson's silver method being the most prominent. These methods were tested with regard to their usefulness for the quantification of melanin.

II.1 Melanosome Staining by Histochemistry

Standard histochemical stains such as toluidine blue and hematoxylin eosin gave a good general overview of the sample. Both staining methods distinguish melanin and sometimes even melanocytes can be detected as they usually appear lighter in colour than the surrounding keratinocytes. Figure 20 displays resin sections of Negroid skin (Fitzpatrick's skin phototype VI). Toluidine blue stains the nuclei purple and the cytoplasm light blue, while melanin appears dark blue (A). The keratinocytes contain a large amount of melanin forming characteristic caps above the nuclei (see white arrowheads).

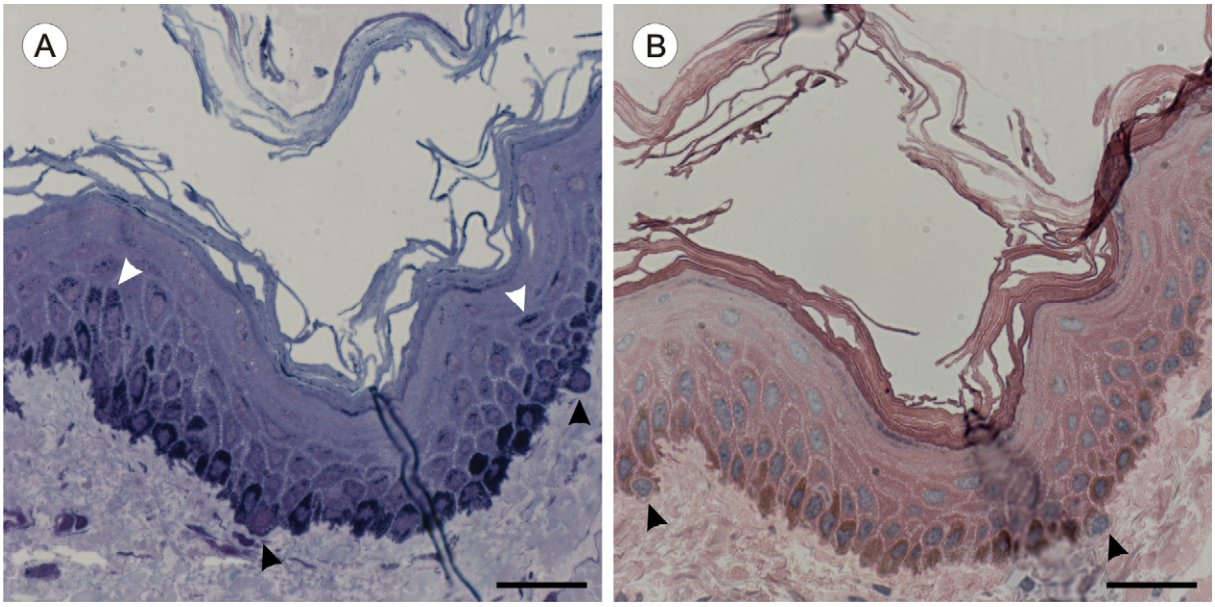

Figure 20: Histochemical standard stains. The samples were high-pressure frozen, freeze-substituted and embedded at low temperature in HM20. 500 nm sections were used for staining. (A) Negroid skin sample stained with toluidine blue: melanin is stained dark blue. Melanosome caps above nuclei (white arrowheads) and melanocytes (black arrowheads) are visible. (B) Hematoxylin eosin staining of the same sample: melanin is stained brown. Here caps above the nuclei are visible only in the SB, but not in superior layers of the epidermis. Melanocytes can be distinguished. *Bars: 25 µm*

The consecutive section of the same sample was stained with hematoxylin and eosin (B). Here the nuclei are stained blue, the cytoplasm pink and melanin appears in brown. Again, the basal keratinocytes are filled with melanin. But due to the similarity of the colours, it is more difficult to distinguish smaller accumulations or single melanosomes and thus no caps above the nuclei are visible only in the SB, but cannot be distinguished in the upper epidermal layers. Some possible melanocytes can be perceived (black arrowheads), but it is not possible to safely assume that these cells really are melanocytes. As it is impossible to discern single melanosomes, only a rough assessment of melanin quantity and distribution can be achieved.

II.2 Nile Blue Staining of Melanosomes

Nile blue is described to stain melanin dark green in frozen sections as well as paraffin sections. Samples treated with chemical fixatives displayed a faint blue colouration of the cytoplasm while the nuclei appear unstained, whereas frozen sections showed no staining of the cytoplasm with dark blue nuclei.

In all cases melanin is stained dark green, but is clearly visible in the paraffin sections only (Figure 21.A). The location correlates with the brown colouration of unstained sections that is produced by melanin (not shown). The frozen sections (Figure 21.B & C) show only a faint green shadow (red arrows) in the lower layers of the epidermis. Single melanosomes cannot be distinguished. In order to clarify whether the detection of melanin with this staining

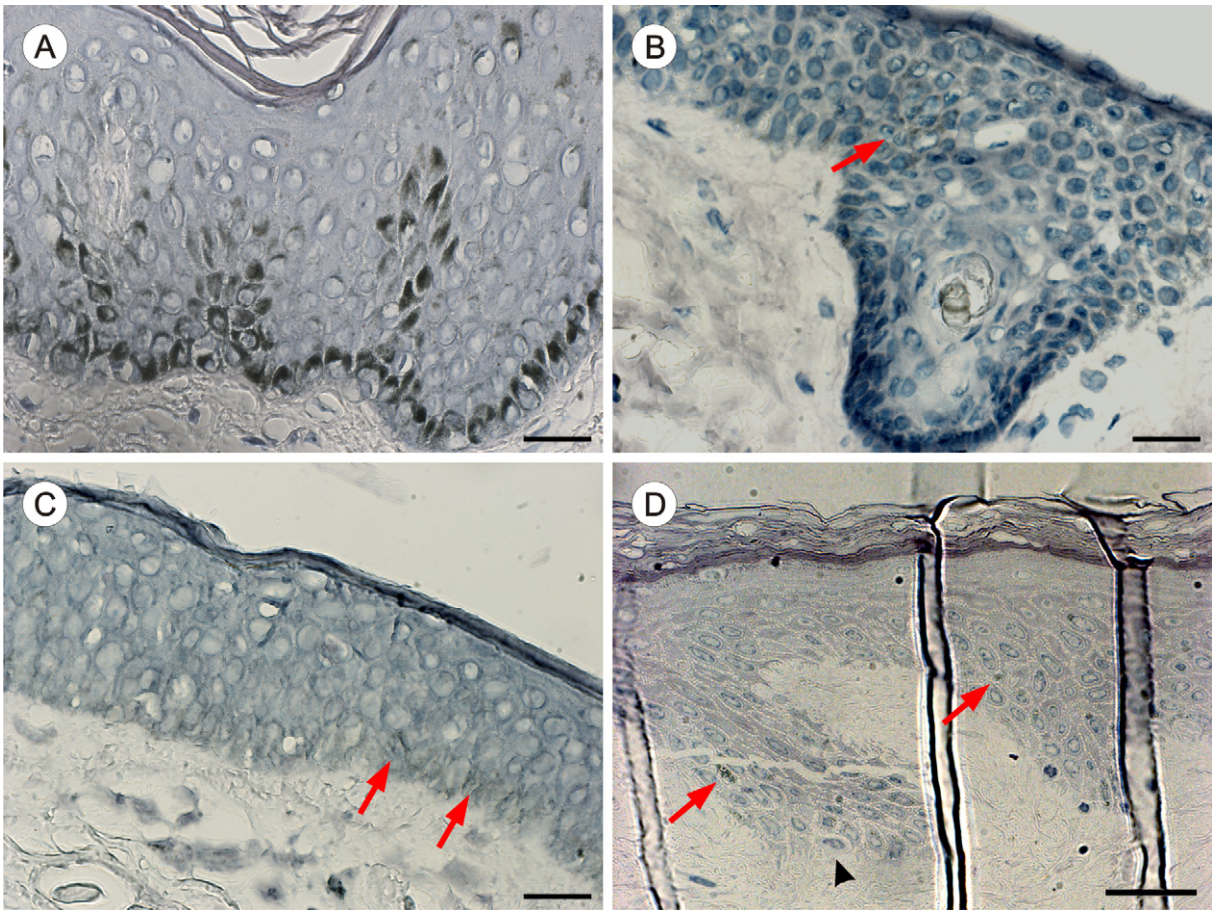

Figure 21: Nile blue staining for melanin. Nile blue is supposed to stain melanin a dark green, while nuclei and cytoplasm appear in blue. (A) Formalin-fixed, paraffin embedded section (4 µm) of Negroid skin. (B) Frozen section (7 µm) without chemical fixative and (C) IEM pre-fixed frozen section (7 µm) of Caucasian skin. (D) High-pressure frozen, freeze-substituted sample of Caucasian skin, embedded in HM20 (500 nm section). On frozen and HM20 sections, Nile blue produced only a faint green staining for melanin (B, C and D; red arrows), while the paraffin sections (A) showed distinct dark green colouration of melanin. Cytoplasm and nuclei are stained light blue. *Bars: 25 µm*

method could be improved by using thinner sections, it was applied to 500 nm sections of high-pressure frozen freeze-substituted samples that were embedded in HM20. Here, the Nile blue staining, like all histochemical standard stains, produced a very detailed overview of the sample, in this case Caucasian skin of Fitzpatrick's skin phototype II (Figure 21.D). Despite the faint staining result, the dark green colouration of melanin is detectable in a few spots (red arrows), but again, smaller accumulations or even single melanosomes are not discernable.

II.3 Fontana-Masson Staining for the Detection of Melanin

The Fontana-Masson silver staining is described to be specific for melanin (Lillie, 1957). It is based on the argentaffin properties of melanin, i.e. the ability of melanin to reduce silver salts to form a metallic silver precipitate, which is easily detected in light and electron microscopy.
The stain produces the most reliable results on formalin-fixed paraffin sections (Figure 22.A). Melanin appears blackish-brown and single particles can be distinguished from the SB up to the SC. Both kinds of frozen sections, without pre-treatment and IEM pre-fixed (B & C), also showed the characteristic staining but it was not possible to discern single particles as there were large accumulations of the black stain, especially in the SB and SSp (white arrows). Especially the standard frozen sections displayed distinct staining in the upper epidermal layers, where little or no melanin would be expected in Caucasian skin (white arrows; Figure 22.B). Post-staining with gold chloride has been omitted, as the staining results did not need blackening.
On resin sections, the Fontana-Masson staining produced a very detailed dark labelling for melanin that stood out well against the neutral red counterstain (Figure 22.D). This dark silver precipitate is quite precisely located in areas where melanin would be expected, i.e. mainly in the lower layers of the epidermis and forming caps above the nuclei (white arrowheads). But the dark labelling could not be observed when the counterstain was omitted, and on closer examination, a lot of the spots were stained dark red rather than black (black arrows), suggesting staining artefacts rather than specific labelling of melanin. The displayed sample was from an age spot (lesional), which explains the large amount of melanin in the SB.
The different staining results obtained for paraffin and frozen sections are remarkable, as the method is described to produce equally good results on frozen sections as on formalin-fixed paraffin sections, although the latter are to be preferred (Romeis, 1968; Churukian, 2002). This might be explained by the differences in fixation, frozen sections being only postfixed in

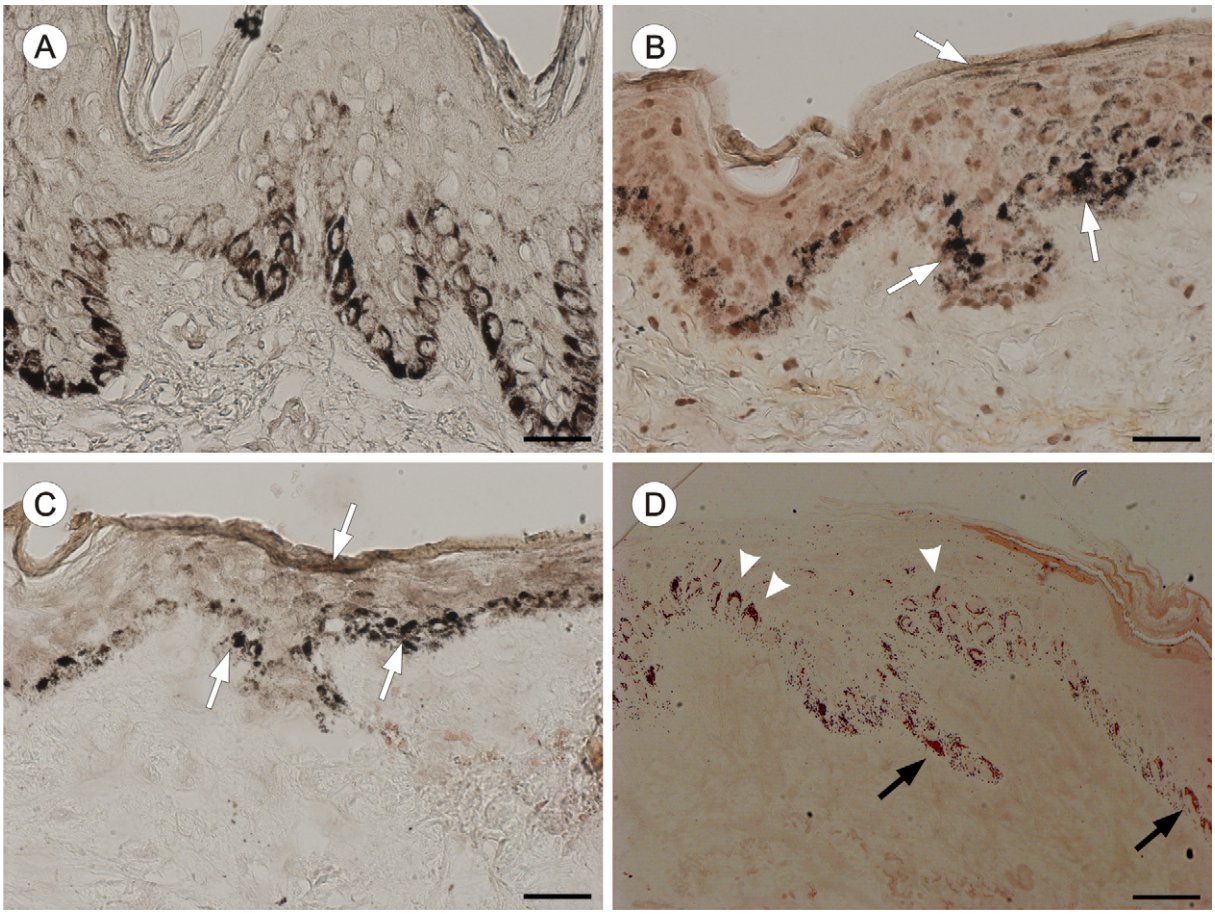

Figure 22: Fontana-Masson staining for melanin. A black silver precipitate indicates the presence of melanin. Neutral red was used as a counterstain. (A) Formalin-fixed, paraffin embedded section (4 µm) of Negroid skin. (B) Frozen section (7 µm), postfixed with formalin before staining and (C) IEM pre-fixed frozen section (7 µm) of Caucasian skin. (D) High-pressure frozen, freeze-substituted sample of Caucasian skin, embedded in HM20 (500 nm section). The black silver precipitate is visible in all sections. The best results were produced on the paraffin sections. The frozen sections showed a slight overreaction (B and C; white arrows), while the resin sections produced only weak staining for melanin, that became visible only after counterstaining with neutral red. Some spots are stained dark red rather that black (D; black arrows). The white arrowheads indicate a few intensely stained supranuclear melanin caps. *Bars: 25 µm*

PFA-fixative for 10 min, while the paraffin sections were treated with fixative for 24 hours. The longer fixation time could be helpful. Aldehydes were found to enhance ammoniacal silver staining (Dion and Pomenti, 1983). Hence, the frozen sections would be expected to show less staining for melanin, rather than the achieved intensive stain. On the other hand, this might be an artefact introduced just by the fixation. To clarify this, frozen sections were processed omitting any chemical fixatives (data not shown), but the results were the same. It is also possible, that the omission of gold chloride post-staining yielded this over-staining. Gold chloride is said to clear weakly impregnated substances (Burck, 1988).

The weak staining results obtained with resin sections can only be explained by masking-effects of the resin on sites of silver affinity, although the sections were etched with H_2O_2

prior to the incubation with the silver solution to remove the resin and uncover the affinity sites. But it is uncertain whether melanin retains its argentaffin properties after resin embedding. Nevertheless, longer incubation with the silver nitrate solution did not improve the staining results.

The over-staining of the frozen sections, as well as the doubtful staining results on resin sections necessitated an assessment of the validity of Fontana-Masson's silver staining regarding the quantitative analysis of the melanin content, or the amount of melanosomes within the epidermis respectively.

For this purpose, 10 µm frozen sections of Caucasian skin (Fitzpatrick's skin phototype II) mounted on a glass slide, were treated according to the Fontana-Masson standard protocol (see chapter C.IV.2.3) followed by dehydration and room temperature embedding in Epon, positioning the skin section parallel to the surface of the resin bloc. After polymerization, the glass slide was removed. Consecutive sections were obtained for investigation in light and electron microscopy. 200 nm sections were mounted on a microscope slide and stained with toluidine blue to gain some contrast (see chapter C.IV.1.2). Subsequently 50 nm sections were obtained, collected on an EM-grid and stained with uranyl acetate for 45 min, followed by lead citrate for one minute. The results are displayed in Figure 23. The light microscopic images (A-C) confirm the presence of the silver precipitate at least in the lower epidermal layers (SSp-SB). Single black granules can be distinguished, mostly in cells of the SB. The characteristic supranuclear location of melanosomes was not apparent and sometimes the silver particles seem to be located underneath or even directly in the nucleus (white arrowheads; Figure 23.B).

The TEM images were obtained in the area around the papilla left of enlargement B. The silver precipitate can be easily distinguished as round black granules, 8-30 nm in diameter.

Figure 23: Fontana-Masson benchmark. (A) 500 nm section of Caucasian skin frozen section, treated according to the Fontana-Masson staining protocol followed by embedding in Epon. Toluidine blue was used as counterstain. The black silver precipitate is visible in the basal cells (see enlargements B & C). The subsequent section was processed for TEM. The silver precipitate is observed throughout the epidermis. Dense accumulations are found on structures resembling melanosomes in shape and size (marked with black arrows). But single silver particles are observed along the cell membranes and within the keratinocytes (black arrowheads). Loose accumulations of silver particles are frequently found with roundish shapes discernable beneath (white arrowheads). (D) Detail of SC. Single silver particles are abundant. (E) Detail of SG, and (F) detail of SSp. Loose silver accumulations are frequently found adjacent to cell borders. Residues of a desmosome are visible nearby (white arrow). (G) The largest amount of silver particles is located in the SB, partially in melanosome-resembling dense accumulations (black arrow), partially loosely scattered in the cells (black arrowheads). N = nucleus. *Bar in (A): 50 µm; bars in (D) - (G): 250 nm*

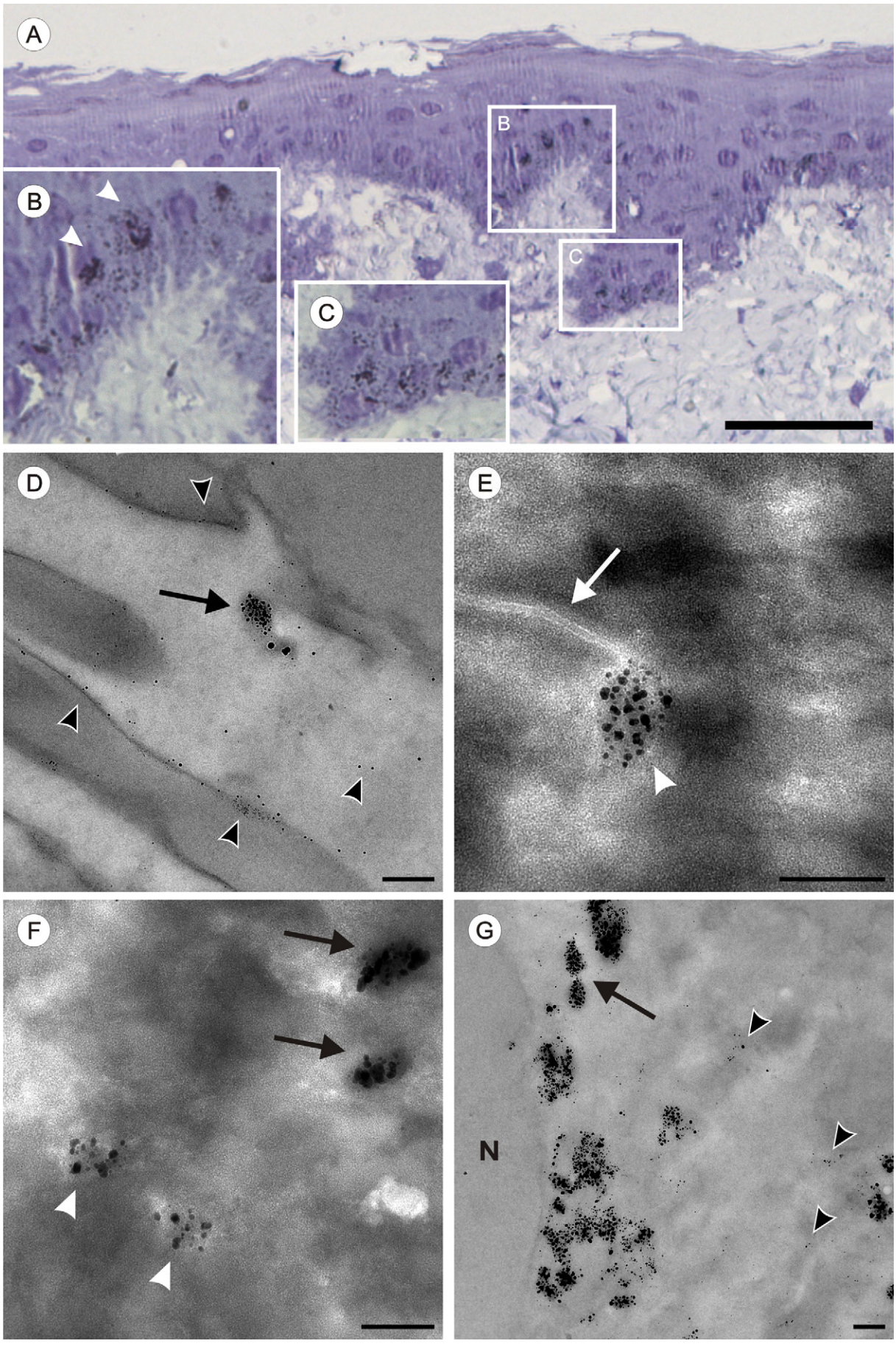
A
B
C
B
C
D
E
F
G
N

The other structures appear more blurred in comparison due to poor contrast, as the tissue was not treated with heavy metals before embedding. Silver granules can be observed throughout the epidermis, with the largest amount of silver particles located in the SB. Dense aggregations of precisely delineated shapes were found on dark, compact structures resembling melanosomes in shape and size (see black arrows, Figure 23.D, F & G). But less dense accumulations are frequently found in the SG and SSp, with roundish organelles discernable beneath, that are not markedly electron-dense, and that are most likely no melanosomes (white arrowheads, Figure 23.E & F). The shape and positioning adjacent to the cell membrane and the desmosome on the left, as well as residues of a membrane opening into the intercellular space, suggest the roundish shape displayed in Figure 23.E to be a lamellar body rather than a melanosome. Additionally, single silver particles were abundantly distributed in the cytoplasm of keratinocytes and especially accumulated along cell membranes in the SC, even on the outside of the cells (black arrowheads, Figure 23.D & G). Figure 23.G shows a part of basal cell, with the nucleus (marked with *N*) visible on the left side. A large amount of silver aggregates are present, but again, the shapes are not always consistent with melanosomes. The accumulations are sometimes much larger than single melanosomes and a lot of single silver granules are visible within the cytoplasm and even in the nucleus.

These findings seem to confirm the assumption, that melanin is not the only substance that is stained by ammoniacal silver. Proteins in general bind low levels of ionic silver. Especially protein side chains consisting mainly of carboxylate-containing residues, thiols and thioether groups, can bind ionic silver. Aldehydes and ketones, including quinones, that are also present in melanin (see chapter B.I.2.1), react rapidly with ammoniacal silver (Lillie *et al.*, 1957). The argentaffin reaction is also described for polyphenols, aminophenols and polyamins (Churukian, 2002). Melanin is most certainly not the only such substance in the human skin.

The longer the incubation with ammoniacal silver, the larger the chance of silver-binding to non-melanin compounds. On the other hand, Humbel *et al.* (1995) report that silver used as an enhancement agent for EM-immunolabelling experiments is not stable, but may be redistributed after exposure to the electron beam of the TEM. Thus, the distribution of single silver granules observed in the cytoplasm of corneocytes and cells of the SG may not represent silver affinity sites, but simply relocated silver particles. However, the reaction is susceptible to artefacts, any contamination of the utilized glassware or reagents must be carefully avoided, as they also give rise to silver precipitates (Burck, 1988). Any variations in the reaction conditions, e.g. pH, composition and temperature of the reaction medium, considerably

affects the quantitative characteristics of this staining method (Gallyas, 1979).

The false-positive staining observed in the TEM images may be considered negligible and too small to be detected in LM. But as the standard application of this staining method is on LM sections, the thickness of the investigated section must be considered, as well as the strong light scattering property of silver colloids. The TEM sections are 200 nm thick, while sections of LM are usually 4-7 µm thick. The thicker the section, the more blurred the resulting image, because of overlapping structures, and thus the false-positive staining is summed up and becomes visible also in LM images. This may lead to overvaluation of melanin content of a sample.

If the method is to be used for quantitative analysis, it is therefore crucial to standardize incubating solutions and incubation time, in order to – at least – minimize inter-experimental variations. Extensive controls are necessary to assess the degree of false-positive staining. Qualitative comparison of the melanin content of different skin samples is certainly possible. But with regard to the possible overassessment, quantitative analysis seems not to be appropriate.

II.4 Melanosomes in CLSM Images of Resin Embedded Samples

Melanin not only absorbs a broad spectrum of light, it has also powerful light scattering properties (Nielsen *et al.*, 2004). These properties can be exploited to visualize melanin, or melanosomes, in skin samples *in vivo* as well as *ex vivo*, by recording the reflection signal of backscattered light (Biel *et al.*, 2003; Viator *et al.*, 2004; Yamashita *et al.*, 2005; Taylor *et al.*, 2006). Here, CLSM was applied to image high-pressure frozen skin samples, that were freeze-substituted in the presence of fluorescent dyes and embedded in HM20 (see chapter C.III.2.2). Nile blue sulphate, to stain the nuclei, was applied in combination with DiIC18 that stains the cell membranes. Safranine O stains nuclei as well as cytoplasm, but the two structures yield fluorescence at different detection wavelengths and can thus be visualized individually.

Figure 24 shows examples of different skin phenotypes imaged in this way. Figure 24.A and B display samples that were stained with Nile blue sulphate and DiIC18. The nuclei are represented in red, the cell membranes of the epidermal cells are displayed in green. The reflection signal is portrayed in blue. Figure 24.A was obtained from a Caucasian skin sample of skin phototype III. It shows a moderate amount of reflection signal that is restricted to the basal

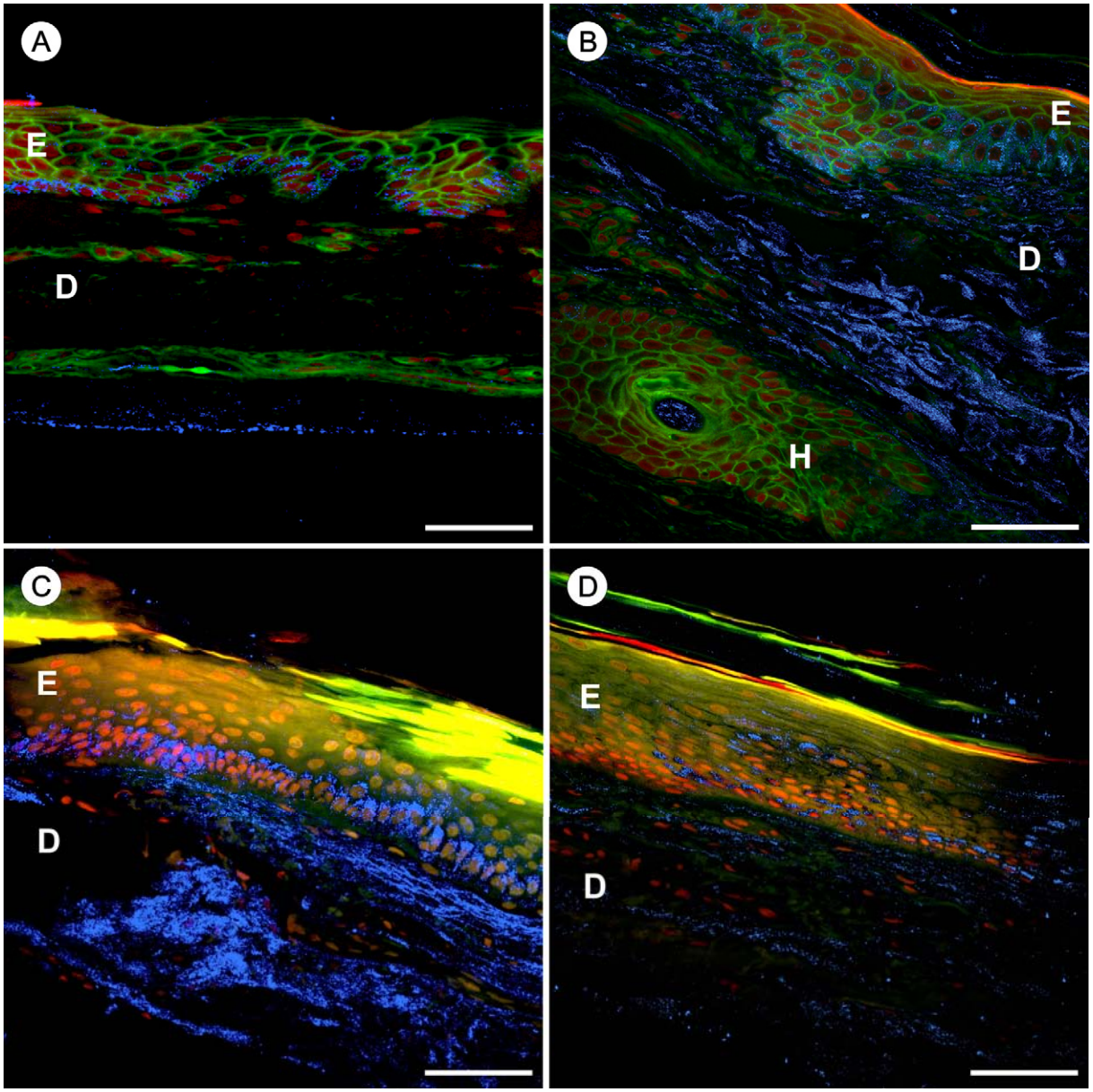

Figure 24: Reflection signal of fluorophore-stained, resin embedded skin samples. The biopsies were high-pressure frozen and freeze-substituted in the presence of fluorescent stains, followed by low-temperature embedding in HM20. (A) Caucasian skin (Fitzpatrick's skin phototype III) and (B) African skin (Fitzpatrick's skin phototype VI). The samples are stained with Nile blue sulphate and DiIC18. Nuclei are displayed in red, cell membranes appear in green. The reflection signal is plotted in blue. The epidermis of the darker phenotype yields a slightly stronger reflection signal that the lighter skin. The reflection obtained from the dermis most likely comes from compact collagen fibres or similar structures, rather than from melanin. A hair follicle is visible in (B), the hair itself yields no fluorescence, but only a faint reflection signal from the contained melanin. (C) A biopsy obtained from the periphery of an age spot and from the lesion itself (D). Both samples were stained with Safranine O. The nuclei displayed in bright orange, while the cytoplasm appears in greenish-yellow colours. Contrary to expectations, the perilesional skin yields the stronger reflection signal, compared to the lesional skin, from the dermis as well as from the epidermis.

E = epidermis, D = dermis, H = hair follicle *Bars: 50 µm*

cells of the epidermis. No reflection is detected in the dermis. The blue line in the lower dermal compartment is a reflection artefact produced by an edge in the resin bloc.

Figure 24.B shows a sample of African skin. It displays a stronger reflection signal that is present not only in the SB but also in the lower layers of the SSp. The reflection detected in the dermal compartment is most likely caused by dense collagen or elastic fibres. Melanin was not present in the dermis, as was determined by light microscopy. A hair follicle is displayed in the lower part of the image. The hair itself is not stained by the fluorescent dyes, but the melanin contained in the cortex and medulla yields a reflection signal.

Figure 24.C and D display samples of senile *lentigines*, lesional (D) as well as from the periphery of the lesion (C). Contrary to expectations, the perilesional sample shows a much stronger reflection signal, from the epidermis as well as from the dermis. In the epidermis, the location of the reflection is strictly limited to the SB and supra-nuclear melanin caps become apparent. In the lesional skin, the reflection signal is also present in the SB, but also in higher layers of the epidermis. This can be explained by the proximity of a papilla, that becomes visible in the histological staining of a section, acquired from the sample after examination in CLSM (Figure 25.B, marked with an asterisk), that shows the reflecting cells to be in the SB.

The displayed section was not obtained from exactly the same depth of the resin bloc as the confocal image, but it is still possible to compare the two images and assess the quality of the reflection signal. In general, the areas that do not contain melanin yield little or no reflection signal. Cells that show explicit melanin caps over the nuclei, give rise to a strong reflection. In addition, these parts do not show any fluorescence, confirming a dense package of melanosomes. On the other hand, some parts of the SG and the dermal compartment show reflection signals, where no melanin is visible in the histological stain (see white arrowheads).

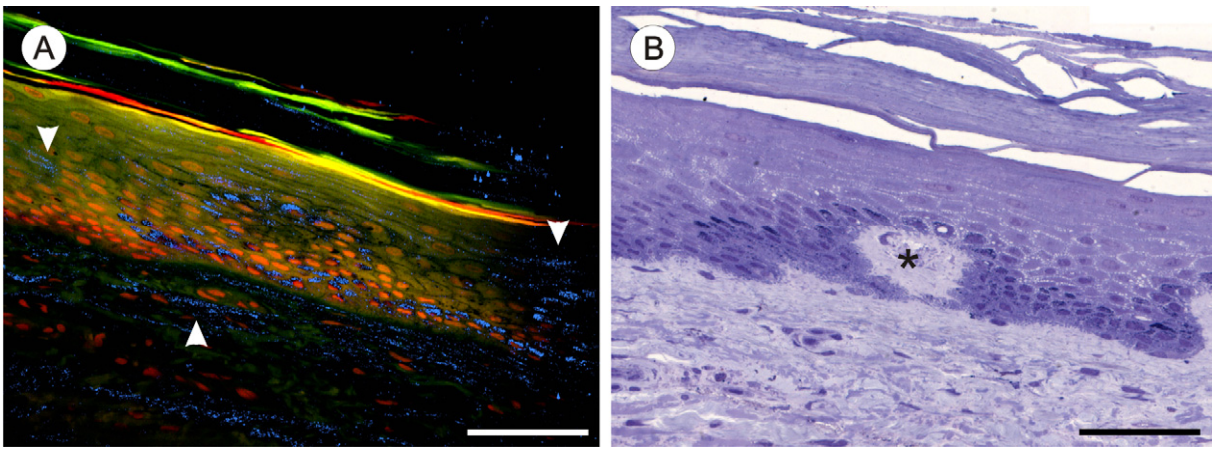

Figure 25: Histological benchmark of the reflection signal. Both images show the same area of the sample. The left image (A) was obtained by CLSM directly on the resin bloc, while the right image (B) shows a 500 nm section from this sample, stained with toluidine blue and visualized by LM. The histological stain shows, that the reflection detected in the SG and dermis does not necessarily come from melanin. *Bars: 50 µm*

In addition, the dermis does not contain melanin, confirming the assumption, that dense epidermal and dermal structures, such as collages fibres or the compact SG, can produce a reflection signal in resin embedded samples when imaged by CLSM. This inaccuracy renders CSLM unemployable for the quantification of melanin.

II.5 Melanosomes imaging by Transmission Electron Microscopy

Even at high magnifications, light microscopy does not enable the exact distinction of single melanosomes nor the identification of subunits. But as the aim of this study was to quantify the epidermal melanin content – or melanosome content, respectively – transmission electron microscopy was employed, because of the superior resolution and the resulting possibility for ultrastructural investigation of the melanosome maturation stages and melanosome types.

Melanosomes can readily be identified in TEM images. Due to the electron absorbing or scattering properties of melanin, melanosomes appear as very dark, dense roundish or oval granules. It is possible to discern single melanosomes and so-called melanosome clusters, aggregations of melanin-filled particles that are grouped to form a melanosome unit, as illustrated in Figure 26. These clusters are usually surrounded by a single membrane and contain two or three, sometimes up to 10 or more subunits.

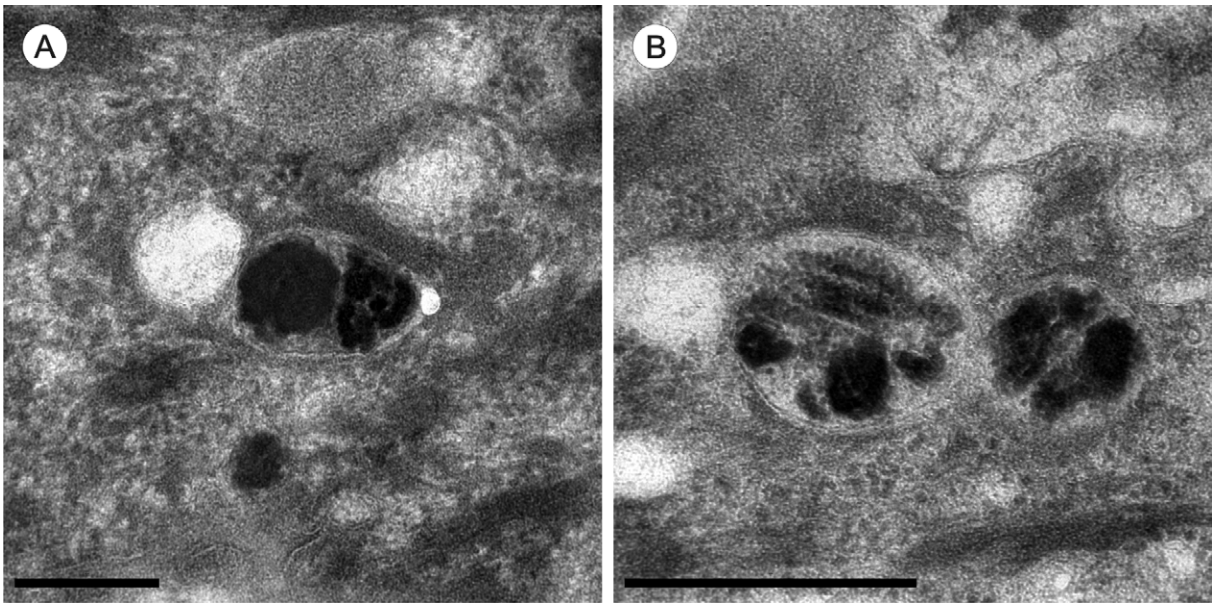

Figure 26: TEM images of melanosomes and melanosome clusters. In TEM images, melanosomes appear as electron dense, compact granules. The melanosomes can be present as isolated particles or form melanosome clusters. The clusters comprise of 2 – 10 subunits and are surrounded by a membrane. (A) Caucasian skin, (B) A sample of *lentigo senilis*, lesional. *Bars: 200 nm*

TEM provides a means to quantify the melanin content of skin samples by directly counting melanosomes and melanosome subunits. Contrary to the chemical determination of melanin content, this method gives information not only on the total melanin content (eu- and pheomelanin), but additionally allows to specify the intra-epidermal distribution of melanin and its polymorphism. This can be achieved by investigating the epidermal layers, like the *Stratum basale* or *Stratum corneum* independently. The results of this investigation are presented in the following chapter E.I.

A wide range of staining techniques microscopic detection techniques, ranging from conventional light microscopy to high-resolution electron microscopy, is available for the identification and description of melanin and melanocytes. But most of the tested methods are suited only for the generation of qualitative statements concerning the presence of melanin in biological tissues – only two methods have proven adequate for the purpose of this project.

Immunocytochemistry allows reliable identification of melanocytes and in combination with CSLM additionally provides 3D-information on their morphology and positioning in the context of the epidermis. This was applied to investigate the melanocyte density and the epidermal melanin unit (chapter E.II).

But as the light microscopic resolution is insufficient for investigations at the level of single melanosomes, TEM was required for the analysis of the epidermal distribution of melanosomes. Moreover, the process of melanosome transfer from melanocyte to keratinocyte and the morphological characteristics of melanosomes in the context of plasma membranes and the cytoskeleton can only be captured by TEM.

E RESULTS

I Epidermal Melanosome Distribution and Melanin Content

The epidermal melanosome distribution and melanin content were investigated on different sample collectives, as illustrated in Table 14. The epidermal distribution of melanosomes was determined for all three groups of samples, with the exception of the Fitzpatrick's skin phototypes, of which only the extremes – phototypes I and VI – were examined. A benchmark experiment was performed to evaluate the manual analysis with respect to different users, using one perilesional sample of *lentigo senilis*. To evaluate a new developed automated analysis tool for counting and grouping melanosomes according to their morphology, the tool was applied to the collective of *lentigo* samples, lesional and perilesional.

Finally, a chemical analysis of the melanin content and parallel reflectance spectroscopy was be applied to the latest sample collective of Fitzpatrick's skin phototypes I-VI to be able to compare and evaluate morphological findings with standard analytical methods used to determine the skin pigmentation in toto.

Table 14: Analyses of melanin content and melanosome distribution.

	Caucasian, Asian, Negroid skin	***Lentigo* (lesional vs. perilesional)**	**Fitzpatrick's skin phototypes**
Manual analysis of melanosome distribution	X	X	X [(1)]
Benchmark test for manual analysis		X [(2)]	
Automated analysis of melanosome distribution		X	
Chemical analysis of melanin content			X
Reflectance spectroscopy (L*a*b values)			X

[(1)] only skin phototypes I and VI
[(2)] only one perilesional sample of *lentigo senilis*

I.1 Stereological Analysis of Epidermal Melanosome Distribution

The epidermal melanosome content of the above specified skin samples was determined by TEM, as described in chapters C.VIII.3 and C.VIII.4. The epidermis was divided into four layers to analyze the intra-epidermal distribution – the *Stratum basale*, the lower and upper part of the *Stratum spinosum* and the *Stratum corneum*. Melanosomes were counted considering aggregations of melanin-filled organelles as one melanosome (see chapter C.VIII.4). The achieved melanosome numbers were correlated to the investigated area of the TEM images and plotted as melanosomes per µm².

I.1.1 Caucasian, Asian and Negroid Skin

Caucasian, Asian and Negroid skin samples obtained from the buttocks were investigated. The different ethnic skin types differed in total melanosome content as well as in the distribution patterns of the melanosomes in the epidermis. The data is displayed in Figure 27. Caucasian skin contained the lowest amount of melanosomes in all four investigated epidermal layers, followed by Asian and Negroid skin. Negroid skin contained not only the most melanosomes in the respective epidermal layers, but also by far the largest total amount of melanosomes. Melanosome numbers were generally highest in the SB, distinctly so in Asian (0.85 mel./ µm²) and Negroid skin (1.85 mel./ µm²), and decreased in the upper layers. The minimum melanosome content was not always found in the SC, as would be expected.

The differences between the ethnic skin types were reflected by the melanosome content of the SB. Asian skin contains double the amount of melanosomes in the SB than Caucasian skin (0.85 mel/ µm² vs. 0.38 mel./ µm²), and Negroid skin again the twofold quantity than Asian skin (1.85 mel./ µm² vs. 0.85 mel./ µm²). This trend is also found in the total amount of melanosomes: Caucasian skin contains a total of 0.82 mel./ µm² in the epidermis, Asian skin holds the 1.8-fold amount (1.51 mel./ µm² epidermis), and the quantity found in Negroid skin is again the twofold of that of Asian skin (3.07 mel./ µm² epidermis). Roughly, a doubling of melanosome content can be found also in the SC. The largest quantity is again found in the Negroid skin (0.30 mel./ µm²), approximately the half of this is found in Asian skin (0.17 mel./ µm²), and again half the amount is counted for Caucasian skin (0.09 mel./ µm²), where hardly any melanosomes are present.

A major difference between Caucasian skin and the darker ethnic skin types is stated in the reduction of melanosome numbers from SB to lSSp. Here, Caucasian skin shows a reduction

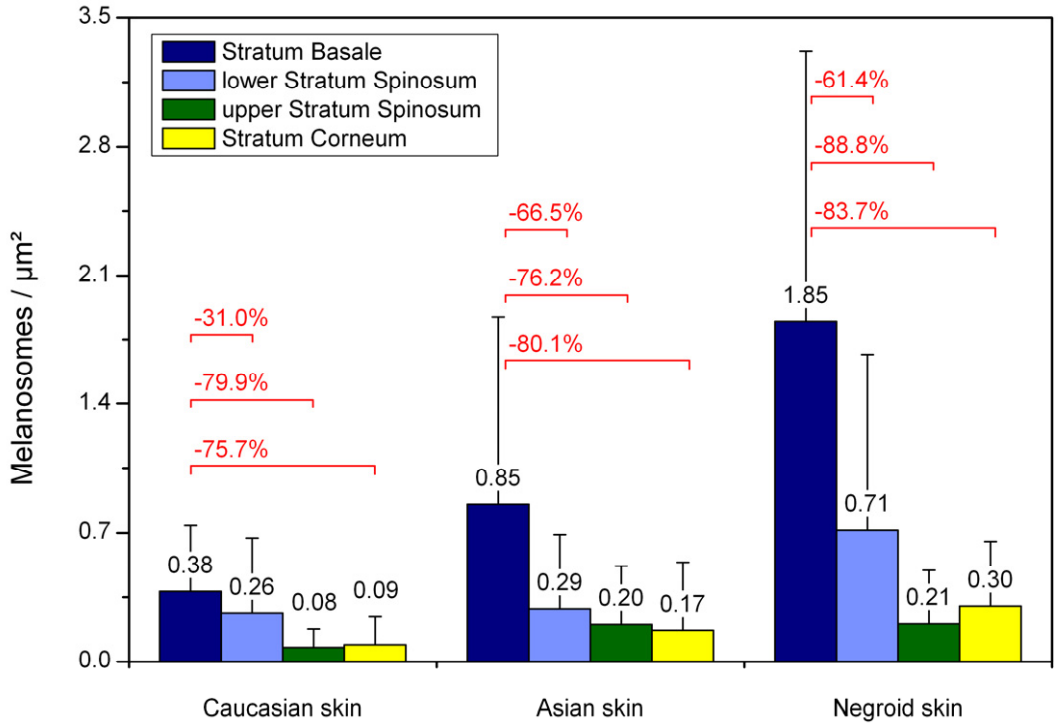

Figure 27: Epidermal melanosomes distribution in ethnic skin types. The total lowest melanosome content is found in Caucasian skin, Asian skin contains approx. double the amount of melanosomes, and the content of Negroid skin is again double than that of Asian skin. All phenotypes have in common, that the highest amount of melanosomes is found in the SB, and the melanosome number decrease in the upper layers of the epidermis. The reduction percentage from SB to the following layers is marked in red. The largest reduction from SB to SC is found in Negroid skin, the lowest in Caucasian skin.

of 31.0 %, while reduction rates of 66.5 % and 61.4 % are found in Asian and Negroid skin, respectively. The total reduction from SB to the skin surface (SC) are scaled again in the succession of melanosome content: Caucasian skin shows the lowest reduction with 75.7 %, followed by Asian skin (80.1 %) and the highest reduction rate is found in Negroid skin with 83.7 %.

As the volunteers for this study were not classified according to Fitzpatrick's skin phototypes, the Asian sample collective comprises a large variety of phenotypes. In an attempt to describe these different subtypes of Asian skin, the samples were further divided according to the countries of origin of the donors. These were Indonesia, India, China and Korea. The Chinese and Korean samples were pooled, as their complexion was assumed to be comparable. This was also expected to be the group of lightest complexion, which would result in the lowest amount of melanosomes.

As Figure 28 shows, this could not be confirmed. The Chinese/ Korean and the Indonesian collectives show comparable melanosome numbers (1.24 mel./ µm² epidermis vs. 1.19 mel./ µm²) and epidermal distribution patterns. The Indian skin contains more than the

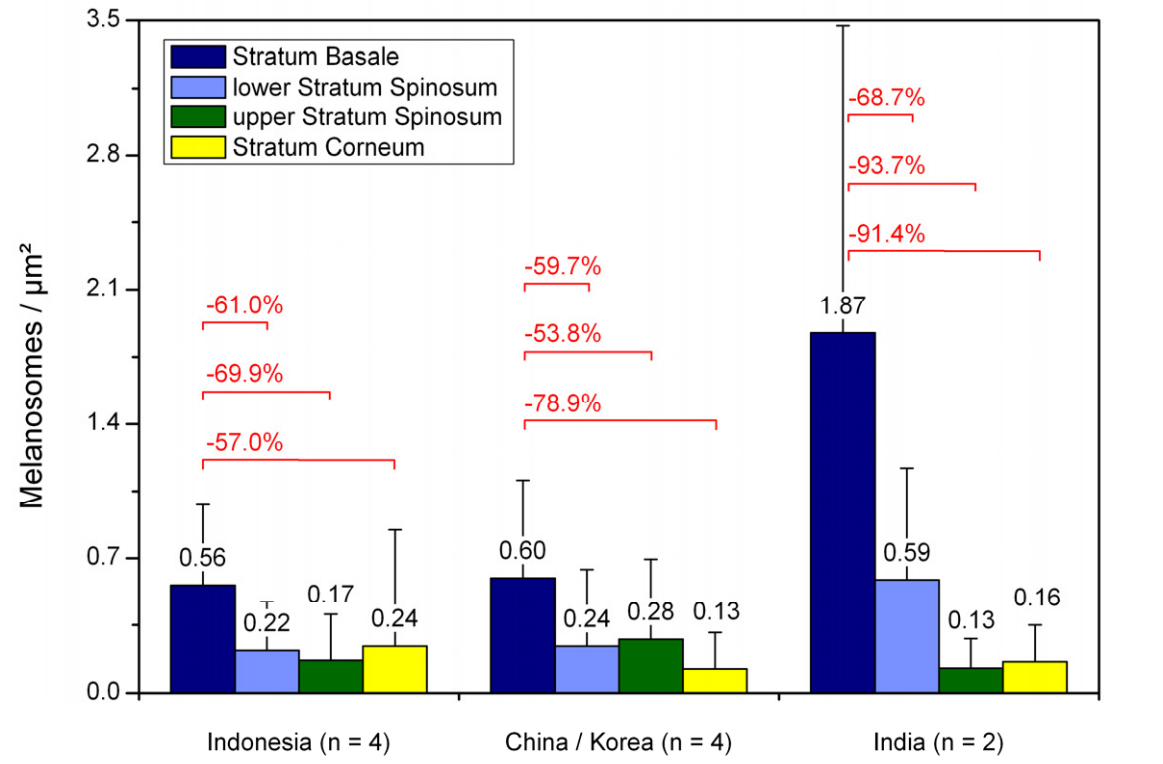

Figure 28: Epidermal melanosome distribution in Asian phenotypes. The collective of Asian skin samples was subdivided to reflect the countries of origin of the donors. Indonesian and Chinese/ Korean skin show comparable distribution patterns and total melanosome numbers. The Indian skin contains more than the threefold amount of melanosomes. The reduction rates from SB to lSSp are comparable in all three phenotypes, while the total reduction from SB to SC differs enormously. Chinese/ Korean skin shows the largest reduction (91 %), followed by Indian skin (79 %). The Indonesian skin samples show a high quantity of melanosomes in the SC, even more than in the SSp, which reduced the total reduction rate to 57 %.

threefold quantity of melanosomes in the SB (1.87 mel./ µm²), and the 2.3-fold amount throughout the epidermis (2.75 mel./ µm² epidermis). The melanosome numbers counted in the SC of all sample groups are comparable.

It must be noted, that only two Indian skin samples were available. The large standard deviation reflects a large difference in the complexion of the two respective volunteers. But both individuals show considerably higher quantities of melanosomes in the respective epidermal layers, as well as in total (2.15 and 3.84 mel./ µm² epidermis), compared to the other two groups of Asian ancestry. The reduction rates from SB to the following lSSp are comparable in all three Asian phenotypes: 61.0 % in Indonesian skin, 59.7 % in Chinese/ Korean skin, and 68.7 % in Indian skin. The striking difference is found in the total melanosome reduction rates from SB to SC. Here, the Indian skin samples show a very efficient reduction of 91.4 %, followed by the Chinese skin (78.9 %). Due to the increased melanosome content in the SC, the Indonesian skin presents a seemingly inefficient total melanosome reduction rate of

57.0 %. These findings not only reflect the diversity of Asian complexion, but confirm the necessity of sample classification according to Fitzpatrick's skin phototypes for exact and representative determination of melanosome content.

I.1.2 Fitzpatrick's Skin Phototypes I vs. VI

Five samples of each Fitzpatrick's skin phototype I and VI, obtained from the buttocks, were investigated in the same way as the samples of ethnic skin types described in the previous chapter. The general trend of epidermal melanosome distribution was confirmed in this second sample collective. The quantity of melanosomes/ µm² (mel./ µm²) was again the largest in the SB, the numbers decreasing in the higher epidermal layers (Figure 29). As expected, the amount of melanosomes in phototype I was much lower than that found in phototype VI, both within the four epidermal layers and throughout the entire epidermis. But with total number of 0.23 mel./ µm² epidermis for phototype I and 2.55 mel./ µm² epidermis for phototype VI, both sample groups stayed below the melanosome number counted for

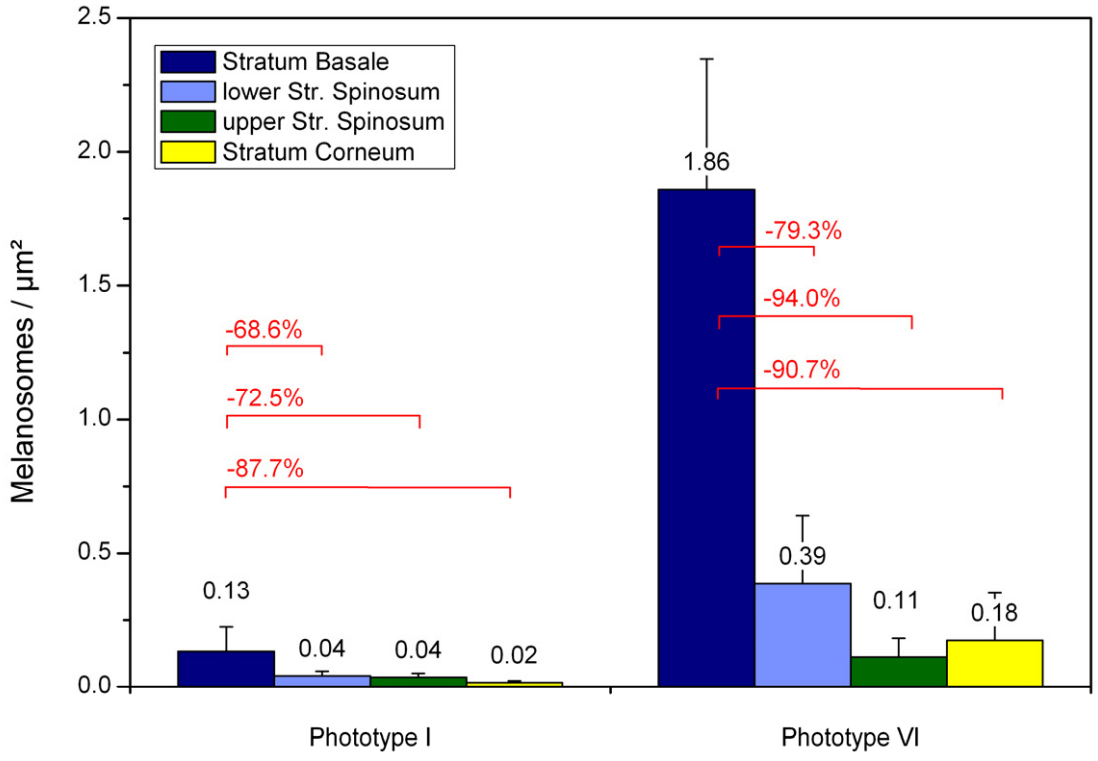

Figure 29: Epidermal melanosome distribution in Fitzpatrick's skin phototypes I and VI. The total amount of melanosomes in skin phototype I was more than tenfold lower than that of the skin samples of phototype VI. The general trend of decreasing melanosome contents from SB to SC was found again, but the counted melanosome numbers were much lower than the obtained data for Caucasian and Negroid skin, in all epidermal layers, except the SB of the phototype VI samples. On the other hand, the reductions rates obtained for phototypes I and VI were distinctly higher, than that of Caucasian and Negroid skin samples.

Caucasian and Negroid skin (0.82 mel./ µm² and 3.07 mel./ µm² epidermis). This was expected for phototype I, as the Caucasian sample collective comprised not only of phototype I, but included phototypes II and III as well. The phototype VI collective and the Negroid skin samples showed consistent results for the SB (1.85 mel./ µm² in Negroid skin and 1.86 mel./ µm² in phototype VI), but the in the upper epidermal layers, the phototype VI sample collective displayed smaller numbers of melanosomes ($lSSp_{Type\ VI}$: 0.39 mel./ µm² vs. $lSSp_{Negroid}$: 0.71 mel./ µm²; $uSSp_{TypeVI}$: 0.11 mel./ µm² vs. $uSSp_{Negroid}$: 0.21 mel./ µm²; $SC_{Type\ VI}$: 0.18 mel./ µm² vs. $SC_{Negroid}$: 0.30 mel./ µm²).

On the other hand, the measured reduction in melanosome quantity from SB to lSSp, and from SB to SC are distinctly higher than the reduction rates obtained for either Caucasian or Negroid skin. The reduction from SB to lSSp was 68.6 % in phototype I, compared to 31.0 % in Caucasian skin. The total reduction from SB to SC averaged 87.7 % in phototype I, as compared with 75.7 % found in Caucasian skin. In Negroid skin, the SB-lSSp reduction rated 61.4 %, and a total reduction of 83.7 % was measured, while the samples of phototype VI showed a reduction of 79.3 % from SB to lSSp, and a total reduction rate of 90.7 %.

I.1.3 Lentigo Senilis and Perilesional Adjacent Areas

Eleven samples from the lesions of senile *lentigines*, obtained from the back of the hands of the volunteers, were examined and compared to the direct periphery of the respective lesion (perilesional sample). Both, the lesion and the perilesional skin showed explicitly increased melanosome numbers throughout the entire epidermis, compared to normal Caucasian skin. The total amount of melanosomes in the lesion (2.50 mel./ µm² epidermis) was threefold higher than that of Caucasian skin and surpassed even Asian skin (1.51 mel./ µm² epidermis) and showed similar values counted for Fitzpatrick's skin phototype VI (2.55 mel./ µm² epidermis). Even the perilesional skin contained a total of 1.43 mel./ µm² epidermis. Caucasian skin averaged 0.82 mel./ µm² epidermis.

The same trend could be found for the single layers of the epidermis. The SB of lesional samples contained the threefold (1.10 mel./ µm²), the perilesional skin the twofold (0.75 mel./ µm²) quantity of melanosomes/ µm², as compared to Caucasian skin (0.38 mel./ mm²). The melanosome amount found in the SC of the lesion (0.27 mel./ µm²) was similar to Negroid skin (0.30 mel./ µm²) and the threefold of that of Caucasian skin (0.09 mel./ µm²). The perilesional skin still contained the 1.8-fold amount of Caucasian SC

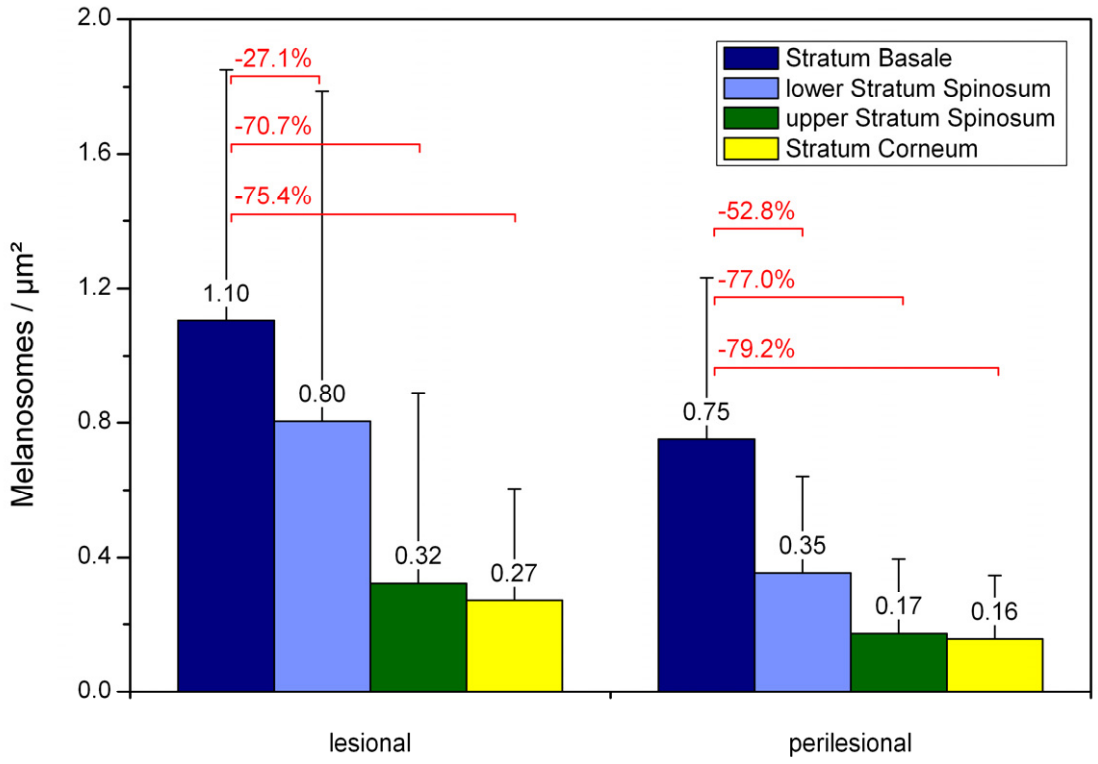

Figure 30: Epidermal melanosome distribution in *lentigo senilis*, lesional and perilesional. Eleven samples of age spots (*lentigo senilis*) were investigated and compared to samples obtained from the direct periphery of the respective senile *lentigines*. Both sample groups showed an increased melanosome content, when compared to normal Caucasian skin. The reduction rates from SB to SC showed comparable values, similar to Caucasian skin. But the reduction from SB to lSSp was distinctly increased in the perilesional skin (53 %), while the lesional skin (27 %) showed a melanosome reduction in the range of normal Caucasian skin (31 %).

(0.16 mel./ µm²), a value comparable to that found in Asian skin (0.17 mel./ µm²) or the samples of Fitzpatrick's skin phototype VI (0.18 mel./ µm²).

The total reduction rates (SB to SC) of both, lesional and perilesional skin (75.4 % and 79.2 %), was equivalent to that of Caucasian skin (75.7 %). The major difference was found in the reduction from the SB to the following lSSp. Here, the lesion showed a similar reduction rate (27.1 %) to the normal Caucasian skin (31.0 %). But the perilesional skin displayed a distinctly more efficient reduction in melanosome numbers (52.8 %).

I.1.4 Melanosome Organisation within the Keratinocytes of Different Skin Types

The epidermal distribution of melanosomes represents one criterion to differentiate ethnic skin types or Fitzpatrick's skin phototypes. But there are also differences in the distribution within the individual keratinocytes. Melanosomes were rarely found in the upper epidermal layers of Caucasian skin, while they are present in considerable numbers in the SC of Asian

and Negroid skin (Figure 31). In the basal keratinocytes, melanosomes were visible in varying quantities (see chapters I.1.1, I.1.2 and I.1.3) in all phenotypes. The bottom row in Figure 31 shows exemplary images of the SB of Caucasian, Asian and Negroid skin. In Caucasian skin, isolated melanosomes and clusters of melanin particles were present. The melanosomes were usually oval-shaped and a little smaller than in the other skin types. In Asian skin, the distribution pattern resembled that of Caucasian skin, except for the size of the melanosomes. The single particles within a cluster were generally smaller than the individually distributed melanosomes, the overall size of the cluster being only slightly larger than the individual particles. The majority of melanosomes found in Negroid skin were isolated particles. They were distinctly larger than that of Caucasian and Asian skin, and showed a more circular shape.

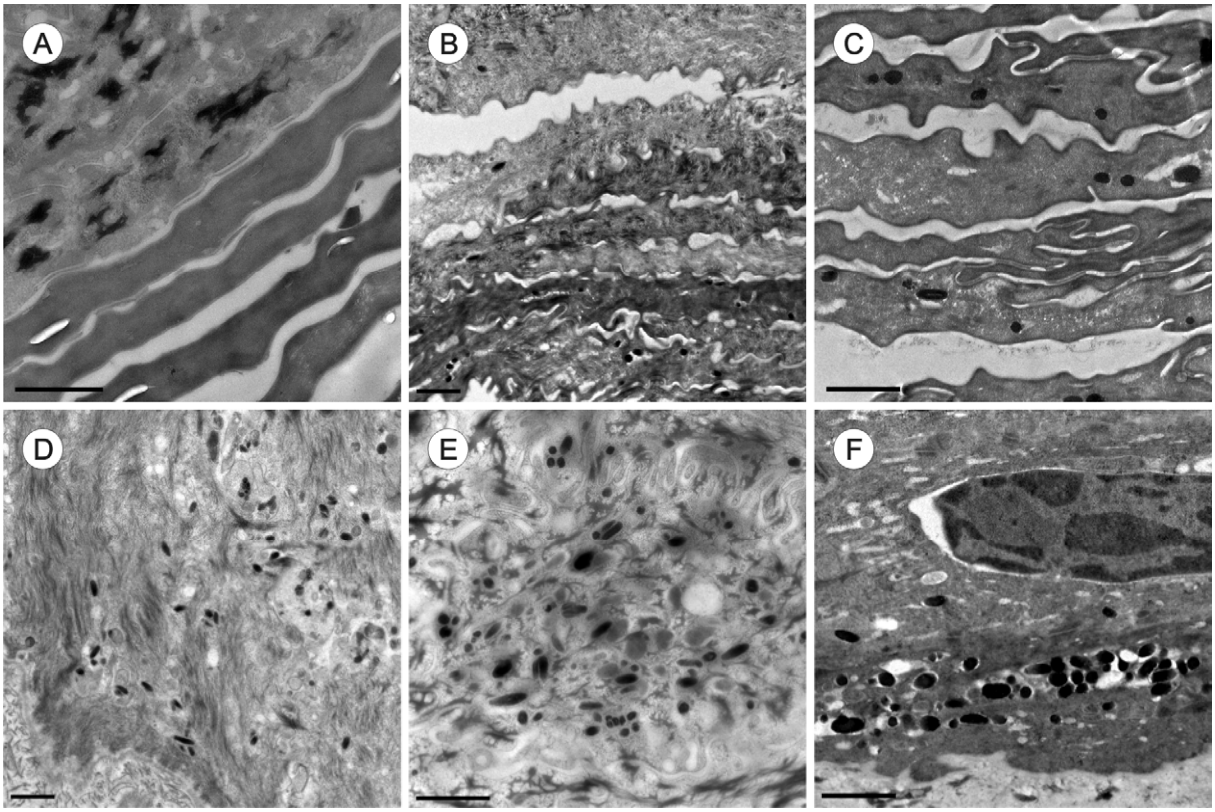

Figure 31: Melanosome distribution in SC and SB of different skin types. The images on top show the SC, the SB is displayed below. (A) No melanosomes were found in the SC of Caucasian skin, while in Asian skin (B) some melanosomes were present in the SC, usually isolated particles, but also some clusters could be observed. (C) Large, individual melanosomes were found in abundance in the SC of Negroid skin. (D) In the SB of Caucasian skin, few melanosomes were present. The bulk of the melanosomes was grouped into clusters and only very few isolated particles could be observed. (E) The SB of Asian skin showed more melanosomes than the Caucasian skin, that were a little larger in size. Clusters were frequently observed, with the single particles forming the cluster being smaller in size than the individually distributed melanosomes. (F) The basal cells of Negroid skin were often filled completely with large individual melanosomes. Clusters were infrequently observed. Lesional samples of *lentigo senilis* resembled Negroid skin in their distribution of melanosomes, but the particles had the dimensions of Caucasian melanosomes. Perilesional skin showed distribution patterns comparable to Caucasian and Asian skin. *Bars: 1 µm*

Frequently, the basal keratinocytes of Negroid skin were completely filled with melanosomes. The lesional samples of *lentigo senilis* showed a distribution pattern comparable to Asian and even Negroid skin, with melanosomes filling the basal keratinocytes and melanosomes present in the SC. But the melanosomes were not as large as in Negroid skin. The perilesional skin resembled Caucasian skin, only the total number of melanosomes was higher (see chapter I.1.3).

The proportion of individual melanosomes compared to melanosome clusters is displayed in Table 15. Basically, the different phenotypes, including *lentigo senilis*, showed comparable percentages of individual melanosomes in all investigated epidermal layers. A clear tendency towards a separation into individual units towards the outmost layer of the epidermis can be found for all skin types and therefore melanosome clusters vanish within lower skin layers during epidermal differentiation. In the SB, approximately 50 % of the melanosomes were present as individual particles, and in the SC, 85 – 90 % of melanosomes were individually distributed. Skin of phototype I and Negroid skin (including phototype VI) constituted an exception. The light skin (phototype I) contained a very high percentage of melanosomes bound in clusters in the SB and only 35.7 % of the melanosomes were individually distributed. In the upper layers, the proportions adapted to the values found in the other phenotypes. In Negroid skin, all epidermal layers showed more than 80 % individual melanosomes.

Table 15: Percentage of individual melanosomes in the epidermal layers of different skin types.

	SB	**lSSp**	**uSSp**	**SC**
Phototype I	35.7 %	53.5 %	68.3 %	93.6 %
Caucasian skin	50.9 %	69.3 %	81.4 %	85.9 %
Asian skin	55.8 %	68.5 %	82.1 %	92.2 %
Negroid skin	87.0 %	85.1 %	83.6%	90.1 %
Phototype VI	76.2 %	78.0 %	83.6 %	94.2 %
Lentigo senilis lesional	51.4 %	55.1 %	75.8 %	87.7 %
Lentigo senilis perilesional	51.9 %	63.6 %	77.9 %	88.8 %

I.1.5 Epidermal Distribution of Melanin Particles in Different Phenotypes

Considering that nearly 50 % of melanosomes in the SB are bound in clusters (with the exception of Negroid skin, where only 23 % of the melanosomes are clustered), it must be contemplated, if counting clusters as one melanosome leads to an appropriate estimation of the epidermal melanin content. Although the single particles constituting a cluster are generally a little smaller than the individual melanosomes, it might be of interest to analyze the epidermal distribution, counting each single melanin unit. The results of the thus modified analysis are displayed in Figure 32 and Figure 33.

As expected, the quantities of melanin particles were higher than that counted for melanosomes, for all phenotypes and in all epidermal layers. The most dramatic changes were observed in the SB, as this was the layer with the largest contingent of clusters. But the general trend remained: the smallest number of melanin particles were found in skin of phototype I, followed by Caucasian, Asian and Negroid skin. The phototype VI samples surpassed the

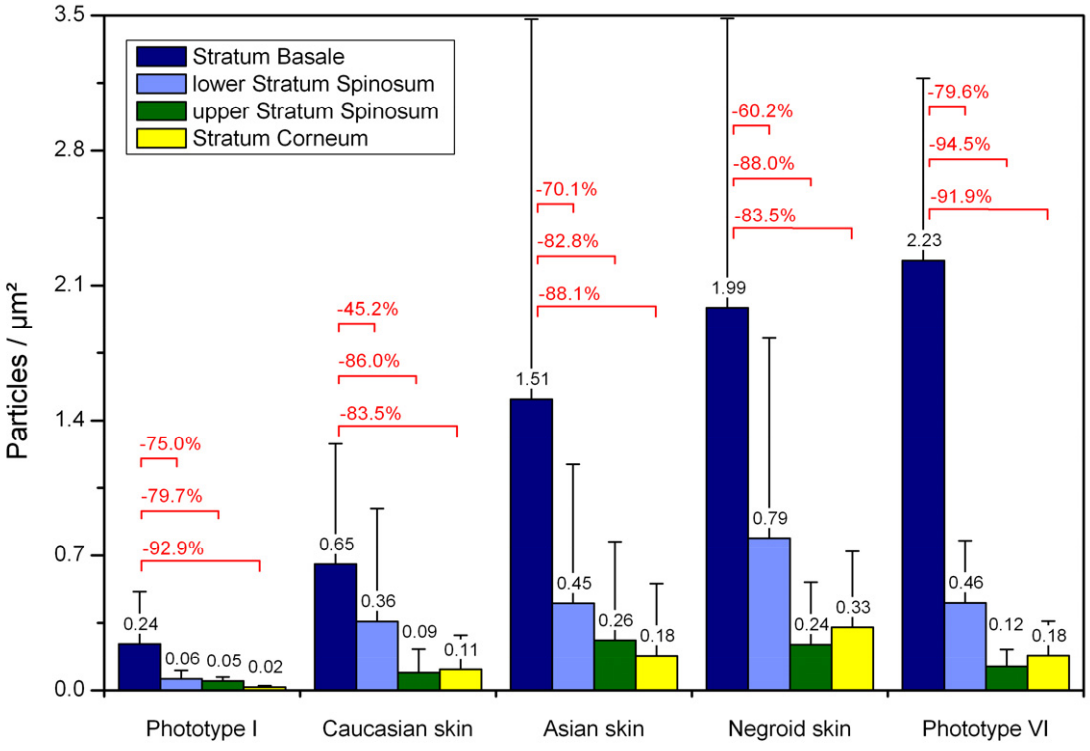

Figure 32: Epidermal distribution of melanin particles in ethnic skin types and phototypes I and VI. For this analysis, clusters were not regarded as one melanosome, but each single melanin particle – bound in a cluster or individually distributed – were counted and correlated to the respective area of the investigated epidermal layers. Expectably, the quantity of melanin particles, was larger than the number of melanosomes in all phenotypes and throughout all epidermal layers, especially in the SB. Skin of phototype I contained the smallest amount of melanosomes, followed by the collectives of Caucasian, Asian and Negroid skin. Due to their higher percentage of clusters, the samples of phototype VI surpassed the collective of Negroid skin samples in the SB. The total melanosome reduction rates were comparable for all skin types.

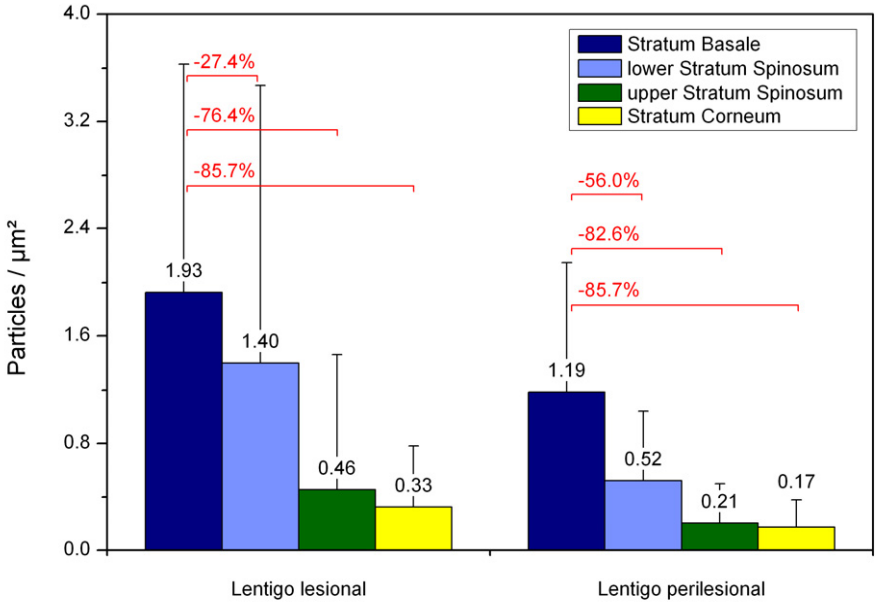

Figure 33: Epidermal distribution of melanin particles in *lentigo senilis*. Again, all melanin particles were counted as an independent unit. The particle quantities per µm² in all epidermal layers were larger than in Caucasian skin in both, lesional and perilesional skin. Lesional skin surpassed even Asian skin. A difference between the lesional and perilesional skin in the reduction rates existed only in the lower epidermal layers, the total reduction from SB to SC showed equal values.

collective of Negroid skin in the SB, due to their larger percentage of clusters in this layer, in the upper epidermal layers, the amount of melanin particles is smaller than in the Negroid skin. In *lentigo senilis* (Figure 33), both lesional and perilesional, the numbers of melanin particles were higher than in Caucasian skin in all epidermal layers. The lesional skin contained even more melanin particles, than Asian skin.

The reduction rates for melanin particles from SB to SC were comparable in all phenotypes, including *lentigo senilis*, and ranged between 83 – 93 %. But major differences were found in the initial reduction from SB to lSSp. Here, the lesional skin of *lentigo senilis* displayed the slightest reduction (27.4 %), while Caucasian skin showed a reduction of 45.2 %. Perilesional skin was comparable to Asian skin (56.0 % vs. 60.2 %). The other skin types exhibit reduction rates of more than 70 %. But compared to the reduction rates obtained when clusters were counted as one melanosome, the clearing rates from the SB to lSSp show an increase of 6 – 15 % in the lighter skin types (Caucasian skin phototype I), but hardly any changes are found in the dark skin types. Whereas the clearing rate in *lentigo senilis* is unchanged in the lower skin layer (SB to lSSp), but is significantly changed toward the upper layers of the epidermis (+ 10 % from SB to SC).

I.1.6 Benchmark Test of the Manual Analysis

To evaluate the significance of the above described manual analysis and estimate susceptibility for misinterpretations in the identification of melanin particles and the allocation to melanosome clusters, a panel of six staff members of the microscopy department volunteered to perform the analysis. Three volunteers were experienced in EM and the interpretation of TEM images of skin. The other three had no experience with TEM images, but a profound microscopic background knowledge. All six volunteers investigated the same sample, a section of a TEM mosaic of a perilesional sample of *lentigo senilis*, covering all four epidermal layers. The image is displayed in Figure 34 (sample number A57-5). The epidermal layers were predefined (see red numbers in Figure 34), and working instructions concerning the definition of melanin particles and melanosome clusters were given. A melanosome was defined as described above (see also chapter C.VIII.4).

The obtained data showed only minor variations for all investigators. Therefore, no distinction was made between EM-experienced and not experienced investigators. The data is shown in Figure 35. The control was extracted from the original analysis of the entire sample collective.

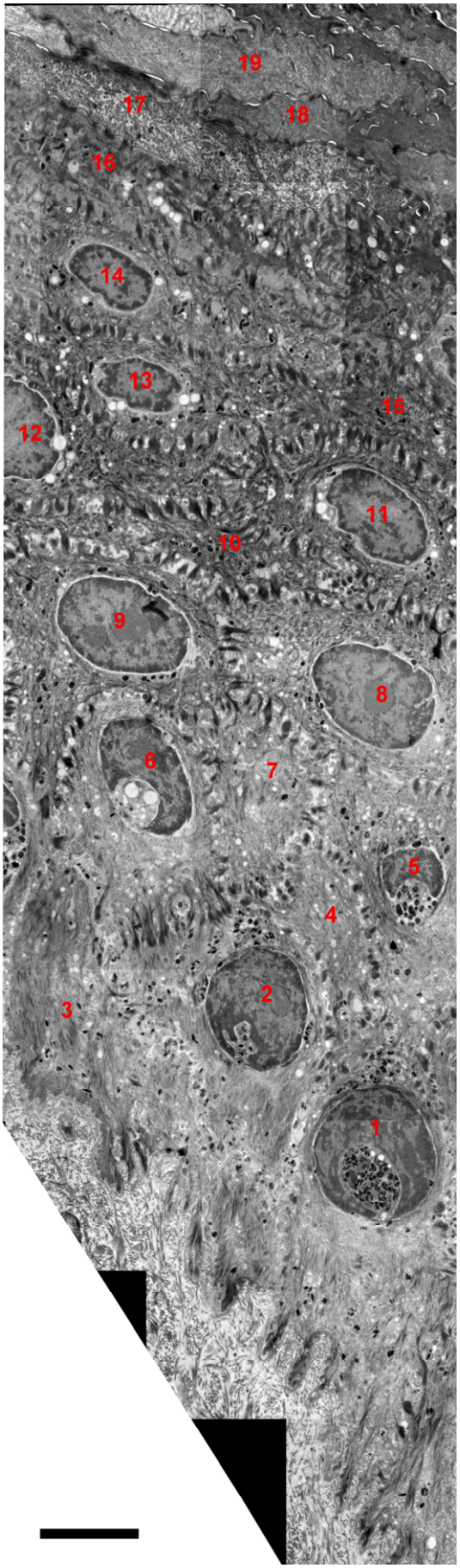

Figure 34: TEM mosaic used for benchmarking the manual analysis. The image shows a perilesional sample of *lentigo senilis*. All four investigated epidermal layers are displayed. The SB comprises of cells 1 – 3 (red numbers), cells 4 – 9 are defined as lSSp, the uSSp consist of cells 10 – 16, and cells 17 – 19 are allocated to the SC. *Bar: 5 µm*

As this data set comprised only a very small number of investigated cells per epidermal layer, the standard deviation was larger than that calculated for the data set obtained by the panel of investigators, which included the entire data of six different analyses.

The quantity of melanin particles counted by the six investigators differed only slightly from the original investigation (see Figure 35, right side), especially in the SB (0.77 part./ µm² for both) and uSSp (0.37 part./ µm² for the panel of investigators and 0.35 part./ µm² in the control). In the lSSp (0.34 part./ µm²) and SC (0.12 part./ µm²), the numbers were only a little higher than in the control (lSSp: 0.27 part./ µm², SC: 0.07 part./ µm²), indicating that the identification of melanin particles posed no difficulties for each of the different investigators, regardless of the grade of experience in the interpretation of TEM images.

On the other hand, the allocation of melanin particles to melanosome clusters, seemed to be more difficult. The quantity of clusters was underestimated in the SB and the respective melanin particles were counted as individual melanosome (see Figure 35, left side), resulting

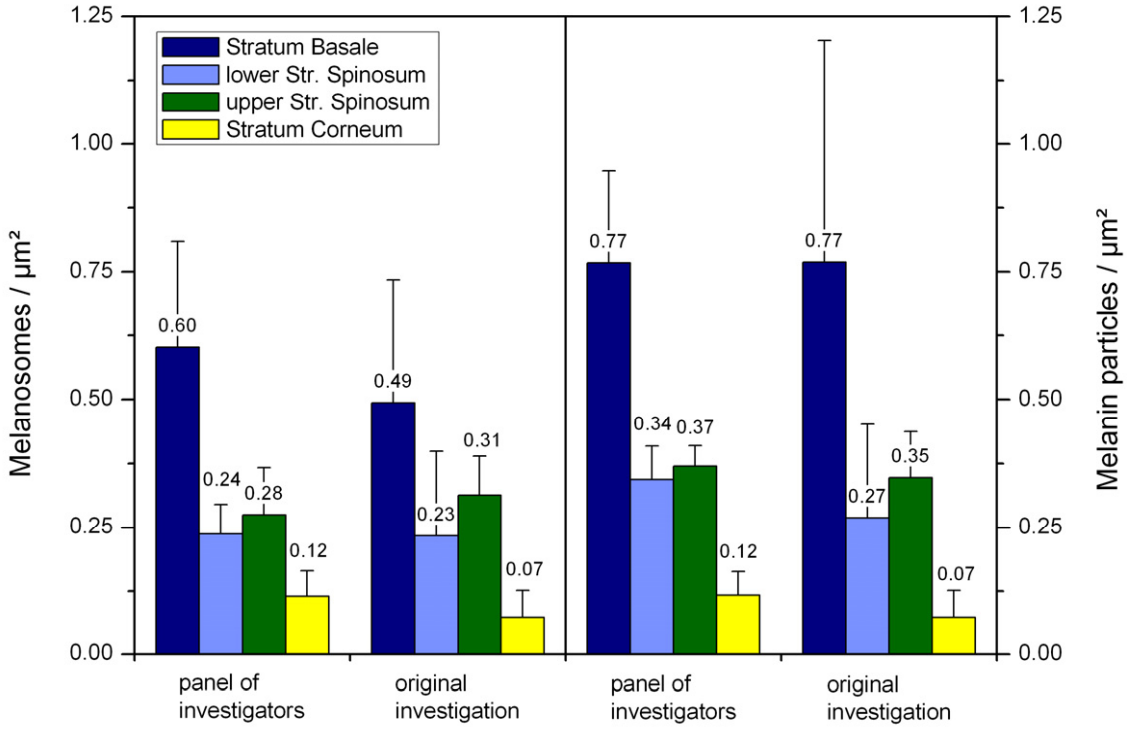

Figure 35: Benchmark test of the manual analysis of melanosome and melanin particle numbers. Six volunteers were asked to perform the above described analysis of melanosome content. Three of the participants had experience in the interpretation of TEM images of skin. The other three had no experience with TEM, but a profound background knowledge of microscopy. All investigated the same sample. The data obtained by both groups showed only minor variations and is therefore pooled. The control shows the original data obtained during the analysis of the entire sample collective. The standard deviation of the panel of users-data included the entire data set of six different analyses, while the control-data included only a very small set of investigated cells, and the values were therefore larger. The quantities of melanin particles (right side) showed a good correlation, especially in the SB, indicating that the particles were well identified. But the number of melanin particles allocated to melanosomes (left side) was underestimated in the SB.

in a larger value for melanosomes (0.60 mel./ µm²) compared to the control (0.49 mel./ µm²). Considering the standard deviation, the correlation was good in the upper epidermal layers. In the SC no clusters were found, which is consistent with the control data. Generally, the benchmark experiment showed a good correlation between the data obtained by different investigators for both, melanin particles and melanosome numbers. The inter-investigator variability was highest in the SC with a standard deviation of 43 %, in the other layers, the standard variation ranged between 25 and 35 %.

I.2 Automated Analysis of Epidermal Melanosome Distribution

As counting melanin particles and melanosomes is very time-consuming, an automated image analysis tool (ZETA) was developed by the Fraunhofer Institute for Applied Information Technology (FIT) in Sankt Augustin, Germany (see also chapter C.VIII.5). The classification of the four epidermal layers still had to be done manually, therefore, the TEM mosaics (see chapters C.VII.3 and C.VIII.3) could not be processed en bloc. Cleavages of the mosaics, covering each epidermal layer, were processed instead, without further fragmentation. Melanosome numbers were determined for each epidermal layer. A melanosome cluster was defined by the spatial configuration of subunits. If the distance between single melanin particles was less than 50 nm, they were rated as a cluster. In addition, the area of the identified melanosomes was measured. An annotated image was generated displaying the areas identified and counted as melanosomes and those melanosomes allocated to clusters. This allowed a visual control of the analysis.

Figure 36: Annotated TEM images illustrating the detection of melanosomes by ZETA. Cleavages of three different samples are displayed, that were processed with ZETA to determine the melanosome content. The annotated images, serving as a visual control of the analysis are displayed on the left. On the right, the respective section without annotation is displayed. (A & B) Example of very good identification and segmentation of melanosomes and melanosome clusters. The sample showed very good structural preservation, although some irregularities in form and location of the nuclei were apparent. But that did not impede with the image processing. (C & D) The structural preservation of this sample was bad, artificial agglomerations of keratin filaments and other artefacts appeared as dark as the melanosomes, and were thus falsely rated as melanosomes (see white arrows). On the other hand, some melanosomes were not identified (see red arrowheads). Often, subunits of melanosome clusters were not identified, and the cluster was rated as one particle (white arrowheads). (E & F) Example of underestimation of melanosome content. Approximately half of the melanosomes were not identified. A lot of the identified segments did not correspond to the actual form of the melanosomes (see white arrowheads). *Bars: 1 µm*

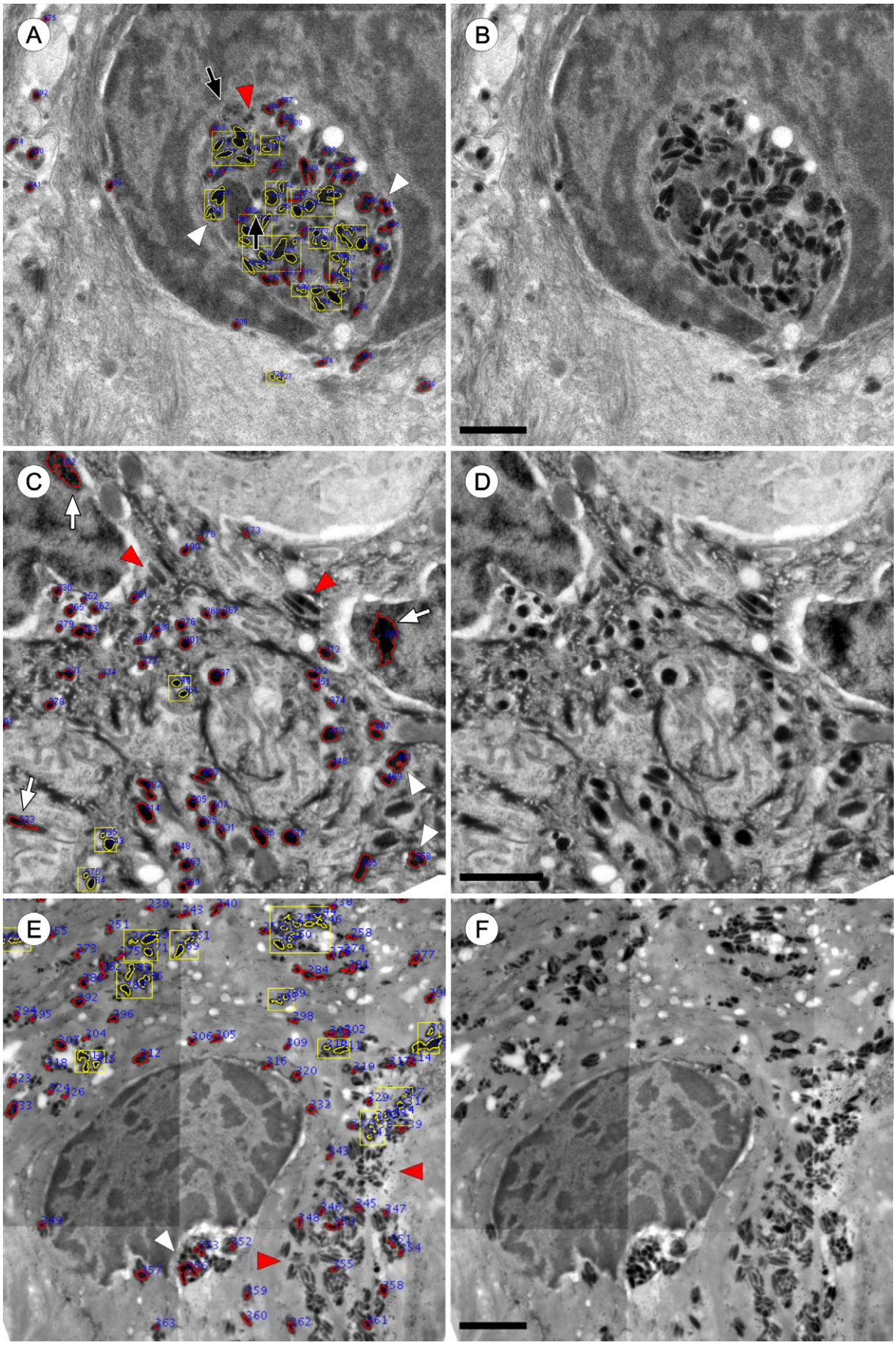
A
B
C
D
E
F

I.2.1 Capability and Limitations of the Automated Analysis

The structural integrity of the sample constituted a major issue for the automated analysis tool. Variations in preservation quality and the presence of artefacts made it impossible to develop a universally valid algorithm for the detection of melanosomes. The software had to be trained separately for samples of good and poor structural preservation, and only images of comparable quality could be processed with identical algorithms. Nevertheless, the automated analysis produced very good results for samples with good structural preservation without artefacts (see Figure 36.A & B). The melanosomes were by far the darkest structures of the respective size in the images, and could thus be easily identified by the segmentation tool. Other organelles that resembled melanosomes in either shape or darkness were not rated as melanosomes (black arrow). The detection of melanin particles and melanosome clusters was good, and only very few melanosomes were not identified (red arrowheads).

But if the structural integrity of the sample was worse, the quality of the melanosome detection was impaired. Preparation artefacts and staining artefacts caused difficulties in the segmentation process. These artefacts appeared as very dark, jagged or fringy shapes, usually larger than the average melanosome. But still, some of these artefacts were counted as melanosomes, despite the different shape and size. Figure 36.C shows an example of a sample with preparation artefacts that would not hinder the manual analysis, but caused considerable difficulties for the image analysis tool. Coagulations of keratin filaments or nucleic acids within the nuclei were falsely detected as melanosomes (white arrows), and subunits of melanosome clusters were often detected as one particle (marked with white arrowheads). On the other hand, some melanosomes were not detected by the software that showed no noticeable variations from the detected melanosomes, in either shape or size (see red arrowheads). Figure 36.E shows an image, that was extraordinarily easy to analyze manually, as – at least in the human perception – the melanosomes stand out against a relatively light background. Contrary to expectations, this image showed a large percentage of undetected melanosomes. And the detected areas displayed uncharacteristic shapes and did not always correspond to actually present melanosomes (white arrowheads). A minor drawback of this analysis tool is the fact that certain a developed algorithm can only be applied to images acquired with identical magnification and resolution. This presents no problem for future investigation, as it can be considered during the acquisition of the images to be analyzed, but it necessitated elaborate post-processing of pre-existing images or even made it impossible.

I.2.2 Comparison of Manual and Automated Analysis on the Basis of Lentigo Samples

To evaluate the results of the ZETA analysis, a part of the collective of *lentigo senilis* samples was processed with the analysis tool, and the results were compared with the existing data of the manual analysis. As mentioned in the previous chapter, the images needed processing before the analysis tool could be applied: each epidermal layer had to be cut out of the overview mosaic of the respective sample and was stored as new image, leaving only the area to be investigated before a white background. Additionally, the resolution of the images had to be adjusted, if necessary, to match the pre-defined value of 8.8 nm/ pixel. Twelve samples (six lesional, and six perilesional samples) were investigated. Each sample yielded at least four images, one for each epidermal layer, sometimes even two, if the imaged area was too small for statistical analysis. Thus, a total of 55 images was processed. But, as mentioned before, the samples were of varying quality, and it was not possible to apply a universally valid algorithm for the detection of melanosomes. Most of the samples had to be processed individually, making a direct comparison of the results as well as of the investigation method difficult. But the major difference between the two analysis methods was the definition of melanosome clusters. While for the manual analysis, melanin particles were defined as part of a cluster, if a surrounding membrane was visible, this criterion could not be implemented in the automated detection system. Therefore, the mere distance between single particles was used as decisive factor. If this distance dropped below 50 nm, the respective particles were identified as parts of a cluster. Therefore, the values obtained for the epidermal melanosomes content could not be compared, but the particle numbers were used instead.

The results obtained for the lesional and perilesional samples of *lentigo senilis* are displayed in Figure 37. The automated analysis resulted in an underassessment of the content of melanin particles in all epidermal layers. In the SB and lSSp, only half of the particles counted in the manual investigation in the respective images, were identified by the automated analysis tool. In the uSSp and SC, the divergence between the two analysis methods was even higher, as in the uSSp of the lesional skin only 24 % of the melanin particles were identified, while in the uSSp of the perilesional skin, the automated analysis tool identified 23 % more particles than actually present, and the SC showed reverse detection rates, with 66 % detected in lesional samples and only 16 % in perilesional skin.

As mentioned before, the structural integrity of the sample was crucial for the quality of the automated detection of melanin particles. Only very few of the investigated *lentigo* samples

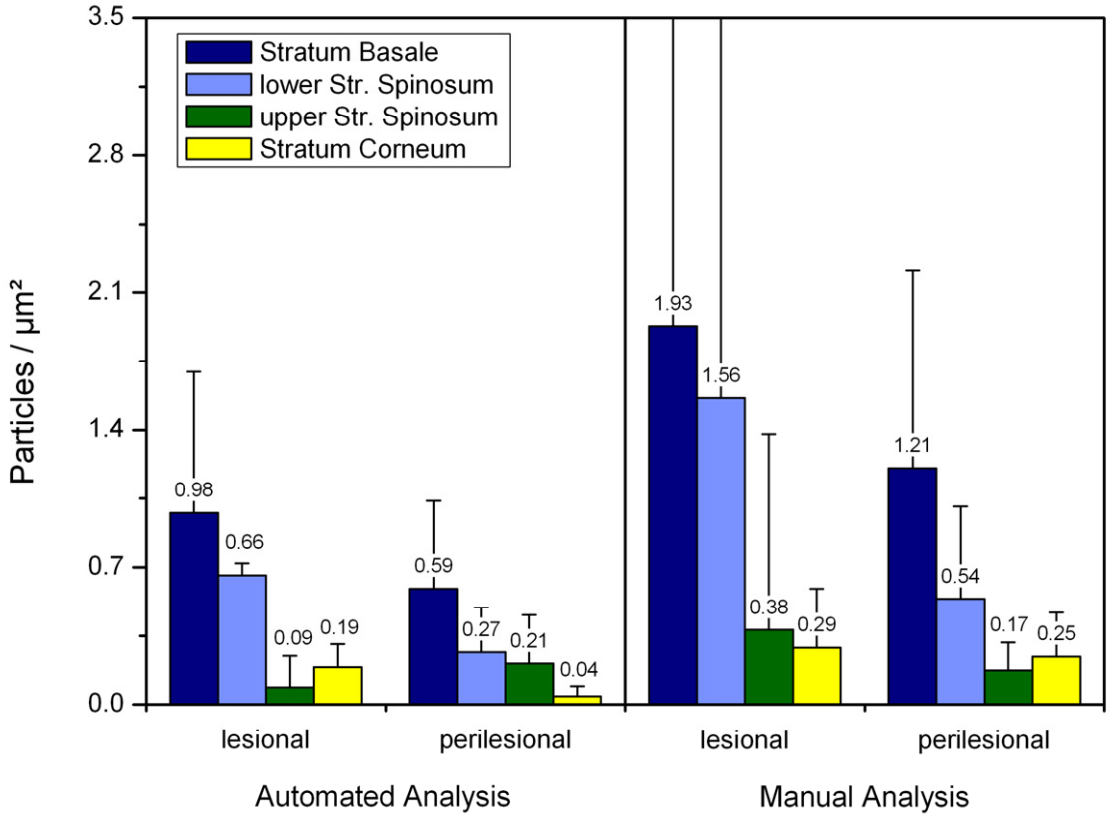

Figure 37: Comparison of automated and manual analysis. For the assessment of the analysis tool, generated by the Fraunhofer Institute for Applied Information Technology (FIT), the sample collective of *lentigo senilis* was processed. The results for melanosome numbers of the two analysis methods can not be compared directly, as they are based on different definitions of melanosomes and melanosome clusters. Therefore, the quantities of melanin particles are used for the comparison. The results of the automated analysis (left) showed a large underassessment of the content of melanin particles compared to the manual analysis. Only 50 % of the particles in the SB and lSSp were identified, in the upper epidermal layers, the recognition rate was even lower.

demonstrated sufficient quality to achieve satisfying results. For these individual samples, the numbers of melanin particles, and melanosomes as well, corresponded well with the results of the manual investigation, as Figure 38 demonstrates. The quantities of melanin particles detected in this perilesional sample (see also Figure 36.A & B) were absolutely comparable to the results of the manual analysis in all epidermal layers, except in the SC, where only 13 % of the particles could be identified. In the other epidermal layers the results were well within the standard deviation of the manually counted values. The discrepancy was 10 – 15 %.

As visible in Figure 36.A and Figure 38, even the allocation to melanosome clusters produced good results. In the lower epidermal layers, the percentage of clustered melanin particles was underestimated by 15 – 35 %, resulting in higher quantities of melanosomes. Again, the SC constituted an exception. Considering the inter-investigator variability of approximately 30 %, the variance in the results of the automated analysis was within a tolerable range.

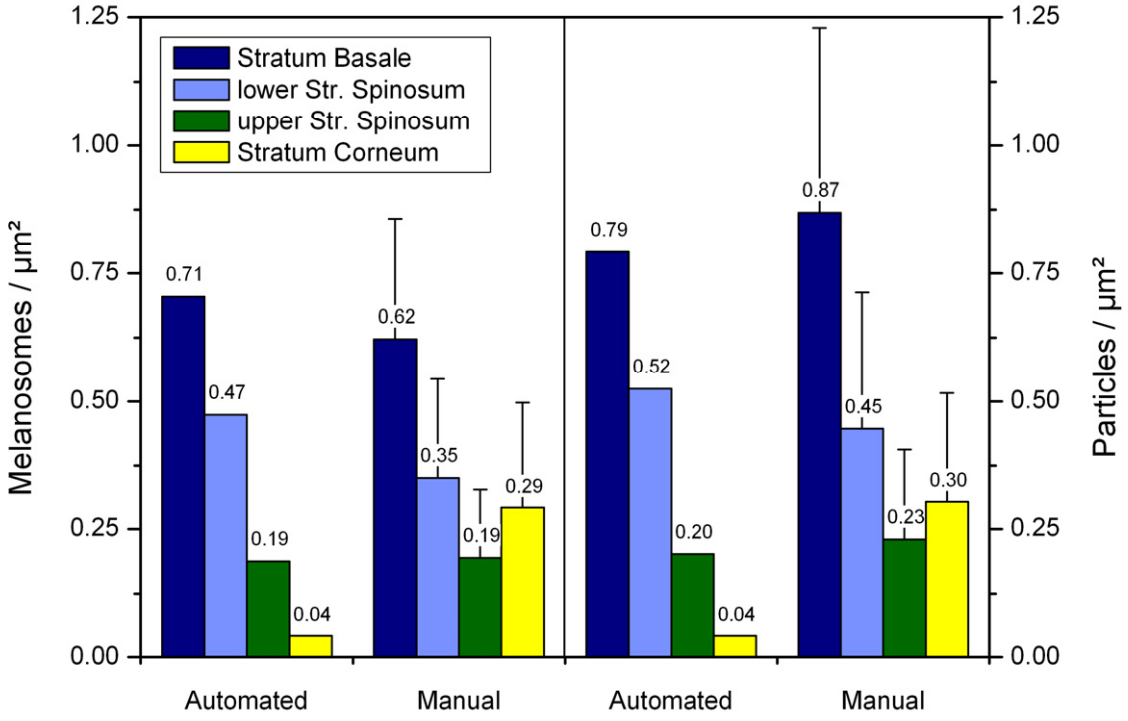

Figure 38: Data of the automated and manual analysis of a perilesional sample (A75-5). This sample showed a good structural integrity, which resulted in a very precise detection of melanosomes (see also Figure 36.A & B). The obtained particle numbers corresponded to the manually counted numbers (right). Only in the SC, the automated detection could not match the manual analysis. Even with the different definition of melanosome clusters, the manually determined melanosome numbers could be reproduced with the automated image analysis tool (left). Again, the SC constituted an exception.

I.3 Chemical Analysis of Epidermal Melanin Content

The sample collective of Fitzpatrick's skin phototypes I-VI comprised of five biopsies of each of the six phototypes. Two biopsies were obtained of each of the thirty volunteers, one was processed for microscopic investigation, the other was chemically analyzed for eumelanin and pheomelanin content as described in chapter C.VI.1. Three samples were lost during shipment to Japan or during the analysis, two of phototype I and one of phototype II (samples #2, #15 and #26). One sample of phototype VI (#16) was not counted for the statistics, as the sample dried out during transport from the UKE to BDF, and the wet weight could not be determined correctly. Here, the values for PTCA and 4-AHP were four times higher than the average for the other phototype VI samples. Following Dr. Wakamatsu's suggestion, sample #27, originally rated phototype V, was classified as phototype VI.

To match the original classification of Caucasian, Asian and Negroid skin, phototypes II and III, and phototypes IV and V were pooled. Phototype I, that is also found in Caucasian skin,

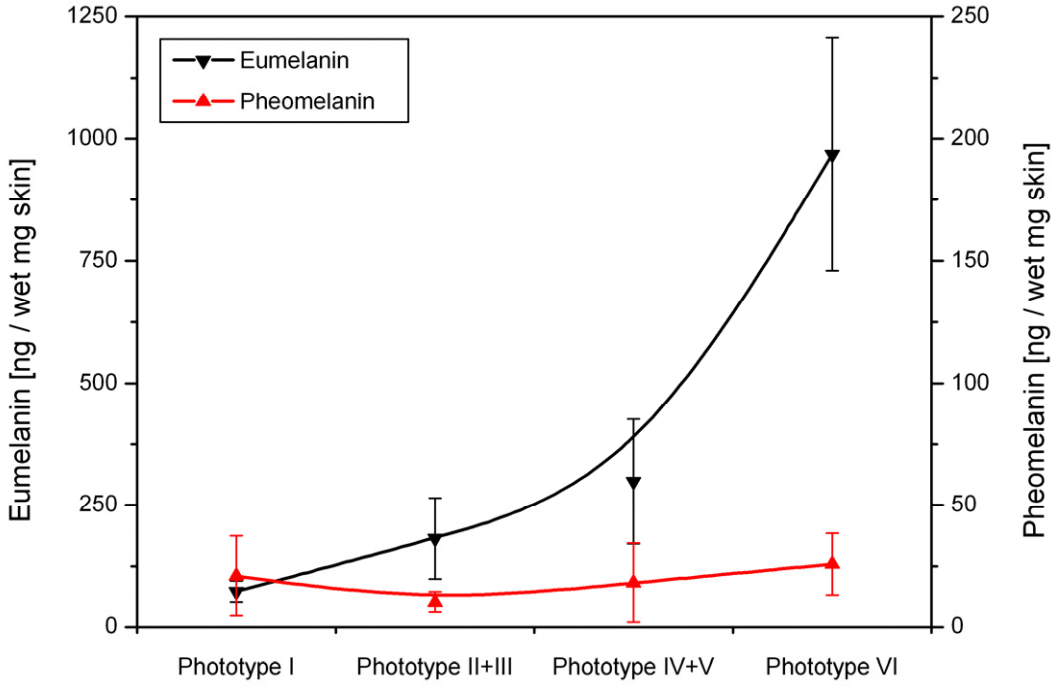

Figure 39: Eu- and pheomelanin content in Fitzpatrick's skin phototypes I -VI. The amount of eu- and pheomelanin were determined chemically, the eumelanin content is displayed in black, the pheomelanin content in red. The grouping of phototypes II+III and IV+V was chosen to match the classification of Caucasian, Asian and Negroid skin. Phototype I was rated individually, because of the large percentage of pheomelanin (22 %). The eumelanin content increased nearly exponentially with the phototype, while the amount of pheomelanin decreased, compared to the total melanin content.

was rated independently to acknowledge the large amount of pheomelanin (22 %). Figure 39 gives an overview of the measured eu- and pheomelanin content, the exact values are listed in Table 16. The eumelanin content increased nearly exponentially with the phototype. Phototype I (74 ng eumel./ wet mg skin) contained only half of the amount of eumelanin measured for phototypes II+III (181 ng eumel./ wet mg skin). On the other hand, the amount of eumelanin found in phototypes IV+V (299 ng eumel/ wet mg skin) was only 1.6-times more than in phototype II+III. By far the largest amount of eumelanin was measured for phototype VI. With approx. 970 ng eumel./ wet mg skin, the eumelanin content was 3.2-times higher than in phototypes IV+V, and 5.3-times more than in phototypes II+III. Especially in phototype VI, the absolute values for eumelanin content showed a high variation, ranging from 720 ng eumel./ wet mg skin to 1340 ng eumel./ wet mg skin.

Compared to the total melanin content, the amount of pheomelanin decreased with the phototype: while in phototype I the amount of pheomelanin was 22 %, it decreased to 5 – 6 % in phototypes II–V, and was even less in phototype VI (2.6 %). The absolute values are more or less constant and rage between 10 – 25 ng pheomel./ wet mg skin.

Table 16: Melanin content in Fitzpatrick's skin phototypes I -VI and percentage of eu- and pheomelanin.

	Phototype I	Phototype II+III	Phototype IV+V	Phototype VI
Eumelanin *[ng/ mg skin]*	73.60	180.98	298.49	968.32
% of total melanin	77.8 %	94.6 %	94.2 %	97.4 %
Pheomelanin *[ng/ mg skin]*	21.03	10.33	18.26	25.83
% of total melanin	22.3 %	5.4 %	5.8 %	2.6 %
total Melanin *[ng/ mg skin]*	94.63	191.31	316.75	994.15

I.4 Investigation of Skin Colour by Reflectance Spectroscopy

For better description and evaluation of the sample collective of Fitzpatrick's skin phototypes I-VI, the participants were reinvited a year after the original punch biopsy study was completed, for reflectance spectroscopy measurement of the area, where the biopsy was taken. Unfortunately, only 16 of the 30 participants could be reinvestigated, three of phototype I, four each of phototype II and III, two of phototype IV and three of phototype VI.

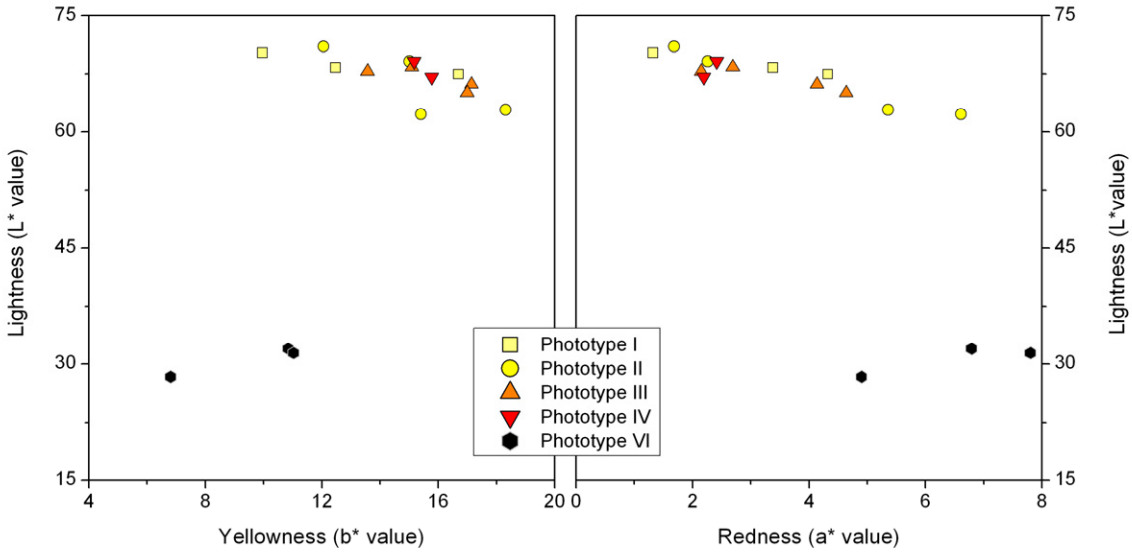

Figure 40: Reflectance spectroscopy of Fitzpatrick's skin phototypes I-IV and VI. Reflectance spectroscopy was applied to determine the *L*a*b**-values of the area, where the biopsy was taken of the collective of Fitzpatrick's skin phototypes I – IV and VI. Not all of the participants could be reinvestigated, thus no data was obtained on phototype V. The *L** values, representative of the lightness of the sample, are displayed in the y-axis. Pigmentation is usually described by the *L** and *b** value, that measures the amount of yellow. The *a** value is used to measure skin redness. The Caucasian and Asian phototypes I-IV could not be distinguished by either *L*a** nor *L*b** values, only the phototypes VI (black symbols) were clearly identified.

No data could be obtained for phototype V. The results were displayed in the *L*a*b* colour system, the *L** value describes the lightness, the *a** value the redness, and *b** value is used to describe the amount of yellow. The *L** value along with the *b** value is generally used to measure pigmentation, while the *a** value best captures erythema or skin redness. The values measured for the 16 volunteers are displayed in Figure 40.

Both notations, *L*b** and *L*a**, showed no clear demarcation between the Caucasian and Asian phototypes I-IV. Interestingly, no distinction could be made for phototype I, neither in lightness (*L** value) nor in redness (*a** value) or the amount of yellow (*b** value). The only group that could clearly be distinguished was that of phototype VI (black symbols). All three samples of this class showed markedly lower lightness values (*L**) and a lesser amount of yellow (*b** value), which was consistent with the darker phenotype.

II Melanocyte Distribution in the Epidermis

II.1 The Epidermal Melanin Unit

Melanocytes are defined as dendritic cells that reside in the basal layer of the epidermis adjacent to the basement membrane. Each melanocyte is said to interact with an approximate 36 keratinocytes providing them with melanosomes. This symbiotic interaction of one melanocyte and a pool of neighbouring keratinocytes, is called an *epidermal melanin unit* (Fitzpatrick and Breathnach, 1963; Nordlund *et al.*, 1998; Jimbow *et al.*, 1999).

As this symbiotic unit is a three-dimensional formation, it would be ideal to image the melanocyte and the associated keratinocytes in their natural context. Therefore, a first approach was to stain entire portions of skin samples, only removing the dermal compartment by collagenase, but leaving the epidermis intact. The samples were fixed with IEM to achieve stability, and stained according to IFA protocol (chapter C.IV.3). Several antibody combinations, including Mel-5, Melanoma Ab-5 (α-gp100), α-S100, α-Keratin and Phalloidin were applied, but no labelling could be observed. Neither elongated incubation with the respective antibody nor the introduction of penetration enhancers, such as Triton X-100, DMSO or Sapponin, produced reasonable results. Antibody-labelling could be detected in the SB, but not in the upper layers of the epidermis and only weak signals could be obtained. A second approach was to stain 40-50 µm thick frozen sections, assuming that the extensive pre-treatment impeded with the staining. But again the antibodies did not penetrate more than

10-15 µm into the section. At last, cryostat sections (15 µm) of high-pressure frozen samples of lesional and perilesional *lentigo senilis* were used, guaranteeing ideal structural integrity of the tissue, as well as good preservation of the melanosomal enzymes (see chapters C.III.1.2.2 and C.III.3.1). The melanocytes were labelled with the primary antibody Mel-5 and fluorescently stained with a Cy5-conjugated secondary antibody. The nuclei were stained with Sytox Green®.

A 3D-volume of a single melanocyte was recorded with CSLM and the image stack processed with Imaris® (see chapter C.VIII.2) to achieve a 3D-representation of the melanocyte. The result is displayed in Figure 41. The inset shows a maximum projection of the image stack, that spans 11.5 µm in depth. The fluorescent signal of the melanocyte (displayed in green) spread over 65 µm along the basement membrane and approx. 40 µm into the spinous layer of the epidermis. The 3D-reconstruction demonstrated impressively the multitude of dendrites, spanning 20-40 µm in length from the nucleus of the melanocyte to the dendrite tips, and

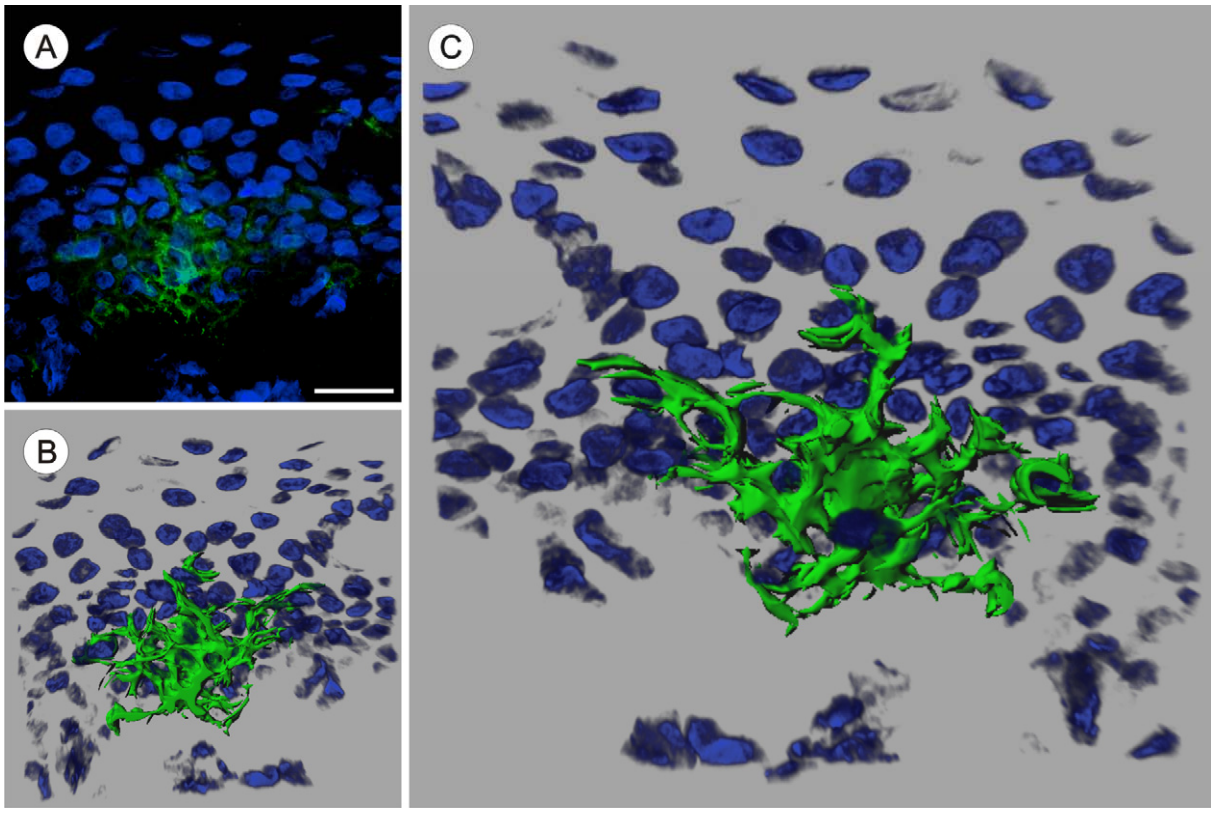

Figure 41: The epidermal melanin unit. Immunofluorescently labelled melanocyte (Mel-5, displayed in green), imaged by CLSM. Nuclei were stained with Sytox Green® and are displayed in blue. (a) Maximum projection of the processed image stack (z = 11.5 µm), displaying the maximum intensity pixel of each sampling point of the image stack. A multitude of dendrites reaching between neighbouring keratinocytes are demonstrated. (B) 3D-recontruction of the melanocyte. (C) 3D-reconstruction, rotated 180°. This melanocyte spans approx. 65 µm along the basement membrane and more than 40 µm from the basement membrane into the SSp. It supplies 39 keratinocytes (counted on the basis of their nuclei). *Bar: 20 µm*

reaching between the neighbouring keratinocytes. The endings of some of the dendrites formed downright envelops around the nuclei of associated keratinocytes. 39 nuclei of surrounding cells in contact with the dendrites were counted in this section.

II.2 Melanocyte Distribution in Fitzpatrick's Skin Phototypes I -VI

Two frozen sections (7 µm) each sample of the Fitzpatrick's skin phototypes I-VI were stained with the melanocyte-specific marker Mel-5 and an antibody directed against the basement membrane component collagen IV, to describe the density of melanocytes and their location in the epidermis. Nuclei were stained with Sytox Green®. Melanocytes were counted only if a nucleus was visible. Melanocyte density was calculated relative to the basement membrane to allow direct comparison between different skin types and compensate different levels of epidermal interleaving with the dermis. Additionally, the skin surface was chosen as reference to assess the influence of melanocyte density on the visible skin colour and allow direct comparability to respective literature (Whiteman *et al.,* 1999; Tadokoro *et al.,* 2005).
The length of the basement membrane and the corresponding stretch of the skin surface were measured using the measurement tool of ImageAccess (chapter C.VIII.1). The SC was not labelled by the applied combination of antibodies, and direct measurement of the length of the SC was therefore not possible. The reference stretch of the skin surface was measured along the outer layers of the *Stratum granulosum* instead. This layer was defined by the uppermost layer of nuclei (see Figure 42, displayed in blue). The mean melanocyte density was determined by correlating the observed number of melanocytes to the reference length of the section.
Figure 42 shows two examples for melanocyte distribution along the basement membrane. The melanocytes are in green, the basement membrane is outlined in red, and the nuclei are presented in blue. Figure 42.A shows an example of light skin (phototype II), and a sample of phototype VI is displayed in Figure 42.B. Interestingly, the lighter skin demonstrated the larger amount of Mel-5 positive cells. Another peculiarity found predominantly in dark skin of phototypes V and VI was the positioning of some of the melanocytes below the basement membrane. They appeared to be "hanging" below the basal cell layer, and the basement membrane formed pouch-shaped envelops around these cells. Examples of hanging melanocytes found in different samples of dark phenotype, are displayed in Figure 42.C – E. The melanocyte density measured for the basement membrane (BM) and the skin surface is illustrated in

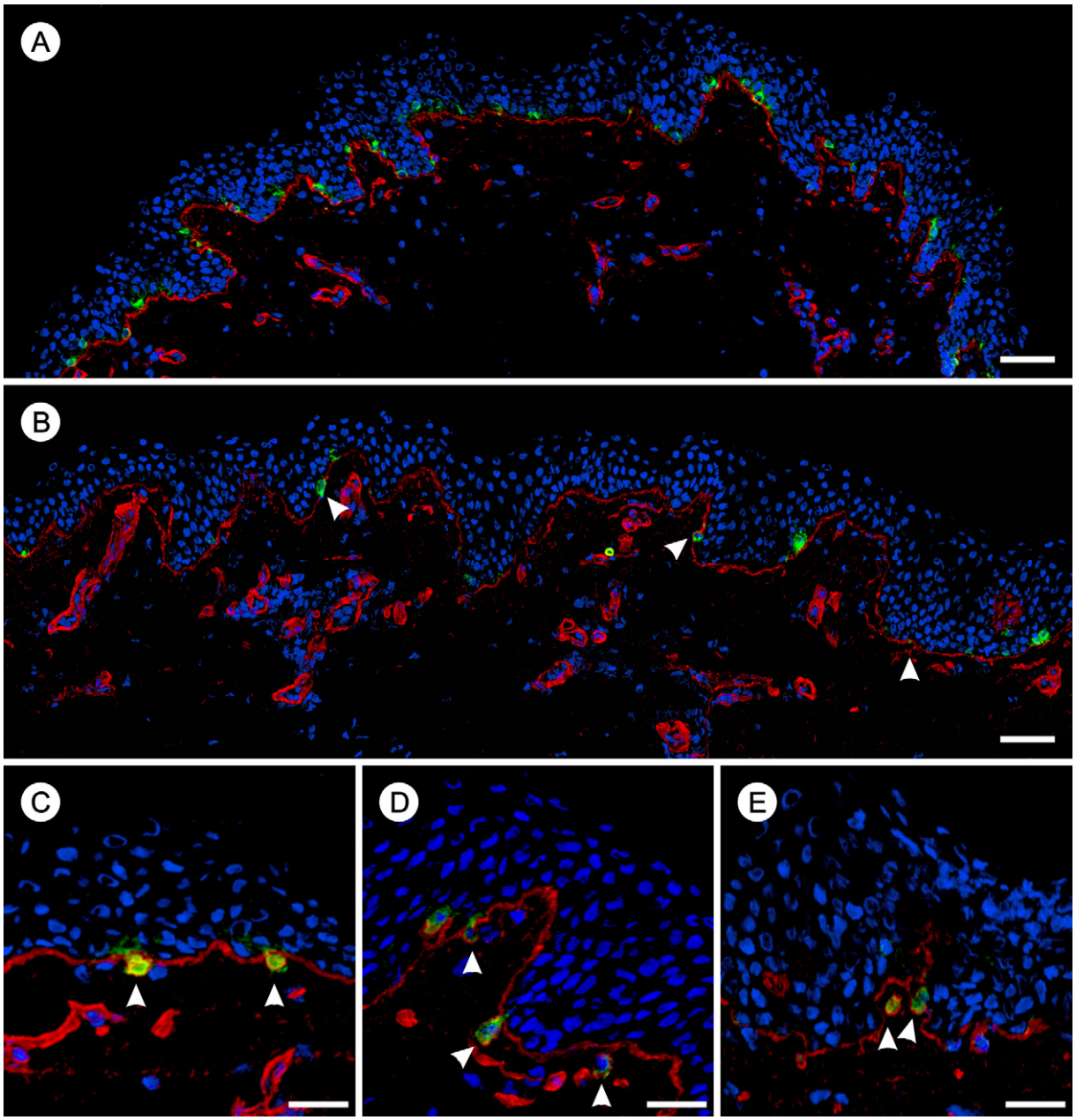

Figure 42: Melanocyte location in the epidermis of skin phototype II and VI. Frozen sections were labelled with Mel-5 (displayed in green) and α-collagen IV (shown in red), to investigate the number and location of melanocytes in Fitzpatrick's skin phototypes I-VI. The nuclei were stained with Sytox Green® (displayed in blue). (A) Skin sample of phototype II. (B) Sample of phototype VI. Less melanocytes were observed than in the darker skin types, than in the lighter phenotypes. Another peculiarity found in dark skin of phototypes V and VI, were melanocytes positioned below the basement membrane, or hanging below the basal cell layer, enveloped by the basement membrane (see white arrowheads). (C) – (E) Enlargements of hanging melanocytes in found in phototypes V and VI. *Bar in (A) and (B): 50 µm; in (C) - (E): 25 µm*

Figure 43. Irrespective of the reference value, the highest melanocyte density was measured in the Caucasian skin phenotypes (phototypes I and II+III). For both groups, comparable melanocyte numbers were measured when correlated to the BM (phototype I: 13.9 melc./ mm BM and 13.6 melc./ mm BM for phototype II+III). When calculated for the reference length

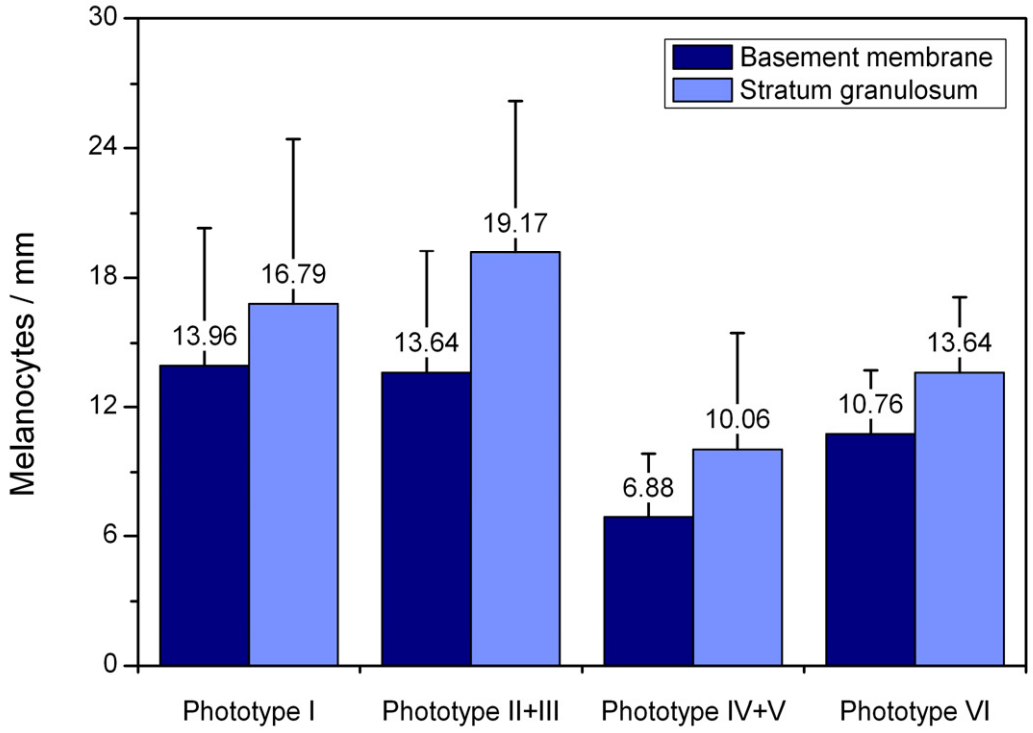

Figure 43: Melanocyte density per millimetre BM and SG in Fitzpatrick's skin phototypes. The melanocyte density was calculated by dividing the counted melanocyte numbers by the reference length of the basement membrane, and the SG respectively. The same tendency was found for both reference lengths: the Caucasian skin types (phototypes I-III) contained the larger amount of melanocytes, than the Asian (phototypes IV-V) and Negroid phenotypes (phototypes IV-VI). The lowest melanocyte density was found in Asian phenotypes.

of the SG, the samples of phototype I exhibited a slightly lower melanocyte density (16.8 melc./ mm SG) than the phototypes II+III (19.2 melc./ mm SG). The Asian phenotypes (phototype IV and V) showed by far the lowest melanocyte density for both correlations: 6.9 melc./ mm BM and 10.1 melc./ mm SG. The samples of phototype VI (Negroid skin) demonstrated medium melanocyte densities, with 10.8 melc./ mm BM and 13.6 melc./ SG.

II.3 Melanocyte Distribution in *Lentigo Senilis* and Adjacent Areas

Four samples each of lesional and perilesional skin of senile *lentigines* were analyzed as described in the previous chapter to determine the melanocyte density – correlated again to the length of the BM as well as the SG. As no standard frozen sections of *lentigo senilis* were available, high-pressure frozen samples obtained during the first study in 2000 – 2001 (see chapter C.II) were investigated. The samples were extracted from the aluminium platelets under liquid nitrogen and transferred into the Cryostat and 5 µm sections were cut as described in chapter C.III.3.1. The sections were stained with Mel-5, α-collagen IV and Sytox

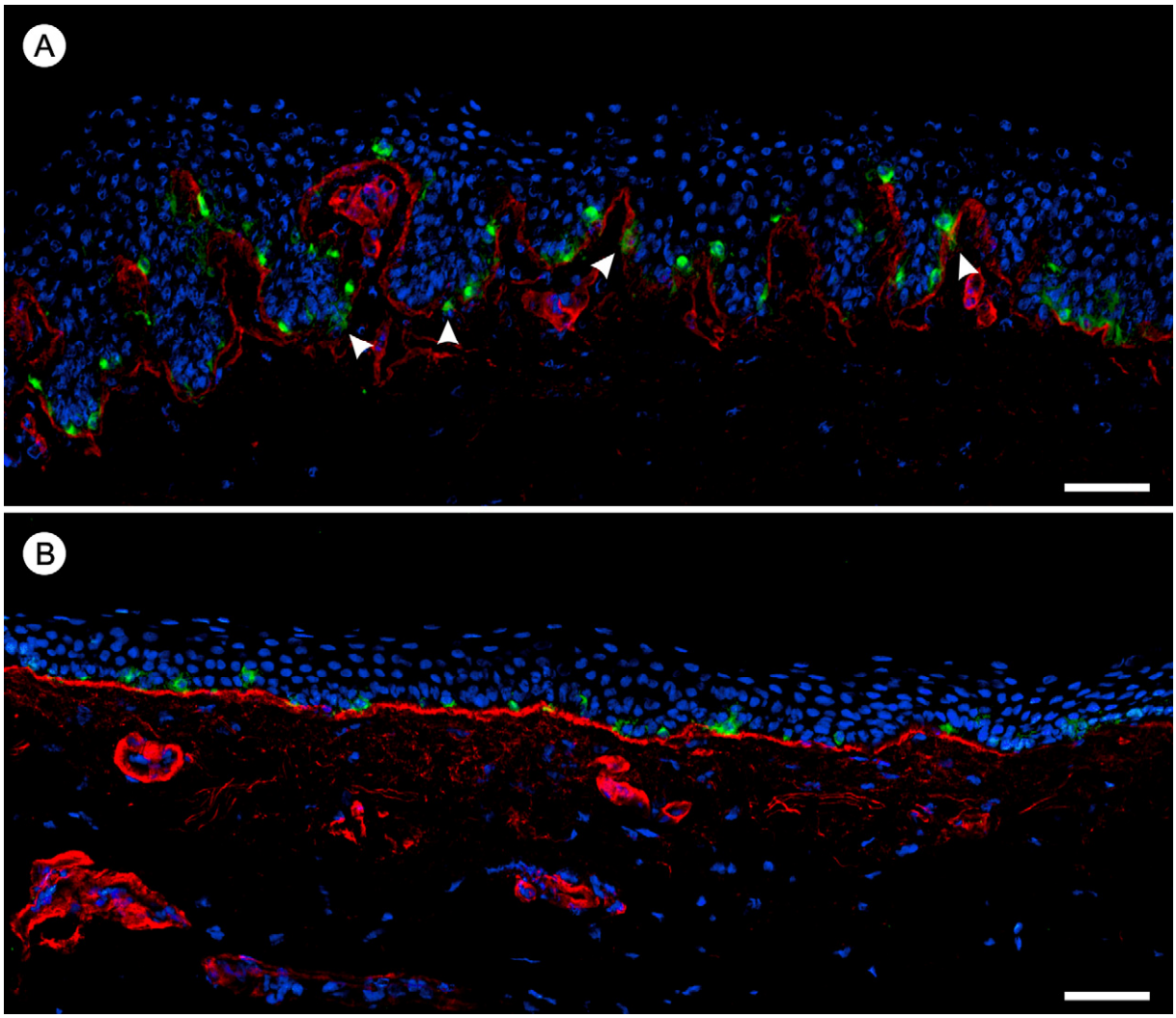

Figure 44: Melanocyte location in *lentigo senilis*. Samples of lesional (A) and perilesional skin (B) of senile *lentigines* were stained with Mel-5 and α-collagen IV, to determine the melanocyte density per millimetre BM and SG. The samples were processed as described for frozen sections, except that they were fixed by high-pressure freezing. The total melanocyte numbers counted in both skin phenotypes were two- to three-fold higher than that measured in normal Caucasian skin. A significant difference between lesional and perilesional skin was observed for the interleaving of epidermis and dermis. Lesional skin showed numerous and deep papillae, while the perilesional skin appeared to have no papillae. This explains the near equalizing of the density values for the SG. *Bars: 50 µm*

Green® to visualize and measure melanocytes, nuclei and the basement membrane. The samples displayed a distinct difference in the dermal-epidermal interleaving (see Figure 44): lesional skin demonstrated deep and numerous papillae, while the BM of the perilesional samples appeared smooth and no papillae were observed. The melanocyte density in both phenotypes was distinctly higher than that found in the matching normal Caucasian skin phototypes I and II+III. As displayed in Figure 45, 20.8 melc./ mm BM were measured in lesional skin (phototype II+III: 13.6 melc./ mm BM). Although Figure 44 implies much larger melanocyte numbers for lesional skin, the average melanocyte density per mm BM measured

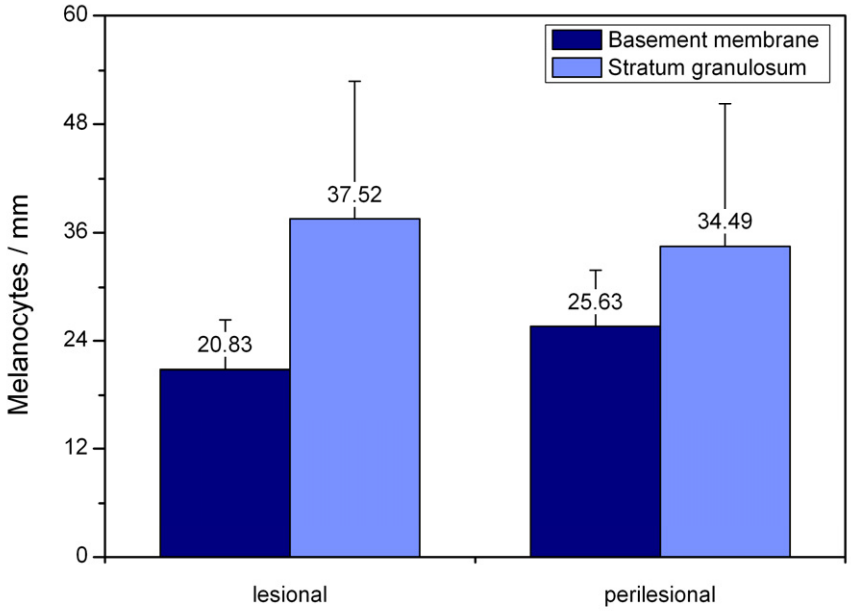

Figure 45: Melanocyte density per millimetre BM and SG in *lentigo senilis*. The melanocyte density was determined for the reference length of the BM and SG representative of the skin surface (n = 4). In lesional skin, the melanocyte density per mm BM was less than in perilesional skin. This situation was reversed when the melanocyte numbers were correlated to the length of the SG.

for perilesional skin was higher than in lesional skin (25.6 melc./ mm BM). But the situation was reversed, when the SG, representative of the skin surface was used as reference. Due to the great decrease in reference length, the melanocyte density of the lesional skin now surpassed the perilesional skin (lesional: 37.5 melc./ mm SG, perilesional: 34.5 melc./ mm SG), but not significantly.

III Characteristics of *Lentigo Senilis*

During the investigation of the senile *lentigines*, it became apparent, that the samples showed distinct disparities in the occurrence of papillae and the numbers of melanocytes. Variations were also observed in the ultrastructure of the basal cell layer. These conspicuous circumstances were systematically and statistically investigated. The results are presented in the following chapter.

III.1 Dermal – Epidermal Interleaving

The most conspicuous difference observed in the *lentigo* samples was the presence or absence of papillae in the lesional specimen. Some samples displayed pronounced elongation of the

rete ridges that protruded deeply into the dermis, while other specimen showed only few or even no papillae and shallow rete ridges. The perilesional samples were equally diverse, some having no papillae at all, and some showing distinct rete ridges.

By definition, senile *lentigines* display distinct elongation of the rete ridges, in addition to an increase in pigmentation in the basal cells and an increased number of melanocytes (Rahman and Bhawan, 1996). To evaluate the sample collective, an integration index was determined for each sample, to measure the level of interleaving of epidermis and dermis. The integration index was calculated by dividing the stretch of the dermal – epidermal junction by the length of the section. The results are displayed in Figure 46. Of the 11 sample pairs (lesional and perilesional skin), only six showed a significantly higher integration index in the lesion, compared to the perilesional skin. These samples (subjects 1-6) were classified as *lentigo senilis*.

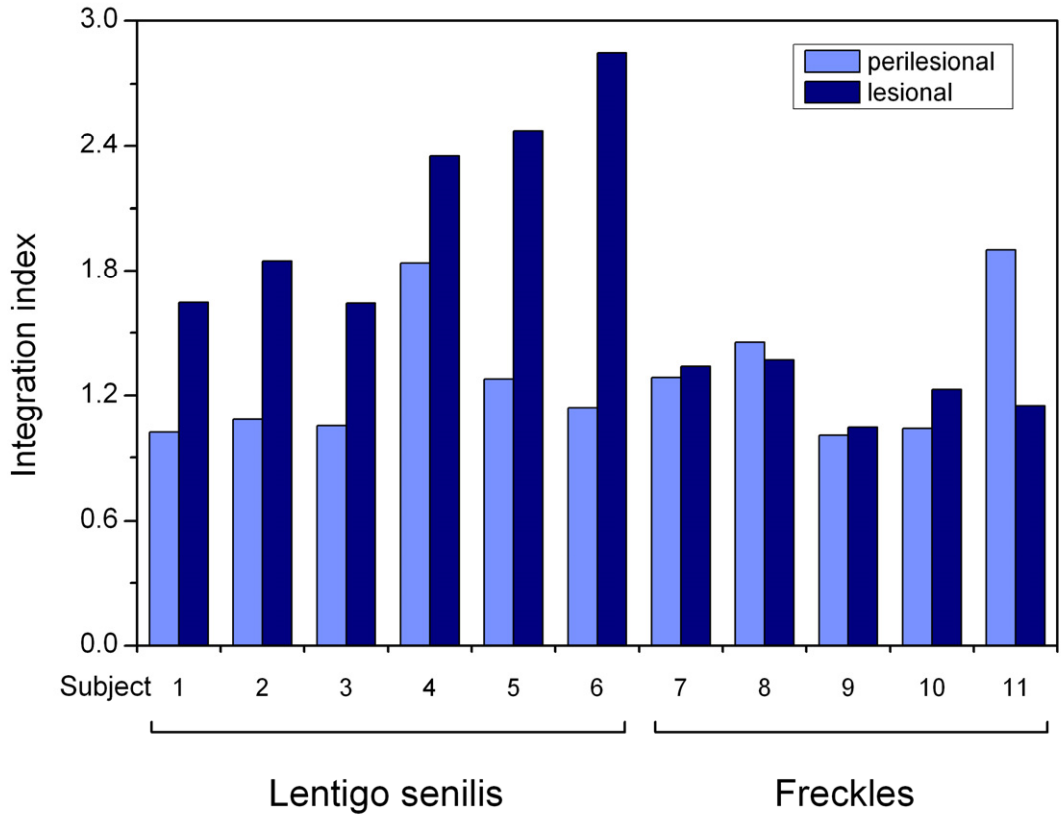

Figure 46: Classification of senile *lentigines* and freckles according to the integration index. By definition, senile *lentigines* show a significant elongation of the rete ridges, compared to the surrounding normal skin. The integration index was calculated by dividing the stretch of the basement membrane by the length of the sample. The sample collective of *lentigo senilis* comprised of 11 pairs of samples, lesional and perilesional skin. Six of the sample pairs showed a significant difference in the integration index, the lesional samples displaying the larger values (subjects 1-6). These samples were classified as *lentigo senilis*. For four sample pairs no difference could be measured (subjects 7-10), and one sample pair showed a significantly higher integration index in the perilesional skin, when compared to the lesion (subject 11). The samples of subjects 7-11 were therefore rated as freckles.

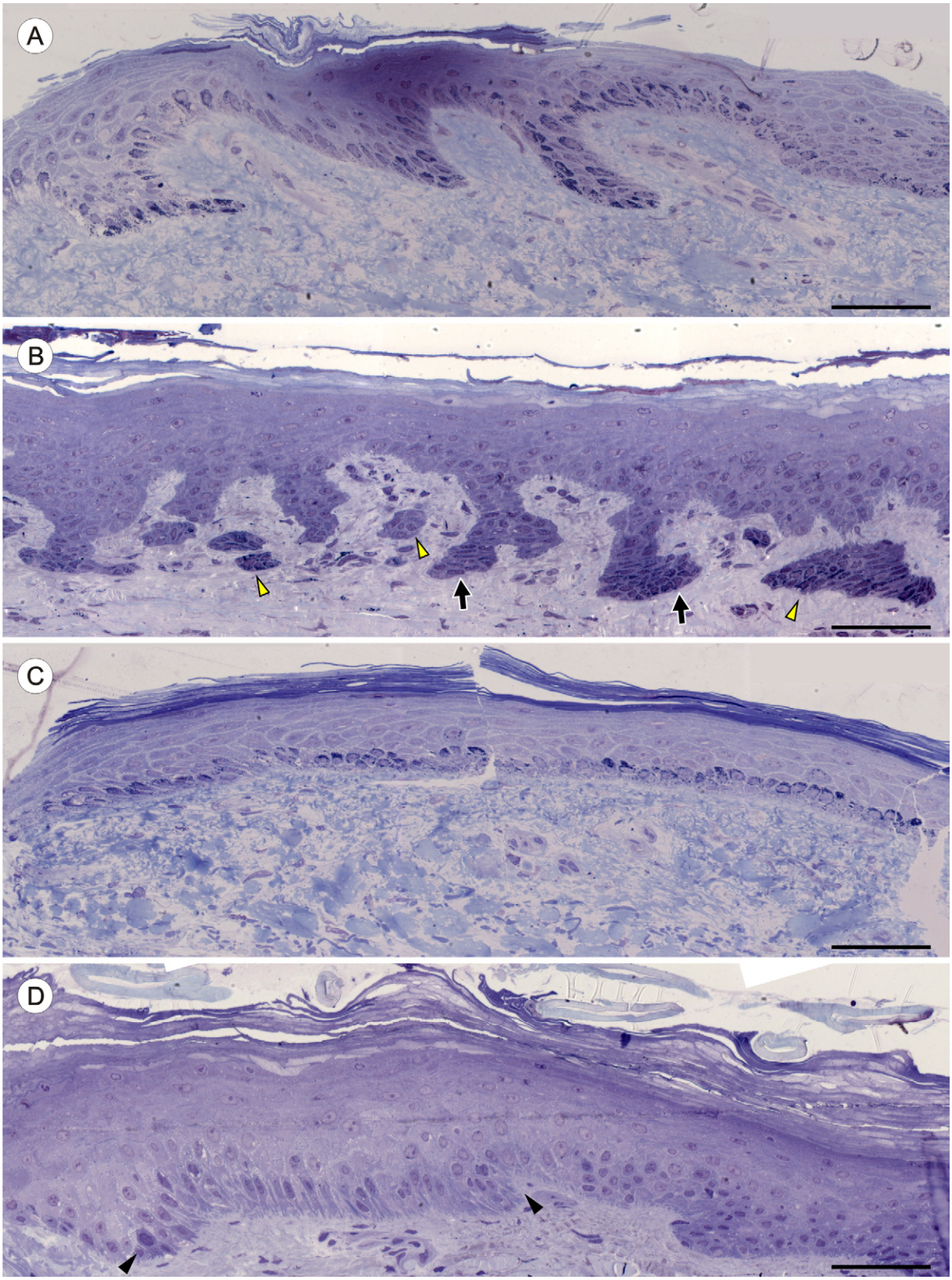

Figure 47: Histological overview of lesional and perilesional samples of senile *lentigines*. (A) Lesional skin contained large numbers of rete ridges, protruding deeply into the dermis. (B) Other lesional phenotypes showed intensive branching of the rete ridges (black arrows), forming islands of epidermal cells (yellow arrowheads). In both phenotypes of ages spots the basal cells were completely filled with melanosomes, and melanosomes were also visible in the upper epidermal layers. (C) & (D) Perilesional skin displayed only few or even no papillae. The basal cells showed supra-nuclear melanin caps. *Bars: 50 µm*

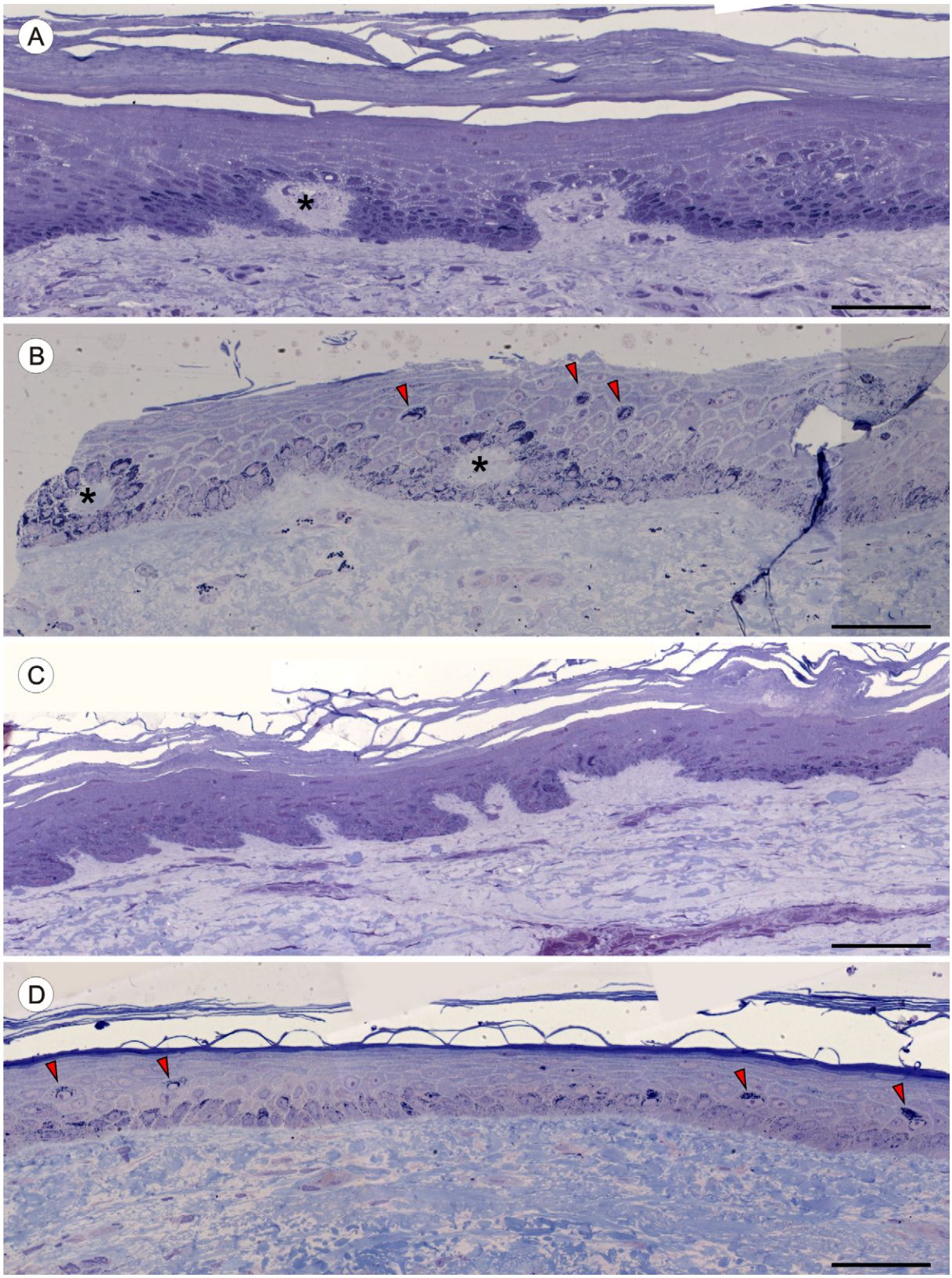

Figure 48: Histological overview of lesional and perilesional samples of freckles. (A) & (B) Lesional skin of freckles displayed fewer and more shallow rete ridges (or papillae resp.), often closing at the basal cell layer to form dermal islands (marked with asterisk). The basal cells were completely filled with melanosomes and supra-nuclear melanin caps were observed even in the upper epidermal layers (see red arrowheads). (C) & (D) In the perilesional skin, less melanosomes were present, although some melanosome-filled cells were observed. The rete ridges were comparable to lesional skin in depth and number. *Bars: 50 µm*

For four of the remaining five sample pairs, no significant difference in the integration index was measured (subjects 7-10). The last pair of samples (subject 11) displayed a reversed combination of integration indices: here the perilesional sample showed a significantly higher integration index, than the lesional sample. These five samples (subjects 7-11) were classified as freckles, according to the definition of Rahman and Bhawan (1996), stating freckles to show no increase in either melanocyte number or elongation of the rete ridges. Apart from that, the two definitions are consistent, as both kinds of macules are found in the same sun exposed areas of the skin, and both show increased pigmentation of the SB.

Despite this classification, both categories demonstrated various phenotypes of lesional and perilesional skin. Variants of *lentigo senilis* are displayed in Figure 47, and freckles are presented in Figure 48. Images A & C and B & D of both figures show matching lesional and perilesional samples of the same subject. The lesion of senile *lentigines* demonstrated a large number of rete ridges, that were explicitly elongated and protruded deeply into the dermis. The basal cells contained many melanosomes, sometimes completely filling the keratinocytes, and melanin caps over the nuclei were visible. Melanosomes were discernable as high up in the epidermis as the SC. The major difference between individual samples was constituted in the form of the rete ridges. While the dermal – epidermal junction of the sample displayed in Figure 47.A showed smooth wave lines, the rete ridges of the sample displayed below (Figure 47.B) branched out (see black arrows) and formed large protrusions and islands of epidermal cells (see yellow arrowheads) in the dermal compartment. These parts were abundantly filled with melanosomes. In accordance with the definition of *lentigo senilis*, the perilesional samples showed no, or only few, and short rete ridges. But mostly, pronounced supranuclear melanosome caps were still observable in the SB (Figure 47.C), although some samples of perilesional skin appeared to contain no melanosomes at all (Figure 47.D).

This last image also demonstrates another feature regularly found in lesional and perilesional samples: frequently, the lower edge of the basal cells appeared jagged and fringy, and the cells were elongated with conspicuously bunched keratin filaments (see Figure 47.D, stretch of BM between the black arrowheads). But these alterations seldom affected the entire section, but were usually restricted to regions of 200-300 µm length.

The perilesional skin of freckles showed similar features as the perilesional samples of senile *lentigines*, only more inhomogeneously. The lesional samples contained a large number of melanosomes, and melanosome-filled cells were abundant in the SB, and completely filled cells were found as high up as the SG (see red arrowheads, Figure 48.B & D). Another

conspicuous feature of the freckles were papillae running parallel to the basement membrane, giving the impression of dermal islands enclosed by epidermal cells of the SB (marked with an asterisk). This closure of the rete ridges may be comparable to the branching of the rete ridges in *lentigo senilis*.

III.2 Ultrastructural Characteristics

As mentioned in the previous chapter, basal cells and basement membrane showed irregularities in some lesional and perilesional samples. The basal cells were elongated and the keratin filaments formed dense bundles stretching along the main axis of the cells. The basal edge of the keratinocytes and the adjacent basement membrane was jagged and fringy. As these features are often associated with inflammatory or other pathological conditions, a fringe integration index was devised, to enable measurement of the described phenomenon and identify possible differences between lesional and perilesional skin.

The fringe integration index was calculated as the quotient of the span of the dermal-epidermal junction and the actual length of the basement membrane as demonstrated in Figure 49.

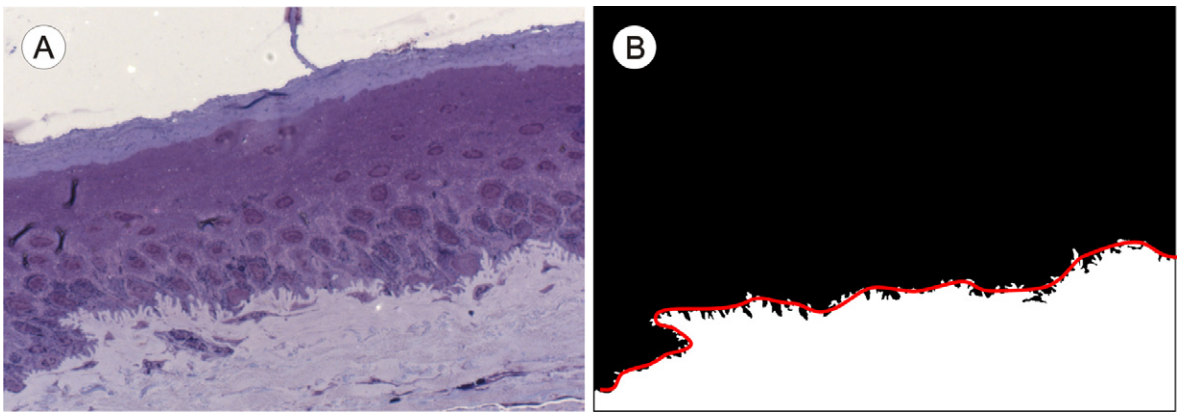

Figure 49: Determination of the fringe integration index. The index was calculated by dividing the actual length of the basement membrane as determined in the original image (A) by the span of the epidermal – dermal junction, illustrated represented in red (B).

The index was determined for both types of lesions, *lentigo senilis* and freckles, as well as for a control collective of normal skin (phototypes I-VI). The results of this investigation are displayed in Figure 50. The fringe integration indices determined for normal skin showed no considerable variations, ranging between 1.25 and 1.66. The *lentigo* samples on the other hand demonstrated a high variability, ranging between 1.38 and 2.62. But no distinct tendency

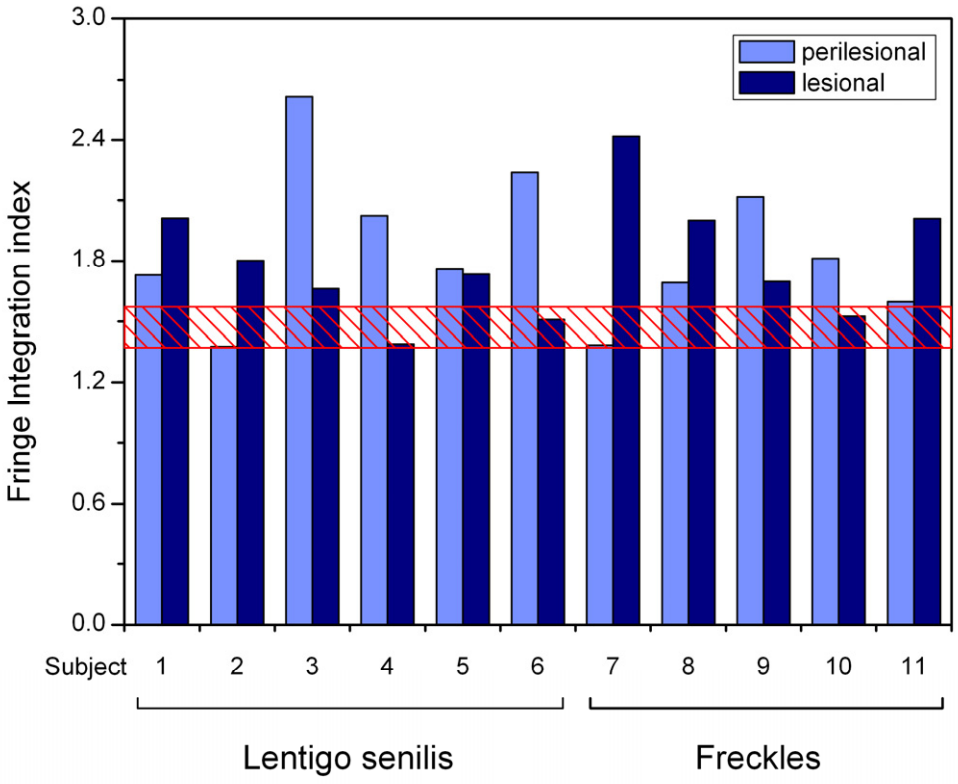

Figure 50: Fringe integration index of the basement membrane of *lentigo senilis* and freckles. The fringe integration index was calculated for all present *lentigo* samples. Lesional and perilesional samples of each subject are displayed. The red demarcation illustrates the fringe indices obtained for the control group of normal skin, including Fitzpatrick's skin phototypes I-VI. Neither lesions nor periphery showed a definite tendency, except that the average values were higher than in the control samples.

could be identified, as to whether lesional or perilesional skin showed more fringes. Nor was it possible to state a difference between *lentigo senilis* and freckles.

These findings were confirmed by TEM investigations of senile *lentigo*. Unfortunately, the ultrastructural preservation of SB and basement membrane of most of the present samples was not sufficient, and only few samples could be investigated. As Figure 51.A & B illustrate, fringy edges of the keratinocytes could be observed in both types of samples (lesional and perilesional), but never affected the entire section and smooth regions were found in the immediate vicinity of fringy keratinocytes. The basement membrane under these keratinocytes was intact and no disruptions were visible. Additionally, the melanocytes in lesional (Figure 51.D) and perilesional samples (Figure 51.C) displayed no irregularity and the adjacent basement membrane exhibited no disruption, irrespective of the presence of fringy keratinocytes.

Another conspicuous feature of age spots is the presence of very large melanosome clusters, consisting of 10 or more melanin particles, massed together in more or less round aggregates.

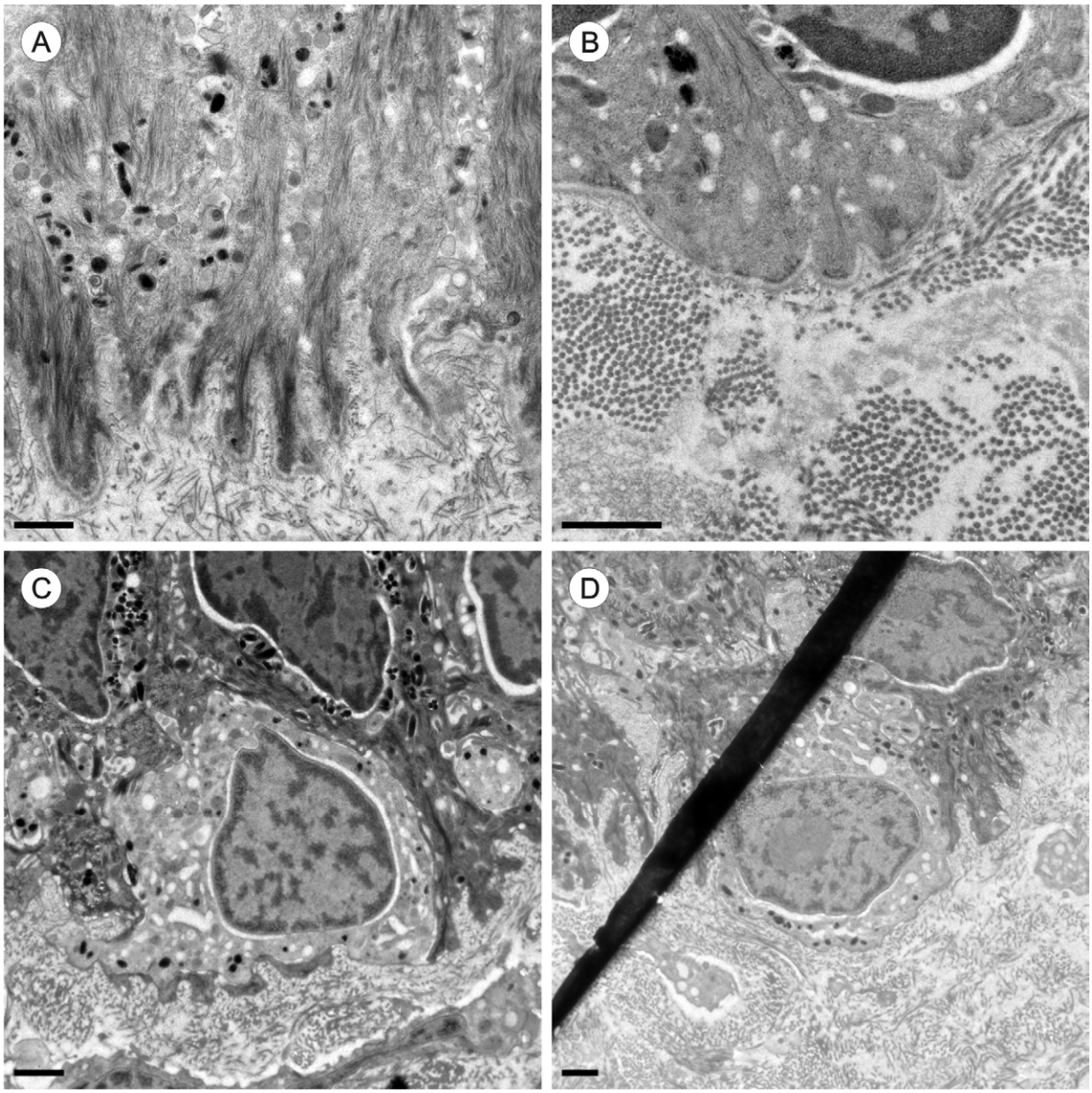

Figure 51: Basement membrane under keratinocytes and melanocytes in *lentigo senilis*. (A) Fringy edges of keratinocytes were frequently found in lesional and perilesional skin of senile *lentigo* and freckles. But the basement membrane showed no disruptions neither in lesional nor perilesional skin. (B) The jagged and fringy keratinocytes never affected the entire section. Regions with smooth basement membrane were found in the immediate vicinity. (C) Melanocyte observed in a perilesional sample. (D) Melanocyte found in a lesional sample of *lentigo senilis*. Disruptions of the BM were not observed, neither under keratinocytes nor under melanocytes. *Bars: 1 µm*

Some examples are illustrated in Figure 52. These so-called macromelanosomes measured up to 800 nm in diameter. They were predominantly observed in the SB and lSSp of lesional skin (Figure 52.A & B), although few were also found in perilesional samples. But usually, the melanosome aggregates observed in perilesional skin were rather smaller, containing 5-7 melanin particles (Figure 52.C), but they were still larger than the average melanosome cluster of 2-3 particles found in normal Caucasian skin.

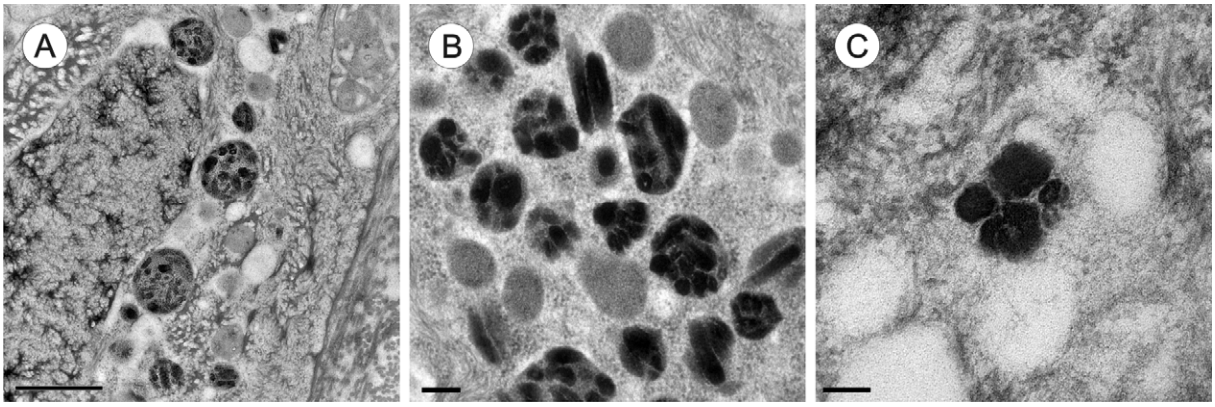

Figure 52: Macromelanosomes in *lentigo senilis*. (A & B) Melanosome clusters of 10 or more melanin particles are found predominantly in the SB and lSSp of lesional samples of senile *lentigo*. (C) Perilesional skin also contained melanosome clusters larger than the average cluster observed in Caucasian skin (usually 2 – 3 melanin particles). *Bars: (A) 1µm, (B) 200 nm, and (C) 100 nm*

III.3 Corrected Melanosome Distribution

According to the above described sub-classification of *lentigo* samples into *lentigo senilis* and freckles, the melanocyte density as well as the epidermal distribution of melanosomes were reinvestigated. Regarding the melanocyte density, *lentigo senilis* and freckles show no distinction: for both references, the BM and the SC, the determined values are within the range of the standard deviation.

The revised melanosome distribution for senile *lentigo* and freckles is shown in Figure 53. The total melanosome content showed only minor differences, with 2.44 mel./ µm² and 1.53 mel./ µm² in lesional and perilesional samples of *lentigo senilis* and 2.53 mel./ µm² and 1.30 mel./ µm² in the lesion of freckles and in the perilesional samples. The melanosome numbers counted in the lower epidermal layers were also comparable, only the lSSp of the freckle lesion displayed increased melanosome numbers compared to the lesion of age spots. The major difference between *lentigo senilis* and freckles was found in the SC. The senile *lentigines* contained considerably more melanosomes (0.35 mel./ µm² lesional, 0.23 mel./ µm² perilesional) than the SC of freckles (0.18 mel./ µm² lesional, 0.05 mel./ µm² perilesional). This was also reflected in the reduction rates measured from SB to SC: 69 % were measured in the lesion and 71 % in perilesional skin of *lentigo senilis,* while in freckles, distinctly higher reduction rates were measured: 84 % in lesional skin and 93 % in perilesional samples. Approx. 40 % of the melanosomes in the SB of the samples rated as freckles, lesional and perilesional, were individually dispersed, compared to the samples classified as real age spots, where 43 % (lesional) and 45 % (perilesional) isolated melanosomes were counted (Table 17).

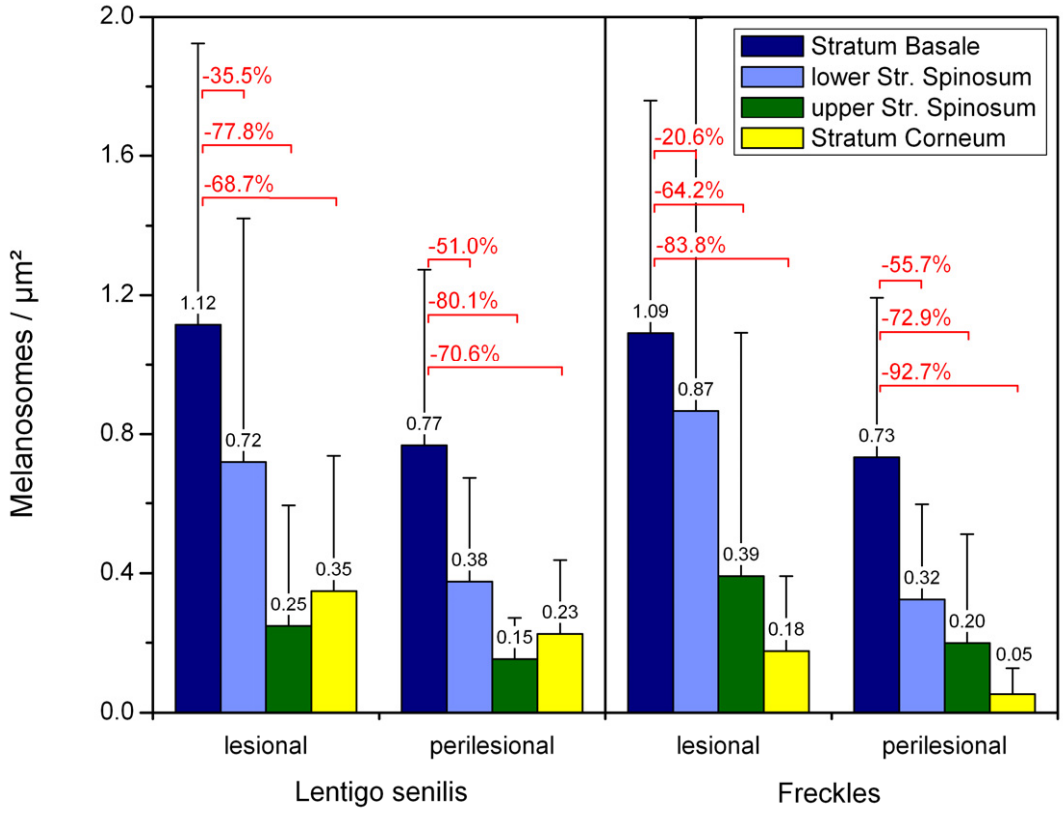

Figure 53: Melanosome distribution in senile *lentigines* and freckles. The melanosome distribution was corrected according to the subdivision of the *lentigo* samples into *lentigo senilis* and freckles. The total melanosome content showed only minor differences, and the melanosome numbers counted in the individual epidermal layers were comparable, with the exception of the lSSp of the freckles (lesional) that displayed an increase in melanosome numbers compared to the lesion of age spots. The major difference was found in the SC of the *lentigines senilis*, where considerably more melanosomes were counted, resulting in lower reduction rates from SB to SC.

Healthy Caucasian with half of the melanosomes individually dispersed, ranged between the two hyperpigmentations. In the lSSp of all phenotypes more than 60 % of the melanosomes were distributed individually, only the lesion of the real *lentigines senilis* showed a considerably lower percentage (48.2 %). Toward the SC, all phenotypes displayed more than 80 %, the age spots even more than 90 % isolated melanosomes.

Table 17: Percentage of individual melanosomes in the epidermal layers of *lentigo senilis* and freckles.

	SB	lSSp	uSSp	SC
Lentigo senilis (lesional)	43.1 %	48.2 %	76.4 %	90.9 %
Lentigo senilis (perilesional)	45.0 %	65.2 %	76.7 %	91.0 %
Freckles (lesional)	58.3 %	60.3 %	75.3 %	83.3 %
Freckles (perilesional)	58.6 %	61.5 %	79.5 %	82.8%
Caucasian skin (buttock skin)	50.9 %	69.3 %	81.4 %	85.9 %

IV Melanosome Transfer – Search for Evidence

If the phenomenon of melanosome distribution and further processing is to be understood, it is crucial to investigate the mechanism of melanosome transfer from the melanocyte to the keratinocytes, as it is the key to comprehending the formation of melanosome clusters or dispersion of single particles within the keratinocytes. The actual mechanism of transfer is still unknown, but several possibilities are discussed, including phagocytosis of dendrite tips, exocytosis of melanosomes from the melanocyte followed by endocytosis by keratinocytes, and direct transfer after membrane fusion of both cell types (see chapter B.I.2.4).

IV.1 Melanosome Transfer in Co-Cultures of Keratinocytes and Melanocytes

Co-culture of melanocytes of Negroid donors and keratinocytes of Caucasian origin (co-cultured for four days before investigation) were investigated by light microscopy to monitor melanosome transfer. The melanocytes showed many dendrites growing in the direction of keratinocytes. These dendrites were full of melanosomes and extensive bidirectional trafficking was observed, into the dendrite tips, and in the reverse direction back to the body of the melanocyte. Along the dendrites, filopodia were detected in abundance (see Figure 54.B, red arrowheads). Many of these protrusions contained melanosomes moving away from the dendrite. But mostly these filopodia were retracted, and the melanosomes returned into the dendrite (Figure 54.B, marked with blue arrowheads). Actual transfer of melanosomes occurred seldom.

An observed event of melanosome transfer is illustrated in Figure 54, the melanocyte dendrite is sketched in red and two keratinocytes are outlined in blue (Figure 54.A). A single melanosome detached from the dendrite (Figure 54.B, marked with an arrow) and moved towards the keratinocyte in the course of 60 sec (Figure 54.C). It lingered at the edge of the keratinocyte for more than one minute (Figure 54.D), before rapidly moving towards the nucleus of the keratinocyte (Figure 54.E). The melanosome then disappeared from view (Figure 54.F), most likely because it was internalized by the keratinocyte, although a definite proof of the transfer was impossible, due to the optical properties of the cell membranes. The entire process lasted only 2 minutes.

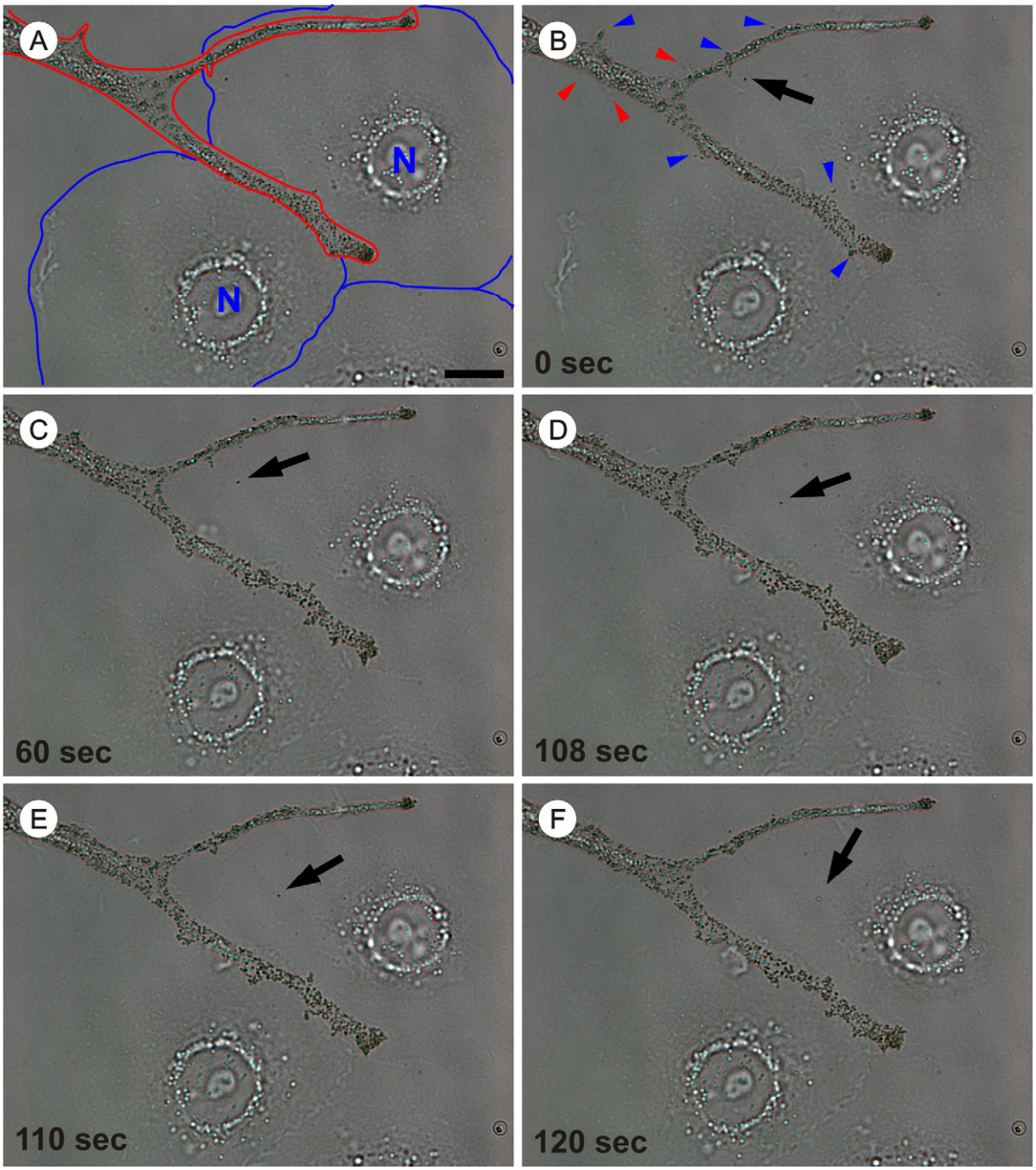

Figure 54: Melanosome transfer observed in co-cultures of melanocytes and keratinocytes. (A) Illustration of the displayed area, the melanocyte dendrite is outlined in red, the two keratinocytes are delineated in blue, the nuclei are marked with N. Several melanosome-filled protrusions from the dendrite (marked with blue arrowheads) and filopodia without melanosomes (marked with red arrowheads) are visible. (B) A melanosome (arrow) detached from the dendrite and moved in the direction of the keratinocyte (C), staying at the edge of the cell for several seconds (D). Then it moved rapidly toward the nucleus of the keratinocyte (E) and disappeared (F). *Bar: 10 µm*

IV.2 Ultrastructural Organisation of Melanosomes within Melanocytes and after Transfer to Keratinocytes

Considering the different theories, trying to explain melanosome transfer to keratinocytes, the number of membranes surrounding individual melanosomes and melanosome clusters may give a clue to solve the riddle.

Within melanocytes, melanosomes were invariably present as single entities, tightly surrounded by a single membrane (see Figure 55), irrespective of the phototype or ethnicity of the investigated skin sample and in every stage of development (see top row). The melanosomes were oval-shaped or round, depending on the section axis, and measured 100-300 nm in diameter.

In keratinocytes of the lower epidermis (SB and lSSp), melanosomes appeared either as solitary particles or were aggregated to melanosome clusters. Negroid skin contained mainly individual melanosomes that were mostly round organelles measuring 150-350 nm in diameter. In contrast, lighter skin types tended to the formation of clusters (see also chapter I.1.4). The melanosomes were predominantly oval-shaped, and measured 50-80 nm crosswise, and 100-300 nm lengthwise. The average cluster was of roundish shape, 400-500 nm in size, sometimes even larger.

Both individual melanosomes and melanosome clusters were again enveloped by a solitary membrane (see Figure 56). However, this membrane did not fit as tightly as observed in melanocytes, but formed a larger, more loosely fitting framing, that often included additional structures of unknown origin (see Figure 56, 2nd row, third and fourth image and bottom row, last image). The larger melanosome clusters often appeared less structured, the comprised particles appearing less dense and blurry, making distinction of single entities difficult (see Figure 56, 1st row, fifth image; 2nd row, first image; and 3rd row, last image).

In the upper layers of the epidermis (SG and SC), melanosome clusters were more rare (see chapter I.1.4) and the present individual melanosomes generally showed no surrounding membrane.

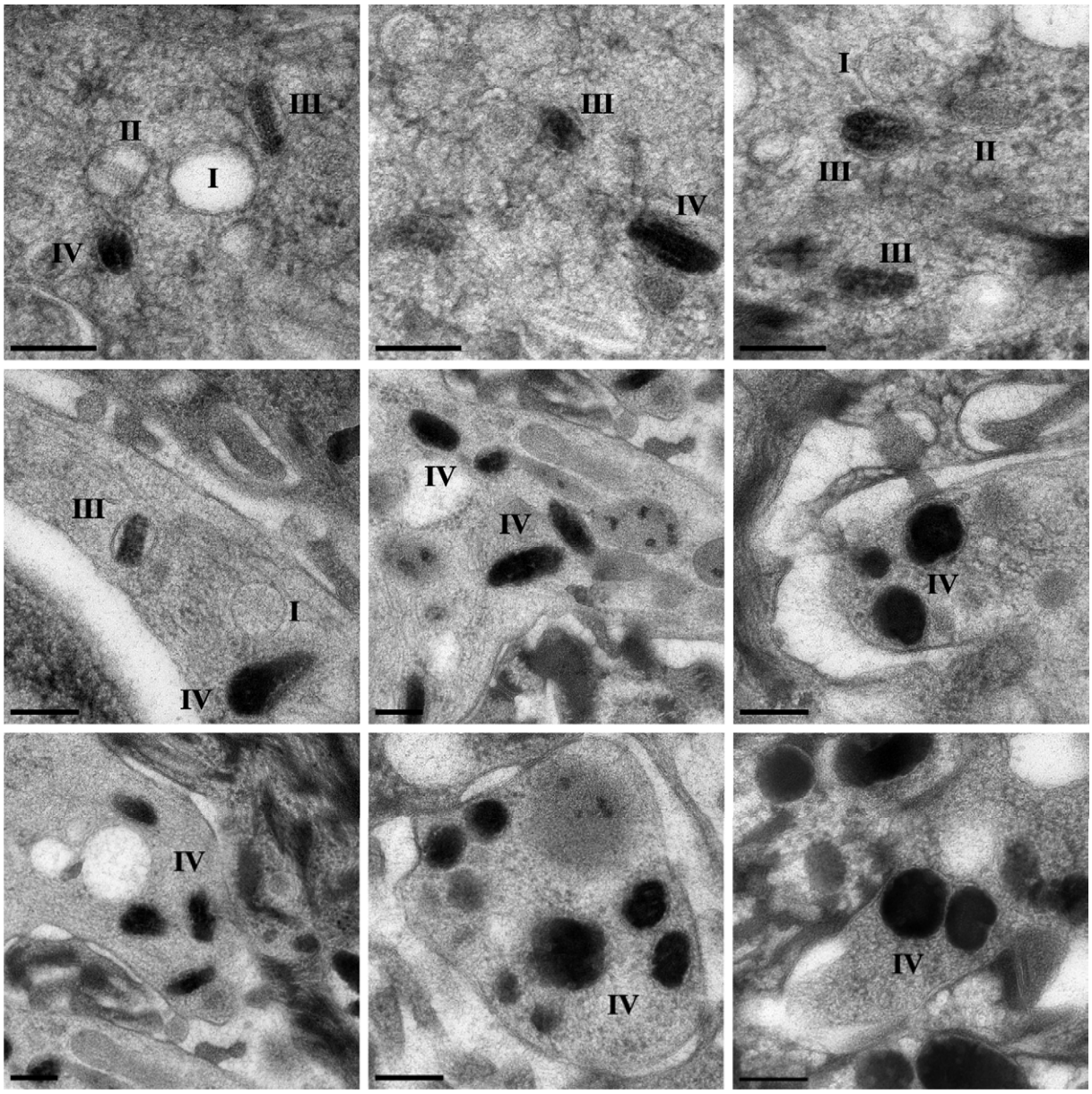

Figure 55: Melanosomes within melanocytes and melanocyte dendrites. Within melanocytes, melanosomes were always found as single, solitary entities, irrespective of phototype or origin of the donor. A single membrane surrounding the melanin-aggregation was present, no matter which stage of development. The maturation stages (chapter B.I.2.3) are annotated with Roman numerals (I-IV). *Bars: 200 nm*

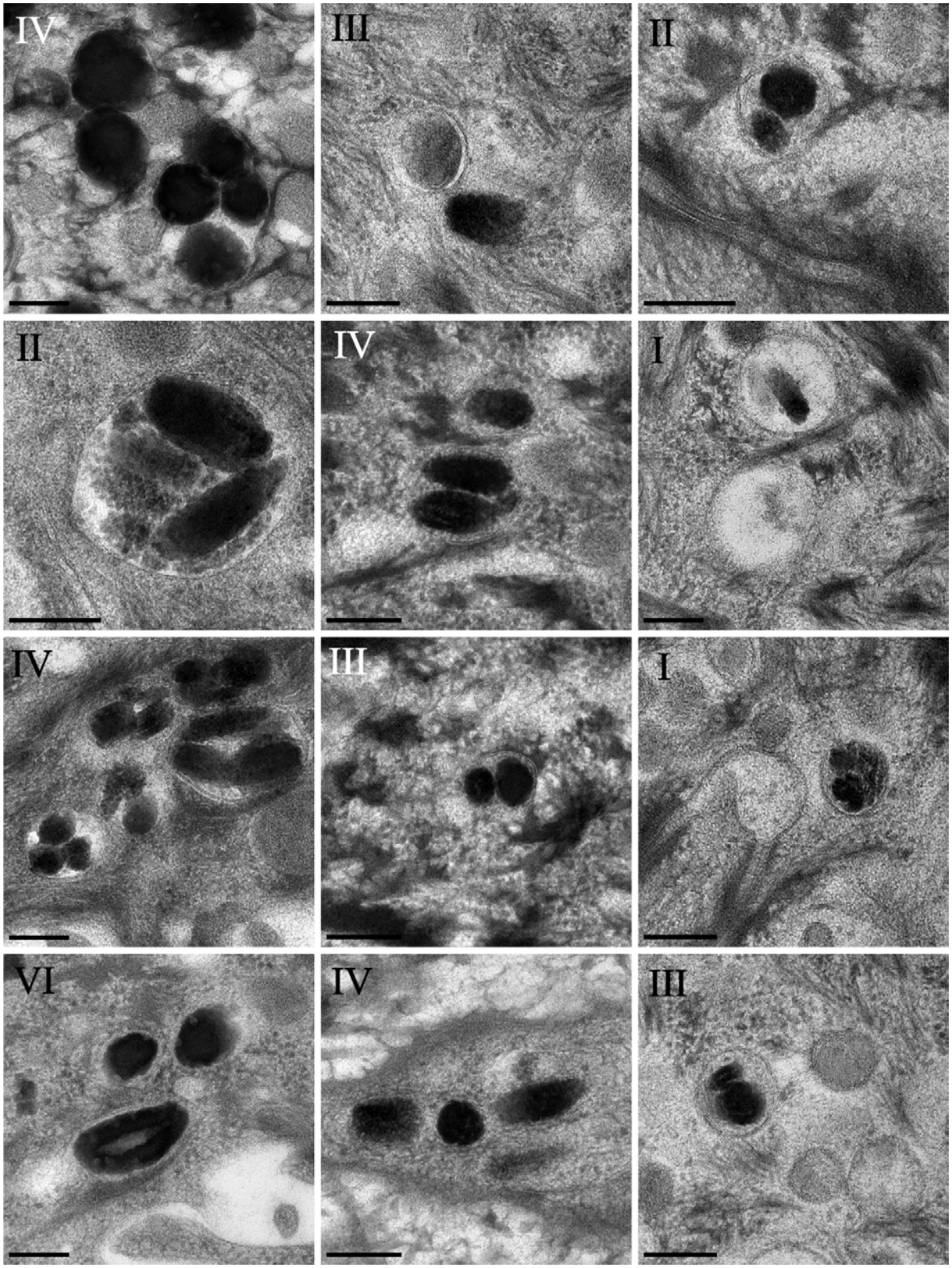
IV
III
II
II
IV
I
IV
III
I
VI
IV
III

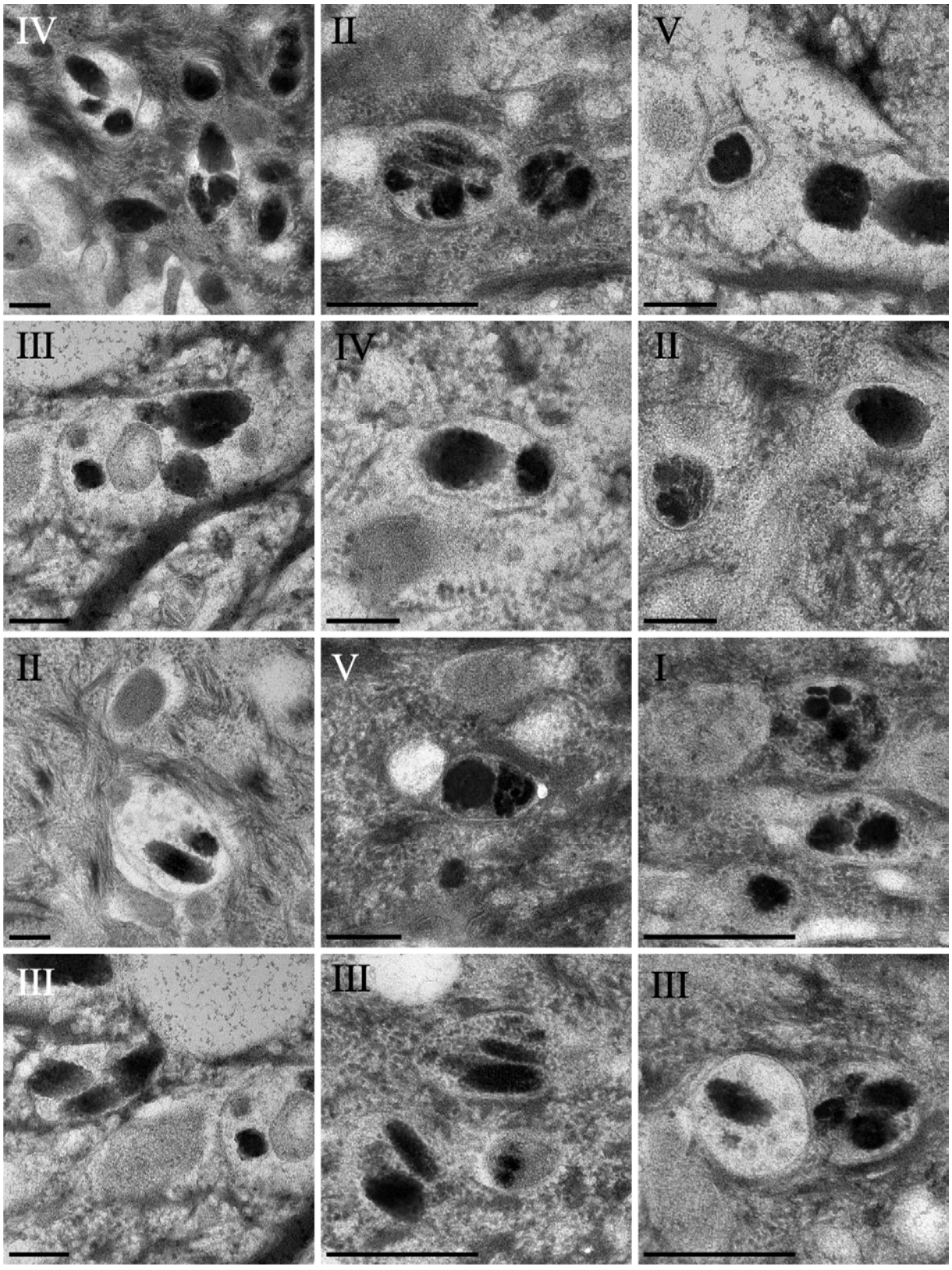

Figure 56 (left & right): Solitary melanosomes and melanosome clusters in keratinocytes of the lower epidermis. The darker the skin type, the larger the melanosomes, and the more individual particles were found. Lighter skin types tended to contain more melanosome clusters of an average size of 2-3 melanin particles. A single membrane loosely surrounded these aggregations of melanosomes, sometimes including other substances of unknown origin (see right page 3rd row, first image & last row, last image). The Roman numerals denominate the phototype of the respective samples. *Bars: 200 nm*

IV.3 Melanosomes in the Intercellular Space

If melanosomes were observed in the intracellular space between keratinocytes, or between melanocytes and keratinocytes, the majority was enclosed in melanocyte dendrites that reached between the adjacent cells (Figure 57, marked with blue arrowheads). The dendrites were usually round or oval-shaped and often showed slender projections, that were most likely filopodia (see Figure 57, top right).

Isolated melanosomes, without any surrounding membrane or cell protrusion were extremely rare, and existed solely in the basal layer of the epidermis, usually in the immediate vicinity of melanocytes. Figure 57 shows some of the few observed examples. “Naked” melanosomes are labelled with red arrowheads.

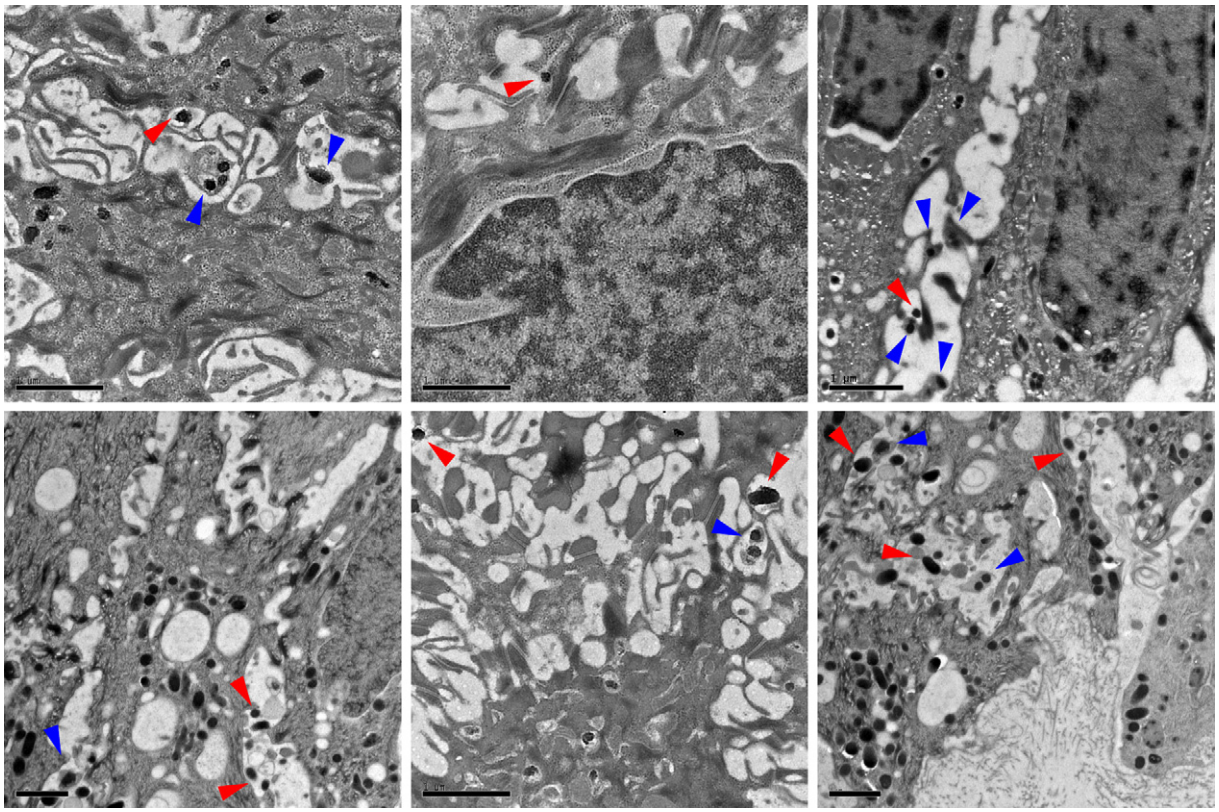

Figure 57: Melanosomes in the intercellular space. The majority of melanosomes found in the space between keratinocytes were present in melanocyte dendrites (marked with blue arrowheads). But infrequently, single melanosomes were observed without any surrounding structure (see red arrowheads), but only in the basal and lowermost layers of keratinocytes. *Bars: 1 µm*

IV.4 Melanosomes at the Interface of Melanocytes and Keratinocytes

Melanocytes formed filopodia not only at the dendrite tips, but all along the dendrites and the melanocyte body. These projections reached into the intracellular space and toward adjacent keratinocytes. In the immediate vicinity of these protrusions, mature melanosomes were observed in abundance, both, within the melanocytes as well as in the adjoining keratinocytes (see Figure 58). In the melanocyte, the melanosomes displayed distinct membranes surrounding a core of compact melanin aggregation. This tight-fitting membrane was not observable after transfer to the keratinocytes, where only one membrane was detected enclosing clusters of melanosomes (see Figure 58.A, tagged with an arrow; and Figure 58.D). In the intracellular space, the filopodia seemed to pinch off the tip, forming buds (Figure 58.C & D). Some of these buds were observable in the intracellular space and near the dendrite in Figure 58.D (red arrowheads). The black arrow labels a single melanosome surrounded by a distinct membrane, with filopodia from the flanking keratinocytes reaching toward it. Many vesicles and melanosome clusters, again surrounded by only one membrane, were detected in the adjoining keratinocytes.

Figure 58.B shows a melanocyte dendrite in direct contact with a keratinocyte. Both cells were interwoven, with protrusions of both cells reaching toward the other. A melanosome was present in a projection of the melanocyte that was directly enveloped by the adjacent keratinocyte (see red arrowhead). Next to this inversion, the keratinocyte membrane formed an envelope engulfing a vesicle, probably containing a melanosome (see black arrowhead). Here, two membranes were observable, one bordering the vesicle itself, the other forming the hollow produced by the keratinocyte during the enclosing process. The space between the two membranes resembled the extracellular space in texture and brightness, indicating an endocytosis. A cluster of two melanosomes, surrounded by a solitary membrane (arrow) and other vesicles were observed next to this engulfed vesicle.

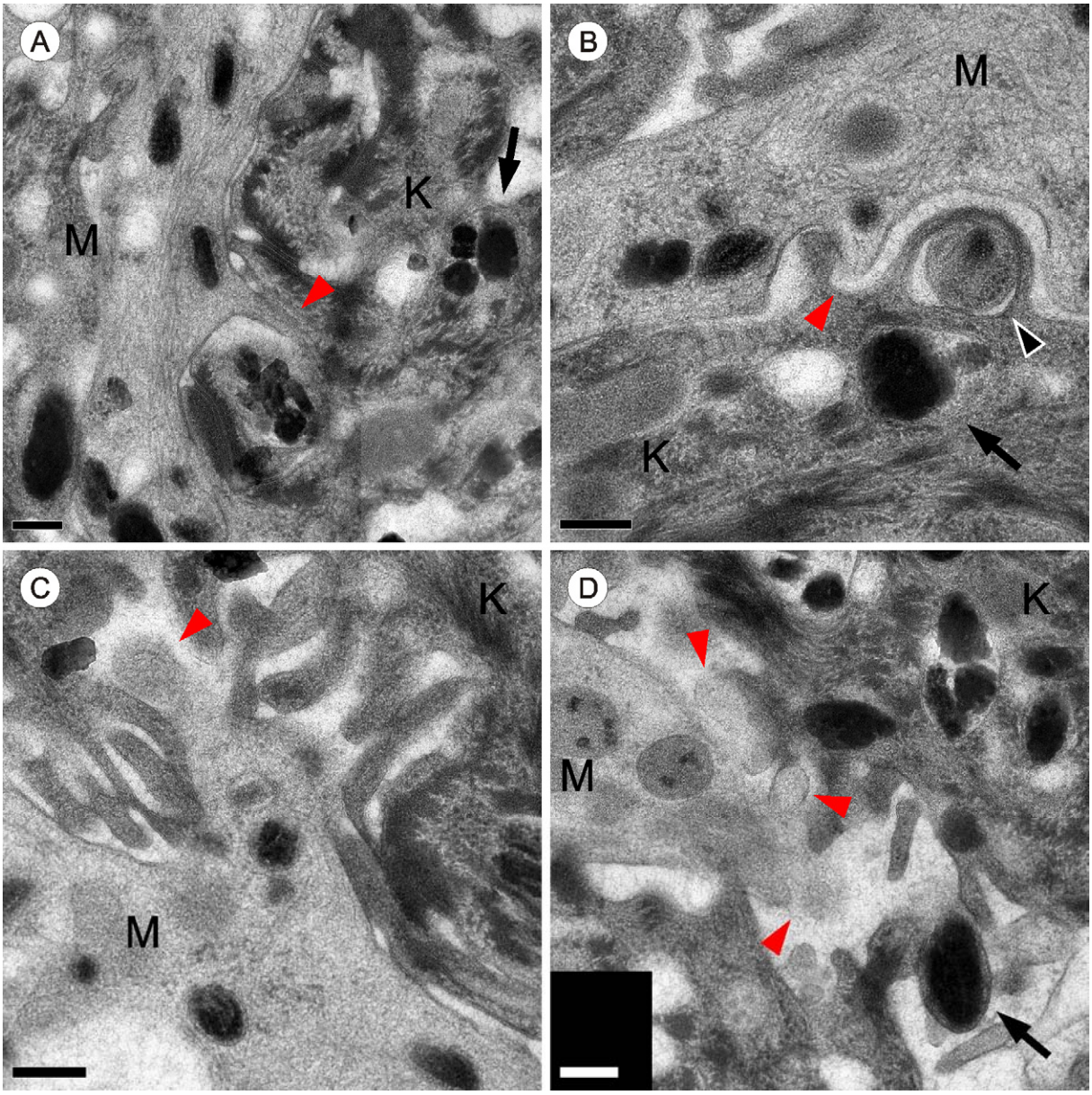

Figure 58: Interaction of melanocyte and keratinocyte. (A) Melanocytes formed filopodia (red arrowhead), that reached toward the keratinocytes. Melanosomes were present in the direct vicinity of the filopodia, within the melanocytes and also in the keratinocytes. In the melanocyte, the melanosome exhibited a distinct membrane around a core containing the melanin aggregation that was not observable in the keratinocytes, where the only visible membrane was detected around clusters of melanosomes (arrow). (B) Projections from the melanocyte were enveloped by the keratinocyte (red arrowhead). Again, melanosomes were found directly in the protrusion as well as in the neighbourhood. In the adjacent keratinocyte, a melanosome cluster surrounded by a solitary membrane (arrow) and other vesicles were observed. The vesicle marked with the black arrowhead showed one membrane forming the vesicle itself, and was additionally enclosed by the keratinocyte-membrane. (C & D) The tips of the filopodium seemed to form buds, detaching from the melanocytes (red arrowheads). A single melanosome was visible in the intracellular space, clearly surrounded by a single membrane (black arrow).

M = Melanocyte; K = Keratinocyte *Bars: 200 nm*

V Melanin Degradation *In Vitro* and Its Detection *Ex Vivo*

Considering the drastic decrease in melanosome numbers from the SB to the SC, measured in all skin types (see chapter I.1), it becomes apparent, that the melanosomes are somehow degraded during the evolution from basal keratinocytes to corneocytes at the skin surface. Melanin is an extremely stable biopolymer. The only reagent capable of degrading melanin, that is present in the skin under physiological conditions, is hydrogen peroxide, arising from superoxide anions generated by the membrane-associated NADPH oxidase (Korytowski and Sarna, 1990; Borovanský and Elleder, 2003). Starting from this hypothesis, the effect of H_2O_2 on melanin was investigated, trying to identify possible degradation products and searching for evidence linking this degradation pathway to the skin. Additionally, the localisation of H_2O_2-production in the epidermis was investigated.

V.1 Degradation of Melanin by Hydrogen Peroxide

As extraction and purification of melanosomes from human epidermis is an elaborate and time-consuming process, yielding only little material (Kushimoto *et al.*, 2001), commercially available *Sepia* melanin (from *Sepia officinalis*) was used as a model substance. This black powdery substance proved to be insoluble in water, and sedimentation was observed soon after suspension in distilled water, leaving the water colourless. When an aqueous solution of hydrogen peroxide (5 %) was added to the melanin suspension, the melanin was dissolved and the solution turned brown within 48 h. Increased concentrations of hydrogen peroxide or irradiation with UV light accelerated the reaction rate of this process. No effect was observed with UV irradiation, omitting H_2O_2.

The untreated *Sepia* melanin consisted of homogeneous globular shaped structures, agglomerated to form larger globules, 30-60 nm in diameter (see Figure 59.A). After incubation with H_2O_2, the round structures were disintegrated. Instead, platelets of 15-20 nm length and 2-5 nm thickness were observed, aligned to stacks of two or three or even up to 100 parallel platelets (see Figure 59.B).

The solution of *Sepia* melanin in H_2O_2 was dried via vacuum pump and analyzed by SEC (see chapter C.VI.3). The resulting chromatogram is displayed in Figure 60. Eight fractions were collected after the elution with retention volumes of 5.20 ml, 6.05 ml, 7.75 ml, 8.29 ml,

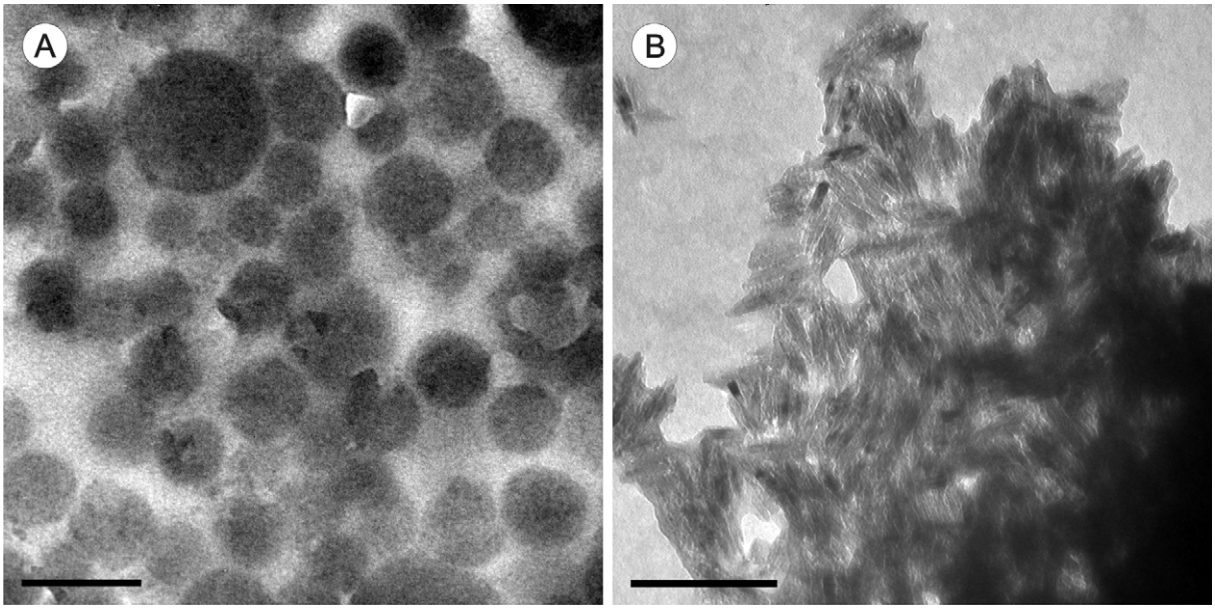

Figure 59: Fragmentation of *Sepia* melanin by hydrogen peroxide. (A) Eumelanin from *Sepia officinalis*. The round homogeneous granules measured 30 – 60 nm in diameter. (B) After treatment with H_2O_2, the round structures were disintegrated to give rise to accumulations of 15 – 20 nm long and 2 – 5 nm thick platelets, packed together in stacks of 2 – 3, sometimes up to 100 pieces. *Bars: 50 nm*

8.76 ml, 9.31 ml, 9.80 ml and 11.47 ml. Unfortunately, the determination of the molecular weight of the individual components of the solution of melanin in H_2O_2 was impossible, as no information existed on the properties of melanin and the identity of possible degradation products. The refractive increment *dn/dc* was determined by analysis of different concentrations of the melanin-H_2O_2 solution. The result of *dn/dc* = 0.1712 can be assumed as an average value for the eight fractions. Based on this *dn/dc*, the molecular masses were determined from the light scattering detector and resulted in values of 26 000 – 891 000 g/mol for the different fractions and are assumed to be implausible. As the proportions of the individual fractions within the melanin–H_2O_2–solution were unknown, is was impossible to determine the *dn/dc*-value for every fraction.

To find out, whether any of the obtained SEC-fractions could be detected in the human skin, biopsies were dissociated to produce a solution investigable by SEC, according to current precipitation protocols (Flanagan *et al.*, 2006). Therefore, skin biopsies were incubated with collagenase type I (0.03 %; overnight at 37 °C), to remove the dermis and the remaining epidermis was further dissociated in trypsin solution from porcine pancreas (10 %; overnight at 37 °C). The SC and adherent hairs were removed and the solution was centrifuged at 6000 rpm (5 min). The residual cells were suspended in PBS buffer and again centrifuged. After renewed suspension in PBS buffer, the cells were minced in a Cell Crusher device and

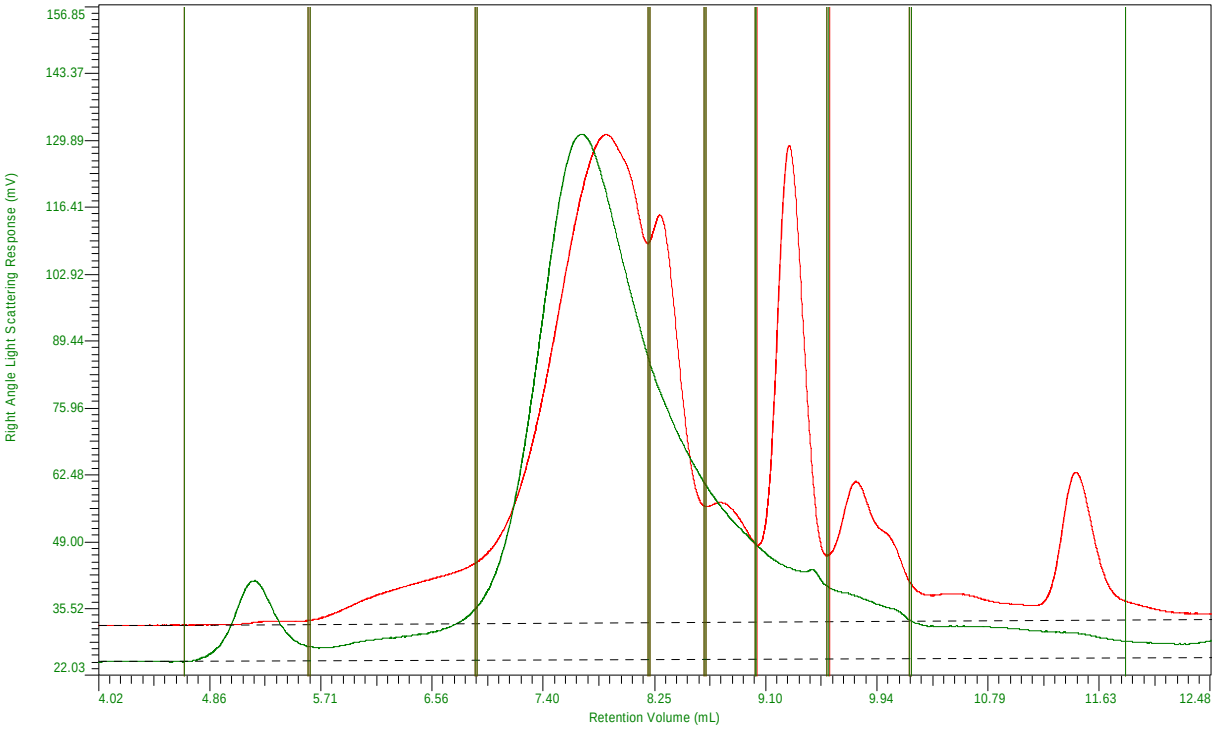

Figure 60: SEC chromatogram of *Sepia* melanin degraded with H_2O_2. The degradation products of *Sepia* melanin were suspended in PBS buffer and analyzed by SEC. 8 fractions were collected, the first had a retention volume of 5.20 ml. The signal obtained from the RI-detector (refractive index) is displayed in red, the signal recorded with the light scattering detector is displayed in green.

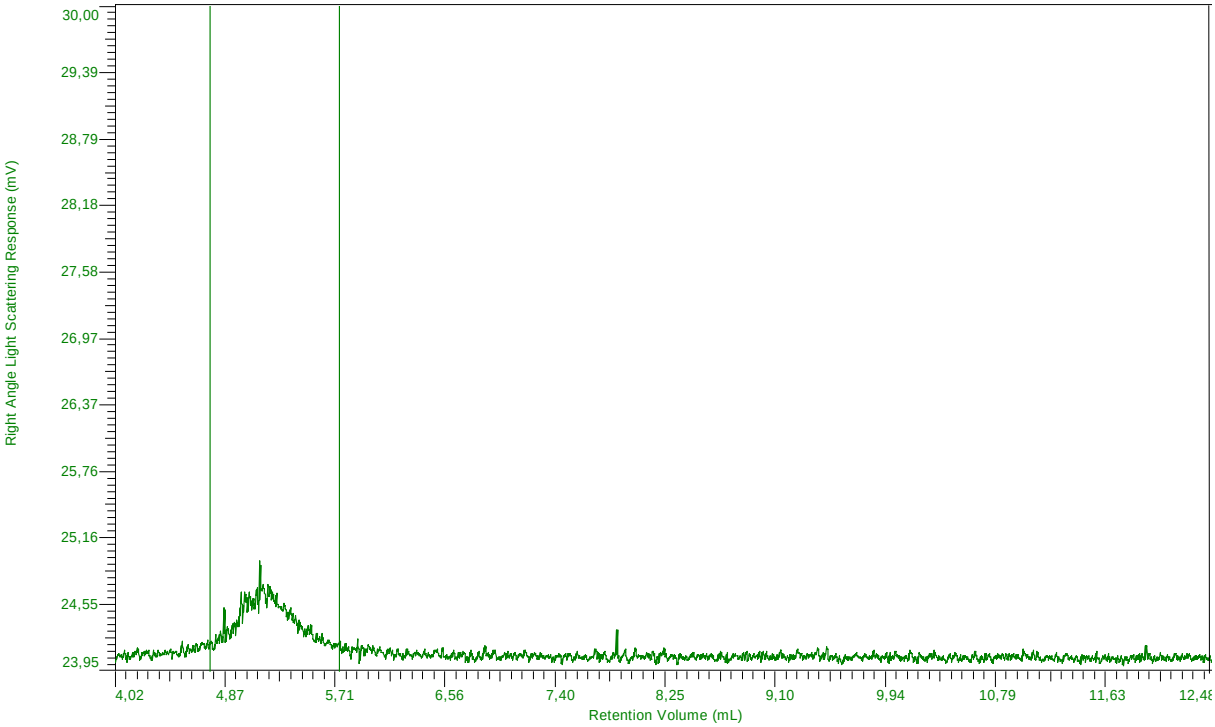

Figure 61: SEC chromatogram of a suspension of human epidermis. A skin biopsy was enzymatically dissociated and suspended in PBS buffer. Residues of cell membranes and hairs were removed. Lipids, proteins and DNA were precipitated with methanol and the suspension was centrifuged. The supernatant was suspended in PBS buffer and analyzed by SEC. The light scattering detector registered one signal with a retention volume of 5.12 ml.

3 ml of methanol were added to precipitate lipids, proteins and DNA, and the solution was again centrifuged. The supernatant was dried and the residue was suspended in PBS buffer and investigated by SEC in the same manner as the H_2O_2 solution of melanin.

For the solution obtained from the skin biopsies, neither RI-detector nor viscosimeter detector detected anything. But the light scattering detector registered a signal with a retention volume of 5.12 ml (see Figure 61), corresponding to the first fraction collected after the elution of the solution of *Sepia* melanin in H_2O_2. This confirms at least the partial transferability of the results obtained with *Sepia* melanin to the pigmentation of the skin.

The 8 fractions obtained from the SEC-analysis of H_2O_2-degraded *Sepia* melanin were dried and resuspended in methanol for analysis by ESI-MS (see chapter C.VI.4). No signal was observed in the mass-to-charge ratio range of 1700-3000 *m/z* for the fractions 1-2 and 4-8. Only the third fraction displayed a periodic mass spectrum, with clusters of peaks in intervals of 149 *m/z* (see Figure 62). Further groups of peaks were detected in smaller intervals of 75 *m/z* and 16 *m/z*.

The mass-to-charge ratios of 1811.4 *m/z*, 1960.4 *m/z* and 2109.5 *m/z* measured for major peak clusters apparent in Figure 62 correspond to DHI, one of the major subunits of the eumelanin oligomer. The DHI polymers occurred in combination with a variety of fragments, such as DHICA, benzene, phenol, benzenediol, indole and hydroxyindole. Furthermore, PTCA polymers (1813.8 *m/z*, 2012.8 *m/z*), that arise during the oxidation of eumelanin with $KMnO_4$ employed to measure the eumelanin content in biological specimen (see chapter C.VI.1), and PDCA (1882.9 *m/z*, 2037.9 *m/z*) were observed in the mass spectrum. The entire list of polymers and possible combinations of polymers, corresponding to the obtained *m/z*-values is displayed in Table 18. The correlation to the *m/z*-values was based on the assumption, that the molecules were present as sodium-adducts.

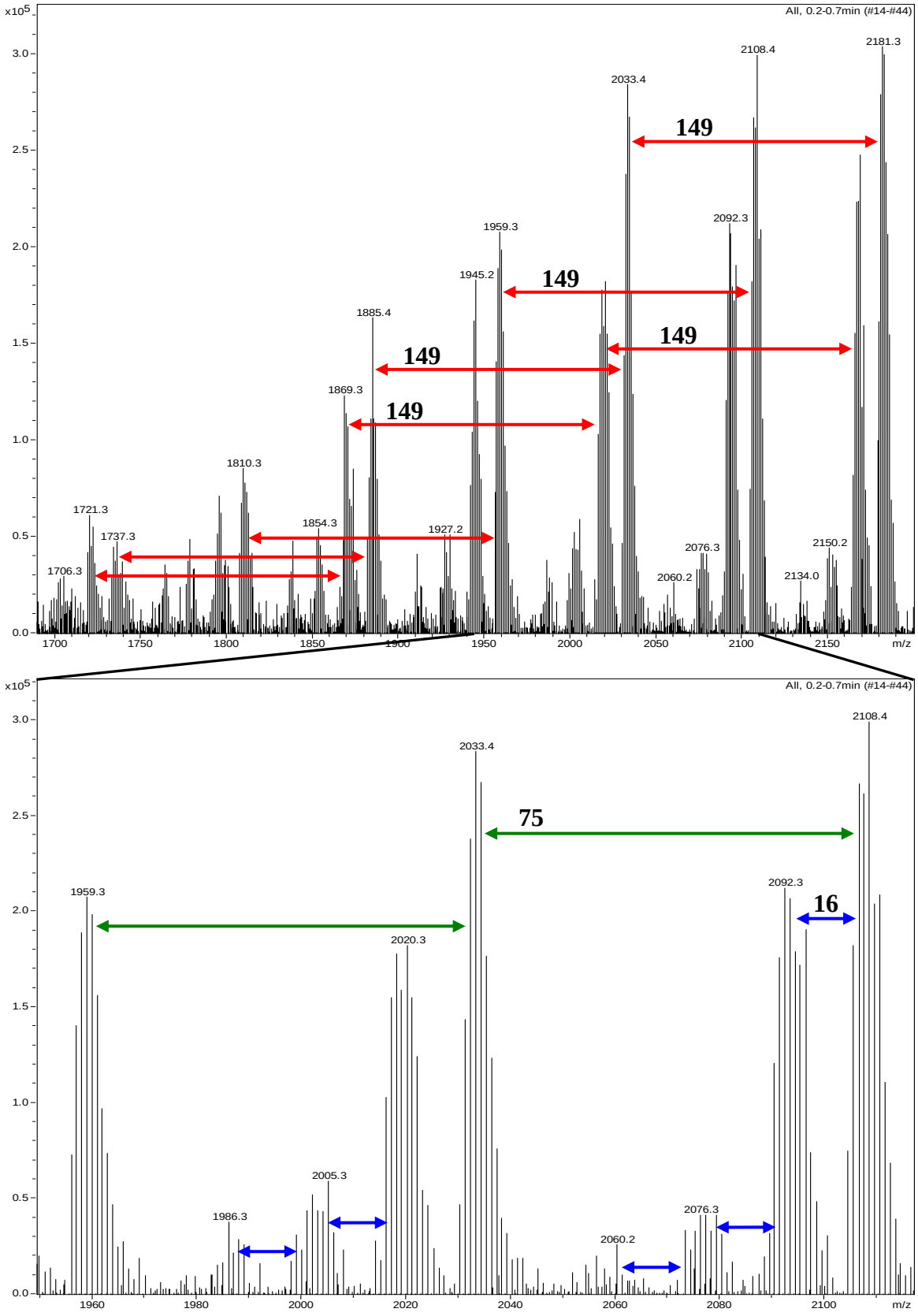

Figure 62: Mass spectrum of the third fraction of the SEC-analysis. The mass-to-charge ratio (*m/z*) is plotted on the x-axis, the y-axis represents the signal intensity of the ions, measured in counts per second (cps). Top: the entire *m/z* range recorded from 1700 *m/z* to 2200 *m/z* is displayed. Bottom: detail in the range of 1945 – 2110 *m/z*. Periodic groups of peaks were detected in intervals of 149 *m/z*, 75 *m/z* and 16 *m/z*.

Table 18: List of polymers, corresponding to the mass spectrum obtained from the third fraction of the SEC-analysis.

Polymer	*m/z*-values
n PTCA	1813.8; 2012.8
n PDCA	1882.9; 2037.9
n Hydroxyindole	1885.6; 2018.6; 2151.7
n DHI	1811.4; 1960.4; 2109.5
n DHI + 1 Benzene	1740.4; 1889.4; 2038.4; 2187.5
n DHI + 2 Benzene	1818.4; 1967.5; 2116.5
n DHI + 1 Phenol	1756.4; 1905.4; 2054.5; 3.5
n DHI + 2 Phenol	1850.4; 1999.5; 2148.5
n DHI + 3 Phenol	1795.4; 1944.5; 2093.5
n DHI + 2 Benzenediol	1733.4; 1882.4; 2031.4; 2180.4
n DHI + 1 Indole	1779.4; 1928.4; 2077.5
n DHI + 1 Hydroxyindole	1795.4; 1944.4; 2093.5
n DHI + 2 Hydroxyindole	1779.4; 1928.4; 2077.5
n DHI + 3 Hydroxyindole	1763.4; 1912.4; 2061.5
n DHI + 1 Benzene + 1 Hydroxyindole	1724.4; 1873.4; 2022.5; 2171.5
n DHI + 1 Benzene + 2 Hydroxyindole	1857.5; 2006.5; 2155.5
n DHI + 1 Phenol + 1 Hydroxyindole	1740.4; 1889.4; 2038.5; 2187.5
n DHI + 1 Phenol + 2 Hydroxyindole	1724.4; 1873.4; 2022.5; 2171.5
n DHI + 1 DHICA	1855.4; 2004.4; 2153.4
n DHI + 1 DHICA + 1 Benzene	1784.4; 1933.4; 2082.4
n DHI + 1 DHICA + 1 Phenol	1800.4; 1949.4; 2098.4
n DHI + 1 DHICA + 1 Benzenediol	1816.4; 1965.4; 2114.4
n DHI + 1 DHICA + 1 Hydroxyindole	1839.4; 1988.4; 2137.4
n DHI + 1 DHICA + 1 Benzene + 1 Hydroxyindole	1768.4; 1917.4; 2066.5
n DHI + 1 DHICA + 1 Phenol + 1 Hydroxyindole	1784.4; 1933.4; 2082.5
n DHI + 1 DHICA + 1 Phenol + 2 Hydroxyindole	1768.4; 1917.4; 2066.5
n DHI + 1 DHICA + 2 Phenol + 1 Hydroxyindole	1729.4; 1878.4; 2027.4
n DHI + 1 DHICA + 1 Benzenediol + 1 Hydroxyindole	1800.4; 1949.4; 2098.4
n DHI + 1 DHICA + 2 Benzenediol + 1 Hydroxyindole	1761.4; 1910.4; 2059.4
n DHI + 1 DHICA + 1 Benzenediol + 2 Hydroxyindole	1784.4; 1933.4; 2082.4

V.2 Localisation of NADPH Oxidase Activity

NADPH oxidase is considered a strong candidate in the quest for the mechanism of melanin degradation (Borovanský and Elleder, 2003). It is rated a possible supplier of H_2O_2, via the production of reactive oxygen species (ROS) that dismutate to H_2O_2. Based on this hypothesis, the localisation of H_2O_2-production in the epidermis was investigated. Therefore, a protocol for the cytochemical detection of H_2O_2 in biological tissues, based on the principles of cerium capture cytochemistry (Ellis and Grant, 2002) was adapted to skin biopsies.

The fine electron dense precipitate, that results from a reaction of H_2O_2 with cerous ions, was visualized by LM and TEM. The amplification reaction with DAB produced no suitable results, as the blue staining of the DAB-cobalt-H_2O_2-complex produced only vague circum-nuclear staining, but could not be clearly identified (Figure 63.A, black arrowheads). A clear staining was observed only along the plasma membranes and in the intercellular space. These areas were also detectable in the reflection mode of CLSM, while no signal was obtained from the sites surrounding the nuclei (Figure 63.B).

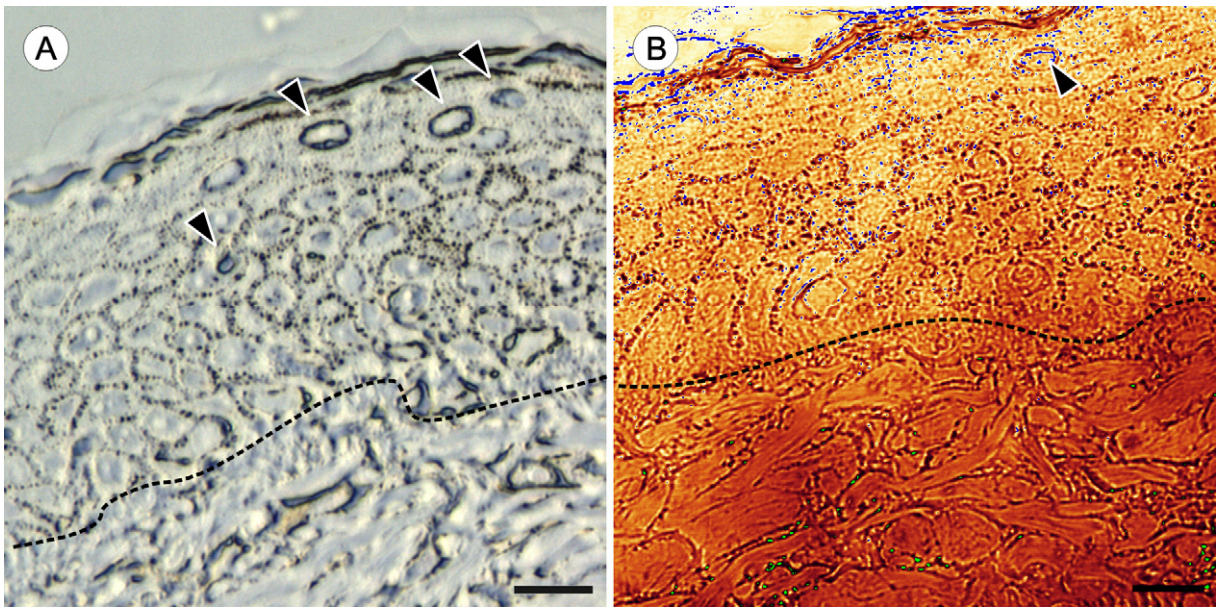

Figure 63: Light microscopic detection of the cerium precipitate demonstrating H_2O_2. H_2O_2 produced via NADPH oxidase reacts with cerium to form a fine electron-dense precipitate, that is detectable by CLSM. The precipitate can be amplified by DAB to visualize its localisation by conventional LM. (A) LM image of Caucasian skin. A faint blue staining is observed surrounding the nuclei. Only few nuclei displayed a distinct dark blue stain (arrowheads). Strong staining is also detected in the intercellular space along the plasma membranes of the keratinocytes. The basement membrane is indicated by the dashed line. (B) The cerium precipitate is visualized reflection mode CSLM. Blue spots indicate strong reflection signal. Again the strongest signal is obtained from the intercellular space. Very few nuclei show surrounding precipitate (arrowhead).
Bars: 20 µm

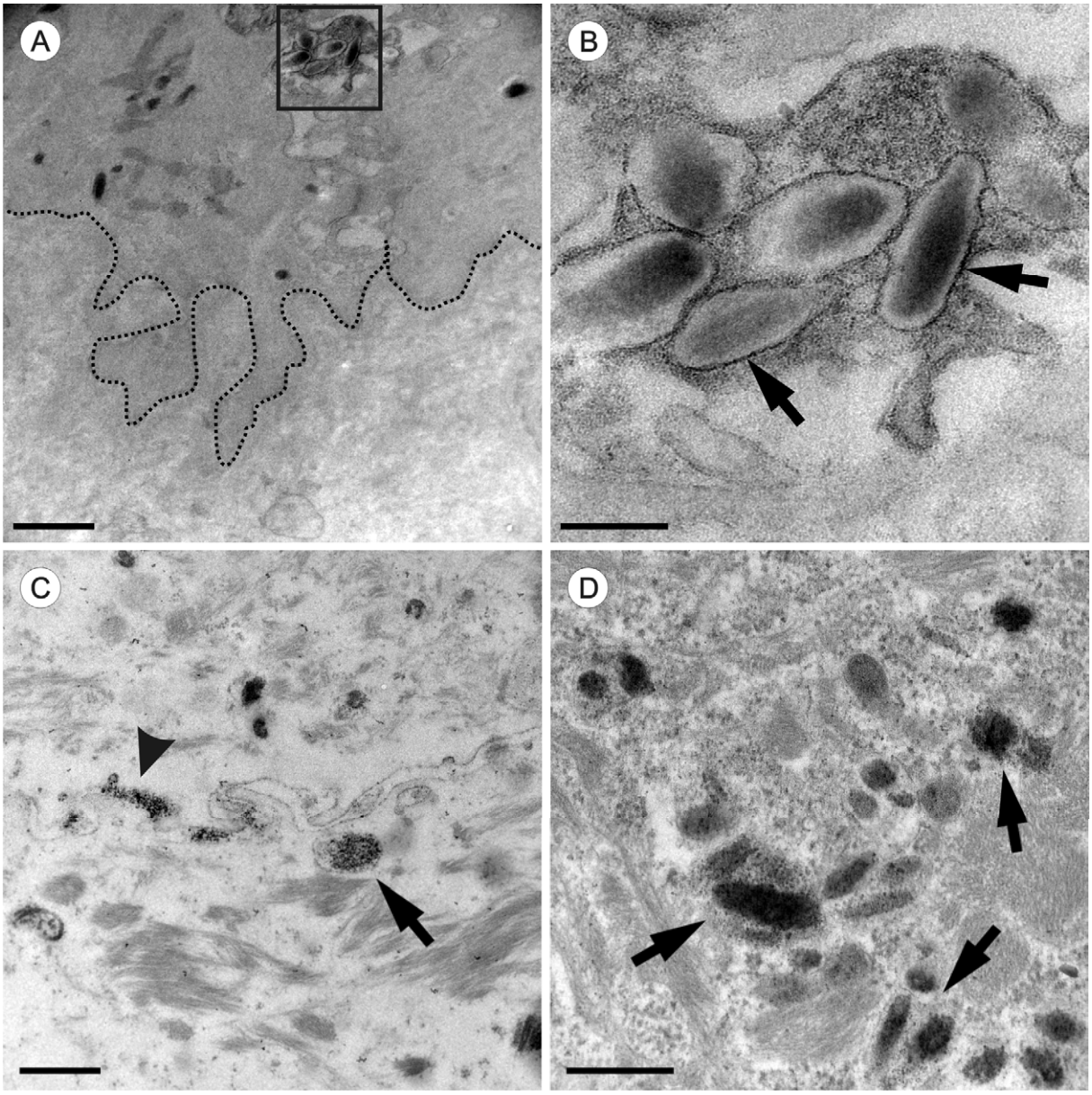

Figure 64: Electron microscopic detection of NADPH oxidase. H_2O_2 produced via NADPH oxidase reacts with cerous ions to form a fine electron-dense precipitate, which is detectable by TEM. (A) Two keratinocytes of the SB with a melanocyte dendrite in the intracellular space between them. The dotted line indicates the basement membrane. Few melanosomes were visible within the keratinocytes (black oval shapes). The area marked by the black frame is displayed in image (B). Several melanosomes were observed in the melanocyte dendrite, framed by the cerous precipitate (black arrows), that was also present in the cytoplasm of the dendrite. (C) Two adjacent keratinocytes of the lSSp are displayed. The cerium-precipitate was observed in the intracellular space (arrowhead) and within the keratinocytes in vesicles, resembling melanosomes in shape and size (arrow). But a melanosome was not discernable within the vesicle. (D) Melanosomes and melanosome clusters in keratinocytes of the SB were often dotted with cerium-granules, although accumulations were not as dense as demonstrated in image (B). *Bars: (A) 200 nm; (B) 50 nm; (C) 200 nm; (D) 100 nm*

For the TEM investigation, the resin sections were not stained with heavy metals, in order to avoid staining artefacts and preserve the visibility of the cerium precipitate contrasting against the ultrastructure of the specimen. Nevertheless, the epidermal cells were clearly distinguished and details of the ultrastructure, such as keratin filaments, vesicles and melanosomes

were identifiable (see Figure 64). The cerium precipitate appeared as fine, dotted enhancement of specific structures. It was detected predominantly in the lower layers of the epidermis (SB and lSSp), along cell membranes and in membrane bound vesicles.

Frequently the precipitate was observed in the intracellular space (see Figure 64.C). Melanocyte dendrites demonstrated particularly distinct accumulation of the dark precipitate, standing out against the adjacent keratinocytes (Figure 64.A). The precipitate was present in the cytoplasm and was explicitly framing the comprised melanosomes (Figure 64.B). Less dense accumulation of precipitate granules were frequently observed around, and even located directly on melanosomes and melanosome clusters (Figure 64.D). In the case of melanosome clusters, the precipitate was evenly distributed within the membrane-bound complex. Vesicles resembling melanosomes in size and shape regularly showed the cerium precipitate (see Figure 64.C, arrow). But, as demonstrated in this example, a melanosome was not always discernable within the membrane-clad structure.

Controls for the specificity of the reaction were performed by (1) omitting the substrate β-NADPH needed for the production of ROS and (2) by addition of a specific inhibitor of NADPH oxidase (DPI). No cerium precipitate was observed in the control samples.

In order to confirm the presence of cerium in the biopsies and to verify its localisation on or near melanosomes, energy-filtered TEM (EFTEM) was performed and an elemental map for cerium was obtained. Figure 65.A displays an overview of basal keratinocytes, acquired by HAADF-STEM (high-angle annular dark field-scanning TEM), the melanosomes are therefore illustrated as bright white shapes. A contamination caused by previous measurement approaches is visible to the right of the nucleus of the left keratinocyte (white square).

The area delimited by the white frame was further investigated by EFTEM, Figure 65.B displays a zero-loss filtered image with two melanosomes (displayed again as dark shapes) discernible. The same area, imaged by EFTEM at an energy loss of 100 eV, corresponding to the energy loss obtained from the N shell electrons of cerium (Figure 65.C). Although the acquired signal is weak, it nevertheless confirms the presence of cerium, and thus the localisation of NADPH oxidase within melanosomes.

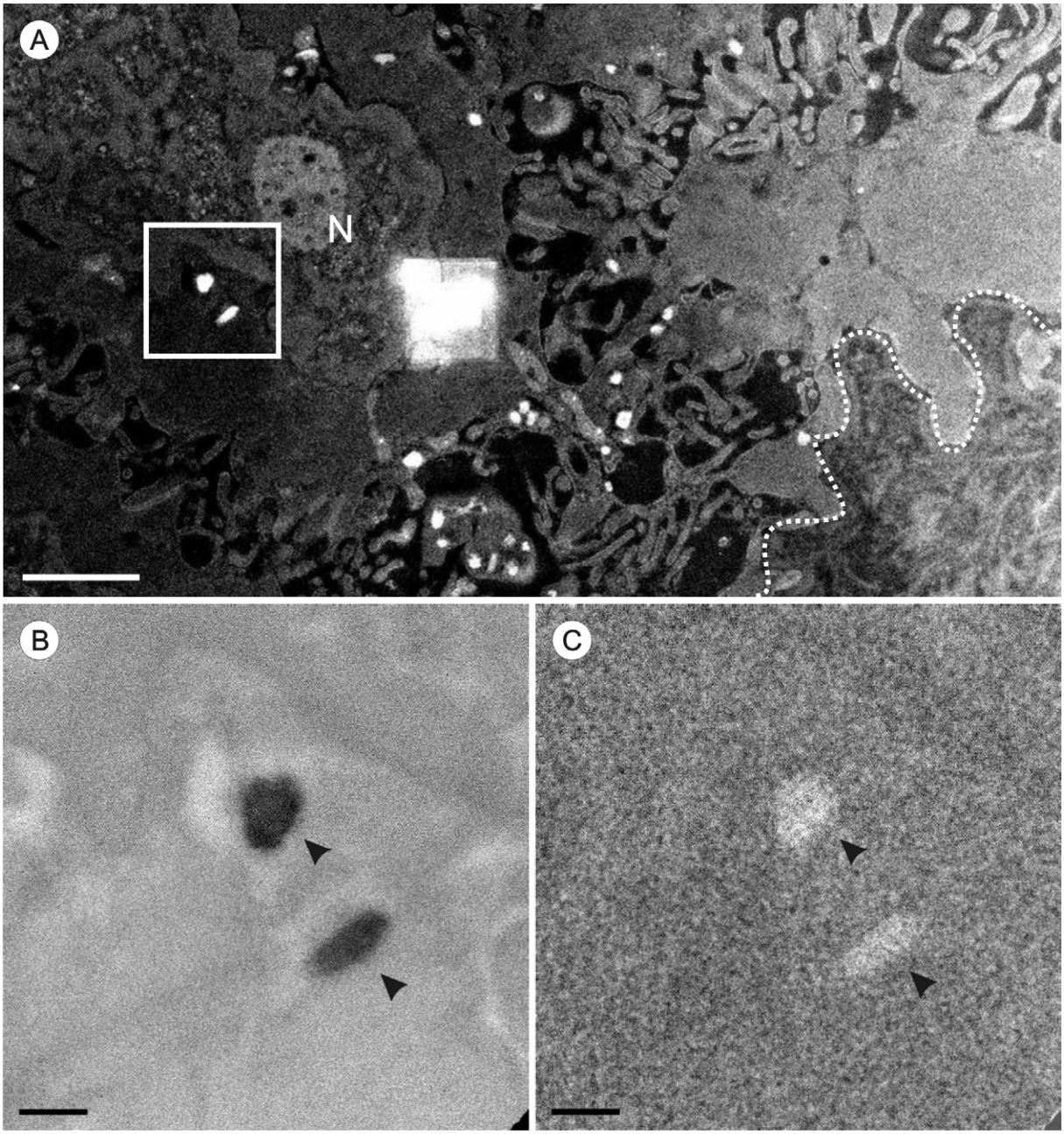

Figure 65: Demonstration of cerium by EFTEM. (A) HAADF-STEM micrograph of basal keratinocytes (the dashed line represents the basement membrane). Melanosomes appear as bright white spots of roundish or oval shape. The white square to the right of the nucleus is caused by a contamination. (B) Enlargement of the area within the white frame. Energy-filtered electron micrograph of two melanosomes (here displayed as dark shapes, see arrowheads). (C) Cerium-map obtained at approx. 110 eV energy loss, representing the same area as image (B). The two melanosomes show a faint signal, confirming the presence of cerium.

N = Nucleus *Bars: (A) 1 µm; (B) & (C) 0.2 µm*

F DISCUSSION & CONCLUSIONS

The purpose of this project was to describe the distribution patterns of melanin in different skin phenotypes and identify morphological and biochemical evidence for the description of melanosome transfer mechanisms as well as melanin processing pathways in the human epidermis. This involved the identification and establishment of appropriate microscopic imaging methods to enable the specific recognition and detailed description of melanocytes and melanosomes at an accurate resolution. Caucasian, Asian and Negroid skin and samples of age spots, including a control area from the periphery of the lesion were investigated by TEM regarding the content of melanosomes in different layers of the epidermis. Additionally, state of the art chemical analysis of epidermal melanin content and reflectance spectroscopy were performed and correlated with the microscopic investigation to evaluate its validity.
Possible mechanisms of melanosome transfer from melanocytes to keratinocytes were again investigated by TEM to identify morphological criteria to prove or disprove the hypotheses described in literature. Based on the obtained data on melanosome distribution and morphology, evidence of a further processing and final degradation of melanosomes was detected, and a possible degradation pathway identified.

I Epidermal Melanosome Distribution Quantified by TEM

As detailed in chapter D.II, the epidermal distribution of melanosomes is ideally characterized by TEM, as the light microscopic resolution is insufficient for investigations at the level of single melanosomes and their distribution. Classifying the epidermis into four sub-layers (the *Stratum basale*, the *Stratum spinosum*, subdivided into a lower and an upper division that includes the *Stratum granulosum*, and the *Stratum corneum*), the melanosome distribution was determined by counting the present melanosomes in each layer. Individual melanosomes and clusters of melanin particles, defined by an enveloping membrane, were each counted as one melanosome. This manual analysis is extremely dependent on the image interpretation of the individual investigator. The benchmark test conducted by six independent investigators

revealed an inter-individual variability of approx. 30 %. While the identification of melanin particles was comparable and showed no major differences, considerably less melanosomes were allocated to clusters, resulting in a substantial increase in the total melanosome numbers of all investigated epidermal layers. This might be explained by uncertainty in interpretation of TEM images due to a lack of background knowledge in the field of pigmentation, as this was not a focal point of the volunteering investigators. On the other hand, intensive engagement in a special subject may also affect the objectivity, and thus the misinterpretation might be on my side as well.

To eliminate this variability and enhance the comparability of individual investigations, an image analysis tool for automated identification and counting of melanosomes was devised, based on the pre-existing ZETA software by the Fraunhofer Institute for Applied Information Technology (FIT) in Sankt Augustin, Germany. This tool is trained manually to define the structure to be analyzed by positive and negative examples, i.e. melanosomes, and enable the distinction from melanosome-resembling structures, such as vesicles (similar in shape) and staining artefacts (similar in grey value) by the algorithm generated during this training phase. The results obtained with this tool displayed a strong dependency on the preservation quality of the analyzed sample: samples with preparation artefacts like agglomeration of proteins and intermediate filaments, or samples with weak contrast posed a problem for the identification of melanosomes by the implemented segmentation tool (see Figure 36).

Another difficulty was the allocation of melanosomes to clusters. While humans are able to recognize a certain structure considering not only shape and colour or grey value, respectively, but also by taking into account the context of the structure in question. A cluster of melanosomes is thus identified as several dark, round-to-oval structures, surrounded by a limiting membrane. The transferability of this a priori knowledge into a computational identification tool is restricted. Therefore, for clusters a spatial criterion had to be applied for the definition of clusters, defining the distance between adjacent melanosomes of a cluster to be less than 50 nm. However, for samples with good structural integrity and a balanced grey value distribution, both, the identification of melanosome as well as the allocation to clusters correlated very well with the manual evaluation. Only the SC – no matter how good or bad the structural integrity of a sample – poses a difficulty for the ZETA software. Even in samples with excellent quality, the corneocytes can appear very dark and homogenous, thus masking the melanosomes (Figure 66.A; white arrowheads), and preparation artefacts in the SC lead to dark filamentous or fringy structures, impeding with the automated detection.

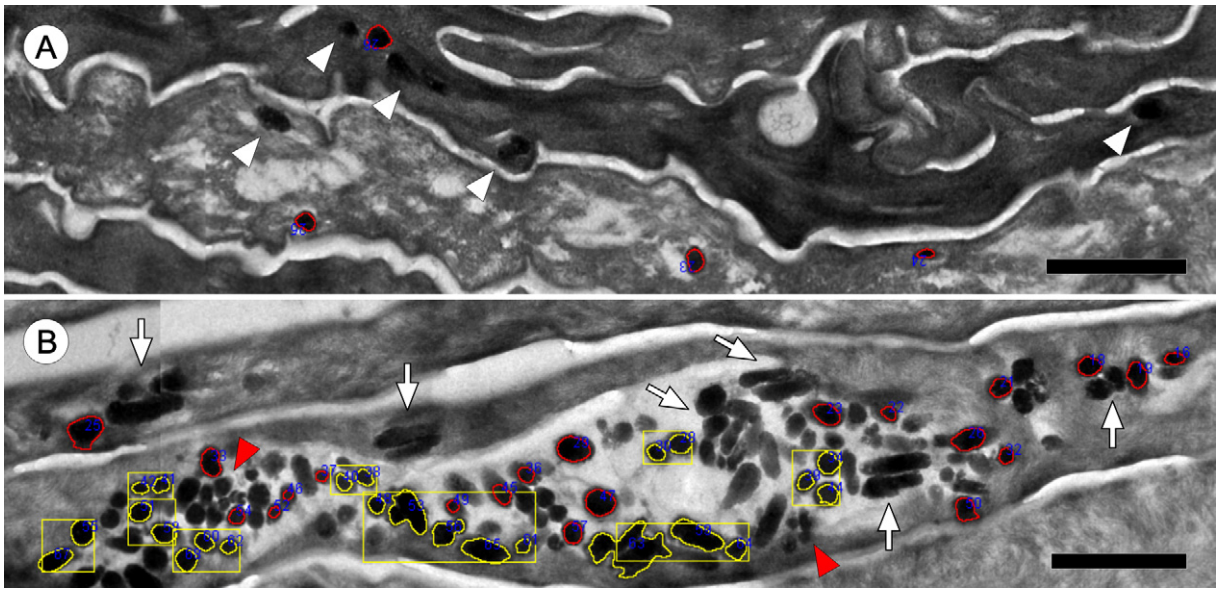

Figure 66: Melanosome detection in SC poses a problem for the ZETA image analysis tool. (A) Detail of the SC of a sample with good quality. In the lower epidermal layers of this sample, ZETA produced excellent results regarding both, the detection of melanosomes and the allocation to clusters (see Figure 36.A & B). But due to low contrast in the SC, about 50 % of the existing melanosomes are not detected (white arrowheads). (B) SC of a sample of Negroid skin. The structural integrity in the entire epidermis is still acceptable, but far less than 50 % of melanosomes are identified by ZETA. Most of the melanosomes are most likely not detected due to aberrant shape (white arrows) or size (red arrowheads). *Bars: 1 µm*

Another problem is given by the different size of the melanosomes found in the SC (Figure 66.B; red arrowheads). The detection algorithm of the ZETA software is based on shape, difference in grey value compared with the surroundings and the size of the sought particles. And although no significant variation in size was observed during the manual analysis, a slight aberration affects the automated detection. The generation of individual training data sets for the SC enhanced the quality of the results, but still, the detection of melanosomes and the allocation to clusters remained sub-standard compared with the lower epidermal layers. Additionally, the application of algorithms based on different training data sets renders the comparability of the results difficult.

The ZETA-based analysis tool is considered a prototype that nevertheless produces very good and stable results, given the relative complexity of electron micrographs. Integration of further shape-related criteria into the segmentation tool to enhance the identification melanosomes may be necessary in order to gain more independence of sample quality. But as ideal sample preservation should be aspired anyway, this drawback can be overcome and the first step toward automated analysis of electron micrographs is done with this self-trainable software.

II Constitutive Pigmentation of Normal Skin Investigated by Microscopy, Chemical Analysis and Reflectance Spectroscopy

Electron microscopy proved to be the most suitable of the available imaging techniques for the quantitative analysis of the epidermal melanosome content in human skin depending on their location. To evaluate the validity of the obtained results in the context of some of the most commonly used state-of-the-art measurement techniques, a direct comparison with reflectance spectroscopy and a the microanalytical method of Ito and Wakamatsu (S. Ito and Jimbow, 1983) was accomplished. Four biopsies of Fitzpatrick's skin phototype I and five samples of phototype VI, were quantitatively investigated by TEM. Corresponding biopsies of each participant were analyzed by Dr. Wakamatsu for eumelanin and pheomelanin content (see chapter E.I.3). Reflectance spectroscopy was performed approximately one year after the draft of the biopsies, in direct proximity of the residual scars (see chapter E.I.4).

Direct comparison of these diverse methods is impossible. But the relation of the two investigated sample collectives can be used for the evaluation. Summing up the melanosome contents determined for the four epidermal layers results in 0.23 mel./ µm² epidermis for phototype I and 2.55 mel./ µm² epidermis for phototype VI. This corresponds to a relative increase of 1017 % (Figure 67). The microanalytical investigation yielded a total melanin content (including eumelanin and pheomelanin) of 94,6 ng melanin/ wet mg skin for phototype I, and 994,1 ng melanin/ wet mg skin for phototype VI, matching a relative increase of 950 %. Considering the dissimilarity of the two employed methods as well as the enormous discrepancy between the two phototypes, these values are well comparable and the divergence of approx. 7 % is negligible. This illustrates, that the melanin content of a tissue sample can be assessed by quantifying melanosomes in electron micrographs, although eumelanosomes are counted predominantly. Pheomelanosomes may be underestimated due to their similarity to other vesicles, as they are spherical and do not appear as electron-dense as eumelanosomes (Jimbow *et al.*, 1983). But the eumelanin proportion predominates in all skin types and only skin of phototype I contains a considerable amount of pheomelanin (Alaluf *et al.*, 2001; Alaluf *et al.*, 2002a; S. Ito and Wakamatsu, 2003). The proportion of pheomelanin in all investigated samples ranged between 3-6 %, only skin of phototype I contained a considerable 22 % (chapter E.I.3). A possible underestimation of the total melanin content due to omission of pheomelanosomes from the analysis is therefore justifiable.

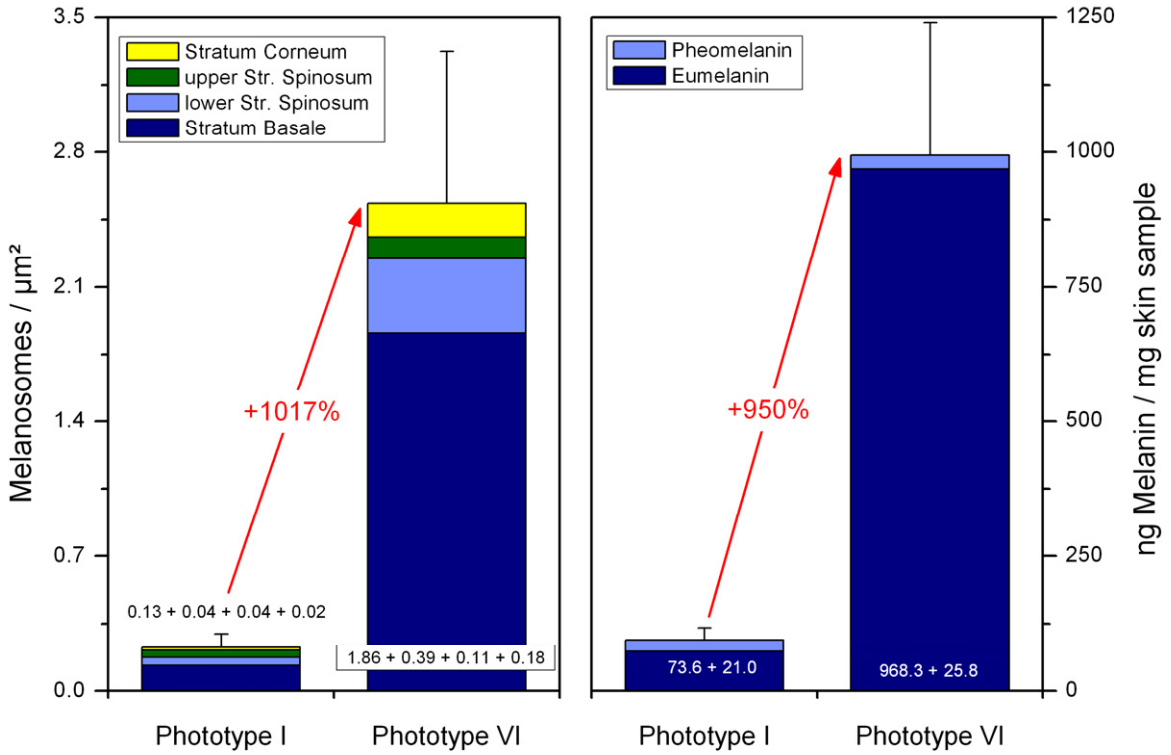

Figure 67: Comparison of microscopic and chemical analysis of epidermal melanin content. Direct comparability of the two diverse methods is impossible, but the proportional difference between the investigated sample collectives can be utilized to correlate chemical and microscopic analysis. The microscopic investigation yielded a total of 0.23 melanosomes/ µm² epidermis for skin of phototype I and 2.55 mel./ µm² for skin samples of phototype VI. This corresponds to a relative increase of 1017 %. The chemical analysis yielded 94.6 ng total melanin/ mg wet skin for phototype I and 994.1 ng/ mg skin in phototype VI, resulting in a relative increase of 950 %. Considering the enormous discrepancy between the two phototypes, the values are well comparable.

Compared with the chemical analysis, the microscopic quantification bears the additional advantage of a spatial resolution, as the distribution of the melanosomes in different layers of the epidermis can be determined and individual as well as clustered melanosomes can be distinguished and quantified at a subcellular level. On the other hand, the distinction between eumelanin and pheomelanin is more accurately achieved by the chemical analysis. Compared with the elaborate preparation procedure for EM, the chemical analysis produces results in a much shorter period of time (S. Ito and Jimbow, 1983). A major drawback of this method is the low yield of specific degradation products, which are utilized for the determination. Originally, the specific marker for DHICA-eumelanin (PTCA) was produced at a yield of only 2.8 %. Although Napolitano *et al.* were able to improve the yield for PTCA to 6.1 % (Napolitano *et al.*, 1995; Napolitano *et al.*, 2000), the calculation of the actual eumelanin content still requires the application of the conversion factor of 160. AHP, specific marker for pheomelanin, gives a yield of 11 % and a conversion factor of 9 is used (Wakamatsu and Ito, 2002). The specific marker for DHI-derived eumelanin, that accounts for 60-70 % of the total

melanin, at least in darker skin types (Alaluf *et al.*, 2001), is produced at a negligible yield of 0.46 %, and is therefore merely used for the determination of the melanin content (Wakamatsu and Ito, 2002). However, this may lead to a considerable underestimation of the actual melanin content, but it remains relative as long as the samples are prepared and analysed in the same batch.

In this context, the assumption that melanosome clusters are to be counted as one melanosome needs to be reconsidered. The relative change in melanosome content from phototype I to VI determined on the basis of this assumption correlates surprisingly well with the chemical analysis of total melanin content. But if the chemical analysis actually underestimates the melanin content, it might be more appropriate to consider each melanin particle as an individual melanosome, and thus estimating the melanin content more correctly. However, the clustered melanin particles are smaller than the individually distributed melanosomes (Thong *et al.*, 2003) and thus contain less melanin. This dilemma might be solved by correlating the counted melanosome numbers with the size of the respective particles, a feature already considered and included in the ZETA software.

Comparison of the results obtained by reflectance spectroscopy with the results of the microscopic and chemical analysis is limited. Phototypes I and VI can be easily distinguished, but the only significant difference was detected in the lightness value (L^* value). Moreover, differentiation of phototypes I, II, III and IV was impossible (see Figure 40). A direct correlation with the other methods was therefore not possible.

The validity of the TEM-based melanin content analysis, proven by the good correlation to the chemically determined total melanin content, allows to use this method to determine the epidermal distribution of melanosomes (melanin content) in skin of different phenotypes. First, a pool of samples classified according to ethnic origin, i.e. Caucasian, Asian and Negroid skin was investigated. A second sample collective comprising of Fitzpatrick's phototypes I to VI was analyzed chemically to determine the total melanin content (see above, and chapter E.I.3). Number and location of the present melanocytes for these latter samples was established by immunofluorescence assay (chapter C.IV.3), and additionally the epidermal melanosome distribution for samples of phototype I and VI was determined by TEM. The Caucasian and Asian skin samples were not sub-classified, but can roughly be allocated to Fitzpatrick's phototypes I-III (Caucasian) and IV+V (Asian). The Negroid skin matches phototype VI. Some of the participants of the first study were from south India and had very dark skin that may be rated as phototype VI rather than V, but precise assignment to

phototypes was not accomplished during this study. However, the necessity for a more precise classification became evident during the investigation of the samples and was considered in the following study design.

For all investigated skin phenotypes, the largest amount of melanosomes is detected in the SB and the quantity gradually decreases toward the outer epidermal layers – a universally confirmed observation (Alaluf *et al.*, 2002a; Bolognia and Orlow, 2003). Expressed as a percentage, the decrease from SB to SC (total clearing rate) is comparable for all investigated samples of normal skin, i.e. skin without any pigmentary disorders. In the first study, Caucasian skin showed a slightly lower melanosome-clearing rate of 76 %, compared to Asian and Negroid skin with 80 % and 84 % (Figure 27). However, the later investigated phototypes I and VI displayed slightly increased clearing rates of approx. 90 % (Figure 29). The initial clearing rate from SB to lSSp already measures approx. 60 % in all phenotypes. Phototypes I and VI of the second investigation even show a melanosome clearing of ~ 70 %. Only the Caucasian sample pool demonstrates a significantly lower clearing rate of 31 %.

The different phenotypes show distinct variations in the intra-keratinocyte distribution patterns of melanosomes in the SB. In Caucasian and Asian skin, roughly half of the melanosomes are organized in membrane-bound clusters. This percentage is significantly increased in phototype I, where approx. 65 % of the melanosomes are clustered. On the other hand, only 13 % clustered melanosomes are observed in Negroid skin and 25 % in phototype VI (Table 15). Toward the upper epidermal layers the quantity of clusters decreases, the efficiency depending on the skin phenotype: the lighter the skin type, the more clusters are observed in the upper epidermal layers. But in the SC a homogenous level of 10-15 % clustered melanosomes is reached in all phenotypes.

The discrepancy in melanosome clustering in the SB of Negroid skin and phototype VI might be explained by variations in the counting procedure, as the two sample pools were not analyzed by the same investigators – an inconsistency avoidable by automated analysis with a refined ZETA software (see chapter F.I). The assumed over-allocation of melanosomes to clusters observed in the analysis of phototype VI would also imply, that the percentage of clusters in phototype I (65 %) is overestimated. However, melanosome clusters are considered a characteristic feature of Caucasian skin, while in Negroid skin, isolated melanosome predominate (Szabo *et al.*, 1969; Konrad and Wolff, 1973). Alaluf *et al.* (2002a) and Thong *et al.* (2003) observed 85 % of the melanosomes organized in membrane-bound clusters in Caucasian skin, and only 11 % clustered melanosomes in Negroid skin. They rated Asian skin as an

intermediate between Caucasian and Negroid skin, with approx. half of the melanosomes clustered. This confirms the observed trend, that the lighter the skin type, the more melanosomes are organized in clusters, while in dark phenotypes the melanosomes are predominantly distributed as isolated entities.

The different phenotypes are best distinguished by their total content of melanosomes. A direct relation can be established between the total epidermal amount of melanosomes and the phototype or ethnicity respectively – the lighter phenotypes containing less, the darker phenotypes more melanosomes (Figure 27). This trend is confirmed by the microanalytical determination of the total melanin content of the sample collective of Fitzpatrick's phototypes I-VI (see above). To match the ethnic classification, phototypes II+III and IV+V were pooled. Phototype I is considered an exception, because of the large proportion of pheomelanin. The total melanin content of samples of phototype I is approx. half of that measured for phototypes II+III, which is again half of the melanin content of phototypes IV+V. And phototype VI contains the threefold amount of melanin, compared with phototypes IV+V (Figure 39). This roughly matches the TEM-based determination of melanosome content for Caucasian, Asian and Negroid skin, the total amount of melanosomes in Caucasian skin being half of that of Asian skin, while Negroid skin contains double the amount compared to Asian skin. Considering the standard deviation of all groups of phototypes, only phototypes I and VI can clearly be distinguished. The samples of phototype II-V are in the same order of magnitude, a fact also manifested in the reflection spectroscopic analysis.

Interestingly, the skin types with the higher melanosome content exhibit the lower quantity of melanocytes in the epidermis (Figure 43). Approx. 14 melanocytes/ mm basement membrane (18 melanocytes/ mm SG) are counted in the phototypes allocated to Caucasian skin, i.e. phototypes I-III. The Asian phototypes IV+V contain approx. 7 melanocytes/ mm BM (10 melc./ mm SG), while in phototype VI (Negroid skin) approx. 11 melanocytes/ mm BM (13 melc./ mm SG) are detected. This implies that the in dark skin phenotypes less melanocytes produce more melanosomes compared to lighter skin types. This phototype dependent density disagrees with the findings of Tadokoro *et al.* (2005), who observed homogenous melanocyte numbers in all Caucasian, Asian and Negroid skin phenotypes, although the results were in a comparable order of magnitude of ~ 12 melanocytes/ mm BM. However, this investigation was accomplished using skin of the dorsum, a chronically photoexposed site, while the above described results relate to an unexposed, photoprotected area (buttock skin). Melanocyte density varies significantly depending of the anatomical site and exposure to UV

light (Szabo, 1954; Staricco and Pinkus, 1957). Whiteman *et al.* (1999) investigated melanocyte densities relative to the SC and found comparable melanocyte densities in (partially) photoexposed sites, like the dorsum (~ 17 melc./ mm SC), upper limb (~ 13 melc./ mm SC) and lower limb (~ 14 melc./ mm SC). However, a considerably lower melanocyte density was observed for the anterior trunk (~ 3 melc./ mm SC), a usually photoprotected site. In default of reference data for buttock skin, the results obtained during the present study are therefore assumed to be probable, although the discrepancy in the relation of melanocyte density and observed melanosome content in Caucasian, Asian and Negroid skin can only be explained by a higher melanin synthesis rate in darker skin.

In conclusion, as the clearing rates are comparable in all skin types, the higher initial melanosome content in the SB of phototype VI (Negroid skin) as compared to lighter skin phenotypes (Caucasian skin, phototype I-III) is maintained throughout the entire epidermis with higher total amounts of melanosomes in the uSSp and SC, accounting for the dark appearance of the skin.

III Facultative Pigmentation of Age Spots and Freckles

Age spots (*lentigo senilis*) and freckles are both rated as solar *lentigines*, UV induced hyperpigmentations of otherwise healthy skin (Rahman and Bhawan, 1996). Both lesions are characterized by explicitly elevated melanosome numbers in the entire epidermis compared to normal skin. In contrast to the directly surrounding skin, age spots exhibit elongated rete ridges, that are increased in number and show branching or bud-like extensions. In the two-dimensional representation of histologic sections, these extensions often appear to merge at the bottom, forming bridges. Freckles on the other hand, miss these distinct features of the rete ridges, and differ from the surrounding perilesional skin only by their increased melanosome numbers.

But while these morphological features are easily revealed by histology, a dermatologist can not distinguish age spots and freckles by mere visual assessment, but requires noninvasive imaging methods like *in vivo* CLSM, that enables 3D-visualization of the rete ridges and papillae (Corcuff *et al.*, 2001; Yamashita *et al.*, 2005). All 11 pairs of lesional and perilesional samples obtained for the present study were assumed to be *lentigo senilis* rather than freckles. Age and tanning or sunburn history of the respective patients lead the investigating derma-

tologist to that assumption, as freckles are described to affect rather younger persons (Rahman and Bhawan, 1996).

Both, *lentigo senilis* and freckles, display elevated levels of melanosomes in all epidermal layers, which is consistent with the literature (Rahman and Bhawan, 1996; Virador *et al.*, 2001). Regarding the total melanosome content, lesional and perilesional of both *lentigo senilis* and freckles are comparable (Figure 53). With 2.44 mel./ µm² in age spots and 2.53 mel./ µm² in freckles, the lesional skin surpasses Caucasian skin (0.83 mel./ µm²) by far and is even comparable to skin of phototype VI (2.54 mel./ µm²). The perilesional skin contains comparable amounts of melanosomes as Asian skin (1.51 mel./ µm²) (Figure 27 and Figure 29). But although freckles and age spots do not differ in the total epidermal amount of melanosomes, the distribution of melanosomes throughout the epidermal layers displays variations. Approx. half of the melanosome content is found in the SB in all lesional and perilesional phenotypes, which is comparable to Caucasian skin. But lesional as well as perilesional skin of *lentigo senilis* contain considerably elevated levels of melanosomes in the SC. Here, 15 % of the total melanosome content is found, while the lesional skin of freckles contains 7 % and in the perilesional skin only 4 % are found. Caucasian, Asian and Negroid each hold 10 % of the melanosomes in the SC. Noteworthy is the difference in melanosome numbers in the lower SSp. Here both lesions contain more melanosomes than the corresponding perilesional skin (30 % in age spots vs. 25 % in perilesional skin, and 35 % in freckles vs. 25 % in perilesional skin).

The total melanosome clearing rates for both, lesional and perilesional skin of *lentigo senilis* measures 70 % and is thus only slightly lower than the clearing rate of Caucasian skin (75 %). However, the clearance rates found in freckles and their surroundings are distinctly higher. Furthermore, the melanosome clearing in the perilesional skin with 93 % is more effective than that observed in lesion (84 %), but both surpass the normal Caucasian skin. It must be noted, that the separately investigated samples of phototype I and VI displayed equally high clearing rates. The described distinctions might therefore fall into the range of normal variations, as the total reduction rates obtained are equal when counting only melanin particles, isolated and clustered, (chapter E.I.1.5). The only conspicuous fact here is the extremely low clearance rate from SB to lSSp in the lesion of freckles: only 5 % of the present melanin particles are degraded.

However, the quantitative reduction of melanosomes from SB to the lower SSp is explicitly more effective in the perilesional skin of both kinds of hyperpigmentation. While in the

perilesional skin, the melanosome number are reduced more than 50 % (clearing rate), the age spots here display a reduction rate of 36 %, and the freckles an even lower clearing rate of 21 % is measured. In Caucasian skin obtained from a photoprotected site, the clearing rate ranges in the same order of magnitude as in the lesions of age spots and freckles (located in a UV exposed area). This becomes even more apparent when melanin particles are counted, without rating the allocation to clusters. The reduction rates in the lesions remain unchanged, while the normal skin types display a significant increase, at least in the lighter phenotypes (chapter E.I.1.5). Considering this, it might be hypothesized that the clearing mechanism in perilesional areas is upregulated as a response to UV exposure, but in locations affected with hyperpigmentation, this upregulation might be impeded, resulting in a stronger and long-lasting tan and hence a strong contrast between perilesional and lesional areas. In any case, the melanosome clearing is delayed in both types of hyperpigmentation, although in total, the reduction reaches comparable levels as in normal skin – an idea already hypothesized by Rahman and Bhawan (1996).

In addition to elevated levels of melanosomes, that are located predominantly in the SB and lSSp of the elongated, club-shaped rete ridges, age spots are described to exhibit increased numbers of melanocytes (Virador *et al.*, 2001). Freckles on the other hand are also characterized by an overproduction of melanosomes, but not by an increase in melanocyte numbers (Rahman and Bhawan, 1996). However, the present samples of age spots and freckles both display more melanocytes than normal skin (E.II.3). Measured along the basement membrane in both, lesion and periphery, the melanocyte numbers are more than 1.5-fold increased compared to normal skin of phototype I-III. Referring the melanocyte numbers to the SG, the numbers are even doubled, compared to normal skin. As no difference was determined for *lentigo senilis* and the samples rated as freckles, it must be considered whether the division of the sample collective into real age spots and freckles is acceptable, or whether the original assumption, that all samples are *lentigo senilis* is more accurate. In any case, apart from shape and depth of the rete ridges, no physiologically relevant distinction could be detected.

When comparing the melanocyte densities of the lesions and the normal skin of phototype I-III, it must be considered, that these data were collected using different types of samples. While the samples of the age spots and freckles were high-pressure frozen and subsequently cut with the Cryostat, the samples of the different phototypes were fixed by plunge-freezing before cutting. Due to this difference in fixation, the frozen sections can be assumed

to show differing affinity for antibody staining (Monaghan *et al.*, 1998; Pfeiffer *et al.*, 2000). This might lead to an overvaluation of the data for the lesions, although it is unlikely, that more the number of melanocytes is affected, but rather the individual melanocytes are displayed in more detail or stronger intensity.

The elevated melanocyte content of the lesional samples is ascribed to a malfunction of the melanocytes resulting in an overproduction of melanin (Virador *et al.*, 2001; Unver *et al.*, 2006). The increased melanocyte numbers alone might account for the elevated melanosome content in the perilesional skin, as here both melanocyte numbers and melanosome content are doubled compared to the Caucasian skin. But in the lesion, twofold numbers of melanocytes produce the threefold quantity of melanosomes.

What causes this overproduction of melanosomes could not be determined during this project, but several morphological conspicuities, apart from the alteration of shape and depth of the rete ridges, could be observed. One feature described for *lentigo senilis* by several investigators is the presence of so-called pendulous melanocytes, meaning that the melanocytes appear to be sinking into the dermis and thus hang below the basement membrane (Cario-Andre *et al.*, 2004; Noblesse *et al.*, 2006). However, this positioning of melanocytes is observed also in normal skin predominantly in dark phenotypes, i.e. phototype V and VI but is rarely observed also in light skin types (chapter E.II.2). This effect is also described by Haake and Holbrook (1999) as a general aspect of postnatal skin. It can therefore not be considered a special feature of *lentigo senilis*, but rather a common aspect of chronically UV irradiated skin (Bacharach-Buhles *et al.*, 1999).

Perturbations of the basement membrane as described by Noblesse *et al.* (2006) could not be observed, because the structural preservation of the samples and the resulting image quality of the TEM micrographs did not allow any interpretation on that score. But the also described jagged and fringy appearance of the interface of basal keratinocytes and the basement membrane, accompanied by elongated cells with bunched keratin filaments were confirmed, although not in all samples and irrespective of lesional or perilesional position (Figure 47.D). This feature is also observed in some inflammatory pathogenic conditions, such as psoriasis (Ackerman *et al.*, 1997).

Increased epidermal melanosome content is the result of enhanced melanosome transfer from the melanocytes to the surrounding keratinocytes. As PAR-2 is given a leading role in the uptake of melanosomes by keratinocytes and is expressed in high levels in highly pigmented skin (Babiarz-Magee *et al.*, 2004), it is noteworthy that this very receptor is implied in trigger-

ing and mediating inflammatory responses to tissue injury (Coughlin and Camerer, 2003). In this context it would be of interest to learn whether the sites affected with *lentigo senilis* had a history of injuries, or even more likely sunburn, as this is also associated with inflammation. Elevated levels of PAR-2 might not be the ultimate trigger of inflammatory processes, but if PAR-2 is recruited to sites of inflammation, it would certainly lead to increased melanosome transfer – a hypothesis that would additionally explain the fact, that hyperpigmentation is a common finding associated with inflammation (Nordlund *et al.*, 1998). The notion of Mackintosh (2001), that melanosomes and melanin are a part of the innate immune system, functioning as a scavenger of bacterial and fungal toxins and inhibitor of microorganism growth in the epidermis, further backs this hypothesis. *Lentigo senilis* would then result from the recruitment of antimicrobial melanosomes to the site of inflammation.

In any case, continuous UV exposure seems to induce a permanent increase in melanocyte numbers and a lasting upregulation of melanin synthesis paired with a reduced clearing efficiency. Regarding the total melanosome content, *lentigo senilis* and freckles are equal and both surpass the constitutive pigmentation of Caucasian skin by factor 3, and the surrounding perilesional skin still shows a doubled melanosome amount. And irrespective of morphological differences or variations in the melanosome clearing rates, both types of hyperpigmentation are perceived as comparable lesions.

IV The Epidermal Melanin Unit Revisited

The epidermal melanin unit is universally described to comprise of one melanocyte supplying melanosomes to 30 – 40 keratinocytes (Nordlund *et al.*, 1998; Bolognia and Orlow, 2003). And prima facie, the embodiment of this symbiotic unit described in chapter E.II.1 seems to agree perfectly, with 39 keratinocytes found in association with one melanocyte. However, this 3D-illustration covers only 11.5 µm in depth. But as the pictured melanocyte spans approx. 65 µm parallel to the basement membrane and 40 µm from the SB into the SSp, it must be assumed, that this expansion is not only lateral, i.e. in the *x-y* axis, but also in depth, i.e. in the *x-z* axis. Assuming that the melanocyte spans another 65 µm in depth (*x-z* axis) and the depicted part is situated in the centre of the cell, the reproduced section, measuring 11.5 µm in depth, represents only approx. one sixth of the entire epidermal melanin unit. This sixth part already holds 39 keratinocytes associated with the melanocyte. Extrapolating to the

assumed depth of the melanocyte, under the assumption that the melanocyte contacts a similar number of keratinocytes in this space, the epidermal melanin unit would de facto encompass more than 200 keratinocytes.

As this number is severely at variance with the literature data, and a single melanocyte, especially from a sample of *lentigo senilis*, might not be representative of normal skin, stereological analysis of representative samples of *lentigo senilis*, three each of lesional and perilesional skin, was performed (Elias and Hyde, 1980; Griffiths, 1993). Melanocytes were stained by Mel-5. Keratinocytes were counted on the basis of their nuclei, stained by Sytox Green®, i.e. corneocytes were not considered. Stereological estimates were determined for the average melanocyte and keratinocyte numbers per µm² epidermis and extrapolated to represent cell quantities per volume (µm³ epidermis). By correlating melanocyte numbers and keratinocyte quantities, the potential maximum size of an epidermal melanin unit was estimated.

This will invariably lead to an overestimation of keratinocyte numbers per melanocyte, as the keratinocytes of the upper epidermal layers can be assumed not to be in contact with melanocytes any more. Additionally, the lesional skin of *lentigo senilis* is characterized by an elongation of the rete ridges, resulting in increased total numbers of keratinocytes. As in lesional and perilesional skin no significant difference is detected in the melanocyte numbers per mm basement membrane, the maximum epidermal melanin unit estimate for the lesional skin comprises more keratinocytes per melanocyte, than that for the perilesional skin.

However, taking into account all potential sources of overassessment of the keratinocyte contingent of the epidermal melanin unit, the estimated maximum ratios of keratinocytes per melanocyte remained well below the reference value of 200 keratinocytes per one melanocyte obtained from the individual melanocyte displayed in 3D. Moreover, no considerable difference was detected between lesional and perilesional skin: both skin types displayed a maximum estimate for the size of the epidermal melanin unit of approx. 90 keratinocytes per melanocyte. Nevertheless, the average maximum estimate of keratinocyte numbers per melanocyte is 2.5-fold larger than the epidermal melanin unit described in the literature. Assuming that by counting all present nuclei of keratinocytes, the number of keratinocytes associated with a melanocyte is overestimated by 40 %, the estimated epidermal melanin unit would still surpass the size propagated by literature by factor 1.5.

This implies that the melanocyte to keratinocyte ratio of 1: 36 represents an underassessment, possibly due to two-dimensional analysis of microscopic images, while neglecting the third

dimension. Another explanation would be, that the ratio of 1: 36 itself represents an estimate, which is consistent with the notion of Fitzpatrick and Breathnach (1963), who provided one of the first descriptions of this symbiotic unit. They already stated that the size of the epidermal melanin unit is variable, depending on the anatomical site and estimates of its size often do not consider the suprabasal keratinocytes. If the ration of 1: 36 is indeed based on basal keratinocytes only, the here obtained estimate of 1: 200 would actually be realistic.

V Melanosome Transfer – Microscopic Evidence and Its Implications

As illustrated in chapter B.I.2.4, the various theories sketching possible mechanisms for melanosome transfer would result in different compartmentalisation of melanosomes within the receiving keratinocytes. In this context, special importance is attached to the membranes surrounding the melanosomes. Membrane fusion between melanocyte and keratinocyte and direct transfer of single melanosomes would lead to isolated melanosomes, maybe grouped together in the keratinocyte, but a membrane surrounding a cluster of melanosomes would not exist. Phagocytosis of dendrite tips would lead to a double membrane surrounding one or more melanosomes, one derived from the melanocyte dendrite, the other originating from the keratinocyte. A third probable theory, exocytosis of melanosomes into the intracellular space, followed by endocytosis by the keratinocytes, would result in a single membrane – derived from the keratinocyte – surrounding one or more transferred melanosomes. In this case, membrane-free melanosomes would be present in the intercellular spare during the transition.

Due to insufficient imaging resolution, light microscopic approaches – although providing the advantage of live cell imaging – supply only limited information regarding the actual mechanism of transfer. Using melanocyte – keratinocyte co-cultures, transfer of melanosomes could be observed, but as described by other researches before, it is an uncommon event in cell culture (Scott *et al.*, 2002). Moreover, it was neither possible to discern whether one single melanosome or several organelles are transferred in one event, nor how they are delivered to the keratinocytes. Based on the LM micrographs, every described mode of transfer is imaginable. The filopodia-like structures described by Scott *et al.* (2002) were observed, but whether melanosomes are released from their tip into the intracellular space or the entire filopodium tip is phagocytosed by the keratinocyte could not be established. Several approaches to stain either melanocyte and/ or keratinocyte membranes or even the melanosomes to identify pro-

cesses involved in the transfer, failed to produce conclusive results (Minwalla *et al.*, 2001a; Berens *et al.*, 2005). By fluorescently staining the plasma membranes of melanocytes prior to co-cultivation with keratinocytes, Minwalla *et al.* showed that the stain is relocated to keratinocytes, concluding that a part of the plasma membrane of the melanocyte is transferred together with the melanosomes (Minwalla *et al.*, 2001a; Boissy, 2003).

However, searching for evidence to prove one or maybe all of the above mentioned theories, namely searching for melanosomal membranes, requires electron microscopic resolution. Within the melanocyte one membrane was observed loosely surrounding single melanosomes. And after the transfer to keratinocytes is accomplished, again only one membrane is discovered, now surrounding either single melanosomes or melanosome clusters (chapter E.IV.2). Assuming that the number of membranes is constant, this condition can only be achieved by exocytosis of melanosomes, followed by phagocytosis by the keratinocyte (see Figure 9). Exocytosis would involve the fusion of the melanosomal membrane with the plasma membrane of the melanocyte to release the melanosome into the intracellular space, resulting in “naked” melanosomes, i.e. melanosomes without enveloping membrane. This was indeed observed but only rarely (chapter E.IV.3). Several other researcher have described “naked” melanin particles in the intracellular space, though it cannot be ruled out entirely, that this is the result of preparation artefacts rather than a description of the biological reality (Swift, 1964; Yamamoto and Bhawan, 1994; Quast *et al.*, 2003). Exocytosis in melanocytes is further backed by the presence of molecules with a well-known role in regulated exocytosis, like SNAREs, mediating the fusion of cellular transport vesicles with the plasma membrane, and Rab27a that helps docking the melanosomes to the plasma membrane (Van Den Bossche *et al.*, 2006). The fact, that “naked” melanosomes are rarely observed might be due to the rapidity of a potential phagocytic uptake and the unlikelihood of capturing this process.

In this context, it must be considered, if an initially existing second surrounding membrane is degraded that rapidly, that this condition is not captured by microscopic investigation either, as suggested by Figure 58.B. The right vesicle (black arrowhead) clearly demonstrates two surrounding membranes, although the dark structure contained inside can not explicitly be identified as a melanosome. In the direct vicinity of this vesicle a melanosome cluster is observed, that again shows only one surrounding membrane. Therefore the vesicle may be represent a vesicle fraction with a dense cargo that is part of a multivesicular structure. Together with the interleaving formation of the plasma membranes of melanocyte and keratinocyte (Figure 58.B; red arrowhead), this would suggest either cytophagocytosis of dendrite tips

as proposed by Okazaki *et al.* (1976) or vesicle shedding by the melanocyte (Hugel *et al.*, 2005; Van Den Bossche *et al.*, 2006). Both processes share the necessity of phagocytic uptake by the keratinocytes, an attribute already confirmed (Potter and Medenica, 1968). And given the important role of PAR-2 in regulating melanosome transfer *in vitro* and *in vivo*, the involvement of phagocytosis seem practically guaranteed (Seiberg *et al.*, 2000a; Seiberg *et al.*, 2000b; Scott *et al.*, 2001; Scott *et al.*, 2003).

Besides, all microscopic evidence stands in contrast with the only theory not involving phagocytosis, namely creating a melanosome transporting channel by membrane fusion, as described by Yamamoto and Bhawan (1994) and Scott *et al.* (2002). The major uncertainty in this context is the formation of membrane-bound melanosome clusters, if they are not formed as a result of the transfer process. Some researches vote that the clustering of melanosomes represents the final stage of melanosome turnover in keratinocytes, indicating that melanosomes might be internalized by the keratinocyte individually and are aggregated into clusters subsequently (Blois, 1968; Potter and Medenica, 1968; Wolff and Konrad, 1971; Wolff *et al.*, 1974). But the data obtained in the present study concerning the epidermal distribution of melanosomes, clearly indicates the contrary, as melanosome clusters decrease toward the upper epidermal layers in favour of isolated melanosomes (chapter E.I.1.4).

Cytophagocytosis, i.e. pinching off and ensuing internalisation of dendrite tips by keratinocytes might be a mere artefact of static two-dimensional imaging. A cross-section of a melanosome dendrite engulfed by a keratinocyte, here interpreted as a pinched off, internalized part of the melanocyte, does not necessarily have to be detached from the melanocyte but could simply be enfolded by the neighbouring cell. As Van Den Bossche *et al.* (2006) point out, this notion, as well as the concept of membrane-fusion originate from a time, when less sophisticated microscopic techniques were applied.

Vesicle shedding presents a second potential mode of transfer resulting in melanosomes engulfed by two membranes. And although proof of a double membrane surrounding one or several melanosomes is scarce, several morphological details have been observed in melanocyte dendrites that may be interpreted as budding or pinching off of vesicles (Figure 58.B, C & D; red arrowheads). It is also possible that these shapes have been interpreted to match Okazakis concept of cytophagocytosis (Okazaki *et al.*, 1976).

The electron microscopic evidence gathered during this study points in the directions of multiple co-existing transfer mechanisms, this notion being supported by several researches (Mottaz and Zelickson, 1967; Yamamoto and Bhawan, 1994; V.J. Hearing, 2005b; Van Den

Bossche *et al.*, 2006). However, definite conclusions on this dynamic process can not be achieved by static two-dimensional imaging alone, but require high-resolution time-lapse imaging to capture such events, followed by correlative electron microscopy combined with proteomics approaches to identify involved proteins.

VI The Impact of Epidermal Melanosome Distribution on the Visual Perception of Skin Colour

In UV unexposed skin, the higher melanocyte density is observed in skin phenotypes with the lesser melanosome content. Together with the circumstance that the melanocyte densities in age spots and freckles – although significantly increased – show no representative difference to perilesional skin (chapter E.II), this implies that melanocyte number and location play a subordinate role in the determination of skin colour. Rather, the relevant distinction is manifested in the total content of melanosomes and their epidermal distribution.

The more melanosomes, the darker the skin appears due to increased absorption of incident light (Nielsen *et al.*, 2006). The melanosome content of age spots and freckles (lesional) distinctly surpasses that of the surrounding skin. And although the total melanosome content of perilesional skin matches that of Asian skin and would thus be expected to appear darker than normal Caucasian skin, it is perceived as skin of white colouration. However. the two sample pools of normal Caucasian and perilesional skin are not fully comparable, as the first sample collective was obtained from a UV protected site (buttock skin) representing the constitutive skin colour, while the second, attained from the back of the hand – a chronically sun exposed site – represents a facultative pigmentation (Kochevar *et al.*, 1999).

The fact that perilesional skin is not perceived as dark as Asian skin might be due to a different distribution of the present melanosomes within the keratinocytes. The lighter the skin phenotype, the more melanosomes are aggregated into clusters, especially in the lower epidermal layers (Table 15). It is noteworthy that the percentage of clustered melanosomes in the Caucasian samples is equal to that measured in the pooled samples of *lentigo senilis* and freckles. But when the two hyperpigmentations are investigated separately, the age spots show slightly more clustered melanosomes than the normal Caucasian skin, while the percentage of aggregated melanosomes in freckles is slightly decreased in the SB (Table 17). The average percentage of clustered melanosomes in Asian skin is only slightly lower than in

Caucasian skin, but the variation between individual samples is much higher. Asian skin seems to represent an intermediate between Caucasian and Negroid pigmentation patterns (Alaluf *et al.*, 2002a; Thong *et al.*, 2003), and here again the samples of lighter phenotype (obtained from Korean or Chinese donors) exhibit much larger amounts of clustered melanosomes (> 50 %) than the samples of dark phenotypes (from India and Indonesia, < 35 %). This supports the finding that the amount of complexes comprising less dense pigment entities is less efficient in light absorption than the denser single eumelanin particles and may explain the visual perception of perilesional areas.

A major function assigned to melanin is the protection of the nuclei by scattering and absorption of the incident UV light (Kochevar *et al.*, 1999; Yamaguchi *et al.*, 2006). Corcuff *et al.* (2001) described melanosomes as “nanomirrors” reflecting UV light, thus limiting its penetration into the nuclei. Individually dispersed melanosomes can be assumed to show different reflecting and scattering characteristics than clusters of melanosomes. Assuming that singly dispersed melanosomes diffusely reflect and/ or scatter incident light, the energy of the light beam is only moderately weakened (Lipson *et al.*, 1997). In contrast, an aggregation of melanosomes has the potential of multiple reflection and scattering events, resulting in a stronger attenuation of the incidental energy, which may lead to a whitening effect by random scattering of visible light. This light (or energy) scattering effect is necessary in light skin types to enhance the efficiency of UV protection, as in total less melanosomes are present. However, in dark skin, due to a larger total amount of melanin, the melanosomes – although singly dispersed – are more tightly packed within the keratinocytes, covering the apical side of the nucleus. Most likely, this will result in comparable light scattering and reflection properties, also quenching the incident energy beams. But in addition, the absorption of eumelanin is higher, resulting in a more efficient reflection of UV light at the melanosomes (mirrors), outweighing the quenching of incident light.

The described distribution patterns represent a sophisticated compromise between UV injury to the nuclei and UV benefits like vitamin D3 synthesis (Mackintosh, 2001; Webb and Engelsen, 2006). The smaller size of the melanosomes observed in light skin types might be a response to insufficient UV light penetration to the sites of the vitamin D3 synthesis. And the size of the particles directly influences their distribution in the keratinocytes (Konrad and Wolff, 1973; Minwalla *et al.*, 2001b; Boissy, 2003), and with that again influences the light scattering properties. This adaptation to different conditions of UV irradiation would explain the large variety of intermediate pigmentation patterns in Asian skin.

However, these characteristics play a minor role in the perception of the skin colour, accounting only for nuances of colouration. As already mentioned, reflection and absorption constitute the major part of the skin colour. At a first glance, it might be considered a paradox, that darker skin yields the stronger reflection of UV light, as measured by Nielsen *et al.* (2004). But a larger content of melanosomes will invariably yield a proportional amount of reflection, while the percentage of absorbed light of different wavelength still dominates and results in a darker appearance of the skin.

In *lentigo senilis* and freckles, an additional deficiency in the melanin degrading system of the skin results in a larger quantity of melanosomes in the upper epidermal layers, which increases the contrast toward the surrounding skin. But like the intra-keratinocyte distribution patterns, the melanosome content of corneocytes is not a sole determining factor for a darker appearance. Otherwise, the colouration of perilesional skin would appear similar to that of Asian skin and the lesions would be perceived as deeply pigmented as Negroid skin, according to their melanosome content in the SC (Figure 27 and Figure 53). Local changes in skin tone as in *lentigo senilis* and freckles only require a sufficiently abrupt gradient to be perceptible – irrespective of the constitutive pigmentation.

VII The Influence of Temporary and Chronic UV Irradiation on Pigmentation

The melanocyte density determined in skin of phototypes I-VI (Figure 43) can be assumed to represent a constitutive condition of the pigmentary system, free of UV stimulation. The obtained values displaying lower melanocyte numbers in the more pigmented skin types, are in disagreement with the findings of Tadokoro *et al.* (2005), who observed equal melanocyte densities in all skin phenotypes, investigating biopsies of the dorsum. Additionally, the melanocyte numbers displayed only minor variations after UV exposure, while other researchers describe a distinct increase after UV stimulation (Gilchrest *et al.*, 1979; Stierner *et al.*, 1989). The dorsum can not be assumed to be a totally photoprotected site and thus the pigmentation status must be considered facultative rather than constitutive, even if direct UV exposure had been avoided before the investigation. Effects of single UV-irradiation even low-dose exposure have been described to produce long standing elevation of pigmentation levels (Yamashita *et al.*, 2005). Therefore it should be considered whether chronic UV expo-

sure may lastingly elevate melanocyte numbers. Gilchrest *et al.* (1979) observed a twofold increase in photoexposed skin compared to unexposed skin. This roughly matches the divergence measured in (unexposed) phototypes I-III and lesional skin of *lentigo senilis* and freckles. In this case the melanocytes would be permanently in a state of UV stimulation and would not react to UV irradiation with further increase in melanocyte numbers. However, Stierner *et al.* (1989) observed an increase in the melanocyte population in both, photoprotected and photoexposed skin, but in addition described the increase to be more pronounced in skin with an initially low melanocyte density. This could explain the lower melanocyte density determined in unexposed skin of phototypes IV-VI. A stronger reaction to UV stimulation of these skin types would then result in an assimilation of melanocyte numbers, as the reaction of lighter skin types I – III would be weaker.

Temporary UV exposure induces tanning, i.e. the darkening of the skin by redistribution of pre-existing melanosomes as well as newly stimulated production of further melanosomes (Yoon *et al.*, 2003). Newly produced melanosomes may be transferred to the surrounding keratinocytes of the SB and lSSp within days of the UV stimulus (Bolognia and Orlow, 2003), and afterwards transmigrate the epidermis within the recipient keratinocytes until their loss by desquamation. This entire process takes approx. 28 days (Bloch *et al.*, 1927; Haake and Holbrook, 1999). Tadokoro *et al.* (2005) measured the melanin content of different skin types in individual epidermal layers by Fontana-Masson staining before and 7 days after a single UV exposure. While the total epidermal melanin content increased 5 – 10 %, the percentage of melanin decreased in the lower layer (corresponding to SB), but increased in the middle layer (corresponding to SSp) of all investigated skin types. The upper layer, comprising the SC showed interesting variations: While Asian and Negroid skin showed no or negligible changes in the melanosome content, the SC of Caucasian skin displayed an increase of 8 %. This redistributed melanin can only originate from the upper SSp or SG, as newly formed melanin can not reach the SC within one week. But as the darker skin types showed no change in the SC, it could be hypothesized, that the melanin degrading system is downregulated or malfunctioning in Caucasian skin after UV exposure.

As the natural photoprotection of Caucasian skin is distinctly lower than that of Asian and Negroid skin (Wulf *et al.*, 2004), this might represent a protection mechanism, designed to increase the efficacy of natural photoprotection. Hyperpigmentations like *lentigo senilis* and freckles might then be interpreted as a deficiency in normalization to restore the balance of photoprotection and insufficient incidence of UV light. Viewed from evolution, it might even

be a permanent return to a higher natural photoprotection level due to chronic UV exposure, reaching a level similar to that found in Negroid skin. However, this is not only achieved by an increased melanin synthesis, but also by reducing the clearing efficiency to reach this "original" state of pigmentation.

As the melanocyte numbers in age spots and freckles are comparable, but the melanosome content is distinctly increased in lesional skin, it would be of interest to compare the levels of the phagocytosis mediator PAR-2 and its activator trypsin in lesional and perilesional skin and other hyperpigmentation disorders (Babiarz-Magee *et al.*, 2004). UV induced activation of PAR-2 has been speculated as mediator for urgent melanosome transfer after UV irradiation (Seiberg *et al.*, 2000a). In this case, PAR-2 could initiate a positive feedback to further enhance melanosome production (Seiberg *et al.*, 2000b; Seiberg, 2001). This could be a potential target either to cosmetically enhance the natural tanning response of the skin or impede with the melanosome transfer in order to achieve a whitening or at least a non-tanning effect – however at the cost of impaired photoprotection.

VIII Degradation of Melanin by H_2O_2 Controls the Skin Colour

The epidermal distribution of melanosomes clearly indicates a sophisticated degrading mechanism to allow sufficient penetration of UV light into the upper layers of the epidermis, while ensuring UV protection of the proliferating basal keratinocytes. A first step comprises the disintegration of melanosome clusters into individual melanosomes (chapter E.I.1.4, Thong *et al.*, 2003). In a second step, the individual melanosomes are destroyed, which has caused a great deal of speculation how this actually is achieved.

Eumelanin, that represents the major component of melanosomes, is a complex, photostable structure, that has proven resistant to acid and alkali (Chedekel, 1982; S. Ito and Jimbow, 1983; Napolitano *et al.*, 2000; Churukian, 2002). Disintegration by lysosomal enzymes, preferentially acid phosphatase, has been favoured by several researchers (Klaus, 1969b; Seiji and Kikuchi, 1969; Olson *et al.*, 1970; Nakagawa *et al.*, 1984). But although acid phosphatase is capable of degrading the protein moiety of the melanosomes, the melanin contingent remains unaffected (Otaki and Seiji, 1971; Saito and Seiji, 1976; Borovanský *et al.*, 1999).

The persistent notion of melanin dust, representing residual parts of melanosomes after or during degradation or even the degradation products of melanin (Rothman and Lorincz, 1963;

Nordlund *et al.*, 1998) could not be confirmed in this study, as no such particles were conceivable in transmission electron micrographs. Degraded melanin particles arising from *in vitro* degradation with H_2O_2 were characterized by SEM and TEM, revealing crystalline Bragg reflection, hence displaying a strong contrast and would consequently be easily detectable within skin sections as well (Glaeser, 2005). Besides, this hypothesis stems from the ill-defined staining of the SC observed after Fontana-Masson silver staining, which has been demonstrated in this project to be prone to false-positive staining and relocation of the formed silver precipitate, which might produce misleading results (chapter D.II.3).

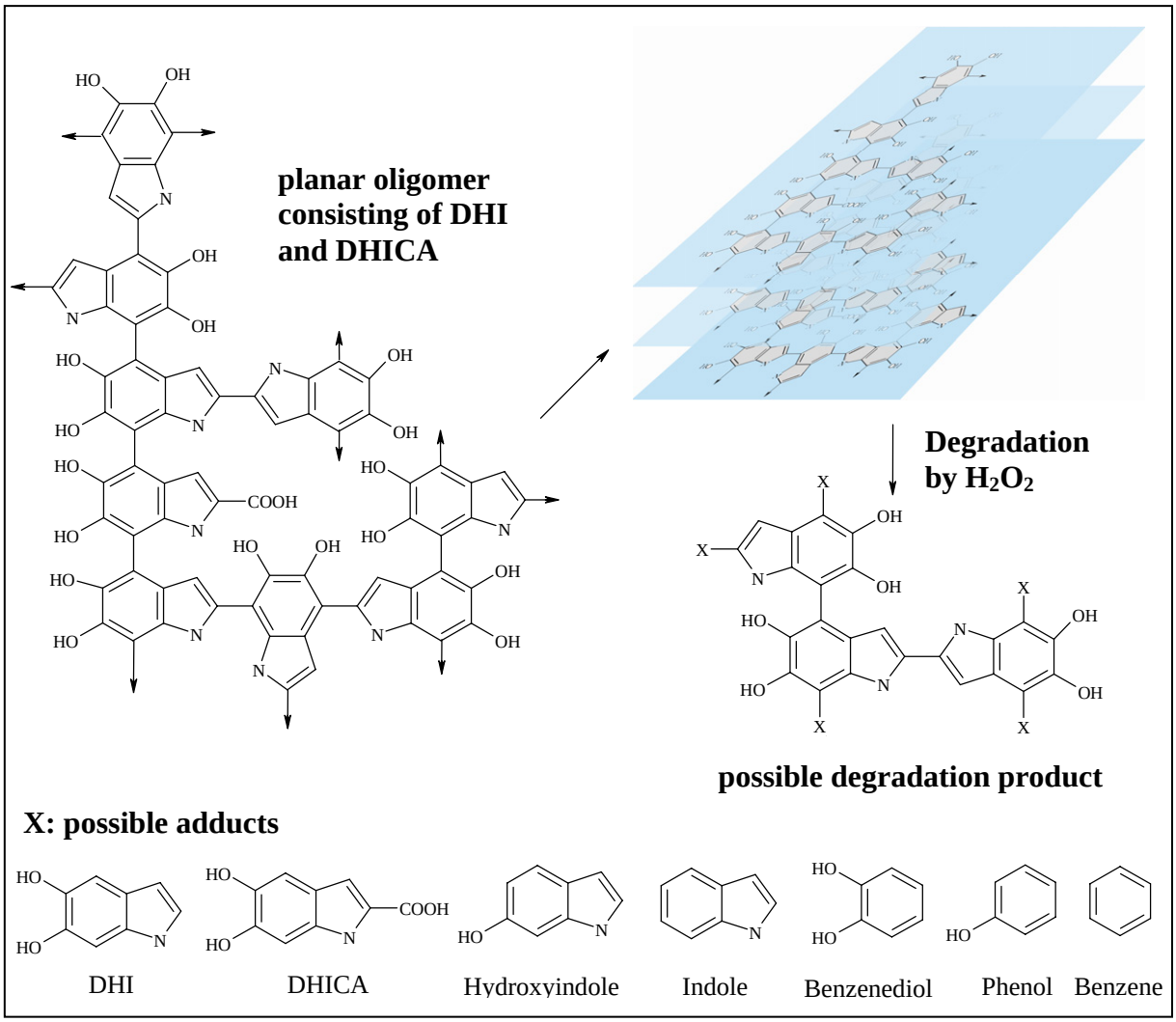

Figure 68: Potential pathway for the degradation of eumelanin by hydrogen peroxide. Eumelanin is assumed to consist of planar subunits built from DHI and DHICA, assembled by π-stacking to form flat cylinders that further assemble into filaments or planar structures. H_2O_2 could both, disintegrate these aggregates into single stacks of DHI – DHICA oligomers, and break the π-π interactions, giving rise to a number of potential degradation products, including DHI, DHICA, hydroxyindole, indole, benzenediol, phenol and benzene.

Oxidative breakdown with strong oxidizing agents such as hydrogen peroxide or permanganate represents the only possible mechanism consistent with *in vitro* degradation of melanin (Prota, 1980; S. Ito and Jimbow, 1983; Borovanský *et al.*, 1999; Elleder and Borovanský, 2001) and the structural organization proposed for eumelanin (Clancy and Simon, 2001). Eumelanin is described to be composed of three or four planar oligomers, each consisting of 4 – 5 units of DHI and/or DHICA, π-stacked to form a flattened cylinder that is further agglomerated into planer sheets or filamentous formations (Figure 5). H_2O_2 could separate the individual cylinders and further disintegrate the oligomers by breakdown of the cohesive π-π interactions, giving rise to fragments of the oligomers, including single DHI and DHICA units and other polymers involved in melanin synthesis (Figure 68). This hypothesis is consistent with the results of the ESI-MS analysis of *in vitro* H_2O_2-degraded *Sepia* melanin (Table 18). In addition to the specific degradation products used for microanalytical quantification of melanin, PTCA and PDCA (chapter B.II.3), DHI was detected in abundance. Several smaller units, possible adducts to the DHI polymer, were identified, including DHICA and some precursors of the DHI and DHICA polymers. This agrees with the notion of Clancy *et al.* (2000) that melanin dust – if indeed existent – might represent one of the self-assembling units of eumelanin.

The observation that disintegration of melanosomes is observed in phagosomes put Borovanský and Elleder (2003) on the track of the membrane-associated NADPH oxidase – a supplier of ROS and possible source for H_2O_2 *in vivo* (Grisham, 2004). The synthesis of hydrogen peroxide in or near melanosomes has already been demonstrated and pathways for its possible photoproduction have been described (Glickman *et al.*, 1993; Borovanský and Elleder, 2003; Chi *et al.*, 2006). By adapting a protocol for cytochemical demonstration of H_2O_2 in biological tissues (Ellis and Grant, 2002), the production of H_2O_2 by NADPH oxidase in the epidermis has been confirmed during this project (chapter E.V.2). This assay was originally described for less complex tissues (Briggs *et al.*, 1975a; Briggs *et al.*, 1975b) and incubation time and concentration of incubating media had to be modified to ensure appropriate penetration into the epidermis of biopsies. Based on the principles of cerium capture cytochemistry, cerium perhydroxide, a fine electron-dense precipitate, is formed in the presence of H_2O_2, thus detecting subcellular sites of H_2O_2 generation *in situ*. The precipitate was detected either by CLSM or TEM, or after amplification with DAB visualized by conventional LM. To ensure the specificity of the reaction, it was validated by omission of the substrate β-NADPH as well as specific inhibition of potentially active NADPH oxidase. Both controls showed no

detectable precipitate. Additionally, the cerium precipitate was confirmed by EFTEM in and near the melanosomes, indicating NADPH to be the source of available H_2O_2 in the epidermis and its participation in the degradation of the melanin moiety of melanosomes.

As the light microscopic imaging resolution is insufficient for the analysis of pigmentation at the single-melanosome level (chapter D.II), exact localisation of the cerium precipitate at the subcellular level is not possible either (Figure 63). However, in transmission electron micrographs, the precipitate can be detected, localised mainly in the SB and lSSp of the human epidermis either directly enveloping melanosomes or in the vicinity (Figure 64). As NADPH oxidase has been demonstrated in keratinocytes (Jones *et al.*, 1996; Turner *et al.*, 1998; Chamulitrat *et al.*, 2004), less dense but still detectable amounts of the precipitate are present in the intracellular space and near the plasma membranes of keratinocytes (Figure 64.C). No precipitate could be detected in the upper epidermal layer, which does not necessarily indicate the absence of H_2O_2 in these regions, but might as well be due to insufficient penetration of the incubating media into the epidermal tissue.

These results at least confirm NADPH oxidase as potential source of H_2O_2 in the vicinity of melanosomes and imply its involvement in the melanin degradation process. As the epidermal distribution of melanosomes is the major determining factor of skin colour, and special importance can be assigned to the presence of melanosomes in the upper epidermal layers (chapter F.VI and F.VII), the efficiency of the melanin degrading mechanism in the lower epidermal layers – especially in light skin types – is of utmost importance. Otherwise, the balance between the benefits of UV light and protection against its harmful effects is impaired. The result would either be hypo- or hyperpigmentation. Here, H_2O_2 and with it NADPH oxidase as the possible source, plays a key role. Exceptionally high levels of H_2O_2 have been detected in the epidermis of vitiligo patients (Rokos *et al.*, 2002). Although this is not the underlying cause of the depigmentation, it might at least be a supportive factor of the removal of melanin from the epidermis.

Hyperpigmentation disorders, like *lentigo senilis* have been associated with inflammation (Ackerman *et al.*, 1997; Cayce *et al.*, 2004). As the production of ROS via NADPH oxidase is part of the immune response of the skin to invading pathogens, inflammatory conditions are characterized by elevated levels of H_2O_2 (Mackintosh, 2001; Grisham, 2004). However, these higher levels of H_2O_2 would be presumed to induce hypopigmentation by enhancing the degradation of melanin, rather than hyperpigmentation. But if a hyperpigmented condition is already manifested, initiated somehow by the epidermal inflammatory response (Nordlund,

1988; Mackintosh, 2001), this could lead to an upregulation of the degradation mechanism via H_2O_2 to dispose of the excess melanin, thus at least creating a positive feedback loop and further enhancing the inflammatory process. Unfortunately, the underlying mechanisms of post-inflammatory hyperpigmentation remain yet unknown and treatment is often difficult (Nordlund and Abdel-Malek, 1988; Cayce *et al.*, 2004). If the generation of H_2O_2 could be regulated specifically in the vicinity of melanosomes without affecting the surrounding tissue, as not to induce inflammatory responses, this could be used to control pigmentation levels. Both, tanning and whitening effects could actively be achieved. However, it will be difficult to introduce any agents into the epidermis, that specifically and exclusively target melanosomes.

G SUMMARY & OUTLOOK

This project was focused on morphological aspects of the pigmentation of the human epidermis, aimed at the identification and description of determining factors accounting for the diversity of phenotypes, and to find unique morphological and biological criteria for the distinction of these phenotypes. In order to achieve this, light and electron microscopic techniques for the investigation of skin pigmentation had to be evaluated, to identify a suitable staining and/ or imaging method for the identification and description of melanocytes, as well as the characterisation and analysis of the epidermal distribution and degradation of individual melanosomes. The latter could only be achieved by transmission electron microscopy, as imaging at the single-melanosome level in the natural context and at a subcellular level, allowing to identify e.g. plasma membranes, cytoskeletal elements etc., requires a resolution that can not be accomplished by light microscopy.

The microscopic quantification of the melanosome content of different epidermal layers was benchmarked against the state-of-the-art method of chemical analysis of epidermal melanin content. The results of the microscopic investigation correlate well with that of the chemical analysis, and provide the further advantage of intra-epidermal spatial resolution, and in the context of light scattering properties, the differentiation of individually distributed or clustered melanosomes. However, distinction between the two types of melanin is more precise in the chemical analysis, which is also the faster – although more complex – method.

By dividing the epidermis into four sub-layers and counting the melanosomes present in each layer, fundamental knowledge of the constitutive epidermal distribution of melanosomes was achieved for the different phenotypes of Caucasian, Asian and Negroid skin, as well as for the facultative pigmentation of elderly Caucasians, with special respect to age spots and freckles. The samples were obtained during two studies approved by the Hamburg ethics committee (internal Beiersdorf AG study numbers: 10684 and 18655).

Two major determining factors for the perception of the complexion were determined: the colour of the human skin is predominantly determined by the present quantity of melanin and its epidermal distribution patterns. The type of melanin plays a subordinate role, as the dark

blackish-brown eumelanin constitutes the major component of human melanosomes. The light reddish pheomelanin, although detectable in all skin phenotypes, has no significant influence on the phenotype. Only skin of phototype I contains a substantial amount, accounting for one fifth of the total melanin moiety. The different phenotypes are best distinguished by their total epidermal melanosome content that displays a direct relationship to the phototype or ethnic origin, with light phenotypes containing less, and dark phenotypes more melanosomes. Age spots and freckles, as well as the surrounding skin, represent a facultative pigmentation status of elderly Caucasian skin with distinctly elevated levels of melanosomes in all epidermal layers. The melanosome content of both lesions is comparable to the constitutive pigmentation levels of Negroid skin, while the perilesional skin matches Asian skin.

However, the perilesional skin is perceived as light Caucasian rather than Asian skin, which is partially due to different distribution patterns and the size of the melanosomes within the keratinocytes. The lighter the skin type, the higher the percentage of clustered melanosomes in the basal keratinocytes. Here, age spots and freckles range in the magnitude of the constitutive Caucasian pigmentation, whereas Negroid skin exhibits predominantly isolated melanosomes. Asian skin shows only slightly elevated levels of individually dispersed melanosomes. As no change is observed in the distribution patterns of hyperpigmented Caucasian skin, temporary or chronic UV irradiation seems to have no influence on the formation of melanosome clusters.

The dispersal of melanosomes as individual or clustered particles is governed by the mode of transfer from melanocyte to keratinocyte. Based on hypotheses elaborately discussed in literature, morphological investigations of single melanosomes and melanosome clusters were aimed at describing the surrounding membranes before and after transfer, in order to prove one or more of the potential transfer mechanisms. The evidence gathered by electron microscopy in this study indicates multiple co-existing modes of transfer, most likely involving exocytosis from the melanocytes, resulting in melanosomes free of surrounding membranes in the intercellular space, that are immediately internalized by adjacent keratinocytes via phagocytic processes.

But neither intra-keratinocyte distribution nor the size of the individual or clustered melanin particles constitute a sole determining factor of the visual perception of the skin colour. Both account only for nuances of the basic colouration. Melanocyte numbers, although elevated in a facultative pigmentation status compared to constitutive pigmentation, do not influence the

perception of the complexion. The major influence is assigned to the total content of melanosomes and the directly related amount of reflection and absorption of incident light.

The largest amount of melanosomes was invariably observed in the SB, with gradually decreasing numbers toward the upper epidermal layers until the SC, where no or only few melanosomes were left. This epidermal melanosome distribution evidently indicates a sophisticated degrading mechanism in the human skin. The clearing effect was quantified for all investigated phenotypes and a potential degrading mechanism was investigated. A cytochemical assay was adapted for the application to skin samples to demonstrate the presence and exact localisation of hydrogen peroxide produced via NADPH oxidase in the epidermis. It was localized in or near melanosomes of the SB and lower SSp, but also on the plasma membranes of keratinocytes. The involvement of H_2O_2 in melanin degradation was demonstrated *in vitro* and *ex vivo* by ESI-MS and GPC analysis of the degradation products of *Sepia* melanin and detection of these degradation products in biopsies of human epidermis.

The importance of this degradation mechanism especially in the lower layers of the epidermis is emphasized by hyperpigmentation disorders like *lentigo senilis* and freckles. Here, distinctly elevated levels of melanosomes are observed in the SB and are maintained throughout the epidermis until the SC, while displaying degradation rates comparable to that of photoprotected Caucasian skin.

The quantitative analysis of melanosomes in the epidermis is quite time-consuming. However, many sub-processes, such as image acquisition and processing, as well as the image analysis have been automated or simplified during this study. Further improvement of the automated detection of melanosomes can be achieved by increasing the data pool for the training data sets for the automated segmentation software.

Further investigations are also needed to ultimately prove the mode of melanosomes transfer to keratinocytes. Nevertheless, potential targets to cosmetically influence epidermal pigmentation levels have been identified. Specific blocking of the melanosome capture in the dendrites of the melanocyte by myosin Va and melanophilin, a vital step for transfer, or inhibition of the phagocytosis mediator PAR-2, thus preventing melanosome uptake into the keratinocytes would lead to skin whitening, since the melanosomes would remain in the intercellular space and would most likely remain in the lower strati of the epidermis. On the other hand, enhancement of these processes could achieve a near-natural tanning effect. Therefore, stable melanocyte-keratinocyte co-cultures are required to establish a screening system for potential transfer inhibitors or stimulating agents. To gain further understating of the development of

lentigo senilis, it would be of interest to investigate the levels of PAR-2 in the affected skin, as increased phagocytosis would invariably result in higher amounts of melanosomes in the keratinocytes. Additionally, the connection between PAR-2, melanosome uptake and inflammation might be of interest.

For the identification of cosmetic agents targeting the production of H_2O_2 via NADPH oxidase, the cytochemical assay for the detection of NADPH oxidase activity would need to be standardized, thus providing a tool to investigate the enhancement or inhibition of melanin degradation *in situ*.

Within the scope of this project is could be demonstrated, that the skin tone is predominantly determined by the epidermal content of melanosomes and is directly related to the amount of eumelanin, while pheomelanin plays a subordinate role and effectively contributes to the skin colour only in phototype I. The perception of skin colour largely depends on the presence of melanosomes in the upper layers of the epidermis. The larger the constitutional amount of melanosomes in the SB, the more melanosomes are able to survive the degradation process and thus reach the upper epidermal layers. Accumulation of melanosomes in the SC as in Negroid skin invariably results in a darker appearance of the skin, since the incident light is already absorbed and/or diffusely scattered in the SC. In contrast, Caucasian skin with less melanosomes provides less possibilities for interactions of UV light with melanin, resulting in less absorption and scattering events – hence the lighter appearance of the skin colour.

H REFERENCES

Ackerman, A.B., Chongchitnant, N., Sanchez, J., Guo, Y., Bennin, B., Reichel, M. and Randall, M.B. (1997) *Histologic Diagnosis of Inflammatory Skin Disease*. 2nd ed., edited by G. Stamathis, Williams & Wilkins, Baltimore, USA.

Alaluf, S., Atkins, D., Barrett, K., Blount, M., Carter, N. and Heath, A. (2002a) *Ethnic Variation in Melanin Content and Composition in Photoexposed and Photoprotected Human Skin*. Pigment Cell Research 15(2): 112-18.

Alaluf, S., Atkins, D., Barrett, K., Blount, M., Carter, N. and Heath, A. (2002b) *The Impact of Epidermal Melanin on Objective Measurements of Human Skin Colour*. Pigment Cell Research 15(2): 119-26.

Alaluf, S., Heath, A., Carter, N., Atkins, D., Mahalingam, H., Barrett, K., Kolb, R. and Smit, N.P.M. (2001) *Variation of Melanin Content and Composition in Type V and VI Photoexposed and Photoprotected Human Skin: the Dominant Role of DHI*. Pigment Cell Research 14(5): 337-47.

Aroca, P., Urabe, K., Kobayashi, T., Tsukamoto, K. and Hearing, V.J. (1993) *Melanin Biosynthesis Patterns Following Hormonal Stimulation*. Journal of Biological Chemistry 268(34): 25650-55.

Astner, S. and Anderson, R.R. (2004) *Skin Phototypes 2003*. Journal of Investigative Dermatology 122(2): xxx-xxxi.

Babiarz-Magee, L., Chen, N., Seiberg, M. and Lin, C.L. (2004) *The Expression and Activation of Protease-Activated Receptor-2 Correlate with Skin Color*. Pigment Cell Research 17(3): 241-51.

Bacharach-Buhles, M., Lubowietzki, M. and Altmeyer, P. (1999) *Dose-Dependent Shift of Apoptotic and Unaltered Melanocytes into the Dermis after Irradiation with UVA 1*. Dermatology 198(1): 5-10.

Barbosa, A.J., Castro, L.P., Margarida, A. and Nogueira, M.F. (1984) *A Simple and Economical Modification of the Masson-Fontana Method for Staining Melanin Granules and Enterochromaffin Cells*. Stain Technology 59(4): 193-6.

Berens, W., Van Den Bossche, K., Yoon, T.-J., Westbroek, W., Valencia, J.C., Out, C.J., Marie Naeyaert, J., Hearing, V.J. and Lambert, J. (2005) *Different Approaches for Assaying Melanosome Transfer*. Pigment Cell Research 18(5): 370-81.

Berson, J.F., Harper, D.C., Tenza, D., Raposo, G. and Marks, M.S. (2001) *Pmel17 Initiates Premelanosome Morphogenesis Within Multivesicular Bodies*. Molecular Biology of the Cell 12(11): 3451-64.

Bhawan, J. (1997) *Mel-5: A Novel Antibody for Differential Diagnosis of Epidermal Pigmented Lesions of the Skin in Paraffin-Embedded Sections*. Melanoma Research 7(1): 43-8.

Biel, S.S., Kawaschinski, K., Wittern, K.-P., Hintze, U. and Wepf, R. (2003) *From Tissue to Cellular Ultrastructure: Closing the Gap Between Micro- and Nanostructural Imaging*. Journal of Microscopy 212(Pt 1): 91-99.

Bloch, B., Pinkus, F. and Spalteholz, W. (1927) *Handbuch der Haut- und Geschlechtskrankheiten - Mikroskopische Technik, Physiologie der Haut, Chemie der Haut*, 2, Julius Springer, Berlin.

Blois, M.S. (1968) *Phagocytosis of Melanin Particles by Human Epidermal Cells In Vitro*. Journal of Investigative Dermatology 50(4): 336-37.

Boissy, R.E. (2003) *Melanosome Transfer to and Translocation in the Keratinocyte*. Experimental Dermatology 12(Suppl 2): 5-12.

Bokoch, G.M. and Knaus, U.G. (2003) *NADPH Oxidases: Not Just for Leukocytes Anymore!* Trends in Biochemical Sciences 28(9): 502-8.

Bolognia, J.L. and Orlow, S.J. (2003) *Melanocyte Biology*. In: J.L. Bolognia, J.L. Jorizzo, *et al.* (Eds), Dermatology, 1st ed., pp. 43-54. Vol. 1. C.V. Mosby.

Borovanský, J. and Elleder, M. (2003) *Melanosome Degradation: Fact or Fiction*. Pigment Cell Research 16(3): 280-86.

Borovanský, J., Hach, P., Smetana, K., Jr., Elleder, M. and Matous-Malbohan, I. (1999) *Attempts to Induce Melanosome Degradation In Vivo*. Folia Biologica (Praha) 45(2): 47-52.

Briganti, S., Camera, E. and Picardo, M. (2003) *Chemical and Instrumental Approaches to Treat Hyperpigmentation*. Pigment Cell Research 16(2): 101-10.

Briggs, R.T., Drath, D.B., Karnovsky, M.L. and Karnovsky, M.J. (1975a) *Localization of NADH Oxidase on the Surface of Human Polymorphonuclear Leukocytes by a New Cytochemical Method*. Journal of Cell Biology 67(3): 566-86.

Briggs, R.T., Karnovsky, M.L. and Karnovsky, M.J. (1975b) *Cytochemical Demonstration of Hydrogen Peroxide in Polymorphonuclear Leukocyte Phagosomes*. Journal of Cell Biology 64(1): 254-60.

Burck, H.-C. (1988) *Histologische Technik*. 6th ed., G. Thieme Verlag, Stuttgart.

Byers, H.R., Maheshwary, S., Amodeo, D.M. and Dykstra, S.G. (2003) *Role of Cytoplasmic Dynein in Perinuclear Aggregation of Phagocytosed Melanosomes and Supranuclear Melanin Cap Formation in Human Keratinocytes*. Journal of Investigative Dermatology 121(4): 813-20.

Cario-Andre, M., Lepreux, S., Pain, C., Nizard, C., Noblesse, E. and Taieb, A. (2004) *Perilesional vs. Lesional Skin Changes in Senile Lentigo*. Journal of Cutaneous Pathology 31(6): 441-7.

Cayce, K.A., McMichael, A.J. and Feldman, S.R. (2004) *Hyperpigmentation: An Overview of the Common Afflictions*. Dermatology Nursing / Dermatology Nurses' Association 16(5): 401-6, 413-6; quiz 417.

Chamulitrat, W., Stremmel, W., Kawahara, T., Rokutan, K., Fujii, H., Wingler, K., Schmidt, H.H. and Schmidt, R. (2004) *A Constitutive NADPH Oxidase-like System Containing gp91^{phox} Homologs in Human Keratinocytes*. Journal of Investigative Dermatology 122(4): 1000-9.

Charles, A. and Ingram, J.T. (1959) *Electron Microscope Observations of the Melanocyte of the Human Epidermis*. Journal of Biophysical and Biochemical Cytology 6(1): 41-4.

Charles, C.A., Marghoob, A.A., Busam, K.J., Clark-Loeser, L. and Halpern, A.C. (2002) *Melanoma or Pigmented Basal Cell Carcinoma: A Clinical-Pathologic Correlation with Dermoscopy, In Vivo Confocal Scanning Laser Microscopy, and Routine Histology*. Skin Research and Technology 8(4): 828-7.

Chedekel, M.R. (1982) *Photochemistry and photobiology of epidermal melanins*. Photochemistry and Photobiology 35(6): 881-85.

Cheng, J., Moss, S.C. and Eisner, M. (1994a) *X-Ray Characterization of Melanins - II*. Pigment Cell Research 7(4): 263-73.

Cheng, J., Moss, S.C., Eisner, M. and Zschack, P. (1994b) *X-Ray Characterization of Melanins - I*. Pigment Cell Research 7(4): 255-62.

Cheun, W.L. (2004) *The Chemical Structure of Melanin*. Pigment Cell Research 17(4): 422-24.

Chi, A., Valencia, J.C., Hu, Z.Z., Watabe, H., Yamaguchi, H., Mangini, N.J., Huang, H., Canfield, V.A., Cheng, K.C., Yang, F., *et al.* (2006) *Proteomic and Bioinformatic Characterization of the Biogenesis and Function of Melanosomes*. Journal of Proteome Research 5(11): 3135-44.

Choi, Y.-G., Bae, E.-J., Kim, D.-S., Park, S.-H., Kwon, S.-B., Na, J.-I. and Park, K.-C. (2006) *Differential Regulation of Melanosomal Proteins after Hinokitiol Treatment*. Journal of Dermatological Science In Press: n/a.

Churukian, C.J. (2002) *Pigments and Minerals*. In: J.D. Bancroft and M. Gamble (Eds), Theory and Practice of Histological Techniques, 5th ed., pp. 243-67. Churchill Livingstone Harcourt Publishers Limited, London.

Clancy, C.M., Nofsinger, J.B., Hanks, R.K. and Simon, J.D. (2000) *A Hierarchical Self-Assembly of Eumelanin.* Journal of Physical Chemistry. B, Condensed Matter, Materials, Surfaces, Interfaces & Biophysical 104: 7871-73.

Clancy, C.M. and Simon, J.D. (2001) *Ultrastructural Organization of Eumelanin from Sepia Officinalis Measured by Atomic Force Microscopy*. Biochemistry 40(44): 13353-60.

Clark, W.H., Jr. and Hibbs, R.G. (1958) *Electron Microscope Studies of the Human Epidermis: The Clear Cell of Masson (Dendritic Cell or Melanocyte).* Journal of Biophysical and Biochemical Cytology 4(6): 679-84.

Corcuff, P., Chaussepied, C., Madry, G. and Hadjur, C. (2001) *Skin Optics Revisited By In Vivo Confocal Microscopy: Melanin and Sun Exposure*. Journal of Cosmetic Science 52(2): 91-102.

Coughlin, S.R. and Camerer, E. (2003) *PARticipation in Inflammation*. Journal of Clinical Investigation 111(1): 25-27.

Dean, N.R., Brennan, J., Haynes, J., Goddard, C. and Cooter, R.D. (2002) *Immunohistochemical Labeling of Normal Melanocytes*. Applied Immunohistochemistry & Molecular Morphology 10(3): 199-204.

Dion, A.S. and Pomenti, A.A. (1983) *Ammoniacal Silver Staining of Proteins: Mechanism of Glutaraldehyde Enhancement*. Analytical Biochemistry 129(2): 490-6.

Donato, R. (2003) *Intracellular and Extracellular Roles of S100 Proteins*. Microscopy Research and Technique 60(6): 540-51.

Duval, C., Régnier, M. and Schmidt, R. (2001) *Distinct melanogenic response of human melanocytes in mono-culture, in co-culture with keratinocytes and in reconstructed epidermis, to UV exposure*. Pigment Cell Research 14(5): 348-55.

Duval, C., Smit, N.P.M., Kolb, A.M., Régnier, M., Pavel, S. and Schmidt, R. (2002) *Keratinocytes Control the Pheo/Eumelanin Ratio in Cultured Normal Human Melanocytes*. Pigment Cell Research 15(6): 440-46.

Echlin, P. (1992) *Low-Temperature Microscopy and Analysis*. 1st ed., Plenum Press, New York, USA.

Elias, H. and Hyde, D.M. (1980) *An Elementary Introduction to Stereology (Quantitative Microscopy).* American Journal of Anatomy 159(4): 412-46.

Elleder, M. and Borovanský, J. (2001) *Autofluorescence of Melanins Induced by Ultraviolet Radiation and Near Ultraviolet Light. A Histochemical and Biochemical Study*. Histochemical Journal 33(5): 273-81.

Ellis, E.A. and Grant, M.B. (2002) *Cytochemical Localization of H_2O_2 in Biological Tissues*. In: D. Armstrong (Ed), Oxidants and Antioxidants: Ultrastructure and Molecular Biology Protocols, pp. 3-12. Vol. 196. Humana Press, Totowa, NJ.

Ellis, E.A., Grant, M.B., Murray, F.T., Wachowski, M.B., Guberski, D.L., Kubilis, P.S. and Lutty, G.A. (1998) *Increased NADH-Oxidase Activity in the Retina of the BBZ/WOR Diabetic Rat*. Free Radical Biology & Medicine 24(1): 111-20.

Feigl, F. (1958) *Spot Tests in Inorganic Analysis*, Elsevier Publishing Co., Inc., New York.

Fitzpatrick, T.B. and Breathnach, A.S. (1963) *Das epidermale Melanin-Einheit-System*. Dermatologische Wochenschrift 147: 481-89.

Fitzpatrick, T.B., Freedberg, I.M., Eisen, A.Z., Wolff, K., Austen, K.F., Goldsmith, L.A. and Katz, S.I., eds. (1999) *Fitzpatrick's Dermatology in General Medicine*. 5th ed. Vol. 1. Edited by T.B. Fitzpatrick, I.M. Freedberg, *et al.* McGraw-Hill, New York.

Flanagan, R.J., Morgan, P.E., Spencer, E.P. and Whelpton, R. (2006) *Micro-extraction Techniques in Analytical Toxicology: Short Review*. Biomedical Chromatography: BMC 20(6-7): 530-38.

Flegler, S.L., Heckman, J.W. and Klomparens, K.L. (1995) *Elektronenmikroskopie: Grundlagen - Methoden - Anwendungen*, Spektrum Akademischer Verlag, Heidelberg.

Fontana, A. (1912) *Verfahren zur intensieven und raschen Färbung des Treponema pallidum und anderer Spirochaten*. Dermatologische Wochenschrift 55: 1003.

Gallyas, F. (1979) *Kinetics of Formation of Metallic Silver and Binding of Silver Ions by Tissue Components*. Histochemistry 64(1): 87-96.

Giddings, T.H. (2003) *Freeze-Substitution Protocols for Improved Visualization of Membranes in High-Pressure Frozen Samples*. Journal of Microscopy 212(Pt 1): 53-61.

Gilchrest, B.A., Blog, F.B. and Szabo, G. (1979) *Effects of aging and chronic sun exposure on melanocytes in human skin*. Journal of Investigative Dermatology 73(2): 141-43.

Glaeser, K. (2005) *Strukturbeschreibung des Biopolymeres Melanin und dessen Abbau in situ und in vitro*. Diplomarbeit, Universität Hamburg.

Glickman, R.D., Sowell, R. and Lam, K.W. (1993) *Kinetic Properties of Light-dependent Ascorbic Acid Oxidation by Melanin*. Free Radical Biology & Medicine 15(4): 453-57.

Gossrau, R., van Noorden, C.J. and Frederiks, W.M. (1989) *Enhanced Light Microscopic Visualization of Oxidase Activity With the Cerium Capture Method*. Histochemistry 92(4): 349-53.

Greatens, A., Hakozaki, T., Koshoffer, A., Epstein, H., Schwemberger, S., Babcock, G., Bissett, D., Takiwaki, H., Arase, S., Wickett, R.R., *et al.* (2005) *Effective Inhibition of Melanosome Transfer to Keratinocytes by Lectins and Niacinamide is Reversible*. Experimental Dermatology 14(7): 498-508.

Griffiths, G. (1993) *Fine Structure Immunocytochemistry*. 1st ed., Springer-Verlag, Heidelberg.

Grisham, M.B. (2004) *Reactive Oxygen Species in Immune Responses*. Free Radical Biology & Medicine 36(12): 1479-80.

Haake, A.R. and Holbrook, K. (1999) *The Structure and Development of Skin*. In: T.B. Fitzpatrick, I.M. Freedberg, *et al.* (Eds), Fitzpatrick's Dermatology in General Medicine, 5th ed., pp. 70-114. Vol. 1. McGraw-Hill, New York.

Hakozaki, T., Minwalla, L., Zhuang, J., Chhoa, M., Matsubara, A., Miyamoto, K., Greatens, A., Hillebrand, G.G., Bissett, D.L. and Boissy, R.E. (2002) *The Effect of Niacinamide on Reducing Cutaneous Pigmentation and Suppression of Melanosome Transfer*. British Journal of Dermatology 147(1): 20-31.

Hall, A.M., Krishnamoorthy, L. and Orlow, S.J. (2004) *25-Hydroxycholesterol Acts in the Golgi Compartment to Induce Degradation of Tyrosinase*. Pigment Cell Research 17(4): 369-406.

Hara, M., Yaar, M., Byers, H.R., Goukassian, D., Fine, R.E., Gonsalves, J. and Gilchrest, B.A. (2000) *Kinesin Participates in Melanosomal Movement Along Melanocyte Dendrites*. Journal of Investigative Dermatology 114(3): 438-43.

Hayat, M.A. (2002) *Microscopy, Immunohistochemistry, and Antigen Retrieval Methods for Light and Electron Microscopy*. 1st ed., Kluwer Academic / Plenum Publishers, New York.

Hearing, V.J. (2005a) *Biogenesis of Pigment Granules: A Sensitive Way to Regulate Melanocyte Function*. Journal of Dermatological Science 37(1): 3-14.

Hearing, V.J. (2005b) *Personal Communication*.

Hohenberg, H., Mannweiler, K. and Muller, M. (1994) *High-Pressure Freezing of Cell Suspensions in Cellulose Capillary Tubes*. Journal of Microscopy 175(Pt 1): 34-43.

Hori, Y., Toda, K., Pathak, M.A., Clark, W.H., Jr. and Fitzpatrick, T.B. (1968) *A Fine-Structure Study of the Human Melanosome Complex and Its Acid Phosphatase Activity*. Journal of Ultrastructure Research 25(1): 109-20.

Hugel, B., Martinez, M.C., Kunzelmann, C. and Freyssinet, J.M. (2005) *Membrane Microparticles: Two Sides of the Coin*. Physiology (Bethesda) 20: 22-27.

Humbel, B.M. and Müller, M. (1984) *Freeze Substitution and Low-Temperature Embedding*. Eurem - Budapest 3(3): 1789-97.

Humbel, B.M., Sibon, O.C., Stierhof, Y.D. and Schwarz, H. (1995) *Ultra-small Gold Particles and Silver Enhancement as a Detection System in Immunolabeling and In Situ Hybridization Experiments*. Journal of Histochemistry and Cytochemistry 43(7): 735-37.

Ito, S. and Fujita, K. (1985) *Microanalysis of Eumelanin and Pheomelanin in Hair and Melanomas by Chemical Degradation and Liquid Chromatography*. Analytical Biochemistry 144(2): 527-36.

Ito, S. and Jimbow, K. (1983) *Quantitative Analysis of Eumelanin and Pheomelanin in Hair and Melanosomes*. Journal of Investigative Dermatology 80(4): 268-72.

Ito, S. and Wakamatsu, K. (2003) *Quantitative Analysis of Eumelanin and Pheomelanin in Humans, Mice and Other Animals: a Comparative Review*. Pigment Cell Research 16(5): 523-31.

Ito, Y., Kanamaru, A. and Tada, A. (2006) *Effects of Methylophiopogonanone B on Melanosome Transfer and Dendrite Retraction*. Journal of Dermatological Science 42(1): 68-70.

Jimbow, K., Fitzpatrick, T.B. and Quevedo, W.C., Jr. (1986) *Formation, Chemical Composition and Function of Melanin Pigments*. In: J. Bereiter-Hahn, A.G. Matoltsy, *et al.* (Eds), Biology of the Integument, 2nd ed., pp. 278-92. Vol. II Vertebrates. Springer-Verlag, Berlin.

Jimbow, K., Ishida, O., Ito, S., Hori, Y., Witkop, C.J. and King, R.A. (1983) *Combined Chemical and Electron Microscopic Studies of Pheomelanosomes in Human Red Hair*. Journal of Investigative Dermatology 81(6): 506-11.

Jimbow, K., Quevedo, W.C., Jr., Prota, G. and Fitzpatrick, T.B. (1999) *Biology of Melanocytes*. In: T.B. Fitzpatrick, I.M. Freedberg, *et al.* (Eds), Fitzpatrick's Dermatology in General Medicine, 5th international ed., pp. 192-219. Vol. 1. McGraw-Hill, New York.

Jones, S.A., O'Donnell, V.B., Wood, J.D., Broughton, J.P., Hughes, E.J. and Jones, O.T. (1996) *Expression of Phagocyte NADPH Oxidase Components in Human Endothelial Cells*. American Journal of Physiology 271(4 Pt 2): H1626-34.

Karnovsky, M.J. (1994) *Robert Feulgen Lecture 1994. Cytochemistry and Reactive Oxygen Species: A Retrospective*. Histochemistry 102(1): 15-27.

Kauser, S., Schallreuter, K.U., Thody, A.J., Gummer, C. and Tobin, D.J. (2003) *Regulation of Human Epidermal Melanocyte Biology by Beta-Endorphin*. Journal of Investigative Dermatology 120(6): 1073-80.

Kitamura, R., Tsukamoto, K., Harada, K., Shimizu, A., Shimada, S., Kobayashi, T. and Imokawa, G. (2004) *Mechanisms Underlying the Dysfunction of Melanocytes in Vitiligo Epidermis: Role of SCF/KIT Protein Interactions and the Downstream Effector, MITF-M*. Journal of Pathology 202(4): 463-75.

Klaus, S.N. (1969a) *Pigment Transfer in Mammalian Epidermis*. Archives of Dermatology 100(6): 756-62.

Klaus, S.N. (1969b) *Post-Transfer Digestion of Melanosome Complexes and Saltatory Movement of Melanin Granules within Mammalian Epidermal Cells*. Journal of Investigative Dermatology 53(6): 440-44.

Kochevar, I.E., Pathak, M.A. and Parrish, J.A. (1999) *Photophysics, Photochemistry, and Photobiology*. In: T.B. Fitzpatrick, I.M. Freedberg, *et al.* (Eds), Fitzpatrick's Dermatology in General Medicine, 5th international ed., pp. 220-29. Vol. 1. McGraw-Hill, New York.

Konig, K. (2000) *Multiphoton Microscopy In Life Sciences*. Journal of Microscopy 200(Pt 2): 83-104.

Konrad, K. and Wolff, K. (1973) *Hyperpigmentation, Melanosome Size, and Distribution Patterns of Melanosomes*. Archives for Dermatological Research 107(6): 853-60.

Korytowski, W. and Sarna, T. (1990) *Bleaching of Melanin Pigments. Role of Copper Ions and Hydrogen Peroxide in Autooxidation and Photooxidation of Synthetic Dopa-Melanin*. Journal of Biological Chemistry 265(21): 12410-16.

Kushimoto, T., Basrur, V., Valencia, J., Matsunaga, J., Vieira, W.D., Ferrans, V.J., Muller, J., Appella, E. and Hearing, V.J. (2001) *A Model for Melanosome Biogenesis Based on the Purification and Analysis of Early Melanosomes*. Proceedings of the National Academy of Sciences of the United States of America 98(19): 10698-703.

Leonhardt, H. (1987) *Hautdecke und Hautsinnesorgane*, Anatomie des Menschen, pp. 498-519. Georg Thieme Verlag, Stuttgart, New York.

Lillie, R.D. (1957) *Metal Reduction Reactions of the Melanins: Histochemical Studies.* Journal of Histochemistry and Cytochemistry 5(4): 325-33.

Lillie, R.D., Henson, J.P. and Burtner, H.C. (1957) *Metal Reduction Reactions of the Melanins: Silver and Ferric Ferricyanide Reduction by Various Reagents In Vitro.* Journal of Histochemistry and Cytochemistry 5(4): 311-24.

Lipson, S.G., Lipson, H.S. and Tannhauser, D.S. (1997) *Optik.* 1 ed., Springer, Berlin.

Liu, Y. and Simon, J.D. (2003) *Isolation and Biophysical Studies of Natural Eumelanins: Applications of Imaging Technologies and Ultrafast Spectroscopy*. Pigment Cell Research 16(6): 606-18.

Lu, H., Edwards, C., Gaskell, S., Pearse, A. and Marks, R. (1996) *Melanin Content and Distribution in the Surface Corneocyte with Skin Phototypes*. British Journal of Dermatology 135(2): 263-67.

Mackintosh, J.A. (2001) *The Antimicrobial Properties of Melanocytes, Melanosomes and Melanin and the Evolution of Black Skin*. Journal of Theoretical Biology 211(2): 101-13.

Masson, P. (1914) *La glande endocrine de l'intestine chez l'homme*. Comptes Rendus Hebdomadaires des Séances de l'Académie des Sciences 158: 59.

Masters, B.R., So, P.T. and Gratton, E. (1997) *Multiphoton Excitation Fluorescence Microscopy and Spectroscopy of In Vivo Human Skin*. Biophysical Journal 72(6): 2405-12.

Matissek, R. (1984) *Hautbräunung und Lichtschutz-Grundlagen, Wirkstoffe und analytische Aspekte. 1. Teil: Hautbräunung und Hautbräunungsstoffe*. Zeitschrift für Lebensmittel-Untersuchung und -Forschung 179(4): 279-87.

Matoltsy, A.G. (1986a) *Dermis*. In: J. Bereiter-Hahn, A.G. Matoltsy, *et al*. (Eds), Biology of the Integument, pp. 272-77. Vol. II Vertebrates. Springer-Verlag, Berlin.

Matoltsy, A.G. (1986b) *Structure and Function of the Mammalian Epidermis*. In: J. Bereiter-Hahn, A.G. Matoltsy, *et al.* (Eds), Biology of the Integument, 2nd ed., pp. 255-71. Vol. II Vertebrates. Springer-Verlag, Berlin.

Minwalla, L., Zhao, Y., Cornelius, J., Babcock, G.F., Wickett, R.R., Le Poole, I.C. and Boissy, R.E. (2001a) *Inhibition of Melanosome Transfer from Melanocytes to Keratinocytes by Lectins and Neoglycoproteins in an In Vitro Model System*. Pigment Cell Research 14(3): 185-94.

Minwalla, L., Zhao, Y., Le Poole, I.C., Wickett, R.R. and Boissy, R.E. (2001b) *Keratinocytes Play a Role in Regulating Distribution Patterns of Recipient Melanosomes In Vitro*. Journal of Investigative Dermatology 117(2): 341-47.

Monaghan, P., Perusinghe, N. and Muller, M. (1998) *High-Pressure Freezing for Immunocytochemistry*. Journal of Microscopy 192(3): 248-258.

Montagna, W., Kligman, A.M. and Charlisle, K.S. (1992) *Atlas of Normal Human Skin*, Springer Verlag, New York.

Mottaz, J.H. and Zelickson, A.S. (1967) *Melanin Transfer: A Possible Phagocytic Process*. Journal of Investigative Dermatology 49(6): 605-10.

Murk, J.L.A.N., Posthuma, G., Koster, A.J., Geuze, H.J., Verkleij, A.J., Kleijmeer, M.J. and Humbel, B.M. (2003) *Influence of Aldehyde Fixation on the Morphology of Endosomes and Lysosomes: Quantitative Analysis and Electron Tomography*. Journal of Microscopy 212(Pt 1): 81-90.

Nakagawa, H., Rhodes, A.R., Fitzpatrick, T.B. and Hori, Y. (1984) *Acid Phosphatase in Melanosome Formation: A Cytochemical Study in Normal Human Melanocytes*. Journal of Investigative Dermatology 83(2): 140-44.

Napolitano, A., Perzzella, A., Vincensi, M.R. and Prota, G. (1995) *Oxidative Degradation of Melanins to Pyrrole Acids: A Model Study*. Tetrahedron 51: 5913-20.

Napolitano, A., Vincensi, M.R., Di Donato, P., Monfrecola, G. and Prota, G. (2000) *Microanalysis of Melanins in Mammalian Hair by Alkaline Hydrogen Peroxide Degradation: Identification of a New Structural Marker of Pheomelanins*. Journal of Investigative Dermatology 114(6): 1141-47.

Nielsen, K.P., Lu, Z., Juzenas, P., Stamnes, J.J., Stamnes, K. and Moan, J. (2004) *Reflectance Spectra of Pigmented and Nonpigmented Skin in the UV Spectral Region.* Photochemistry and Photobiology 80(3): 450-55.

Nielsen, K.P., Zhao, L., Stamnes, J.J., Stamnes, K. and Moan, J. (2006) *The Importance of the Depth Distribution of Melanin in Skin for DNA Protection and Other Photobiological Processes*. Journal of Photochemistry and Photobiology. B, Biology 82(3): 194-98.

Noblesse, E., Nizard, C., Cario-Andre, M., Lepreux, S., Pain, C., Schnebert, S., Taieb, A. and Kurfurst, R. (2006) *Skin Ultrastructure in Senile Lentigo*. Skin Pharmacology and Physiology 19(2): 95-100.

Nordlund, J.J. (1988) *Postinflammatory Hyperpigmentation*. Dermatologic Clinics 6(2): 185-92.

Nordlund, J.J. and Abdel-Malek, Z.A. (1988) *Mechanisms for Post-Inflammatory Hyperpigmentation and Hypopigmentation*. Progress in Clinical and Biological Research 256: 219-36.

Nordlund, J.J., Boissy, R.E., Hearing, V.J., King, R.A. and Ortonne, J.-P. (1998) *The Pigmentary System: Physiology and Pathophysiology*, Oxford University Press, New York.

Odland, G.F. (1991) *Structure of the Skin*. In: L.A. Goldsmith (Ed), Physiology, Biochemistry and Molecular Biology of the Skin, pp. 3-62. Vol. I. Oxford University Press, Oxford.

Okazaki, K., Uzuka, M., Morikawa, F., Toda, K. and Seiji, M. (1976) *Transfer Mechanism of Melanosomes in Epidermal Cell Culture*. Journal of Investigative Dermatology 67(4): 541-47.

Olson, R.L., Nordquist, J. and Everett, M.A. (1970) *The role of epidermal lysosomes in melanin physiology*. British Journal of Dermatology 83(1): 189-99.

Otaki, N. and Seiji, M. (1971) *Degradation of Melanosomes by Lysosomes*. Journal of Investigative Dermatology 57(1): 1-5.

Pawley, J.P. (1995) *Handbook of Biological Confocal Microscopy*, Plenum Press, New York.

Perry, A. (2005) *Could You Please Make Me a Shade Lighter?* TIME Magazine 166(23): 41.

Pfeiffer, S., Vielhaber, G., Vietzke, J.-P., Wittern, K.-P., Hintze, U. and Wepf, R. (2000) *High-Pressure Freezing Provides New Information on Human Epidermis: Simultaneous Protein Antigen and Lamellar Lipid Structure Preservation. Study on Human Epidermis by Cryoimmobilization*. Journal of Investigative Dermatology 114(5): 1030-38.

Potter, B. and Medenica, M. (1968) *Ultramicroscopic Phagocytosis of Synthetic Melanin by Epidermal Cells In Vivo*. Journal of Investigative Dermatology 51(4): 300-303.

Prota, G. (1980) *Recent Advances in the Chemistry of Melanogenesis in Mammals*. Journal of Investigative Dermatology 75(1): 122-27.

Quast, T., Wehner, S., Kirfel, G., Jaeger, K., De Luca, M. and Herzog, V. (2003) *sAPP as a Regulator of Dendrite Motility and Melanin Release in Epidermal Melanocytes and Melanoma Cells*. FASEB Journal 17(12): 1739-41.

Rahman, S.B. and Bhawan, J. (1996) *Lentigo*. International Journal of Dermatology 35(4): 229-39.

Raposo, G., Fevrier, B., Stoorvogel, W. and Marks, M.S. (2002) *Lysosome-Related Organelles: A View from Immunity and Pigmentation*. Cell Structure and Function 27(6): 443-56.

Raposo, G. and Marks, M.S. (2002) *The Dark Side of Lysosome-Related Organelles: Specification of the Endocytotic Pathway for Melanosome Biogenesis*. Traffic 3(4): 237-48.

Raposo, G., Tenza, D., Murphy, D.M., Berson, J.F. and Marks, M.S. (2001) *Distinct Protein Sorting and Localization to Premelanosomes, Melanosomes, and Lysosomes in Pigmented Melanocytic Cells*. Journal of Cell Biology 152(4): 809-23.

Rawe, J. (2006) *Why Teens Are Obsessed With Tanning*. Time Magazine 168(6): 54-56.

Robinson, J.M., Ohira, T. and Badwey, J.A. (2004) *Regulation of the NADPH Oxidase Complex of Phagocytic Leukocytes. Recent Insights from Structural Biology, Molecular Genetics, and Microscopy*. Histochemistry and Cell Biology 122(4): 293-304.

Rokos, H., Beazley, W.D. and Schallreuter, K.U. (2002) *Oxidative Stress in Vitiligo: Photo-Oxidation of Pterins Produces H_2O_2 and Pterin-6-Carboxylic Acid*. Biochemical and Biophysical Research Communications 292(4): 805-11.

Romeis, B. (1968) *Mikroskopische Technik*. 16th ed., R. Oldenbourg Verlag, München.

Rothman, S. and Lorincz, A.L. (1963) *Defense Mechanisms of the Skin*. Annual Reviews of Medicine 14: 215-42.

Saito, N. and Seiji, M. (1976) *Degradation of Melanosomes In Vitro and In Vivo*. Pigment Cell 3: 348-92.

Sasai, Y., Kumano, S., Takahashi, M. and Nakano, H. (1978) *Histochemical Quantification of Dopa Oxidase (Tyrosinase) Activity in Epidermal Melanocytes*. Histochemistry 55(3): 235-43.

Sauermann, K., Clemann, S., Jaspers, S., Gambichler, T., Altmeyer, P., Hoffmann, K. and Ennen, J. (2002) *Age Related Changes of Human Skin Investigated With Histometric Measurements by Confocal Laser Scanning Microscopy In Vivo*. Skin Research and Technology 8(1): 52-56.

Schraermeyer, U. (1993) *Does Melanin Turnover Occur in the Eyes of Adult Vertebrates?* Pigment Cell Research 6(4 Pt 1): 193-204.

Schwarz, R., Berlage, T. and Knieps, T. (2006) *Trainierbare Bildanalyse für High-Content-Screening*. Labor Praxis März.

Scott, G., Deng, A., Rodriguez-Burford, C., Seiberg, M., Han, R., Babiarz, L., Grizzle, W., Bell, W. and Pentland, A. (2001) *Protease-Activated Receptor 2, a Receptor Involved in Melanosome Transfer, is Upregulated in Human Skin by Ultraviolet Irradiation*. Journal of Investigative Dermatology 117(6): 1412-20.

Scott, G., Leopardi, S., Parker, L., Babiarz, L., Seiberg, M. and Han, R. (2003) *The Proteinase-Activated Receptor-2 Mediates Phagocytosis in a Rho-Dependent Manner in Human Keratinocytes*. Journal of Investigative Dermatology 121(3): 529-41.

Scott, G., Leopardi, S., Printup, S. and B.C., M. (2002) *Filopodia are Conduits for Melanosome Transfer to Keratinocytes*. Journal of Cell Science 115(Pt. 7): 1441-51.

Seabra, M.C. and Barral, D.C. (2004) *The Melanosome as a Model to Study Organelle Motility in Mammals*. Pigment Cell Research 17(2): 111-19.

Seiberg, M. (2001) *Keratinocyte - Melanocyte Interactions During Melanosome Transfer*. Pigment Cell Research 14(4): 236-42.

Seiberg, M., Paine, C., Sharlow, E., Andrade-Gordon, P., Costanzo, M., Eisinger, M. and Shapiro, S.S. (2000a) *The Protease-Activated Receptor 2 Regulates Pigmentation via Keratinocyte-Melanocyte Interactions*. Experimental Cell Research 254(1): 25-32.

Seiberg, M., Paine, C., Sharlow, E., Andrane-Gordon, P., Constanzo, M., Eisinger, M. and Shapiro, S.S. (2000b) *Inhibition of Melanosome Transfer Results in Skin Lightening*. Journal of Investigative Dermatology 115(2): 162-67.

Seiji, M., Fitzpatrick, T.B. and Birbeck, M.S. (1961) *The Melanosome: A Distinctive Subcellular Particle of Mammalian Melanocytes and the Site of Melanogenesis*. Journal of Investigative Dermatology 36: 243-52.

Seiji, M. and Kikuchi, A. (1969) *Acid Phosphatase Activity in Melanosomes*. Journal of Investigative Dermatology 52(2): 212-16.

Skepper, J.N. (2000) *Immunocytochemical Strategies for Electron Microscopy: Choice or Compromise*. Journal of Microscopy 199 (Pt 1): 1-36.

Smoller, B.R., Hsu, A. and Krueger, J. (1991) *HMB-45 Monoclonal Antibody Recognizes an Inducible and Reversible Melanocyte Cytoplasmic Protein*. Journal of Cutaneous Pathology 18(5): 315-22.

Staricco, R.J. and Pinkus, H. (1957) *Quantitative and Qualitative Data on the Pigment Cells of Adult Human Epidermis*. Journal of Investigative Dermatology 28(1): 33-45.

Stierner, U., Rosdahl, I., Augustsson, A. and Kagedal, B. (1989) *UVB Irradiation Induces Melanocyte Increase in Both Exposed and Shielded Human Skin*. Journal of Investigative Dermatology 92(4): 561-64.

Swift, J.A. (1964) *Transfer of Melanin Granules from Melanocytes to the Cortical Cells of Human Hair*. Nature 203: 976-77.

Szabo, G. (1954) *The Number of Melanocytes in Human Epidermis*. British Medical Journal 1(4869): 1016-17.

Szabo, G., Gerald, A.B., Pathak, M.A. and Fitzpatrick, T.B. (1969) *Racial Differences in the Fate of Melanosomes in Human Epidermis*. Nature 222(5198): 1081-82.

Tadokoro, T., Yamaguchi, Y., Batzer, J., Coelho, S.G., Zmudzka, B.Z., Miller, S.A., Wolber, R., Beer, J.Z. and Hearing, V.J. (2005) *Mechanisms of Skin Tanning in Different Racial/Ethnic Groups in Response to Ultraviolet Radiation*. Journal of Investigative Dermatology 124(6): 1326-32.

Taylor, S., Westerhof, W., Im, S. and Lim, J. (2006) *Noninvasive Techniques for the Evaluation of Skin Color*. Journal of the American Academy of Dermatology 54(5, Supplement 2): S282-S290.

Telek, G., Scoazec, J.Y., Chariot, J., Ducroc, R., Feldmann, G. and Roz, C. (1999) *Cerium-Based Histochemical Demonstration of Oxidative Stress in Taurocholate-Induced Acute Pancreatitis in Rats. A Confocal Laser Scanning Microscopic Study*. Journal of Histochemistry and Cytochemistry 47(9): 1201-12.

Thong, H.-Y., Jee, S.-H., Sun, C.-C. and Boissy, R.E. (2003) *The Patterns of Melanosome Distribution in Keratinocytes of Human Skin as Determining Factor of Skin Colour*. British Journal of Dermatology 149(3): 498-505.

Turner, C.P., Toye, A.M. and Jones, O.T.G. (1998) *Keratinocyte Superoxide Production*. Free Radical Biology & Medicine 24(3): 401-7.

Unver, N., Freyschmidt-Paul, P., Horster, S., Wenck, H., Stab, F., Blatt, T. and Elsasser, H.-P. (2006) *Alterations in the Epidermal-Dermal Melanin Axis and Factor XIIIa Melanophages in Senile Lentigo and Ageing Skin*. British Journal of Dermatology 155(1): 119-28.

Van Den Bossche, K., Naeyaert, J.-M. and Lambert, J. (2006) *The Quest for the Mechanism of Melanin Transfer*. Traffic 7(7): 769-78.

Vancoillie, G., Lambert, J., Mulder, A., Koerten, H.K., Mommaas, A.M., Van Oostveldt, P. and Naeyaert, J.M. (2000) *Kinesin and Kinectin can Associate with the Melanosomal Surface and Form a Link with Microtubules in Normal Human Melanocytes*. Journal of Investigative Dermatology 114(3): 421-29.

Velangi, S.S. and Rees, J.L. (2001) *Why are Scars Pale? An Immunohistochemical Study Indicating Preservation of Melanocyte Number and Function in Surgical Scars.* Acta Dermato-Venereologica 81(5): 326-28.

Viator, J.A., Komadina, J., Svaasand, L.O., Aguilar, G., Choi, B. and Stuart Nelson, J. (2004) *A Comparative Study of Photoacoustic and Reflectance Methods for Determination of Epidermal Melanin Content*. Journal of Investigative Dermatology 122(6): 1432-39.

Virador, V.M., Matsunaga, N., Matsunaga, J., Valencia, J., Oldham, R.J., Kameyama, K., Peck, G.L., Ferrans, V.J., Vieira, W.D., Abdel-Malek, Z.A., *et al.* (2001) *Production of Melanocyte-Specific Antibodies to Human Melanosomal Proteins: Expression Patterns in Normal Human Skin and in Cutaneous Pigmented Lesions.* Pigment Cell Research 14(4): 289-97.

Virador, V.M., Muller, J., Wu, X., Abdel-Malek, Z.A., Yu, Z.-X., Ferrans, V.J., Kobayashi, N., Wakamatsu, K., Ito, S., Hammer, J.A., *et al.* (2002) *Influence of Alpha-Melanocyte-Stimulating Hormone and Ultraviolet Radiation on the Transfer of Melanosomes to Keratinocytes*. FASEB Journal 16(1): 105-07.

Wakamatsu, K. and Ito, S. (2002) *Advanced Chemical Methods in Melanin Determination*. Pigment Cell Research 15(3): 174-83.

Wakamatsu, K., Ito, S. and Rees, J.L. (2002) *The Usefulness of 4-Amino-3-Hydroxyphenylalanine as a Specific Marker of Pheomelanin*. Pigment Cell Research 15(3): 225-32.

Webb, A.R. and Engelsen, O. (2006) *Calculated Ultraviolet Exposure Levels for a Healthy Vitamin D Status*. Photochemistry and Photobiology in print.

Whiteman, D.C., Parsons, P.G. and Green, A.C. (1999) *Determinants of Melanocyte Density in Adult Human Skin*. Archives for Dermatological Research 291(9): 511-16.

Wilson, J.M., De Hoop, M., Zorzi, N., Toh, B.-H., Dotti, C.G. and Parton, R.G. (2000) *EEA1, a Tethering Protein of the Early Sorting Endosome, Shows a Polarized Distribution in Hippocampal Neurons, Epithelial Cells, and Fibroblasts*. Molecular Biology of the Cell 11(8): 2657-71.

Wolff, K., Jimbow, K. and Fitzpatrick, T.B. (1974) *Experimental Pigment Donation In Vivo*. Journal of Ultrastructural Research 47(3): 400-19.

Wolff, K. and Konrad, K. (1971) *Melanin Pigmentation: An In Vivo Model for Studies of Melanosome Kinetics Within Keratinocytes*. Science 174(13): 1034-35.

Wu, X., Rao, K., Bowers, M.B., Copeland, N.G., Jenkins, N.A. and Hammer, J.A. (2001) *Rab27a Enables Myosin Va-Dependent Melanosome Capture by Recruiting the Myosin to the Organelle*. Journal of Cell Science 114(Pt 6): 1091-100.

Wulf, H.C., Sandby-Moller, J., Kobayasi, T. and Gniadecki, R. (2004) *Skin Aging and Natural Photoprotection*. Micron 35(3): 185-91.

Yamaguchi, Y., Takahashi, K., Zmudzka, B.Z., Kornhauser, A., Miller, S.A., Tadokoro, T., Berens, W., Beer, J.Z. and Hearing, V.J. (2006) *Human Skin Responses to UV Radiation: Pigment in the Upper Epidermis Protects Against DNA Damage in the Lower Epidermis and Facilitates Apoptosis*. FASEB Journal 20(9): 1486-8.

Yamamoto, O. and Bhawan, J. (1994) *Three Modes of Melanosome Transfers in Caucasian Facial Skin: Hypothesis Based on an Ultrastructural Study*. Pigment Cell Research 7(3): 158-69.

Yamashita, T., Kuwahara, T., Gonzalez, S. and Takahashi, M. (2005) *Non-Invasive Visualization of Melanin and Melanocytes by Reflectance-Mode Confocal Microscopy*. Journal of Investigative Dermatology 124(1): 235-40.

Yoon, T.-J., Lei, T.C., Yamaguchi, Y., Batzer, J., Wolber, R. and Hearing, V.J. (2003) *Reconstituted 3-Dimensional Human Skin of Various Ethnic Origins as an In Vitro Model for Studies of Pigmentation*. Analytical Biochemistry 318(2): 260-69.

Zajac, G.W., Gallas, J.M., Cheng, J., Eisner, M., Moss, S.C. and Alvarado-Swaisgood, A.E. (1994) *The Fundamental Unit of Synthetic Melanin: A Verification by Tunnelling Microscopy of X-ray Scattering Results*. Biochimica et Biophysica Acta 1199(3): 271-78.

I APPENDIX

I Punch Biopsy Studies

The two studies (internal Beiersdorf AG study numbers: 10684 and 18655) conducted to obtain the skin samples investigated during this project were approved by the Hamburg ethics committee. The first study, titled "Studie zur Untersuchung spezieller Aspekte negroider und kaukasischer Haut", approved by the ethics committee Nov. 24, 1999 (catalogued under OB), was accomplished from Feb. 2000 to May 2001. The second study ("*Ex vivo*-Studie zur Untersuchung des Einflusses von Fibroblasten auf die Pigmentierung in der menschlichen Haut") was approved Apr. 1, 2004 (catalogued under OB-024/04) and was carried out from Apr.-July 2005. Ethics proposal and declaration of consent, to be stated by each participant are detailed in the following. They are comparable for both studies.

I.1 Ethics Proposal (Ethikantrag)

Fragen-Katalog der Ethik-Kommission bei der Ärztekammer Hamburg:

***Ex vivo*-Studie zur Untersuchung des Einflusses von Fibroblasten auf die Pigmentierung in der menschlichen Haut**

1. Persönliche Angaben

1.1 Namen und Dienststellungen der Versuchleiter und ihrer Mitarbeiter
- Frau Prof. Dr. med. I. Moll, Direktorin der Hautklinik des UKE
- Frau Dr. E. Knußmann-Hartig, Wiss. Mitarbeiterin, Hautklinik des UKE
- Dr. rer. nat. F. Stäb, Abteilungsleiter, Beiersdorf AG Hamburg
- Dr. rer. physiol. R. Wolber, Laborleiter, Beiersdorf AG Hamburg

1.2. Angaben über wissenschaftliche Qualifikation des Versuchsleiters
Versuchsleiter sind Frau Prof. Dr. I. Moll, Direktorin der Hautklinik des UKE, Fachärztin für Dermatologie und Venerologie und für dieses Fach seit 1991 an der Universität Heidelberg habilitiert, und Herr Dr. F. Stäb, wissenschaftlicher Mitarbeiter und Abteilungsleiter bei der Beiersdorf AG.
Zweijährige Erfahrung in der klinischen Prüfung von Arzneimitteln liegen vor.

1.3. Finanzierung der Studie ?
Die Studie wird aus Mitteln der Beiersdorf AG Hamburg finanziert.

2. <u>Beschreibung und wissenschaftliche Begründung des Projektes</u>

2.1. Erläuterung des Versuchszieles

Es ist bekannt, dass menschliche Haut des Phototyps V-VI einen zehnfach höheren Eigenschutz vor UV-Strahlung und einen bis zu tausendfach höheren Schutz vor der Entwicklung von Hautkrebs hat als diejenige der geringer pigmentierten Phototypen, insbesondere die Phototypen I-II. Das Zusammenspiel der in der Epidermis lokalisierten Melanozyten und Keratinozyten im Pigmentierungsprozess der Haut ist bereits Gegenstand intensiver Forschung. Kontrovers diskutiert wird dagegen die Rolle der Fibroblasten im Pigmentierungsgeschehen. Im Rahmen dieser Studie soll der Einfluss von Dermiszellen (Fibroblasten) unterschiedlicher Phototypen (I-VI) auf Epidermiszellen (Keratinozyten, Melanozyten) *in vitro* in sogenannter 3D-Hautmodelle untersucht werden. Es werden 2 Biopsien im Bereich des Gesäßes entnommen, in Kultur die dermalen Fibroblasten isoliert und expandiert und mit Melanozyten enthaltenden Epidermismodellen kokultiviert. Anschließend sollen die Modelle histologisch und biochemisch hinsichtlich verschiedener Pigmentierungs- und Wachstumsparameter (Tyrosinaseaktivität, Melaningehalt, Differenzierung, ßFGF) untersucht werden. Ziel ist es, die Rolle der Fibroblasten in der Pigmentierung der menschlichen Haut und damit deren Einfluss auf den endogenen Hauteigenschutz vor ultraviolettem (UV-) Licht bei unterschiedlichen Phototypen zu charakterisieren. Gentechnologische Untersuchungen erfolgen nicht.

2.2. Darstellung des heutigen Wissenstandes:

Die so genannte Minimale Erythemale Dosis (MED) oder auch der Eigenschutz der Haut vor UV-Strahlung ist bei stark pigmentierter menschlicher Haut 10 bis 15fach höher als bei geringer Pigmentierung. Um den Faktor 500 bis 1000 höher ist sogar der Schutz vor der Entwicklung von Hautkrebs (Kollias et al., 1991). Zurückzuführen ist dies nicht etwa auf eine höhere Anzahl von Melanozyten in stärker pigmentierter Haut sondern u. a. auf die etwa zehnfach höhere Tyrosinaseaktivität (Iozumi et al., 1993; Iwata et al., 1990) (Tyrosinase ist das geschwindigkeitsbestimmende Enzym der Melanogenese), die unterschiedlichen Größen und Formen der Melanosomen (Toda et al., 1972) und die Prozessierung der Melanosomen in den Keratinozyten (Szabo et al., 1969).
Die Regulation der Pigmentierung über den Austausch parakriner Faktoren zwischen Keratinozyten und Melanozyten nach Stimulierung durch UV-Strahlung ist seit langem Gegenstand der Forschung. So konnte z. B. gezeigt werden, dass durch UVB-Strahlung der Protease-aktivierte Rezeptor (PAR)-2 auf Ebene der Keratinozyten aktiviert wird und es zu einer verstärkten Aufnahme von Melanosomen durch Keratinozyten kommt (Seiberg, 2001).
Weniger erforscht ist dagegen die Rolle der Fibroblasten in der Pigmentierung der Haut. Diese wird in der Literatur kontrovers beschrieben. Es wurde gezeigt, dass die Kultivierung von Melanozyten auf einem Dermisäquivalent, welches lebende Fibroblasten enthielt, die Lebensfähigkeit der Melanozyten nach UV-Bestrahlung steigert. Vermutet wurde hier ein Zusammenhang zwischen der Bildung u.a. von Neurotrophinen durch Fibroblasten, die als eine Art von Überlebensfaktor für Melanozyten nach UV-Stress gelten (Archambault et al., 1995). Hedley et al. zeigten anhand eines rekonstruierten Humanhaut Modells der Phototypen I und II, dass das Hinzufügen von Fibroblasten die spontane Pigmentierung der Melanozyten in diesem Modell unterdrückt bzw. das Weglassen der Fibroblasten eine verstärkte Pigmentierung, Lokalisation der Melanozyten auch oberhalb der basalen Keratinozyten und eine schlechte Stratifizierung des Modells zur Folge hatte. Auch wurde hier in einem Versuch mit Melanozyten des Phototyps I/II bzw. IV auf einem Modell mit Keratinozyten/Fibroblasten Typ I/II gezeigt, dass die Hautmodelle in der Pigmentierung dem Melanozyten-Spender ähnelten (Hedley et al., 2002).
In einer weiteren Untersuchung an einem Hautmodell-System des Phototyps IV wurden diese Daten in sofern bestätigt, dass auch hier die Pigmentierung (Melaningehalt) makro-sowie mikroskopisch in Modellen mit Fibroblastenpopulation deutlich verringert war als in Abwesenheit von Fibroblasten. In der immunhistologischen Untersuchung wurde außerdem gezeigt, dass die Anzahl proliferierender Keratinozyten sehr hoch und die Anzahl der Melanozyten sehr niedrig in der Anwesenheit von Fibroblasten war. Wiedersprüchlich dazu erscheinen die Ergebnisse mit Melanozyten-Monokulturen, welche mit konditioniertem Medium (mit löslichen Faktoren, welche die Fibroblasten ins Medium abgeben) inkubiert scheinbar eine gesteigerte Proliferation aufwiesen (Lee et al., 2003).
In allen bisherigen Untersuchungen wird der Einfluss von Fibroblasten/Keratinozyten im Allgemeinen untersucht, phototyp-abhängige Untersuchungen konzentrieren sich in der Hauptsache auf Melanozyten von Spendern unterschiedlicher Phototypen. In dieser Studie sollen nun Fibroblasten von Spendern unterschiedlicher Phototypen mit Hautmodellen eines immer gleichen Phototyps kokultiviert und deren Wechselwirkungen dokumentiert werde.

2.3. Ergebnisse pharmakologisch-toxikologischer Vorprüfungen:

Entfällt, da keine Medikamente oder Medizinprodukte eingesetzt werden; es werden nur 2 Biopsien je Spender entnommen.

2.4. Begründung der Notwendigkeit von Humanversuchen
Für das unter 2.1. dargestellte Versuchsziel existiert kein Tiermodell, das eine adäquate Übertragung auf die Verhältnisse in menschlicher Haut zulässt. Daher müssen die Untersuchungen an frisch gewonnen Biopsien von Probanden durchgeführt werden.

2.5. Schilderung der geplanten Versuchsdurchführung
Von hautgesunden Probanden aus der Altersgruppe 20-45 Jahre, die in drei Gruppen eingeteilt den Phototypen I/II (heller Hauttyp), III/IV(mittlerer Hauttyp) und V/VI (dunkler Hauttyp) zuzuordnen sind, werden im Bereich des Gesäßes (weitestgehend unbestrahlte Haut) insgesamt 2 Biopsien (Durchmesser 5 mm) entnommen in Kulturmedium transferiert. Anschließend wird *in vitro* mittels Skalpell die Dermis von der Epidermis getrennt, und eine Partikelkultur zur Isolierung und Vermehrung der dermalen Fibroblasten mit den Dermisstücken angelegt. Nach der weiteren Expansion der Fibroblasten-Monokulturen sollen diese mit einer kommerziell erhältlichen melanozytenenthaltenden Epidermis ko-kultiviert werden und verschiedene *in vitro*-Tests zur (UV-induzierten) Pigmentierung durchgeführt. Die Epidermis wird für vergleichende histologische Untersuchungen kryokonserviert, um später eine Korrelation zwischen der Pigmentierung der Haut und dem Einfluss der Fibroblasten auf die Melanogenese herstellen zu können: Hierbei werden mit klassischen biochemischen und zellbiologischen Verfahren die Aktivitäten der Enzyme untersucht, die an der Melaninbildung beteiligt sind (Melanogeneseassay, insbesondere Tyrosinase). Ferner werden die Mediatoren untersucht, die für die Zell-Zell-Kommunikation wichtig sind (bFGF mittels ELISA-Techniken) und klassisch morphologische Techniken (Histologie zur Bestimmung des Melaningehalts, der Melanozytenzahlen etc.) herangezogen. Gentechnische Analysen sind im Rahmen dieser Studie nicht geplant. Alle Untersuchungen finden an Zellen statt, die nach Biopsieentnahme aus den Biopsien isoliert werden.
Je Phototypengruppe sollen 10 Probanden herangezogen werden, insgesamt sollen somit 30 Probanden teilnehmen.

2.6. Literaturangaben
Archambault, M., Yaar, M., Gilchrest, B.A. (1995) J Invest Dermatol 104: 859-67
Hedley, S. J., Layton, Ch. et al. (2002) Pigment Cell Res 15: 49-56
Iozumi, K. Hoganson, G. E. et al (1993) J Invest Dermatol 100: 806-11
Iwata, M, Corn, T. et al. (1990) J Invest Dermatol 95: 9-15
Kollias, N., Sayre, R. M. et al (1991) Photochem Photobiol B 9:, 135-60
Lee, D.-Y., Lee, J.-H. et al. (2003) Arch Dermatol Res 294: 444-446
Seiberg, M. (2001) Pigment Cell Res 14: 236-42
Szabo, G., Gerald, A. B. et al (1969) Nature 222: 1081-2
Toda, K., Pathak, M. A. et al (1972) Nat New Biol 236: 143-5

2.7. Ist das Projekt schon bei einer anderen Ethik-Kommission vorgelegt worden ?
Nein.

3. <u>Schilderung der voraussehbaren Belastungen und Risiken für die Versuchspersonen</u>
Belastungen und Risiken bestehen bei dieser Studie nur im Hinblick auf Entnahme der Probeexzisionen, da alle weiterführenden Arbeiten an den frisch ex vivo genommenen Biopsien, i.e. nicht in situ erfolgen.
Bei einer Stanzbiopsie wird aus der Haut ein 5 mm durchmessender Gewebezylinder in örtlicher Betäubung entnommen. Es verbleibt ein diesem Zylinder entsprechender Gewebedefekt, der mittels einer kleinen Hautnaht verschlossen wird und rasch unter Hinterlassung einer kleinen Narbe abheilt. Voraussehbare Risiken bestehen in der Möglichkeit einer Unverträglichkeit gegenüber dem Lokalanästhetikum, einer Nachblutung, einer Wundinfektion sowie einer ungewöhnlichen Narbenbildung.

3.1. Kontraindikationen, Ein - und Ausschlusskriterien
<u>Kontraindikationen</u>:
- Hinweise auf ungewöhnliche Lichtreaktionen der Haut
- Schwangerschaft
- systemische Erkrankungen
- floride Infektionen
- bekannte Unverträglichkeit gegenüber Lokalanästhetika

<u>Einschlusskriterien</u>:
- Lebensalter 20 bis 45 Jahre
- Phototypen I-VI (siehe 2.5)

Ausschlusskriterien:
- Vorliegen einer Kontraindikation
- Lebensalter unter 20 Jahren oder über 45 Jahren
- Probanden mit eingeschränkter Geschäftsfähigkeit
- Einnahme von Medikamenten, insbesondere solcher Medikamente, die ausgeprägte UV-abhängige Reaktionen zeigen (Glucokortikoide, nichtsteroidale Antiphlogistika)
- Nikotin oder Alkoholabusus

Abbruchkriterien:
- Unverträglichkeit gegenüber dem Lokalanesthetikum

3.2. Möglichkeit weiterer, derzeit nicht überschaubarer Risiken
Weitere, derzeit nicht überschaubare Risiken bestehen nach dem aktuellen Erkenntnisstand nicht.

4. Voraussichtliche Vorteile und Bedeutung des Versuchs für den Menschen
a) in der Heilkunde
Für die präklinische Identifikation und Untersuchung von pigmentierungsstimulierenden Substanzen *in vitro*, die den Eigenschutz der Haut vor UV-Strahlung durch erhöhte Melaninsynthese verstärken können. Dies könnte völlig neuartige Ansatzpunkte für die Prävention von Hautkrebs und sonstige UV-bedingte Hautschädigungen liefern.

b) in der Forschung
Die Studie dient der *in vitro* Untersuchung der Pigmentierung und speziell deren Beeinflussung durch Fibroblasten in einem 3D-Hautmodell, welches sehr nahe an der *in vivo*-Situation ist. Ferner sind möglicherweise grundlegende Erkenntnisse über die Ursachen der Pigmentierung und des Hauteigenschutzes bei unterschiedlichen Phototypen zu erwarten.

4.1. Gesunde Minderjährige betroffen ?
Nein, da Minderjährige in die Studie nicht aufgenommen werden.

4.2. Individuelle Indikation
Die individuelle Indikation ergibt sich aus den unter 3.1. aufgeführten Kriterien. Die selbstverständlich freiwillige Teilnahme an der Studie ist allen Probanden, die den Einschlusskriterien (siehe 3.1.) entsprechen und keine Kontraindikationen (siehe 3.1.) aufweisen, möglich.

5. Güterabwägung zwischen den Nachteilen und Risiken einerseits und dem voraussichtlichen Nutzen andererseits
Nachteile und Risiken der Studie sind unter 3. ausführlich aufgeführt. Sie bestehen lediglich in der Entnahme von 2 Probeexzisionen in örtlicher Betäubung im Bereich des Gesäßes zu einem Zeitpunkt.
Ein unmittelbarer Nutzen für die an der Studie teilnehmenden Probanden ist nicht gegeben. Die voraussichtlichen Vorteile und die Bedeutung in Heilkunde und Forschung sind unter 4. aufgeführt.

5.1. Vorrang der Belange der Versuchspersonen
Die Belange der Versuchspersonen stehen unbedingt im Vordergrund. Probanden, denen durch die Teilnahme an der Studie eventuell Nachteile entstehen, werden in die Studie nicht aufgenommen (s. Einschlusskriterien).
Eine Zuordnung der gewonnenen Daten zu den persönlichen Probandendaten ist nicht möglich.

5.2. Beschränkung der Zahl der Versuchspersonen auf das unbedingt notwendige Maß
Die Zahl der Versuchspersonen wird auf das unbedingt notwendige Maß beschränkt. Aufgrund unserer experimentellen Erfahrungswerte aus *in vitro*-Kultursystemen ist die Durchführung der Experimente bei jeweils 10 freiwilligen Spendern vom Phototyp I/II, Phototyp III/IV und Phototyp V/VI ausreichend.

5.3. Strengere Anforderungen an die Vertretbarkeit bei Versuchen an gesunden Probanden, denen keine therapeutischen Vorteile aus dem Versuch erwachsen, als bei neuartigen Heilversuchen an Patienten
Entfällt, da keine Heilversuche geplant sind.

5.4. Blind- und Doppelblindversuche
Entfällt.

6. <u>Angaben über den Inhalt der Aufklärungsgespräche mit den Versuchspersonen</u>
Das Aufklärungsgespräch wird individuell mit jedem Studienteilnehmer geführt. Es wird in Aufklärungsbögen inhaltlich dokumentiert, vom Probanden unterzeichnet und dem Probanden in Kopie ausgehändigt (siehe Punkt 7).

6.2. Aufklärung über die Widerruflichkeit der Einwilligung
Im Aufklärungsbogen wird ausdrücklich darauf hingewiesen, dass der Teilnehmer jederzeit das Recht auf Widerruf seiner Einwilligung hat.

6.3. Aufklärung über Probandenversicherung einschließlich Umfang und Verhaltensregeln
Eine Probandenversicherung in erforderlichem Umfang besteht über das Forschungszentrum der Beiersdorf AG. Diese Versicherung ist mit der Allianz-AG unter der Vers.Nr. IHA 30/445/0163550/240 abgeschlossen.

6.4. Aufklärung bei
a) randomisierten Studien
b) Blind- und Doppelblindstudien
c) Placebo-kontrollierten Studien
Entfällt, da entsprechende Studien nicht durchgeführt werden.

6.5. Beachtung der Sonderregeln bei Minderjährigen und in ihrer Geschäftsfähigkeit beeinträchtigten Probanden
Minderjährige und in ihrer Geschäftsfähigkeit beeinträchtigte Probanden werden nicht in die Studie aufgenommen.

7. <u>Beifügung eines Musters für die zu erteilende Aufklärung</u>
Ein Aufklärungsbogen liegt dem Antrag bei.

8. <u>Nachweis einer ausreichenden Probandenversicherung</u>
Auf eine Probandenversicherung in erforderlichem Umfang über das Forschungszentrum der Beiersdorf AG wird der Proband aufmerksam gemacht.

9. <u>Darstellung der Erfüllung etwaiger sonstiger Voraussetzungen für die Durchführung des Vorhabens (z.B. § 40(1) Nr. 3,6,7 AMG, Strahlenschutzverordnung §§ 41-43)</u>
Entfällt.

10. Maßnahmen bei Veränderung der Risikolage
Entfällt.

10.1. Sicherstellung, dass bei Veränderungen der Risikolage während des Versuches die Güterabwägung im Sinne von Ziffer 5 jeweils erneut durchgeführt wird und bei nachteiliger Veränderung der Risikolage auch erneute Aufklärungsgespräche mit den Versuchspersonen stattfinden
Diese Sicherstellung ist gegeben; insbesondere werden Patienten bei Veränderungen ihrer Risikolage von der Teilnahme ausgeschlossen.

10.2. Mitteilung der veränderten Abbruchkriterien an die Ethik-Kommission
Bei Veränderung der Abbruchkriterien wird die Ethik-Kommission entsprechend informiert.

I.2 Declaration of Consent (Einwilligungserklärung)

<u>Aufklärung und Einwilligung zur Teilnahme an der „*Ex-vivo*-Studie zur Untersuchung des Einflusses von Fibroblasten auf die Pigmentierung in der menschlichen Haut“</u>

Frau Wessel hat mir heute in einem persönlichen Gespräch folgendes erklärt:
Die Beiersdorf AG plant eine Studie zur Charakterisierung von Pigmentierungsprozessen (Prozesse der Hautbräunung) und deren Beeinflussung durch Zellen der tieferen Hautschichten (dermale Zellen). Dazu sollen 2 kleine Hautproben aus dem Gesäß in örtlicher Betäubung entnommen werden.

Aus den gewonnenen Proben wird in einem speziellen Verfahren zunächst ein bestimmter Zelltyp (Bindegewebszellen) isoliert und damit dann in einem besonderen Kultur-Verfahren (Kokultur, 3D-Modell) Untersuchungen vorgenommen. Diese erlauben Rückschlüsse auf die Rolle dieses Zelltyps in der Pigmentierung der menschlichen Haut. Die Zellen bleiben ca. zwei Wochen in Kultur. Dazu werden die Daten in einer den gesetzlichen Vorschriften entsprechenden Art und Weise anonymisiert, so dass es nicht mehr möglich ist, die gewonnenen Untersuchungsergebnisse einzelnen Probanden zuzuordnen.

Mögliche Belastungen und Risiken der Entnahme einer Hautprobe:
Die zwei Hautproben werden folgendermaßen gewonnen: Zunächst werden kleine Hautareale lokal betäubt. Dann wird aus diesem Bereich eine kleine Hautprobe mittels einer speziellen Nadel (Durchmesser maximal 5 mm) entnommen. Es verbleibt eine kleine, oberflächliche Wunde mit einem Durchmesser von maximal 5 mm, die zur Beschleunigung der Wundheilung mit einer kleinen Hautnaht und einem Pflasterverband versorgt wird. Die Entnahmestellen sollten mindestens 1 Woche nicht nass werden oder bei unbeabsichtigtem Nasswerden anschließend vorsichtig abgetrocknet und mit einem frischen Pflaster versorgt werden. Der Pflasterverband sollte anfangs täglich, später alle 2 bis 3 Tage gewechselt werden. Nach etwa 10 bis 12 Tagen ist die Entnahmestelle in der Regel unter Hinterlassung einer kleinen Narbe abgeheilt, so dass der Hautfaden entfernt werden kann.
Mögliche Belastungen und Risiken bestehen in einer eventuellen Unverträglichkeitsreaktion auf das Betäubungsmittel, in einer gewöhnlichen Narbenbildung sowie der Möglichkeit einer Wundinfektion.
Falls Sie im Anschluss an die Entnahme der Hautproben oder während der Wundheilungsphase ungewöhnliches bemerken, wenden Sie sich bitte an die **Poliklinik in der Hautklinik, Telefon-Nr. 040-42803-2650 (8.00-16.00h)** oder an die **Station 4 der Hautklinik, Telefon-Nr. 040-42803-6348 (16.00-8.00h, Wochenenden)**. Dort kümmert sich der Diensthabende Arzt der Hautklinik um Sie.

Name, Vorname des Probanden: …….

Geburtsdatum: …….

Lokalisation der Hautproben: Gesäß, links oder rechts

Erklärung zur Probandenversicherung:
Ich wurde darüber informiert, dass für mich als Teilnehmer der Studie eine entsprechende Probandenversicherung durch die Beiersdorf AG abgeschlossen wurde.

Hamburg, den …….

Unterschrift des Probanden: …….

Unterschrift des aufklärenden Arztes: …….

Erklärung zur Probandenversicherung:
Bei einer klinischen Studie sind die Studienteilnehmer nach Maßgabe der dafür geltenden Allgemeinen Versicherungsbedingungen (AVB/P) versichert.
Die Probandenversicherung (Studienversicherung) wurde durch die Beiersdorf AG mit der Allianz Versicherungs-AG (Police-Nr. IHA 30/445/0163550/240) abgeschlossen.
Der Versicherungsschutz besteht für Gesundheitsschäden, die spätestens fünf Jahre nach Abschluss der beim Versicherten durchgeführten klinischen Prüfung eingetreten sind und nicht später als zehn Jahre nach Beendigung der klinischen Prüfung dem Versicherer gemeldet werden. Die Gesundheitsschädigung gilt als ab dem Zeitpunkt eingetreten, in dem der Geschädigte erstmals einen Arzt wegen Symptomen konsultiert hat, die sich bei diesem Anlass oder später als Symptome der betreffenden Gesundheitsschädigung erweisen.
Ersetzt wird der Vermögensschaden, der durch die Gesundheitsschädigung herbeigeführt wird. Der Umfang der Versicherung für eine Versuchsperson beträgt mindestens € 500.000,-.
Ausgeschlossen von der Versicherung sind Schädigungen oder Verschlimmerungen bereits bestehender Leidenszustände, die auch ohne Teilnahme an der klinischen Prüfung eingetreten wären oder fortbestünden, genetische Schädigungen sowie Schädigungen, die darauf beruhen, dass die Versuchsperson vorsätzlich ausdrücklichen Anweisungen bei der klinischen Prüfung zuwider gehandelt hat.

Um den Versicherungsschutz nicht zu gefährden, muss die Versuchsperson folgendes beachten:
1. Während der Dauer der Untersuchung darf sich die Versuchsperson einer anderen Behandlung nur im Einvernehmen mit dem Prüfarzt unterziehen. Im Notfall kann selbstverständlich umgehend jeder andere Arzt aufgesucht werden.

2. Eine Gesundheitsschädigung, die als Folge der Untersuchung eingetreten sein kann, muss die Versuchsperson der Allianz Versicherungs-AG, Police-Nr. IHA 30/445/0163550/240,
Anschrift: Zweigniederlassung für Norddeutschland, Großer Burstah 3, 20457 Hamburg
Telefon: 040/3617-0
unverzüglich anzeigen.
3. Die Versuchsperson muss alle zweckmäßigen Maßnahmen treffen, die der Aufklärung der Ursache oder des Umfangs eines Schadens sowie dessen Minderung dienen.
4. Verletzt die Versuchsperson vorsätzlich oder grob fahrlässig eines nach Eintritt von ihr zu erfüllende Obliegenheit, ist der Versicherer von der Verpflichtung zur Leistung frei. Bei grob fahrlässiger Versicherung besteht die Leistungspflicht weiter, sofern die Verletzung ohne Einfluss auf die Feststellung des Versicherungsfalles oder des Leistungsumfanges geblieben ist.
5. Im Falle des Todes geht die Informationspflicht auf die Rechtsnachfolger (Erben) über.

Erklärung über Datenschutzbestimmungen (gemäß §40(1)2, AMG)

1. Ich bin damit einverstanden, dass im Rahmen der klinischen Prüfung bzw. wissenschaftlichen Studie meine personenbezogenen Daten/Krankheitsdaten aufgezeichnet und anonymisiert (d. h. ohne Namensnennung)
a) An den genannten Auftraggeber der Studie zu ihrer wissenschaftlichen Auswertung
sowie
b) An die zuständige Überwachungsbehörde oder die zuständige Bundesoberbehörde zur Überprüfung der ordnungsgemäßen Durchführung der Studie weitergegeben werden.
Die Verarbeitung und Nutzung meiner anonymisierten Daten erfolgt auf Fragebögen und elektronischen Datenträgern für die Dauer von 10 Jahren.
2. Außerdem bin ich damit einverstanden, dass ein autorisierter und zur Verschwiegenheit verpflichteter Beauftragter des Auftraggebers oder der zuständigen Überwachungsbehörde bzw. der zuständigen Bundesoberbehörde in meine beim Prüfarzt vorhandenen personenbezogenen Daten Einsicht nimmt, soweit dies für die Überprüfung der Studie notwendig ist.
3. Für den Fall, dass die klinische Prüfung in mehreren Ländern durchgeführt wird, bin ich damit einverstanden, dass zur Überprüfung der Studie meinen aufgezeichneten Daten anonymisiert auch an die zuständige ausländische Überwachungsbehörde weitergeleitet werden und dass ein zur Verschwiegenheit verpflichteter Beauftragter der zuständigen ausländischen Überwachungsbehörde in meine personenbezogenen Daten Einsicht nimmt, soweit dies für die Überprüfung der Studie notwendig ist.
4. Wenn ich meine Einwilligungserklärung zur Teilnahme an der Studie widerrufe, werden die bereits gespeicherten Daten gelöscht.

Erklärung der Versuchsperson nach dem Aufklärungsgespräch:

Frau Wessel hat mich vollständig über das Wesen und die Bedeutung der geplanten Studie aufgeklärt. Dabei konnte ich alle mich interessierenden Fragen stellen. Ferner hatte ich Gelegenheit, das Merkblatt genau durchzulesen und auch dazu Fragen zu stellen. Ein Exemplar des Merkblattes ist mir zum Verbleib ausgehändigt worden.
Ich wurde darüber informiert, dass ich meine Einwilligung zur Teilnahme an der Studie jederzeit und ohne Angabe von Gründen widerrufen kann, ohne dass mir daraus Nachteile bezüglich einer laufenden oder zukünftigen Behandlung entstehen.
Ich weiß, dass die im Rahmen der Studie erhobenen Daten und persönlichen Mitteilungen der ärztlichen Schweigepflicht unterliegen und zur Auswertung nur ohne Patientenname (anonymisiert) zusammengeführt werden.
Ich bestätige durch meine Unterschrift, dass ich die Aufklärung verstanden habe und ich mich mit der Durchführung der genannten Studie einverstanden erkläre. Zugleich erkläre ich, dass ich mit der im Rahmen der Studie erfolgenden Aufzeichnung von (Krankheits-) Daten und ihrer Weitergabe an den Auftraggeber, die zuständige Überwachungsbehörde oder die zuständige Bundesoberbehörde und, soweit es sich um personenbezogene Daten handelt, mit deren Einsichtnahme durch Beauftragte des Auftraggebers oder der Behörden einverstanden bin.

Unterschrift des Probanden:	Unterschrift des aufklärenden Arztes:
…….	…….....
Hamburg, den …….	Hamburg, den …….

I.3 Information on Study Participants

I.3.1 Study 10684

Sample	Date of biopsy	Gender	Phenotype
1	05.09.2000	male	Lentigo senilis, lesional
2	05.01.2001	male	Lentigo senilis, lesional
3	04.05.2001	male	Lentigo senilis, lesional
4	22.11.2001	male	Lentigo senilis, lesional
5	22.11.2001	female	Lentigo senilis, lesional
6	22.11.2001	female	Lentigo senilis, perilesional
7	22.11.2001	male	Lentigo senilis, perilesional
8	04.05.2001	male	Lentigo senilis, perilesional
9	05.01.2001	male	Lentigo senilis, perilesional
10	05.09.2000	male	Lentigo senilis, perilesional
11	21.02.2000	male	Asian skin, Indonesia
12	22.02.2000	male	Asian skin, Korea
13	22.02.2000	female	Asian skin, Korea
14	25.02.2000	male	Asian skin, India
15	25.02.2000	female	Asian skin, Indonesia
16	25.02.2000	female	Asian skin, Indonesia
17	04.05.2001	male	Negroid skin, Ghana
18	04.05.2001	male	Negroid skin, Ghana
19	11.05.2001	male	Negroid skin, Ghana
20	18.05.2001	male	Negroid skin, Ghana
21	18.05.2001	female	Negroid skin, Ghana
22	18.05.2001	male	Negroid skin, Ghana
23	05.01.2001	male	Caucasian skin, Germany
24	18.05.2001	male	Caucasian skin, Germany
25	23.05.2001	male	Caucasian skin, Germany
26	23.05.2001	male	Caucasian skin, Germany
27	01.08.2001	male	Caucasian skin, Germany
28	01.08.2001	female	Caucasian skin, Germany
29	20.09.2001	female	Asian skin, India
30	11.05.2001	male	Negroid skin, Ghana
31	23.11.2001	female	Lentigo senilis, lesional
32	23.11.2001	female	Lentigo senilis, perilesional
33	11.05.2001	male	Negroid skin, Ghana
34	23.11.2001	female	Lentigo senilis, perilesional
35	23.11.2001	female	Lentigo senilis, lesional
36	05.12.2001	male	Negroid skin, Ghana
37	21.09.2001	male	Asian skin, China
38	22.11.2001	female	Lentigo senilis, perilesional
39	22.11.2001	female	Lentigo senilis, lesional
40	23.11.2001	female	Lentigo senilis, lesional
41	23.11.2001	female	Lentigo senilis, perilesional

42	05.12.2001	female	Lentigo senilis, lesional
43	05.12.2001	female	Lentigo senilis, perilesional
44	05.12.2001	male	Negroid skin, Ghana
45	05.12.2001	female	Lentigo senilis, lesional
46	05.12.2001	female	Lentigo senilis, perilesional
47	22.02.2000	female	Asian skin, Indonesia
48	28.09.2001	male	Asian skin, Korea
49	05.01.2001	female	Negroid skin, Ghana
50	06.07.2001	male	Caucasian skin, Germany
51	06.07.2001	male	Caucasian skin, Germany
52	05.12.2001	male	Caucasian skin, Germany
53	05.12.2001	female	Caucasian skin, Germany

I.3.2 Study 18655

Sample	Date of Biopsy	Gender	Age	Phototype	Phenotype
1	24.02.2005	female	23a	II	Caucasian skin, Germany
2	24.02.2005	female	23a	II	Caucasian skin, Germany
3	24.02.2005	female	54a	IV	Asian skin, Korea
4	24.02.2005	female	46a	I	Caucasian skin, Germany
5	24.02.2005	female	56a	IV	Asian skin, Korea
6	24.02.2005	male	50a	III	Caucasian skin, Germany
7	09.03.2005	male	39a	VI	Negroid skin, Ghana
8	09.03.2005	female	33a	VI	Negroid skin, Ghana
9	09.03.2005	female	23a	III	Caucasian skin, Germany
10	09.03.2005	female	22a	IV	Caucasian/ Negroid skin
11	09.03.2005	female	20a	II	Caucasian skin, Germany
12	09.03.2005	female	22a	I	Caucasian skin, Germany
13	29.03.2005	female	30a	III	Caucasian skin, Germany
14	29.03.2005	male	30a	III	Caucasian skin, Germany
15	29.03.2005	male	26a	I	Caucasian skin, Germany
16	30.03.2005	male	61a	VI	Negroid skin, Ghana
17	30.03.2005	female	47a	VI	Negroid skin, Ghana
18	30.03.2005	female	24a	II	Caucasian skin, Germany
19	30.03.2005	male	42a	I	Caucasian skin, Germany
20	20.04.2005	male	25a	II	Caucasian skin, Germany
21	20.04.2005	male	24a	IV	Caucasian skin, Germany
22	27.04.2005	female	40a	V	Hispanic or Latino skin, South
23	27.04.2005	male	20a	III	Caucasian skin, Germany
24	04.05.2005	male	22a	IV	Caucasian skin, Germany
25	04.05.2005	female	61a	V	Hispanic or Latino skin, South
26	04.05.2005	female	23a	I	Caucasian skin, Germany
27	29.06.2005	male	30a	V	Asian skin, India
28	29.06.2005	female	25a	VI	Negroid skin, Kenya
29	29.06.2005	female	53a	V	Asian skin, Philippines
30	29.06.2005	male	43a	V	Asian skin, Philippines

II Safety Information for the Applied Chemicals and Reagents

Hazard symbols

A = substance not characterized, **C** = corrosive, **E** = explosive, **F** = flammable, **F+** = highly flammable, **N** = environmentally dangerous**, O** = oxidizing, **T** = toxic, **T+** = extremely toxic, **Xn** = harmful, **Xi** = irritating,

Substance	Hazard symbols	R phrases	S phrases
Acetic acid	C	34	23.2-26-36/37/39-45
Acetone	F, Xi	11-36-66-67	9-16-26
Acrolein	F, T+, N	11-24/25-26-34-50	23-26-28-36/37/39-45-61
Allopurinol	T	25-43	28-36/37-45
Aminotriazol	Xn, N	48/22-51/53-63	13-36/37-61
Ammonia	C, N	34-50	26-36/37/39-45-61
β-NADPH	T	23/24/25-39/23/24/25-26-36/37/38-45	36/37/39
Cerium chloride	Xi	36/37/38	26-36
Cobalt chloride	T, N	49-22-42/43-50/53	22-45-53-60-61
Collagenase type I	Xn	36/37/38-42	22-24-26-36/37
DAPI	-	22-24/25	-
DOPA	Xi	36/37/38	26-36
Epon DDSA	Xi	36/37/38	26-36
Epon DMP 30	Xn	22-36/38	26-28
Epon NMA	Xn	22-36/37/38-42	39
Ethanol	F	11	7-16
Glutaraldehyde	T, N	22-23-34-42/43-50	26-36/37/39-45-61
HM20	Xi	10-36-37-38-43	16-26-27-28-36/37/39
Hydrochloric acid	C	34-37	26-36/37/39-45
Hydrogen peroxide	C	34	3-26-36/37/39-45
Lead citrate	T, N	20/22-33-50/53-61-62	45-53-60-61
Maleic acid	Xn	22-36/37/38	26-28.1-37
Methanol	F, T	11-23/24/25-39/23/24/25	7-16-36/37-45
Nile blue sulphate	Xi	36/38	22
Osmium tetroxide	T+	26/27/28-34	7/9-26-45
Paraformaldehyde	Xn	20/22-36/37/38-40-43	22-26-36/37
potassium permanganate	O, Xn, N	8-22-50/53	60-61

Substance	Hazard symbols	R phrases	S phrases
Saponin	Xi	36/37	26-37/39
Silver nitrate	C, N	34-50/53	26-45-60-61
Sodium cacodylate trihydrate	T,N	23/25-50/53	20/21-28-45-60-61
Sodium hydroxyde	C	35	26-36/37/39-45
Sodium tetrabortate decahydrate	-	24/25	-
Sulphuric acid	C	35	26-30-45
Trifluoroacetic acid	C	20-35-52/53	26-36/37/39-45-61
Tris	Xi	36/37/38	26-36
Triton X-100	Xn	22-41	26-36/39
Trypsin	Xn	36/37/38-42	22-24-26-36/37
Uranyl acetate	T+, N	26/28-33-51/53	20/21-45-61

Indication of Particular Risks (R-phrases)

R 8 Contact with combustible material may cause fire
R 10 Flammable
R 11 Highly Flammable
R 20 Harmful by inhalation
R 22 Harmful if swallowed
R 23 Toxic by inhalation
R 25 Toxic if swallowed
R 26 Very Toxic by inhalation
R 33 Danger of cumulative effects
R 34 Causes burns
R 35 Causes severe burns
R 36 Irritating to the eyes
R 37 Irritating to the respiratory system
R 38 Irritating to the skin
R 40 Limited evidence of a carcinogenic effect
R 41 Risk of serious damage to eyes
R 42 May cause sensitization by inhalation
R 43 May cause sensitization by skin contact
R 45 May cause cancer
R 49 May cause cancer by inhalation
R 50 Very Toxic to aquatic organisms
R 61 May cause harm to the unborn child
R 62 Possible risk of impaired fertility
R 63 Possible risk of harm to the unborn child
R 66 Repeated exposure may cause skin dryness or cracking
R 67 Vapours may cause drowsiness and dizziness

Combination of Particular Risks

R 20/22 Harmful by inhalation and if swallowed
R 23/24/25 Toxic by inhalation, in contact with skin and if swallowed
R 23/25 Toxic by inhalation and if swallowed
R 24/25 Toxic in contact with skin and if swallowed
R 26/27/28 Very Toxic by inhalation, in contact with skin and if swallowed
R 26/28 Very Toxic by inhalation and if swallowed
R 36/37 Irritating to eyes and respiratory system
R 36/37/38 Irritating to eyes, respiratory system and skin
R 36/38 Irritating to eyes and skin
R 39/23/24/25 Toxic: danger of very serious irreversible effects through inhalation, in contact with skin and if swallowed
R 42/43 May cause sensitization by inhalation and skin contact
R 48/22 Harmful: danger of serious damage to health by prolonged exposure if swallowed

R 50/53	Very Toxic to aquatic organisms, may cause long-term adverse effects in the aquatic environment
R 51/53	Toxic to aquatic organisms, may cause long-term adverse effects in the aquatic environment
R 52/53	Harmful to aquatic organisms, may cause long-term adverse effects in the aquatic environment

Indication of Safety Precautions (S-phrases)

S 3	Keep in a cool place
S 7	Keep container tightly closed
S 9	Keep container in a well-ventilated place
S 13	Keep away from food, drink and animal feeding stuffs
S 16	Keep away from sources of ignition - No smoking
S 22	Do not breathe dust
S 23	Do not breathe gas/fumes/vapour/spray (appropriate wording to be specified by the manufacturer)
S 24	Avoid contact with skin
S 26	In case of contact with eyes, rinse immediately with plenty of water and seek medical advice
S 27	Take off immediately all contaminated clothing
S 28	After contact with skin, wash immediately with plenty of ... (to be specified by the manufacturer)
S 30	Never add water to this product
S 36	Wear suitable protective clothing
S 37	Wear suitable gloves
S 39	Wear eye/face protection
S 45	In case of accident or if you feel unwell, seek medical advice immediately (show label where possible)
S 53	Avoid exposure - obtain special instruction before use
S 60	This material and/or its container must be disposed of as hazardous waste
S 61	Avoid release to the environment. Refer to special instructions safety data sheet

Combination of Safety Precautions

S 7/9	Keep container tightly closed and in a well-ventilated place
S 20/21	When using, do not eat, drink or smoke
S 36/37	Wear suitable protective clothing and gloves
S 36/37/39	Wear suitable protective clothing, gloves and eye/face protection
S 37/39	Wear suitable gloves and eye/face protection

III Curriculum Vitae

Miriam Susanna Droste

born November, 2nd 1974 in Hamburg, Germany

Education

July 2003 – Present

Doctoral thesis at Beiersdorf AG
R&D Microscopy Department, Unnastraße 48, PO Box 518, 20245 Hamburg, Germany
Supervisor: Dr. Roger Wepf

In cooperation with the University of Hamburg
Institute of Physical Chemistry, Grindelallee 17, 20146 Hamburg Germany
Supervisor: Prof. Dr. Stephan Förster

Oct. 2001 – May 2003

M.Sc. in Environmental Engineering at the Hamburg University of Applied Sciences
Lohbrügger Kirchstraße 65, 21033 Hamburg, Germany

Master's thesis at Beiersdorf AG
R&D Microscopy Department, Unnastraße 48, PO Box 518, 20245 Hamburg, Germany
Supervisors: Dr. Stefan Biel and Dr. Roger Wepf

Thesis title: "Development of a non-invasive cell swelling measurement assay for in situ cell culture"

Mar. 1996 – Aug. 2001

Diploma in Environmental Engineering at the Hamburg University of Applied Sciences

Diploma thesis at the University of Hamburg
Institute of Soil Science, Allende-Platz 2, 20146 Hamburg, Germany
Supervisor: Dr. Dietmar Goetz

Thesis title: "Mobilität von technischen Ölen in Bodenmaterialien bei ungesättigter Wasserbewegung"

Oct. 1994 – Feb. 1996

Study of Geography at the University of Hamburg.

July 1985 – June 1994

Comprehensive secondary school, Gymnasium Bondenwald, Hamburg, Germany
Main subjects for the Abitur: Geography, English, Mathematics and Art

IV Publications & Conference Contributions

Droste, M.S., Glaeser, K., Wolber, R., Wenck, H., Wittern, K.P. and Wepf, R.: *Skin Pigment Distribution in Various Skin Types and Pigmentation Disorders: Reassessment by Light and Electron Microscopy*. (in preparation for Skin Pharmacology and Physiology)

Droste, M.S., Wolber, R., Wenck, H., Wittern, K.P. and Wepf, R.: *Reviewing the Epidermal Melanin Unit: Melanocytes Visualized in 3D Contact More Keratinocytes Than Hitherto Anticipated*. (in preparation for Experimental Dermatology)

Droste, M.S. and Wepf, R.: *High-Pressure Freezing Enhances Antibody Binding Efficiency in Cryo-Sections*. (technical note, in preparation for Journal of Microscopy)

Publications:

Droste, M.S., Biel, S.S., Terstegen, L., Wittern, K.P., Wenck, H. and Wepf, R.: *Noninvasive Measurement of Cell Volume Changes by Negative Staining*. Journal of Biomedical Optics 10(6): 064017 (2005)

Conference Proceedings:

Droste, M.S., Glaeser, K., Wolber, R., Wenck, H., Wittern, K.P. and Wepf, R.: *Correlative Microscopy for the Melanosome Distribution in Lentigo Senilis Compared with Caucasian, Asian and Negroid Skin*. Scanning 28(2): 60 (2006)

Droste, M.S., Wolber, R., Wenck, H., Wittern, K.P. and Wepf, R.: *Melanosome Distribution in Caucasian Skin with Lentigo Senilis Compared to Normal Caucasian, Asian and Negroid Skin*. Journal of Investigative Dermatology 125(6): A25-A32 (2005)

Conference Contributions:

Droste, M.S., Glaeser, K., Wolber, R., Wenck, H., Wittern, K.P., Wepf, R.: *Correlative Microscopy for the Melanosome Distribution in Lentigo Senilis Compared to Caucasian, Asian and African Skin*. SCANNING, Washington (2006)

Droste, M.S., Wolber, R., Wenck, H., Wittern, K.P., Wepf, R.: *Distribution of Melanosomes in Lentigo Senilis Compared with Different Ethnic Skin Types*. SCUR & ISP Meeting, Hamburg (2005)

Droste, M.S., Delekat, T., Schmucker, R., Herbst, M., Wepf, R., Biel, S.S.: *Development of a non-invasive cell swelling measurement assay for in situ cell culture*. Aquaplug Meeting, Aarhus (2003)

Droste, M.S., Biel, S.S., Wepf, R., Delekat, T., Schmidt-Rose, T.: *Measurement of Cell Volume Changes by Confocal Laser Scanning Microscopy*. Aquaplug Meeting, Hamburg (2002)

V Acknowledgements

It is a pleasure to thank the many people who made this thesis possible.

I would like to express my sincere gratefulness to my supervisor, Dr. Roger Wepf, for his enthusiasm, his inspiration, and the unfailing precision with which he helped me shape the ideas in this thesis. Going over the concepts with him again and again was always a distinct pleasure. I am grateful for the opportunity to join his team in Zurich and to continue learning.

I am indebted to Prof. Dr. Stephan Förster for willingly patronizing this project from the part of the University of Hamburg and accommodating me in his team.

To Prof. Dr. Horst Weller I am obliged for taking over the part of second referee.

I would like to thank Dr. Ulrich Hintze, Dr. Horst Wenck and Prof. Dr. Klaus-Peter Wittern of Beiersdorf AG for the initializing and supporting this interesting project. I thank Dr. Rainer Wolber for his special support of this project.

To Dr. Stefan Biel I owe particular gratitude for introducing me to the field of microscopic research and calling back on a Friday afternoon. – Thank you for constructive criticism, guidance and encouragement. I really enjoyed our endless discussions, concerning far more than skin research.

I am indebted to Katja Gläser, who energetically supported this project and accomplished a wonderful Diploma thesis. – Without your work, this thesis would be incomplete. Thank you!

I genuinely appreciate the support of all members of the Microscopy Department, they all gave generously of their time and challenged me to look at problems in new ways. – Thank you for making me feel at home.

Special thanks to Dr. Elisabeth Müller Gubler for performing last-minute EFTEM analysis.

I wish to thank my best friends Lisa Werner and Inga Fleissner for remaining friends throughout these difficult times, and for all the emotional support, camaraderie, and entertainment they provided.

A very special thanks to Falk Lucas for putting up with me and this thesis. – Thank you for your understanding, patience, support and caring.

Lastly, and most importantly, I wish to thank my parents, Hadwig and Manfred Droste. They bore me, raised me, supported me, taught me, and loved me. To them I dedicate this thesis.

VI Eidesstattliche Versicherung

Hiermit versichere ich, Miriam Droste, geboren am 2. November 1974 in Hamburg, an Eides statt, dass ich die vorliegende Dissertation selbständig durchgeführt habe. Alle verwendeten Quellen und Hilfsmittel sind von mir als solche gekennzeichnet worden.

Diese Arbeit ist zuvor weder in gleicher, noch ähnlicher Form einem Prüfungsausschuss zur Erlangung des Doktorgrades vorgelegt worden.

Hamburg, den 12. Dezember 2006

Miriam Droste